WASM: Minerals, Energy and Chemical Engineering

Comparison of Diesel Particulate Matter Simulation Models and Ventilation Optimisation by Using Computational Fluid Dynamics

Ping Chang

This thesis is presented for the Degree of
Doctor of Philosophy
of
Curtin University

June 2019

Declaration

To the best of my knowledge and belief this thesis contains no material previously published by any other person except where due acknowledge has been made.

This thesis contains no material which has been accepted for the award of any other degree or diploma in any university.

The research does not include any human and animal ethics issue.

Signature:

Date: 05/06/2019

Acknowledgement

Time passed quickly and it was like yesterday when I started my Ph.D. study. I never expected I could meet so many difficulties and challenges during my doctoral study before I started it. Fortunately, with the help of my research group members and others, I overcame all of the challenges I met and came to the final stage finally.

First I would like to thank my supervisor, Dr. Guang Xu, for giving me helps in both daily life and my research. When I first came to Kalgoorlie, he provided me with so many suggestions and tips about living here, which helped me getting used to the local life quickly. In addition, he also devoted so much time to my research. He revised each of my papers patiently and gave me so many valuable comments to improve the quality of my papers. I believe I was not able to publish these papers with the help of him.

I also want to thank my research group members, Xuhan Ding, Yinping Chen, Jinxin Huang and Zidong Zhao, for their support to my research. During my study, they provided me with great help in my simulation and experiments. I enjoyed so much in everything we did together.

I am grateful to Dr. Benjamin Mullins and S. Abishek for giving me so many supports in my CFD study. Especially for Dr. S. Abishek, who is a CFD expert, I would like to thank him for helping me to set up the supercomputer and solvers for the simulation. Besides, I also appreciate them for giving so many valuable feedbacks on my papers and research.

I also want to thank the Pawsey Supercomputing Centre, Perth, WA, for providing high-performance communication and computing facilities for my CFD simulation.

I would like to thank Sunrise Dam Gold Mine, WA for supporting me to conduct the experiments and tests on the mine site.

At last, I want to express my sincere thanks to my parents. For the past three years, they gave both financial supports and metal supports. They always gave me support for each decision I made. Each time I was feeling down, they were always the first one who gave me encouragement.

Thanks for all your supports and encouragements.

Abstract

Diesel particulate matter (DPM) is generated due to the incomplete combustion in the diesel engine. Since the 1960s, the diesel equipment has been continuously used in the mining industries because of its high efficiency, strong power and long duration compared to the gasoline equipment. With the increasing use of diesel equipment, the miners, especially for the underground miners who work in the confined area, has the potential to exposure to a high concentration of DPM. It is reported that the DPM concentration in underground mines could be a hundred times higher than the normal environment. Research shows that both long-term and acute exposure to the high concentration of DPM could lead to an adverse health impact on human health. In the past two decades, many studies suggested a positive relationship between long-term DPM exposure and lung cancer. In 2012, based on the solid evidence provided by numbers of animal and epidemiological studies, the International Agency for Research on Cancer identified DPM as a carcinogen (Group 1). To minimize the DPM hazard in underground mine, a number of DPM control methods have been applied on the mine site. However, ventilation is still the main and common used method to maintain the DPM level in the underground mine. To control the DPM effectively by the optimizing the ventilation design, it is important to understand the DPM dispersion behaviours and identify the high DPM concentration zones. To achieve this, this study used the computational fluid dynamics (CFD) modelling to analysis the DPM dispersion and concentration distribution characteristics in the underground mine.

A review of the health effects of DPM was first provided in the beginning to address the health issues caused by DPM. The regulation and limit of DPM in different countries were also provided based on current studies. It showed the 0.1 mg/m^3 of DPM (measured as elemental carbon) was recommended by the Australian Institute of Occupational Hygienists for the underground mines. According to the health issues, the DPM control strategies on the mine site were then reviewed. The ventilation was the main control method in the underground mine. According to this, the CFD method was confirmed to study the DPM concentration distribution and optimize the ventilation design to better control DPM.

A CFD modelling was first constructed based on a published report, and a new numerical method which called Eulerian-Lagrangian method was used to study the air-DPM two-phase flow behaviours. Then the results were further compared with another numerical method. Then, an onsite experiment was conducted and the CFD modellings

were built based on the onsite experiment. The CFD modelling was used to optimize the auxiliary ventilation design in a development face. After that, a comparison study was conducted to compare the three most commonly used numerical models to simulate the DPM. The difference among three methods was provided and the advantages and disadvantages were also suggested based on the simulation results. The DPM distributions under different mining activities (shotcreting, loading, and charging) in a development face were also simulated and the ventilation system was evaluated. Finally, a dynamic mesh technology which used to represent the dynamic mining activity was introduced, and the DPM distributions were analysed.

The research provides a timesaving, effective and high accurate method to study the DPM dispersion and concentration distribution characteristics. The results and method presented in this study could help the mining industry to identify the high DPM concentration areas, optimize the auxiliary ventilation design and improve the working environment for the underground miners.

List of the Publications Included in this Thesis

This thesis includes four published journal papers and two conference papers. The relevant papers' copyright have been checked and they could be used in the thesis. The below is the list for the papers.

Journal Papers

1. Chang, P., & Xu, G. (2017). A review of the health effects and exposure-responsible relationship of diesel particulate matter for underground mines. International Journal of Mining Science and Technology, 27(5), 831-838. DOI: https://doi.org/10.1016/j.ijmst.2017.07.020
2. Xu, G., Chang, P., Mullins, B., Zhou, F., & Hu, S. (2018). Numerical study of diesel particulate matter distribution in an underground mine isolated zone. Powder technology, 339, 947-957.
   DOI: https://doi.org/10.1016/j.powtec.2018.08.075
3. Chang, P., Xu, G., Zhou, F., Mullins, B., Abishek, S., & Chalmers, D. (2019). Minimizing DPM pollution in an underground mine by optimizing auxiliary ventilation systems using CFD. Tunnelling and Underground Space Technology, 87, 112-121. DOI: https://doi.org/10.1016/j.tust.2019.02.014
4. Chang, P., Xu, G., Zhou, F., Mullins, B., & Abishek, S. (2019). Comparison of underground mine DPM simulation using discrete phase and continuous phase models. Process Safety and Environmental Protection, 127, 45-55.
   DOI: https://doi.org/10.1016/j.psep.2019.04.027

Conference Papers

1. Chang, P., & Xu, G. (2019). Review of Diesel Particulate Matter Control Methods in Underground Mines. Paper presented at the Proceedings of the 11th International Mine Ventilation Congress.
2. Chang, P., & Xu, G. (2019). Numerical study on DPM dispersion and distribution in an underground development face based on dynamic mesh. Paper presented at the Proceedings of the 17th North American Mine Ventilation Symposium.

Contents

List of Tables

List of Figures

List of Abbreviations

AIOH	Australian Institute of Occupational Hygienists
CFD	Computational Fluid Dynamics
DPFs	Diesel Particulate Filters
DPM	Diesel Particulate Matter
EC	Elemental Carbon
EEM	Eulerian-Eulerian Method
ELM	Eulerian-Lagrangian Method
IARC	International Agency for Research on Cancer
LHD	Load-haul-dump Truck
MSHA	Mine Safety and Health Administration
NIOSH	National Institute for Occupational Health and Safety
OC	Organic Carbon
OEM	Original Equipment Manufacturer
SCR	Selective Catalytic Reduction
SIMPLE	Semi-Implicit
STM	Species Transport Method
TCS	Torque Converter Stall
TWA	Time Weighted Average
WHO	World Health Organization

List of Nomenclature

A_p	Projected area of particle
C_c	Cunningham slip correction factor
C_d	Drag force coefficient
C_i	Passive scalar
D	Diffusion coefficient in air
d_p	Particle diameter
$\boldsymbol{F_d}$	Drag force
$\boldsymbol{F}$	Sum of other forces act on particles
$\boldsymbol{g}$	Gravity acceleration
G_k	Turbulent production
$\boldsymbol{I}$	Unit tensor
k	Turbulent kinetic
m_p	Particle mass
M	Gas molar mass
p	Air pressure
Re_p	Particle Reynolds number
R	Ideal gas constant
S	Source term
S_{Ct}	Turbulent Schmidt number
T	Gas temperature
t	Simulation time
$\boldsymbol{u_g}, \boldsymbol{v_g}$	Air velocity
$\boldsymbol{u_g}, \boldsymbol{v_p}$	Particle velocity
β	Interphase momentum exchange coefficient

ρ_g	Gas density
ρ_p	Particle density
ε	Volume fraciton
μ_t	Turbulent viscosity
μ	Molecular viscosity
$\boldsymbol{\tau}$	Viscous stress tensor
λ	Mean free path of gas molecules

1 Introduction

Outline

1. Background and Motivation
2. Research Aims and Objectives
3. Thesis Structure

1.1 Background and Motivation

The diesel-powered equipment has been largely used in mining industries since the 1960s according to the good performance, high efficiency and long durability of the diesel engine. Meanwhile, the extensive utilization of diesel equipment together with the increased depth of underground mine causes challenges in maintaining the diesel particulate matter (DPM) at an acceptable level in the underground mine. As a result, the underground miners have a high risk of over-exposure to high concentrations of DPM due to the confined work environment. In the development face in underground mines where the diesel equipment works more frequently during the mining activities, with the poor ventilation conditions, this issue could be magnified many times. It was reported that the DPM concentrations in such areas could be a hundred times high than the normal environment (US.EPA, 2002). DPM is mainly composed of an insoluble elemental carbon (EC) core and an adsorbed surface coating of relatively soluble organic carbon (OC), both of which are in submicron range (US.EPA, 2002). A study showed that more than 90% of the total number of diesel particles are less than 0.1 μm (D. B. Kittelson, 1998). Due to DPM's ultra-fine characteristics, it is able to penetrate the human's respiratory system and deposit in the deepest part of the human lung. For this reason, it brings negative health effects to people who are exposed to it. Such effects include both short-term risk such as acute irritation, asthma, cough and lightheadedness, and long-term exposure risk of lung cancer (Attfield et al., 2012; DMP, 2013; B. Rudell et al., 1996; Silverman et al., 2012; Turner, 2007; US.EPA, 2002). In 2012, based on the sufficient evidence from both animal studies and epidemiological studies, the International Agency for Research on Cancer declared the DPM as a carcinogen to humans (Group 1) (Lyon, 2012).

According to the potential risk of DPM, many countries have set the limit of DPM level for underground mines to protect the miners. However, in Australia, there is no national exposure standard for DPM. The Australian Institute of Occupational Hygienists suggested an 8-hour time-weighted-average exposure standard of 0.1 mg/m^3 (measured as EC) of DPM concentration for mining industries. Many states, such as Queensland and Western Australia, in Australia have applied this value as a recommended exposure limit for mines.

To control the DPM concentration, current DPM control method includes source controls, which control the DPM before it emits to the work environment, and exposure controls, which control the DPM after it emits from the diesel engine. The source controls mainly include the diesel engine maintenance, the improvement of diesel engine

design, and the usage of alternative fuel. The exposure controls include the usages of diesel filters, mine ventilation and the application of environmental cabs and personal protective equipment. For the mining industry, ventilation is still the main approach to control DPM. Thus, to understand the DPM dispersion characteristics and identify the high DPM concentration zones are important for a better ventilation design and the making of a DPM control strategy.

Currently, some Australian mines have exceeded the recommended limit and some miners even lack the knowledge and skill to monitor the DPM levels on mine site. Moreover, to measure the DPM levels for each area on the mine site by humans is labour consuming and uneconomic. Especially in some space-confined areas, such as the development face, it is not allowed for the miners to measure the DPM concentrations around the diesel equipment when the diesel vehicle is working according to the safety considerations. In addition, for the airflow complicated areas, the DPM dispersion may highly rely on the airflow distribution. It is also hard for the miners to understand the locations of such areas. Therefore, a method should be required for helping the mining industry to solve the above issues. Such a method should be (1) economic, high efficiency, more safety and less labour intensive to identify the high DPM concentration areas and (2) able to evaluate the ventilation performance on maintaining the DPM levels and (3) easily to optimize the auxiliary ventilation systems in the development face. With the development of computing technology. Computational fluid dynamics method has become an effective, economic and timesaving technique to solve the health-related issues on mine site. CFD is a proper method to solve the above issues and it meets all the requirements mentioned.

1.2 Research Aims and Methodology

The mining industry is challenged to meet the current recommended DPM limit, and the related health issues might be more serious than it is recognised. The main aim of this research is to provide an effective method (CFD) for the industry to understand the DPM dispersion characteristics and help them to optimize the ventilation design to control the DPM efficiency. The aim was accomplished by two major objectives.

The first major objective is to understand the health effects, monitor method, control strategies of DPM and determine the applicability of CFD on this study. The objective in this phase could be achieved by the detailed literature review as following:

1. Determination of the current existing health problems caused by DPM and suggesting the regulation of the DPM for the mining industry.

2. Evaluation and comparison of the performance of the different DPM monitors. Providing a systematic monitoring approach to the mining industry.
3. Investigation of the currently DPM control strategies and determining the commonly used method on the mine site.
4. Determining the applicability of CFD simulation on this study.

The second objective is to use the CFD method studying the DPM behaviours and evaluate the ventilation system performance under different mining activities. This stage could be achieved by the following steps:

1. Developing an appropriate numerical method to simulate the DPM behaviours and validate it with the onsite experiment.
2. Predicting the DPM distributions and identify the high DPM concentration areas by CFD modelling.
3. Comparison of the current modelling methods which were used to simulate the contaminant in underground mines and determination of an optimum method for the DPM simulation based on different cases.
4. Investigation of the auxiliary ventilation system performance on the maintaining of DPM.
5. Evaluating ventilation performance under different mining activities.
6. Recommendation of the good control strategies and improving the underground work environment based on the simulation results.

To conduct the CFD simulation, both an open source software-OpenFOAM and a commercial software - ANSYS were used. OpenFOAM is short for Open-source Field Operation And Manipulation, which is a Linux system based C++ toolbox. This software enable the users to develop solvers based on the requirement. OpenFOAM is used to simulate airflow and DPM dispersion behaviours. All the meshes were generated by ICEM, a package of ANSYS and the post-processing has been done by ParaView. Fluent, a CFD simulation pack of ANSYS, was used for the dynamic mesh simulation.

Development face is one of the most common working layouts in the underground mine, and most of the mining activities (shotcreting, loading and charging) are conducted in this area. Due to the confined space, the DPM concentration is usually higher in a development face than other areas on the mine site. Thus, the development face is the main study objective ofthis thesis. The ventilation system evaluation and DPM concentration distribution are also analysed in the development face.

1.3 Thesis Structure

This thesis consists of 8 chapters. This chapter presents the introduction and the main aim of this study. Chapter 2 to chapter 7, are presented by the published journal paper, or conference paper, or the paper is under reviewed or the paper is going to be submitted. The status of each paper is presented at the beginning of each chapter. Chapter 8 is the conclusion part which summarizes the main findings, analysis of the current limits of this study and presents the plan of the future work. The detailed description of chapter 2 to 7 are illustrated in follows:

Chapter 2 consists a comprehensive literature reviews on the current DPM research. This chapter consists of four parts. The review of DPM health effects, DPM monitoring approaches, current DPM control methods on the mine site, and the CFD application on the mining industry. The review identified the current challenge on the mine site and determine the suitability of the CFD method for this study.

Chapter 3 presented a CFD numerical study on the DPM distribution characteristics in an underground isolated zone. The simulation models were built according to a published report. Compared to the previous study, a different simulation method was used to present the DPM behaviours, which gave a close agreement with the onsite data. This method was also used in the following chapter.

In Chapter 4, a CFD study was conducted to optimize the auxiliary ventilation design in an underground development face. An onsite experiment was first conducted. Then the CFD simulation was built according to the onsite measurement.

Chapter 5 is a comparison study of different numerical models used to simulate DPM. Three main numerical models used in the previous study to simulate the DPM were included and the disadvantages and advantages of each model were summarized. The applicability of each method was also suggested. Based on this, a fast and accurate model was used to study the DPM behaviours in chapter 6 and 7.

Chapter 6 studied the DPM concentration distribution characteristics in a development face under various mining activities (shotcreting, loading and charging). The performance of the auxiliary ventilation was also evaluated.

Based on the limitation of the current simulation method presented in the previous chapters. Chapter 7 introduced a new simulation method which called dynamic mesh method to study the DPM behaviours with the impact of a moving vehicle.

2 Literature Review

This chapter consists of four parts as following:

1. "A review of the health effects and exposure-responsible relationship of diesel particulate matter for underground mines" This part has been published as a journal paper on International Journal of Mining Science and Technology. It was entirely written by Ping Chang with the editorial suggestion by Dr Guang Xu. Please cited it as:
   Chang, P., & Xu, G. (2017). A review of the health effects and exposure-responsible relationship of diesel particulate matter for underground mines. International Journal of Mining Science and Technology, 27(5), 831-838. DPM Measurement
2. "Review of Diesel Particulate Matter Control Methods in Underground Mines" This part has been presented on the 11th International Mine Ventilation Congress, Xi'an, China. It was entirely written by Ping Chang with the editorial suggestion by Dr Guang Xu. Please cited it as:
   Chang, P., & Xu, G. (2019). Review of Diesel Particulate Matter Control Methods in Underground Mines. Paper presented at the Proceedings of the 11th International Mine Ventilation Congress.
3. CFD Application for Mining
4. Summary

This chapter presented the adverse health effects of high concentration DPM exposure, current DPM measurement methods, DPM control strategies and DPM limitation in different countries. Then the applicability of CFD method on the DPM studies was approved. Hundreds of previous literatures were reviewed. The methods for DPM simulation were summarised and had been further discussed in the following chapter.

2.1 A Review of the Health Effects and Exposure-Responsible Relationship of Diesel Particulate Matter for Underground Mines

2.1.1 Abstract

The increasing use of diesel-powered equipment in confined spaces (underground mines) has the potential to overexpose underground miners under the threat of diesel particulate matter (DPM). Miners in underground mines can be exposed to DPM concentrations far more than workers in other industries. A great number of animal and epidemiological studies have shown that both short-term and long-term DPM exposure have an adverse health effect. Based on reviews of related studies, especially some recent evidence, this paper investigated the long and short-term health effects based on animal studies and epidemiological studies. The exposure-response relationship studies were also explored and compared to the current DPM regulation or standards in some countries. This paper found that the DPM health effect studies specifically for miners are not sufficient to draw solid conclusions, and a recommendation limit of DPM concentration can be put in place for better protection of miners from DPM health risk. Current animal studies lack the use of species that have similar lung functions as humans for understanding the cancer mode of action in human. And finally, the DPM health hazard will continue to be a challenging topic before the mode of action and reliable exposure-response relationship are established.

2.1.2 Introduction

As diesel-powered equipment has good power performance, high economy, efficiency as well as durability, its use has continuously increased in both underground coal and metal/non-metal mines since the 1960s. Various types of diesel-powered equipment are operated in the mining industry. Compared to gasoline equipment, diesel-powered equipment is more efficient and emits less carbon dioxide (a greenhouse gas) per unit of work. Nevertheless, diesel-powered equipment emits much more particulate matter than gasoline equipment during the combustion process. This is a problem in confined spaces, such as underground mines, where it has great potential for miners to be

overexposed to diesel particulate matter (DPM). Miners in underground mines can be exposed to far higher DPM concentrations than in other industries. For example, in 1996, the US nationwide average DPM exposure was estimated to be 1.4 $\mu g/m^3$. On the other hand, investigators showed that exposure for the workers in coal mines and noncoal mines ranges from 10 to 1,280 $\mu g/m^3$, with environmental equivalent exposure of 2 to 269 $\mu g/m^3$ (US.EPA, 2002).

In 1988, based on the results of a series of animal and epidemiologic studies, the National Institute for Occupational Health and Safety (NIOSH) in the US recommended that DPM had potential carcinogenic effects on humans (NIOHS, 1988). In the following year (1989), International Agency for Research on Cancer (IARC), a part of the World Health Organization (WHO), published a monograph which classified DPM as a probable carcinogen to humans (group 2A) (IARC, 1989). A number of animal studies have been conducted, which showed that long-term exposure to DPM has the potential to cause lung tumours (Heinrich et al., 1995; Heinrich et al., 1986; Iwai et al., 2000; Mauderly, Jones, Griffith, Henderson, & McClellan, 1987; Nikula et al., 1995; Walter et al., 2005). There are also many epidemiological studies on humans that have suggested the association between health effects and long-term DPM exposure (Attfield et al., 2012; Boffetta et al., 2001; Garshick et al., 2012; Garshick et al., 2004; Garshick, Laden, Hart, Smith, & Rosner, 2006; Järvholm & Silverman, 2003; Laden, Hart, Eschenroeder, Smith, & Garshick, 2006; Laden, Hart, Smith, Davis, & Garshick, 2007; Silverman et al., 2012; Steenland, Deddens, & Stayner, 1998; Vermeulen et al., 2014). These studies concluded that long-term exposure to high concentrations of DPM could increase the lung cancer risk. In addition, many studies showed that short-term or acute exposure to DPM could also induce negative health effects, such as acute irritation, asthma, cough, light-headedness (HEI, 2003; Lucking et al., 2011; B. Rudell et al., 1996; B. Rudell et al., 1994; B Rudell, Sandström, Stjernberg, & Kolmodin-Hedman, 1990; Salvi et al., 1999; Salvi et al., 2000; Turner, 2007; US.EPA, 2002). In 2012, based on sufficient evidence of animal and epidemiological studies, IARC classified DPM as carcinogenic to humans (Group 1). For these reasons, health issues associated with DPM exposure are receiving substantial attention from the public, government agencies and academia.

In order to minimize DPM health hazards, the DPM concentration should be maintained below an acceptable standard. Germany, Canada and the USA have already set their limit or standard for DPM exposure for mining industries. Germany sets the DPM limit for underground noncoal mines and other surface workplaces at 0.3 and 0.1 mg/m^3, respectively. The Canada Centre for Mineral and Energy Technology sets the

standard of DPM at 0.75 mg/m^3 (Cantrell & Watts Jr, 1997). In the US, the Mine Safety and Health Administration (MSHA) has an exposure standard of DPM for metal/nonmetal mines of 0.16 mg/m^3 (measured as total carbon) (MSHA, 2006). The development of regulations and standards for the DPM exposure in underground mines is still in its early stage in Australia (AIOH, 2013). Currently, the official limit for DPM exposure for underground mines is still not established, and the level of regulation in different states varies. In Australia, many regulatory agencies have considered 0.1 mg/m^3 (measured as elemental carbon, TWA) of DPM as a recommended exposure limit, and this is also recommended by the Australian Institute of Occupational Hygienists (AIOH) (DMP, 2013).

Due to the hazards of DPM, many studies of DPM have been carried out; however, very few detailing the health effects review impacts on mining workers, especially for the underground miners. The aim of this paper is to provide a review of the health effects of DPM on underground miners, especially some recent evidence, and the regulations in some major mineral producing countries with a new trend on what data is more appropriate to reflect the DPM dose. This paper conducted a scientific review of a great number of available literature published over the past three decades. Based on the published animal and epidemiological studies, this paper determined the potential relationship between both long-term and short-term DPM exposure and health effects. This paper also aims to determine whether there was an exposure-response relationship for cancer effects. Available data from animal and human studies have been used to evaluate the exposure cancer unit risk and the cancer mode of action. A recommended exposure limit of DPM for underground mining industry was concluded based on a summary of the published literature and regulation in different countries.

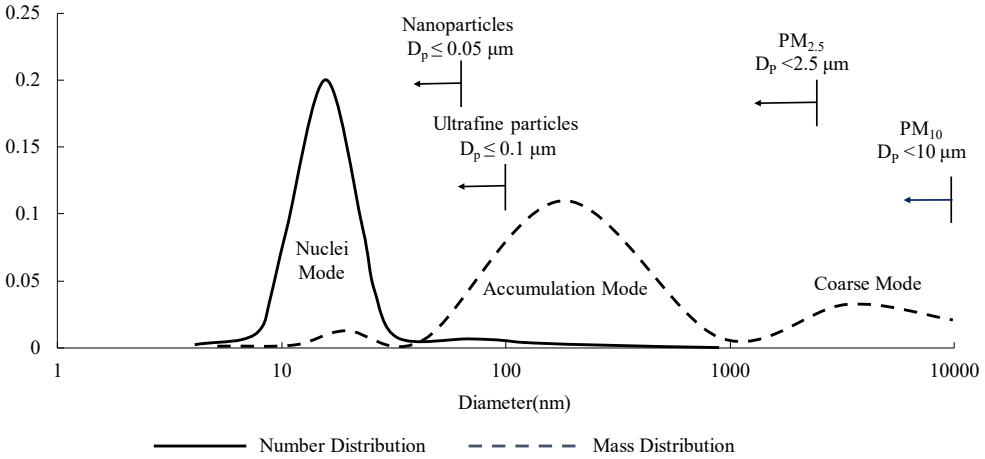

Figure 1 Diesel particulate matter size distribution (Modified after Kittelson (D. B. Kittelson, 1998))

2.1.3 Health effects of DPM

2.1.3.1 Deposition mechanisms

The main way for DPM to enter the respiratory system is inhalation. It was reported that particles could deposit within the human respiratory tract (US.EPA, 2002). Studies showed that the filtering capacity of the nose would be very low when particles' size was less than 0.5 μm (Schwab & Zenkel, 1998; US.EPA, 2002). When the particle size is less than 1 μm, it is able to deposit in the deepest ranges of lungs. Figure 1 shows the typical mass-weighted and number-weighted size distributions of diesel particles. As can be seen, more than 90% of the particles' diameters are below 1 μm, which are capable of entering the deepest ranges of the lungs. Many studies have shown that airborne PM, in which DPM is the main component, contributes to the respiratory mortality and morbidity (Anderson, Thundiyil, & Stolbach, 2012; HEI, 2002).

2.1.3.2 Long-term effects

2.1.3.2.1 Laboratory animal studies

A high number of animal studies have been carried out to evaluate the potential health effects of long-term DPM exposure. Many animal studies, including on rats, mice, hamster and monkey, have demonstrated that long-term exposure to high concentrations of DPM contributes to increasing the risk of lung tumour.

Almost all the animal studies have shown a lung tumour response in rats after long-term exposure to a high concentration of DPM (>2.5 mg/m^3). Heinrich U et al. conducted a long-term study with rats, mice, and hamsters exposed to unfiltered and filtered DPM to understand its carcinogenicity (Heinrich et al., 1986). All experimental animals were aged 8 to 10 weeks before the exposure. The exposure was 19 h a day, 5 days a week. The maximum exposure duration for mice, rats and hamsters was 120, 140 and 120 weeks, respectively. The concentrations of unfiltered DPM in this study were about 4 mg/m^3. Each group included 96 animals. There was a clean air exposure chamber for the control groups with equal sample size. A high lung tumour rate in rats (18%, 17/95) had been observed after long-term exposure to DPM compared with the controls (0%, 0/96). Mauderly et al. (Mauderly et al., 1987) conducted a carcinogenicity study of rats that were exposed to soot (a primary composition of DPM) at high, intermediate, and low concentrations (0.35, 3.5, 7.0 mg/m^3 respectively) for up to 30 months (7 h/day, 5 days/week). The result showed that the rate of lung tumour for high and intermediate exposure groups was 13% and 4% respectively, which was higher than that of the control group (1%). Iwai et al. (Iwai et al., 2000)conducted an inhalation study to estimate the relationship between oxidative DNA damage and lung tumour in 48 F344 female rats which were exposed to diesel exhaust at 2.1 to 4.9 mg/m^3 for up to 12

months (17 h/day, 3days/week). After 12 months' exposure, the experimental rats were transferred to a clean room and maintained for another 18 months for observation. The results showed that the rate of lung tumours in rats increased gradually with the exposure duration after 6 months and reached the peak at the 9th month; the exposed rats had high rates of death compared with the controls. Many other studies also showed similar results (Heinrich et al., 1995; Henderson et al., 1988; Nikula et al., 1995; Walter et al., 2005). From the studies above, DPM is considered carcinogenic in rats after long-term exposure. However, a study conducted by Lewis et al. gave an opposite conclusion (Lewis, Green, Moorman, Burg, & Lynch, 1989). In this study, three different animals (monkeys, rats and mice) were exposed to different experimental environments for up to 2 years, including clean air (controls group), 2 mg/m^3 coal dust, 2 mg/m^3 DPM, and 1 mg/m^3 coal dust and 1 mg/m^3 DPM mixture. No significant difference in the rate of lung tumour for rats was found between the four exposure groups (2%, 4%, 4% and 4%, respectively). Compared to other studies, this study lacks the post-exposure period for rats, which could be a reason for the different results. It is also noticed that the DPM concentration in this study was lower than other studies, which could also be a limitation for the results.

Some animal studies also selected mice as one of the tested animals. However, discrepant results were achieved in some of those mice studies. Heinrich et al. pointed out that the lung tumour incidence in exposed mice (32%) was about three times that of the controls (11%) (Heinrich et al., 1986). However, a carcinogenic response failed to show in his later study (Heinrich et al., 1995). In this study, mice were exposed to clean air, filtered diesel exhaust (particle free) and unfiltered diesel exhaust (4.5 and 7.0 mg/m^3 DPM) for 13.5 months (18 h/d, 5 d/week). No lung tumour incidence increase was observed in the mice. Although the earlier study provided some evidence for the carcinogens of DPM, no tumorous response was observed in the larger sample size and well-designed later study. Thus, the carcinogenic effect of DPM on mice is inconclusive. The reason for the discrepant results are still not identified.

In contrast to the studies of rats and mice, a lack of significant tumorous response was found in hamsters and monkeys. In Heinrich et al.'s study, no tumours were observed in both the DPM exposure group and the control group for the hamsters (Heinrich et al., 1986). The monkey group showed a similar result as that of rats in the report by Lewis et al. which is mentioned above (Lewis et al., 1989). In summary, DPM did not induce lung tumours either in hamsters or in monkeys. The limited observation

time and the difference in lung burden ability between monkeys, hamsters and rats may cause different results.

In summary, almost all the studies in rats indicated an apparent increase in the risk of lung tumours except for one study (Lewis et al., 1989). None of the hamster studies showed the same increasing trend as rats in the risk of lung tumours. The results of the mice studies varied. Only one study involved monkeys, but no lung tumours were found in monkeys after long-term DPM exposure (Lewis et al., 1989). The animal studies in rats have provided sufficient evidence for the carcinogenicity of DPM, but future studies still need to be conducted to determinate the carcinogenicity of DPM exposure for other animals.

2.1.3.2.2 Epidemiological studies

Animal studies have already provided a number of evidence and experimental data for the positive link between DPM exposure and adverse health effects. Although it is possible that long-term DPM exposure contributes to lung cancers in humans, it does not mean that the dose-response information from the carcinogenicity in rats is applicable to humans. Many studies showed that it is the overload of the lung which resulted in the high risk of lung tumour in rats (Heinrich et al., 1995; Iwai et al., 2000; Nikula et al., 1995). For humans, the clearance and burden function of the lung is much greater than rats. In other words, the deposition of DPM in the lungs is different for animals and humans even when breathing the same dose of DPM. Thus, adopting the laboratory animals' DPM exposure concentration as the guidance for human DPM exposure is inappropriate (US.EPA, 2002). For this reason, a number of occupational studies have been conducted, which provided epidemiologic evidence relevant to the association between DPM exposure and the risk of lung cancer.

In 1986, NIOSH published the report "*Evaluation of the potential health effects of occupational exposure to diesel exhaust in underground coal mines*". This report included a series of animal studies and epidemiological studies with regard to the health effects of long-term DPM exposure. In 1988, NIOSH further analysed the data in the 1986 report and concluded that long-term exposure to high concentrations (over 4 mg/m^3) of diesel exhaust could significantly increase the risk of lung tumour for tested animals. However, only two epidemiological studies cited in the report illustrated that the lung cancer mortality of the railroad workers increased after long-term exposure to DPM emissions (Garshick et al., 1987, 1988). While another epidemiological study showed that there was no significant increase in the lung cancer mortality of workers who were exposed to the DPM emissions compared with the general group, this result is

less reliable due to the small size of the analysed population (Garshick et al., 1987). Based on sufficient animal studies and limited evidence of epidemiological studies, NIOSH recommended that DPM had potential carcinogenic effects on human (NIOHS, 1988). In 1988, IARC held a review conference with a working group of experts to evaluate the health effects of DPM exposure. Similar to the NIOSH recommendation, IARC classified the DPM as a probable carcinogen to humans (group 2A), and this conclusion was reported in the 1989's publication "*Diesel and gasoline engine exhausts and some nitroarenes*" (IARC, 1989). The review mainly evaluated more than ten cohort studies related to different occupations (railroad workers, drivers and miners) and case-control studies related to various diseases (lung cancer, bladder cancer, etc.). However, the association of long-term DPM exposure and the incidence of lung cancer could not be identified due to limited evidence of epidemiological studies. After 24 years, in 2012, IARC conducted another review following the first review in 1988. A major result of this review was that DPM has been changed to be classified to carcinogenic to humans (Group 1), and this evaluation was published in a report in 2013 (IARC, 2013). The animal and limited epidemiological studies reviewed in the previous report provided the evidence to support the probable carcinogenicity of DPM (IARC, 1989). In the latest report, new evidence for the association between lung cancer and DPM exposure has been provided by epidemiological studies (IARC, 2013). Two studies cited in the report, an occupational cohorts study and a case-control study, in particular, provided powerful evidence for the association between lung cancer and long-term DPM exposure (Silverman et al., 2012).

A number of epidemiological studies for different job titles which were reviewed in the IARC report provided strong evidence for the carcinogenicity of DPM (IARC, 2013). Garshick et al. found that the relative risk (RR) for lung cancer mortality among long-term exposure railroad workers was 1.40 (95% CI: 1.30-1.51) compared with those workers without regular exposure to DPM emissions (Garshick et al., 2004). However, this study did not adjust for the smoking history, which is a potential confounding factor for the result. For this reason, Garshick et al. conducted a further study with the smoking history adjustment (Garshick et al., 2006). The results of the study showed that the RR of lung cancer were 1.22 (95% CI: 1.12-1.32) and 1.35 (95% CI: 1.24-1.46) with and without smoking history adjustment, respectively. This data showed that there was a small difference in the risk of lung cancer mortality after considering the smoking history. Large sample size and long duration period in this study allowed reliable conclusions to be drawn. Similar results were also found in epidemiological studies of

trucking industry workers, construction workers and other DPM exposure related areas (Boffetta et al., 2001; Olsson et al., 2011; Parent, Rousseau, Boffetta, Cohen, & Siemiatycki, 2007).

Compared to other diesel engine related jobs, underground miners usually are exposed to higher concentrations of DPM due to the confined working space and poor ventilation conditions. However, only three epidemiological studies on underground mines in the last decade have been found. These studies provide strong evidence for the association between high risk of lung cancer and long-term DPM exposure. In a cohort mortality study, a large sample size of 12,315 mineworkers who were exposed to DPM emissions at 8 American non-metal mines was selected (Attfield et al., 2012). All the workers had been employed for more than 1 year during which time the diesel equipment was used in the mine. The mortality information for miners was followed until the end of 1997. The study selected the respirable EC as the surrogate of DPM for each case study at eight mining facilities (including all kinds of surface and underground jobs). In the assessment, the exposure was estimated based on the measurement of personal respirable EC (REC) levels between 1998 and 2001. The historic REC concentration (before 1998) was speculated based on the data collected between 1998 and 2001. This study also takes other factors, such as sex, job titles, date of birth, into consideration. However, smoking history was not available to use in the study. The results of the study showed that the mean DPM concentration for the surface workers and underground workers were 1.7 and 128.2 $\mu g/m^3$, respectively. The RR of lung cancer mortality for ever-underground workers and surface only workers were 1.21 (95% CI: 1.01-1.45) and 1.33, respectively. When the cumulative DPM concentration was above 946 $\mu g/m^3$ a year, the RR for underground miners was 2.21 (95% CI: 1.19-4.09). This data illustrated that the high DPM concentration exposure group (underground miners) has a higher risk of lung cancer mortality than that of the low-exposure group (surface miners). Also, the results showed a rising trend in the hazard ratios for lung cancer mortality with increasing DPM exposure time. Based on this study, a nested case-control study was conducted by Silverman et al., with the same group of miners as the research sample (Silverman et al., 2012). With the inclusion of smoking history and previous respiratory disease as factors, the adjusted results still supported the conclusions of the original study by Attfield et al. (Attfield et al., 2012). For both smokers and non-smokers, the risk of lung cancer mortality increased with the increasing exposure time (15-year lag). The underground miners who were exposed to high concentrations of DPM for a long-term (15 years or more) had a higher risk of lung

cancer mortality (4 times) than surface miners who were exposed to a lower concentration of DPM. In another cohort study, 5,862 German potash miners were followed from 1970 to 2001 (Neumeyer-Gromen, Razum, Kersten, Seidler, & Zeeb, 2009). Total carbon (TC) was selected as a surrogate of DPM. Cumulative diesel exposure was estimated by multiplying the concentrations of TC by the miners' exposure period. Smoking history of miners was considered as a confounder factor in this study. The standardized mortality ratio (SMR) for lung cancer was 0.73 (95% CI: 057-0.93); the lung cancer SMR for the whole cohort and sub-cohort were 1.28 (95% CI: 0.61-2.71) and 1.50 (95% CI: 0.66-3.43), respectively, at the cumulative DPM exposure of 4.9 mg/m^3-years compared with the low exposure group after smoking adjustment. The results showed a positive link between the mortality of lung cancer and DPM exposure, and the RR grows with increasing exposure time.

However, the study conducted by Möhner et al. drew a different conclusion (Möhner, Kersten, & Gellissen, 2013). This study reanalysed Neumeyer-Gromen's study and aimed to reassess the cancer risk in potash miners after long-term exposure to DPM (Neumeyer-Gromen et al., 2009). EC was used to represent the level of total DPM. The results indicated that there was no apparent relationship between cumulative DPM exposure and lung cancer risk. However, the result is not convincing due to the small sample size.

To summarize, the epidemiologic studies have supported the positive relationship between the long-term DPM exposure and the risk of lung cancer, which is unlikely to be caused by chance. Only a few studies were found directly on underground miners, but three of such studies indicated a positive relationship between lung cancer mortality and prolonged high DPM concentration exposure. Further studies are still needed to focus on the underground miner group as the DPM concentrations underground are higher than other workplaces. Besides, other contaminants, such as dust, should also be considered in the study, because such contaminants might exacerbate the health effect of DPM.

2.1.3.3 Short-term effects

Although the diesel exposure studies were mainly focused on the carcinogenicity of long-term DPM exposure (i.e., lung cancer), the health effects of short-term or acute DPM exposure are also investigated in various studies. These studies are divided into laboratory animal studies and human studies in this section.

2.1.3.3.1 Laboratory animal studies

Due to the similar non-carcinogenic responses to the short-term DPM exposure in human and experimental animals, many animal studies are used to evaluate the DPM

short-term effect. Rat is the preferred animal species in such studies, and the DPM dosage is either through exposing the animal to the DPM environment or through intratracheal instillation or injection of a dose of DPM directly into the test animal.

A number of inhalation studies showed that short-term exposure to DPM could affect the brain, cardiovascular and lung system, but these effects are reversible after a period of stay in a DPM-free environment. Campen et al. conducted a study to estimate the association of acute DPM exposure and cardiovascular effects in spontaneously hypertensive rats (Campen et al., 2003). The study exposed rats to five different levels of DPM (0, 0.03, 0.1, 0.3, 1 mg/m^3) for 6 h/day for one week. Mild effects on lungs for the exposure group were observed in this study. Both HR and PQ intervals showed a significant difference in the male exposure rats, but less difference was found in the female exposure group. The limited experimental data in this study prevented the result providing enough evidence to reveal the association between cardiovascular effects and DPM exposure. This association was further studied by Campen et al. using mice as the study subject. The results showed that both DPM and non-particle compounds in the diesel exhaust had adverse effects on cardiovascular systems (Campen et al., 2005). Berlo et al. conducted a study to estimate the relationship between short-term DPM exposure and adverse effects on rat lungs and brains (Berlo et al., 2010). This study exposed male Fischer F344 rats, aged 9 weeks, to 1.9 mg/m^3 DPM and purified air (controls) for 2 h and then followed by a 4 or 18 h recovery exposure. The results showed that an increase in HO-1 level, a material to protect the brain from injury, was observed in the brain for the exposure group. However, only light inflammation was observed in the lungs. Thus, concluding that short-term DPM exposure has adverse effects on the brain but limited effects on the lungs. Hazari et al. exposed male spontaneously hypertensive rats to low (0.5 mg/m^3) and high (0.15 mg/m^3) concentrations of whole diesel exhaust (wDE) and filtered diesel exhaust (fDE) and filtered air (controls) for 4 h to study the link between increased risk of triggered arrhythmias and diesel exhaust exposure (Hazari et al., 2011). Slightly higher heat rates were observed in wDE and fDE exposure groups compared with the controls. The findings illustrated that a high rate of arrhythmias could be triggered by short-term exposure to DE for that heart sensitivity group. Gordon et al. exposed 12 male Wistar-Kyoto rats to 3 experimental environments (unfiltered DPM, filtered DPM and clean air) for 2 exposure periods (2 days and 4 weeks) (Gordon, Schladweiler, Krantz, King, & Kodavanti, 2012). The results showed a reduction in BP and HR in both filtered and unfiltered DPM exposure groups after 4 weeks exposure compared with the controls, but

there was no apparent difference in HR between the 3 groups in the first exposure week. Apparent inflammation in the lungs was found in both the 2 days and 4 weeks exposure groups. Apparent reduction of cardiac contractility was observed only in the unfiltered DPM exposure group after 4 weeks exposure. However, all the adverse effects disappeared after a period of recovery. This study indicated that short-term DPM exposure can cause adverse effects on both heart and lungs, but the adverse effects are reversible after a period of recovery. Overall, short-term DPM exposure could result in a series of adverse effects on the brain, lungs and cardiovascular system. From the study, it is concluded that the brain and cardiovascular system are more sensitive to the DPM exposure than the lungs. However, the adverse effects will disappear after a period of recovery in clean air.

Some instillation and injection studies also linked the DPM to the adverse effects on the lungs and cardiovascular system, such as inflammation in lungs, arrhythmia and myocardial ischemia. Yokota and his co-workers conducted a series of intratracheal instillation studies to estimate the DPM's adverse effects on the cardiovascular system and lungs in rats (Yokota et al., 2004; Yokota, Ohara, & Kobayashi, 2008; Yokota, Seki, Furuya, & Ohara, 2005). In the study, a pre-instillation of 1 mg DPM dose was received by rats before the ischemia/reperfusion experiment. Arrhythmia and inflammation in the lungs were observed in the experiment, which indicated that short-DPM exposure might cause dysfunction on the lungs and the cardiovascular system. Nemmar et al. conducted an injection study to demonstrate the cardiovascular and lung inflammatory effects induced by DPM in rats. Different doses of DPM (0.02. 0.1 and 0.5 mg/kg) were injected into the tail vein of rats (Nemmar, Al-Maskari, Ali, & Al-Amri, 2007). The study supports the same conclusion that the existence of DPM in systemic circulation can induce pulmonary inflammation and cardiovascular changes. However, there was no post-exposure procedure in these studies, which leads to uncertainty for its reversibility.

2.1.3.3.2 Human studies

The available human research indicated that short-term or acute exposure to DPM results in some non-cancer health effects, such as acute irritation, asthma, cough, light headedness. Especially for asthma patient and sensitive groups, who are more easily affected by the DPM.

A series of studies have been conducted by Rudell et al. to access the health effects of short-term DPM exposure on humans (1996; 1994; B Rudell et al., 1990). These studies exposed healthy non-smoking volunteers to DPM exhaust for a short-period. The results suggested that short-term exposure could cause bronchial inflammation, eye

irritation, nasal irritation and headache, etc. Salvi et al. conducted some similar studies on healthy human volunteers (Salvi et al., 1999; 2000). These studies demonstrated that acute or short-term exposure to high concentration DPM could cause a pulmonary inflammatory response in the lungs and cause respiratory health effects. However, the DPM level data was not available in these studies. Nordenhall et al. conducted studies of the adverse effects of short-term DPM exposure on the airway in humans (Nordenhall et al., 2000; 2001). In these studies, 15 non-smoking healthy and 14 asthmatic volunteers were exposed to diesel exhaust at a PM_{10} concentration of 0.3 mg/m^3 and clean air (controls) for 1 h. Inflammation in airways was observed both in the healthy and asthmatic groups 6 h after the exposure. For the asthmatic group, significant airway hyper responsiveness, which is the fatal factor of asthma, was found in the DPM exposure group but not in the controls. This means that asthma could be triggered after short-term exposure to DPM among asthmatics. To estimate the health effects of short-term DPM exposure on vascular and endothelial function in humans, Mills et al. exposed 30 non-smoking healthy male volunteers to 0.3 mg/m^3 DPM and clean air for 1 h (Mills et al., 2005). During the exposure, the volunteers were asked to do intermittent exercise. The adverse effects on vascular and fibrinolytic function were observed in the DPM exposure group, but there was less effect on the heart rate and blood pressure for the same group. Mills et al. conducted a similar study to estimate the effects of short-term DPM exposure on myocardial, vascular and fibrinolytic functions in coronary heart disease patients (Mills et al., 2007). The results showed that short-term DPM exposure could aggravate the impairment of myocardial and vascular functions for stable coronary heart disease patients when doing exercise. The two studies indicated a positive relationship between short-term DPM exposure and adverse effects on cardiovascular functions. Lucking et al. conducted a study to estimate the particle capture effects of particle traps (Lucking et al., 2011). This study exposed 19 healthy male volunteers to 0.3 mg/m^3 DPM with and without particle traps for an hour. The results showed a higher rate of vascular function impairment and thrombus formation in the exposure group without particle traps compared to the group with particle traps. Although the aim of this study is to evaluate the performance of the particle traps, the findings provided the support for the positive association between short-term DPM exposure and the adverse effects of cardiovascular functions.

From the studies above, it is concluded that short-term DPM exposure is associated with adverse health effects on humans, including respiratory and cardiovascular disease. Especially for the sensitive population, they are more easily affected by acute DPM

exposure. However, no cancer effects have been observed for short-term DPM exposure. In fact, many cancers are caused by one or more risk factors, like long-term exposure.

2.1.4 Exposure-response relationship and regulation

2.1.4.1 Exposure-response relationship

Understanding the exposure-response relationship may help to control the DPM effectively. Currently, there are mainly two ways to evaluate the exposure-response relationship (US.EPA, 2002). The first approach is to evaluate the relationship between the potential cancer risk to humans and certain levels of long-term DPM exposure (mg/m^3). Another way is by the cancer mode-of-action information.

The first approach could be achieved by evaluating the available human and animal data. Many animal studies showed that lung cancer response in rats had been observed under a high concentration of DPM exposure, but this concentration is not suitable for humans because of the difference in burden ability of lungs. Therefore, human data is more applicable than animal data. A number of occupational epidemiological studies mentioned above have provided substantial data to evaluate the exposure-response relationship. According to these studies, a positive relationship between the incidence of lung cancer and long-term DPM exposure has been demonstrated. Several epidemiological studies for underground miners have provided some available data for the evaluation of the exposure-response relationship. Neumeyer-Gromen et al. concluded that the smoking adjusted ratio of lung cancer mortality for miners (15-year duration of exposure) was 1.0 (baseline) when the cumulative DPM exposure levels were below 1.29 mg/m^3-year (measured as TC) (Neumeyer-Gromen et al., 2009). The mortality ratio (MR) increased with increasing levels of DPM exposure. When the DPM exposure levels were above 4.9 mg/m^3-year, the MR rose to 1.28 (95% CI: 0.61-2.71) and 1.50 (95% CI: 0.66-3.43) for the whole cohort and sub-cohort, respectively. Attfield et al. indicated that the RR (not adjusted for smoking habit) of lung cancer mortality for the underground miners (15-year lag) was 1.0 (baseline) when the cumulative DPM exposure levels were below 0.108 mg/m^3-year (measured as EC) (Attfield et al., 2012). The RR increased to 2.21 (95% CI:1.19-4.09) when the cumulative DPM concentration was above 0.946 mg/m^3-year (measured as EC). On the basis of Attfield et al.'s study, Silverman et al. adjusted the smoking habit in his study. This study showed that the smoking adjusted ratio of lung cancer mortality for underground miners was 1.0 (baseline) when the cumulative DPM concentration was below 0.003 mg/m^3-year (measured as EC) (Attfield et al., 2012). When the concentration was above 0.536 mg/m^3-year (measured as EC), the SMR increased to 2.83 (95% CI: 1.28-6.26). Overall,

although these epidemiological studies have provided some available data, they are inadequate to determine the exposure-response relationship. In another word, cancer unit risk cannot be identified by the available data. First, different measurements (TC and EC) of DPM could lead to different DPM levels. Compared with TC, EC is a more sensitive and specific surrogate of DPM. In addition, baseline exposure is not normal environmental exposure. Comparing the specific occupational exposure (underground mines) with the normal environmental exposure could provide more information to the evaluation of the response-exposure relationship. However, the data still provides some useful information. An increasing trend of lung cancer mortality risk with increasing concentrations of DPM exposure could be observed from the data.

Another way to evaluate the exposure-response relationship is based on cancer mode-of-action information. Many animal studies used a bio-marker to evaluate the effects of DPM exposure. Nikula et al. pointed out that alveolar epithelial hyperplasia could be considered as the beginning of lung tumours in rats exposed to DPM (Nikula et al., 1995). Iwai et al. selected 8-OH-dG production to detect the DNA damage in the lungs in the DPM exposure rats (Iwai et al., 2000). In addition, heart rate, PQ interval, neutrophil count, oxygen radical production, HO-1 level, arrhythmias, etc., have been used to assess the health effects of DPM exposure in rats (Berlo et al., 2010; Campen et al., 2003; Gordon et al., 2012; Hazari et al., 2011; Yokota et al., 2004). For humans, some symptoms, like nose and eyes irritation, headache, bad smell and bronchial inflammation, have been selected to evaluate the health effects of short-term DPM exposure on humans. Most of the animal and human studies only provided the mode of non-cancer action information. However, the cancer mode-of-action for long-term DPM exposure in humans has not been established. The current studies mainly focused on the association between the incidence of lung cancer and long-term DPM exposure. Fewer studies mentioned the mechanism of DPM that induces lung cancer. In some animal studies, the lung overload response in rats could be treated as a cancer mode-of-action. However, this is not applicable to humans. Further studies are needed to evaluate the cancer mode-of-action or carcinogenesis mechanism of DPM.

2.1.4.2 Regulation

To protect miners, many countries have assigned limits or passed regulations to control DPM levels for underground mines based on available studies.

Germany was the first to set the limit for DPM in underground mines. In 1990, Germany classified DPM as a carcinogen. The government then set the limit for DPM at 0.2 mg/m^3 for general surface workplaces and 0.6 mg/m^3 for non-coal underground

mines. With the development of the limit, Germany reduced the DPM limit for underground non-coal mines and other surface workplaces to 0.3 and 0.1 mg/m^3, respectively (AIOH, 2013).

In Canada, the exposure standard for DPM was set by each individual province. Most provinces set 1.5 mg/m^3 for DPM measured as RCD (respirable combustible dust) as the standard exposure for non-coal mines at first. This standard had remained constant for a long time. Then, the Canada Centre for Mineral and Energy Technology finally reduced the standard for DPM to 0.75 mg/m^3 for the underground mines (Cantrell & Watts Jr, 1997). Quebec then changed this standard to 0.6 mg/m^3 (measured as RCD), while other provinces still use 1.5 mg/m^3 of DPM as the exposure standard (Sean McGinn, 2009).

In the US, MSHA published a final rule for DPM exposure in January 2001, which recommends the interim limit for DPM concentration at 0.4 mg/m^3 (measured as TC) for metal/nonmetal mines (MSHA, 2001a). In 2005, MSHA changed the interim exposure limit to permissible exposure limit and regulated the new DPM exposure standard at 0.308 mg/m^3 (measured as EC) (MSHA, 2005b). In 2006, MSHA set the final DPM exposure standard at 0.16 mg/m^3 (measured as TC), and this limit has been implemented from 2008 (MSHA, 2006).

In Australia, the regulation and standard for the DPM exposure for underground mines are still at its developing stage (AIOH, 2013). The official limit for DPM exposure for underground mines is still not established, and the limit of DPM concentration varies for different states. In the past, the old NSW guideline recommended the limit of DPM exposure at 0.2 mg/m^3. Currently, many regulatory agencies in Australia have adopted 0.1 mg/m^3 of DPM concentration (measured as EC) as the standard limit for underground mines. In 2008, the NSW Department of Primary Industries published a new guideline for DPM management in underground mines, which adopted 0.1 mg/m^3 for DPM concentration for 8 h (one work shift) as a recommended exposure standard (MSOD, 2008). In 2012, the Queensland Mines Inspectorate adopted the same DPM exposure limit for its underground mines; in the same year, the Department of Mines and Petroleum in Western Australia (WA) published a guideline (draft) with a recommended exposure standard of 0.1 mg/m^3 as well (AIOH, 2013). Based on the available information, AIOH adopted 0.1 mg/m^3 DPM concentration for 8 working hours as a recommended DPM exposure standard for underground mines in Australia (AIOH, 2013).

2.1.5 Discussion

The available animal and epidemiological studies have shown that both short-term and long-term exposure to DPM could pose a risk to health. From the animal studies, it is suspected that long-term DPM exposure can increase the risk of lung tumour. The available animal studies showed that four animal species had been used: rats, hamsters, mice and monkeys. Rat is the most sensitive animal to DPM exposure among the four species. The lung tumour response in rats had been observed after long-term exposure to a high concentration of DPM (>2.5 mg/m^3). However, this exposure-response relationship cannot be used for humans directly. An impaired clearance function of lungs had been found among the rats. The overload of DPM in lungs resulted in the high risk of lung tumours in rats. The lung clearance and burden function of human beings is much greater than that of rats. In addition, the occupational environmental DPM concentration is usually lower than the animal experimental DPM concentration. For these reasons, an overload condition in a human's lungs is not expected to happen. Besides, one study showed that monkeys did not develop lung tumours after two years exposed to whole diesel exhaust (2 mg/m^3 of DPM) (Lewis et al., 1989). Therefore, the increased risk of lung tumours in rats is inadequate to evaluate the exposure-response relationship for humans. Further animal studies should be carried out to solve this problem. Two suggestions have been given for further studies:

(1) More species of animals should be considered in the study, especially for some animals which have similar lung clearance function as humans. Examples: apes, orangutans.

(2) Long-term exposure time is necessary. In Lewis et al.'s study, monkeys did not develop lung tumours. One possible reason for this result is the short exposure period (Lewis et al., 1989).

The epidemiological studies indicated that long-term exposure to DPM resulted in a higher risk of lung cancer. The epidemiological studies included miners, railroad workers, trucking industry workers and construction workers. The relative risk of lung cancer ranged from 1.13 to 5.10 under different DPM exposure conditions (duration, concentration, smoking history, etc.). Although a number of epidemiological studies have been carried out to determine the carcinogenicity of DPM, few studies are related to miners. However, compared to other occupations, the miners, particularly underground miners, have the potential to be in a higher concentration DPM environment due to the confined spaces. Four epidemiological studies for miners have been conducted. Three epidemiological studies for underground miners have demonstrated the positive relationship between high risk lung cancer mortality and long-term DPM exposure based

on the large samples (Attfield et al., 2012; Neumeyer-Gromen et al., 2009; Silverman et al., 2012). However, there were still several limitations in the studies preventing an accurate result. In Neumeyer-Gromen et al.'s study, TC was selected as the surrogate of DPM (Neumeyer-Gromen et al., 2009). Compared with EC, TC is more easily influenced by other interferences, like cigarette smoke, coal dust and oil mist (Janisko & Noll, 2008; James Noll, Janisko, & Mischler, 2013). The selection of surrogate for DPM will directly influence the accuracy of the study results. Another limitation is the sample size. Only 3,087 participants' exposure and smoking behaviour were validated in this study. If a large sample size was selected, more reliable conclusions will be drawn. Attfield et al. did not take smoking history into consideration. Smoking could be an interference factor for the relative risk of lung cancer, so it is necessary to control for the smoking effects on the results (Attfield et al., 2012). Besides, no historical exposure data are available for DPM concentration in both Attfield and Silverman et al.'s studies (Attfield et al., 2012; Silverman et al., 2012). All the past data was estimated based on the measurement of personal respirable EC (REC) levels between 1998 and 2001. For this reason, the historical exposure data might be overestimated or underestimated. Although limitations exist in these studies, they still provide strong evidence for the relationship between long-term DPM exposure and a high risk of lung cancer. Another epidemiological study conducted by Moher et al. drew a different conclusion with that concluded by other scholars. The sample size could be one possible reason for this different result (Möhner et al., 2013). Therefore, further study is still needed to arrive at a more reliable result. Three suggestions have been given for further studies:

(1) To get a more accurate and reliable result, EC should be chosen as the surrogate of DPM because TC is more easily influenced by other interferences, especially in some high dust concentration environments.

(2) Large sample size and long duration should be considered in the studies because these factors allow reliable conclusions.

(3) More potential confounders such as smoking and previous employment history should be controlled during the study in order to obtain reliable results.

From the short-term animal studies, it is concluded that short-term DPM exposure, injection or instillation DPM dosage can cause adverse effects on the brain, lungs and cardiovascular system. Most of these effects are reversible after a period of recovery. In addition, it is noticed that the rat is still the main experimental animal species. Only Campen et al. selected mice as the experimental animal. In order to get a more convincing result, different kinds of animal could be used in further study, especially

some kinds of primates (Campen et al., 2005). The human studies indicated that short-term DPM exposure is linked with some non-cancer adverse health effects, such as acute irritation, asthma, cough, light headedness. From three studies, it is noticed that the sensitive group, such as asthmatics and heart disease patients, is more likely to be affected by DPM (Mills et al., 2007; Nordenhall et al., 2000; Nordenhäll et al., 2001). Therefore, more attention should be paid to this group of people when working in a high DPM concentration environment.

The exposure-response relationship could be evaluated by DPM exposure data (a cancer unit risk potency for DPM) and the mechanisms or mode of cancer action information in studies. Understanding the exposure-response relationship may assist to better control DPM and protect miners from DPM health risks. However, the exposure-response relationship cannot be established based on the available animal and human studies. The animal studies did provide some exposure data, but this data was not suitable for humans due to the different lung clearance capacity and burden function of rats and humans. Epidemiological studies also provided limited information due to the uncertainties in these studies, such as different surrogates of DPM, confounding (smoking history) in the studies. Currently, it is noticed that the available animal and human studies provided limited mechanisms or mode of cancer action information. Not too many studies focused on the mechanism by which DPM induces lung cancer in humans. Overall, further studies are still needed before the mode-of-action and reliable exposure-response relationships are established.

Many countries have developed limits or regulations for DPM for mining industries to protect the underground miners. From the regulations, many markers (TC, EC and RCD) have been selected as a dosimeter for DPM and all these markers are measured in mass units (mg/m^3). However, TC and RCD are easily influenced by other interferences, like cigarette smoke, coal dust and oil mist (Janisko & Noll, 2008; James Noll et al., 2013). EC has been considered as an accurate and reliable dosimeter for DPM because it could be monitored even at a low concentration and there are no other known interferences for EC in underground mines. In addition, EPA's report indicated that respirable-sized particles could also be used as dosimeters for DPM (US.EPA, 2002). However, there are several uncertainties related to using respirable-sized particles as the dosimeter. First, compared with other dosimeters, historical data of respirable-sized particles is not available. Second, the accuracy and reliability are not mentioned in EPA's report. Due to these uncertainties, future studies are needed to determine the most accurate and reliable dosimeter for health effect purposes.

2.1.6 Conclusions

Based on the available health effects' data, this review has demonstrated that both short-term and long-term exposure to DPM is contributing to adverse health effects, especially in a high DPM concentration environment (underground mine). For this reason, many DPM regulations have been developed to guarantee underground miners' health.

A number of epidemiologic and animal studies have demonstrated that long-term exposure to high concentrations of DPM could increase the risk of lung cancer. Two recent epidemiologic studies provided strong evidence for the positive association between long-term DPM exposure and high risk lung cancer mortality among underground miners. Short-term or acute exposure to high concentrations of DPM (0.3 mg/m^3) can cause acute irritation, asthma, cough, light-headedness, etc., but no evidence demonstrated the relationship between short-term or acute exposure to high concentrations of DPM and lung cancer. However, the exposure-response relationship or a cancer unit risk potency for DPM could not be determined due to the limitation of animal study data and uncertainties in the available epidemiologic data. Many countries have developed their own DPM emission standard or limit to guarantee their underground miners' health. Germany set the DPM limit for underground non-coal and other surface workplaces at 0.3 and 0.1 mg/m^3, respectively. In Canada, most provinces set 1.5 mg/m^3 for DPM measured as RCD (respirable combustible dust) as the standard exposure for non-coal mines. America and Australia recommended the exposure standard for DPM at 0.16 mg/m^3 (measured as TC) and 0.1 mg/m^3 (measured as EC). These limits or standards are developed based on various dosimeters for DPM measurement. With the studies continuing, an accuracy and proper dosimeter will be selected to measure the DPM standards for the underground mining industries.

2.2 DPM Measurement

To control DPM concentration in underground mines effectively, it is important to select an optimum DPM measurement methods. In this section, various DPM measurement methods were reviewed and the advantages and disadvantages of each method were summarized in Table 1.

Table 1 Comparison of DPM measuring methods

Category	Methods	Country	Advantages	Disadvantages
Elemental Carbon-based Methods	NIOSH method 5040	USA	1. Benchmark DPM measurement method 2. Accurate and reliable	1. Real-time data is not available 2. Long-time process 3. Uneconomic for each sample
	Method ZH 1/120.44	Germany	Accurate and reliable	
Gravimetric Method	Respirable combustible dust (RCD) method	Canada	Easy procedures	1. Real-time data is not available 2. Cannot be used on coal mine
Real-time DPM Monitor	Airtec monitor	N/A	1. Real-time data display 2. Small, light, wearable 3. Durable (at least 12 hours)	Interfered by dust and smoking
	D-PDM Monitor	N/A		Interfered by respirable dust, smoking and oil mist
	Aethalometer	N/A	1. Real-time data display 2. Long-term measuring (up to several days)	1. A stationary monitor 2. Measurement can be influenced by movement and vibration 3. Personal sampling is not possible

2.2.1 Elemental Carbon-based Methods

An ideal method to monitor DPM in the underground mine is to find a signature for diesel emissions, which could be used to increase the accuracy of exposure measurement (HEI, 2002). As the main component of DPM is carbon, carbon measurement is an effective method. In the past, some researches considered total carbon (TC) as the surrogate to measure the DPM level because TC consists of the over 80% of DPM (D. B. Kittelson, 1998; MSHA, 2001b). Nevertheless, TC (TC=OC+EC) can be influenced by other interferences, such as cigarette smoke, coal dust and oil mist (Janisko & Noll, 2008; James Noll, Gilles, Wu, & Rubinstein, 2015; James Noll et al., 2013). Nowadays, it is increasing clear that EC is a better surrogate to measure DPM level than TC, because EC could be monitored even at a low concentration and there are no other known interferences for EC in underground mines (M. Birch & R. Cary, 1996; Birch, 2003; M. E. Birch & R. A. Cary, 1996; Birch, Dahmann, & Fricke, 1999; Birch & Noll, 2004; DMP, 2013; J. D. NOLL, 2007; James Noll et al., 2013; JD Noll et al., 2006). Several DPM measurement methods (method 5040, method ZH/120.44) are used EC as a surrogate to measure DPM level.

2.2.1.1 NIOSH method 5040

NIOSH method 5040 is a temperature-based thermo-optical method to measure the DPM level by determining the EC concentration (HEI, 2002). Before analyzing in the laboratory, a full-shift personal sample is collected in an underground environment. The sampling device consists of a cyclone, a submicron impactor, a filter cassette and a personal sampling pump (JD Noll et al., 2006). The submicron impactor is inserted between the cyclone and filter cassette, which can separate the DPM from other interferences (coal dust etc.). The pump is operated at an accurate flow rate of 1.7 lpm.

After the sampling process, the sample is sent to a laboratory for analysis of the EC and TC. The analytical method has two stages. In the first stage, the sample is placed in a sample oven, which is filled with pure helium (He). When the oven temperature steps up to about 870℃, it is noticed a visible darkening of the filter deposit. Under this temperature, OC is oxidized to CO_2; while the EC will not evolve due to the lack of oxygen. After that, the CO_2 converts to CH_4 in a methanator. The CH_4 is finally measured by a flame ionization detector (FID). In the second stage, an O_2-He mixture is introduced in the oven. The oven temperature reduces to about 600℃ first and then again increased to 900℃. Under this condition, EC reacts with O_2 and converts to CO_2 finally. Like the first stage, the CO_2 then converts to CH_4 and finally measured by the FID. In this approach, both OC and EC are measured. And the sum of OC and EC is TC. Due to its accurate and reliable, NIOSH method 5040 has been recommended as a standard DPM measurement method by many studies.

2.2.1.2 Method ZH 1/120.44

Method ZH 1/120.44 is an official method for determining OC and EC of DPM in Germany. This method, or variation of it, has been applied in many European countries since the 1990s (Birch et al., 1999). Both personal samples and area samples are used for method ZH 1/120.44. The personal sampling device consists of a cyclone preseparator, a filter and a personal sampling pump. The cyclone preseparator separates the respirable fraction from large particles. The filter diameter is 37mm and installed on a sampling pump. The flow rate of the pump is 2 lpm during the sampling. For area sample, an instrument with a horizontal elutriator is used. The filters' diameter of this instrument is 47 mm and the flow rate is 46.5 lpm. The analytical process of method ZH 1/120.44 is similar as of the NIOSH method 5040. First, the sample is heated under a temperature of 500℃ for 8 minutes. Not like the NIOSH method 5040, in method ZH 1/120.44, the gas in the oven is nitrogen (N_2) instead of helium (He). In this stage, OC is oxidized to CO_2,

and then the CO_2 is determined by the coulometric determination. After this, oxygen is introduced. The temperature first reduces to the room temperature; and then increases to 300℃ in 30 seconds and continually rises to 800℃ in 4 minutes. During this period, EC is oxidized to CO_2 and then measured by the coulometric determination (Dahmann & Bauer, 1997). Although the analytical principle between NIOSH 5040 and ZH 1/120.44 are similar, the results between the two methods are different because different thermal programs are used. However, the difference between the two methods is quite small (Birch et al., 1999).

2.2.2 Gravimetric Method

Except for the elemental carbon-based method, the gravimetric method has also been employed for DPM measuring. One approach which called respirable combustible dust (RCD) method has been widely applied in Canada for measurement of DPM concentration in the mining industry (M. Birch & R. Cary, 1996). Like the other two methods, samples collecting is the first step. The sampling device consists of a 10-mm nylon cyclone, a silver membrane filter and a sampling pump are used (Turcotte, Edwardson, & Laflamme, 1998). The cyclone removes the non-respirable dust from respirable dust. The pump flow rate is 1.7 lpm too. After the sampling, the sample is placed in a muffle furnace at a temperature of 500℃. Under this temperature, the carbon of the respirable combustible dust is oxidized to carbon dioxide by the catalyzing effect of the silver membrane filter. The filter mass is weighed before and after heated. The combustible dust in the respirable sample is measured as the difference in filter mass. Finally, the concentration of DPM is determined by calculating the mass difference, the flow rate and the total sampling time (M. Birch & R. Cary, 1996).

Although the laboratory-based methods are usually accurate and reliable methods for measuring the DPM concentration, these methods have some apparent disadvantages. First, these three methods only provide the average concentration of DPM over the sampling period. The most apparent drawback is that the whole process of these methods can last for several weeks before the results come out. When the results come out, the miners may work in a different environment. Besides, the method 5040 is not economic. It would cost more than 100$ to generate a single sample (James Noll et al., 2013). In addition, the RCD method can only be used in non-coal mines because the analytical result of this method is easily influenced by interferences, such as coal dust, sulphide components in the airborne dust etc. (Gillies & Wu, 2005; Robert A. Haney, 1997).

2.2.3 Real-time DPM Monitor

Although laboratory measurement methods for DPM are accurate and reliable, they are not capable of the real-time DPM measurement. Conversely, real-time measurements can provide workers with real-time information about DPM level. For this purpose, some real-time DPM monitors have been developed recent years.

2.2.3.1 Airtec monitor

In the US, NIOSH has developed a laser absorption technique to monitor DPM concentration in underground mines (James Noll & Janisko, 2007). A real-time DPM monitor called Airtec has been developed based on this technique. The Airtec monitor is produced by FLIR Inc. It is a small, light (about 0.7 kg) and wearable device. The monitor consists of a laser, a rechargeable lithium-ion battery, a filter cassette, a photodiode and a diaphragm pump. The battery enables the device to work at least 12 hour's shift even under a high concentration DPM environment. EC is a highly light absorbing material because of conduction electrons associated with the graphitic structure (Watson, Chow, & Chen, 2005). For this reason, the laser mainly detects EC rather than other less absorbing materials. The filter in the monitor can be replaced when it is fully loaded with black carbon. When the filter is overloaded, the monitor can give a filter saturation alert. The pump has the capability to work at a rate of 1.7 lpm (high flow) and 0.85 lpm (low flow). A particle size selector is usually installed on the device to remove the potential interferences from the DPM during the sampling. The Airtec is able to provide both the real-time and an eight-hour TWA EC level on an LCD display. It can also display TC level. After sampling, the data can be downloaded to a PC with a USB port (James Noll & Janisko, 2007; James Noll et al., 2013; Takiff & Aiken, 2010).

In order to test the performance and accuracy of the Airtec, Noll J et al. (James Noll et al., 2013) had conducted a serious of detailed laboratory analysis of the device. These analyses include calibration curve, NIOSH accuracy criteria, the limit of detection (LOD) and limit of quantification (LOQ), and interferences test. The results of analyses showed that the device has met the NIOSH accuracy criteria (an average bias less than 10 percent). In addition, the measurement of the device would not be interfered by humidity and oil mist. Without a submicron per-selector on the device, dust can interfere with the measurements. However, with a submicron per-selector on it, dust would not be a trouble. When collecting samples inside an enclosed cab, cigarette smoke can cause a measurement bias greater than 10 percent. While in open areas, the cigarette would not be an interference anymore. In addition, a recent study conducted by Gaillard et al. (Gaillard, McCullough, & Sarver, 2016) also demonstrated the accuracy of the Airtec monitor.

2.2.3.2 D-PDM monitor

Another real-time DPM monitor called D-PDM monitor, which is developed on the base of the Thermo Fisher Scientific Personal Dust Monitor (PDM) unit. The PDM is a portable and durable device which utilized a tapered element oscillating microbalance (TEMO) system to measure particles on a filter of the device. It was reported that the PDM has met the NIOSH accuracy criteria for mass concentration measurements (J Noll, Volkwein, Janisko, & Patts, 2013). Besides the PDM unit, the D-PDM consists of a 0.8μm cut point impactor, a BGI cyclone. When sampling, the device is operated at a flow rate of 1.7 lpm. Under this flow rate, the impactor can separate the DPM from coal or other dust and enable the instrument to measure the DPM concentration effectively.

Wu H and Gillies A (Wu & Gillies, 2008)had tested the D-PDM in 5 Australian mines. During the test, almost all the samples are collected at the longwall face where the dust concentrations below 500 $\mu g/m^3$. The results in this study showed that the D-PDM is success in measuring DPM changing trend in the underground mines. However, one study by NIOSH (A. D. Bugarski, Cauda, Janisko, Mischler, & Noll, 2011) showed that there are many interferences may influence the D-PDM accuracy, such as respirable dust, cigarette and oil mist. It was reported that the measurement of DPM had a bias of 20% to 40% when sampling under a high dust concentration environment (200 $\mu g/m^3$ DPM and 2000$\mu g/m^3$ dust). If the dust concentration is over 2000$\mu g/m^3$ in some mines, the bias might be larger.

2.2.3.3 Aethalometer

The Aethalometer is also a direct-reading device to measure DPM level. It is developed by Magee Scientific Co. Berkeley, California. This device is a stationary monitor designed for long-term black carbon (BC, a component of DPM) measurement in the atmosphere by optical absorption of carbonaceous particles. The Aethalometer consists of a filter, a transparent mask with a 5 mm diameter hole, two logarithmic amplifiers, a pair of high-intensity LED lamps, two photodiode detectors and a pump. Not like the previous two monitors, the pump of Aethalometer works at a flow rate of 1-6 lpm when sampling. The transparent mask covers on the filter can remove the interferential particulate matter so the measured particulate matter can deposit on the filter. Every 5 minutes during sampling, the absorption of an 880 nm light beam transmitted through the deposit is determined. The Aethalometer is able to display the five minutes' average BC concentration (Hansen, Rosen, & Novakov, 1984).

J. Borak and his colleagues (Borak, Sirianni, Cohen, Chemerynski, & Wheeler, 2003) have conducted a study to make a comparison between the NIOSH 5040 method

and the Aethalometer. This study showed that the Aethalometer should be calibrated before measuring. The Aethalometer should be strictly kept stationary during the measurement because the movement and vibration easily influence the accuracy of the results. In addition, personal sampling is not possible by this instrument.

2.2.4 Other DPM Sampling or Measurement Methods

There are many other instruments and methods for DPM sampling and measuring. These methods include a standard sampling method (SSM) by the MSHA (MSHA, 2005a); a high-volume sampling (HV) method (A. Bugarski, Schnakenberg, et al., 2004); a Tapered Element Oscillating Microbalance (TEOM) series 1400a ambient particulate monitor; an scanning mobility particle sizers (SMPS) which can measure the particulate numbers and size distribution (S. E. Mischler, Bugarski, & Noll, 2006). However, these methods or instruments also have some disadvantages. The SSM needs a long time for sampling at low DPM concentration. Both the SSM and the HV may take a long time before the measurement results can be obtained. Personal sampling is not possible for the HV, the TEOM and the SMPS (S. E. Mischler et al., 2006). In addition, these methods mainly based on the particles size selection to measure the DPM concentration. For this reason, some interferences, such as coal dust, cigarette smoke, oil mist etc., easily influence the accuracy of the measurement.

2.3 Review of Diesel Particulate Matter Control Methods in Underground Mines

2.3.1 Abstract

Diesel-powered equipment is widely used in the mining industry due to its superb performance, cost-effectiveness, efficiency as well as durability. However, there is a potential for miners in underground mines to be overexposed to high diesel particulate matter (DPM) concentrations with the increasing use of diesel engines. In 2012, the International Agency for Research on Cancer (IARC) classified DPM as a carcinogen to humans (group 1) based on sufficient evidence from animal and epidemiological studies. Regulations and control methods have been developed to minimize DPM health hazard in underground mines. This paper firstly reviewed the adverse health effects of DPM on humans based on related animal and epidemiological studies. Findings indicated that both short-term and long-term exposure to high concentrations of DPM have adverse impacts (acute irritation, asthma, cough, light-headedness, lung cancer, etc.) on humans, and a recommended limit of DPM concentration (0.1 mg/m3, measured as element carbon) should be established to help reduce miners' risk of lung cancer. The effects of

DPM control methods were also evaluated, which include source controls and exposure controls. Finally, an optimum DPM controlling strategy was obtained to lower DPM concentrations and provide a safe and healthy working environment for miners.

2.3.2 Introduction

The mining industry has been using the diesel-powered equipment extensively since the 1960s due to superb power performance, cost-effectiveness, efficiency as well as durability. Compared to gasoline engine, the diesel-powered engine emits less carbon dioxide and nitrogen oxide (Neeft, Makkee, & Moulijn, 1996), but emits much more particulate matters. The wide utilization of diesel engines in mining industries puts the underground miners under the threat of diesel particulate matter (DPM) exposure. Working in confined areas, underground miners can be over-exposed to DPM exhaust, which is much higher than for workers in other industries. It was reported that the DPM concentration in underground mines can be at least 100 times higher than that measured in other environments where the use of diesel engines is also common (Birch & Noll, 2004; JD Noll et al., 2006).

In the past three decades, numerous animal and human researches which relate to DPM have shown that both long- and short-term exposure to DPM can result in negative health effects. In 1998, the US National Institute for Occupational Health and Safety (NIOSH) pointed out that DPM was a potential carcinogen to humans (NIOHS, 1988). In 1989, the International Agency for Research on Cancer (IARC), classified DPM as a probable carcinogen to humans (group 2A) based on the evidence from abundant animal studies and limited epidemiologic studies (IARC, 1989). In 2012, based on further evidence in epidemiologic studies, the IARC reclassified DPM as a carcinogenic to humans (group 1). In addition, short-term DPM exposure also results in adverse health effects, such as acute eye irritation, asthma, cough, light-headedness etc. For these reasons, health issues as a result of DPM exposure have drawn much attention from both the public and governments.

To minimize the health hazards caused by DPM exposure, the DPM concentration needs to be maintained below an acceptable level. Many countries set the DPM concentration limit or standard for mining industries. In order to maintain the DPM levels under the recommendation standard, two main control approaches are commonly used, source controls and exposure controls. Source controls deal with the elimination of DPM before it is emitted outside the diesel engine, which includes engine design improvement, engine maintenance and the use of alternative fuel. Exposure control tries to contain DPM exhaust after it is ejected to the working environment. These are mainly

achieved through dilution using adequate ventilation, the use of aftertreatment (DPM filter) and protective equipment.

The aim of this article is to provide an overview of the performance of different DPM control methods in underground mines, and then recommend an efficient and economic DPM control strategy to the mining industry. The paper firstly illustrates the DPM characteristics and the potential health effects on humans by both long-term and short-term DPM exposure. Then, several DPM controlling methods are evaluated in this article. Finally, an optimum DPM controlling strategy is obtained to lower DPM concentrations and provide a safe and healthy working environment for miners based on the summary of the current DPM control technology.

2.3.3 Characteristics of DPM

2.3.3.1 Composition of DPM

DPM is produced by the incomplete combustion of fuel in the diesel engine. It is a complex mixture with thousands of components in it (ZHENG, 2011). The particulate components mainly consist of elemental carbon (EC), organic carbon (OC), adsorbed condensed hydrocarbons, and sulphate, although its composition is highly variable (Steven E Mischler & Colinet, 2009). EC is the main component of DPM, which can range from about 30% to 90% of DPM. Commonly, around 30% of DPM is composed of unburned oil and fuel. Other components include condensed inorganic oxides (sulphate), water and ash (contains trace metals) (HEI, 2002).

The range of size distribution of DPM varies. The diameter of DPM ranges from 5 nm to 10 μm. However, more than 90% of the number of particles are less than 1 μm (D. Kittelson, Watts, & Johnson, 2002). It was reported that the filtering capacity of the human nose would be very low when particles' sizes are less than 0.5 μm (Schwab & Zenkel, 1998; US.EPA, 2002). With the ultra-fine characteristics, DPM is able to penetrate the respiratory tract and deposit in the deepest ranges of lungs.

2.3.3.2 Health Effects

In recent years, a lot of animals and epidemiological studies have been conducted to analyse the adverse health effects of DPM exposure. Numbers of studies have demonstrated the positive association between long-term DPM exposure and the risk of lung cancer.

In 1986, NIOSH conducted a study which reviewed a number of studies of the DPM health effects on bacterial cultures, animals and humans to identify the possible hazard of DPM exposure (NIOSH, 1986). This report concluded that long-term exposure

to high concentration DPM resulted in cancer in animals, however, these effects were not confirmed on humans. In 1988, NIOSH published another report (NIOHS, 1988) which reanalyzed the data in the 1986's report and included several relatively new animal and human studies since the release of the 1986 report. The results from new animal studies (Heinrich et al., 1986; Mauderly et al., 1987) associated with the risk of cancer with the exposure to high concentration DPM. Three human studies (Edling, Anjou, Axelson, & Kling, 1987; Garshick et al., 1987, 1988) cited in this report indicated an increased lung cancer mortality from the railroad and bus station workers after long-term exposure in high DPM concentration environment. However, one study conducted by Edling et al. (Edling et al., 1987) is questionable due to the small size of samples. The limited epidemiological studies were still not enough to draw a solid relationship between high risk of cancer and long-term exposure although two studies. Thus, NIOSH considered DPM as a potential carcinogen to humans and the gaseous fraction of diesel exhaust may also cause cancer. In the same year, IARC reviewed a great number of animal and human data from the previous studies to evaluate the potential hazard of DPM. Based on the studies, a report (IARC, 1989) was released in 1989 which classified the DPM as aa probable carcinogen to humans (Group 2A). Compared to NIOSH's report, more epidemiological studies which related to various occupations were included. However, the positive relationship between lung cancer morality and long-term DPM exposure were not confirmed due to the limited data. This conclusion did not change until 2012. In this year, IRAC changed the DPM's classification from Group 2A to Group 1. They reclassified the DPM as carcinogenic to humans with the solid evidence of the association between lung cancer and DPM exposure from the epidemiological studies after the last report. In the latest report (IARC, 2013) which released on 2013, sufficient animal and human studies had been evaluated to draw the conclusion. Except to the animal studies, it is worth noting that various human studies were reviewed in this report which included cohort studies with a wide range of diesel engine related occupations, case-control studies and meta-analyses according to different kinds of cancers. Although some limitations, such as not continuous historical data, not detailed work histories, and lack of smoking information, were existed in some studies, the data was enough to demonstrate the association between lung cancer and long-term DPM exposure.

In addition, short-term or acute exposure to DPM exhaust is linked to some respiratory diseases and other adverse effects on human, such as asthma, cough, chest tightness and light-headedness (Mills et al., 2007; Nordenhäll et al., 2001; B. Rudell et al., 1996; Salvi et al., 2000). This is especially the case for asthma patients and sensitive

groups, who are more easily affected by DPM exposure. It is worth noting that most of these effects are non-cancer effects and recoverable.

From the studies above, it is a hazard for both long- and short-term DPM exposures. This is particularly the case for long-term DPM exposure, which has potential carcinogenic effects on humans. Due to the adverse effects of DPM exposure, the workers who work in diesel related environment should be given extra attention and protective.

2.3.3.3 Standard Limit for DPM

To minimize the DPM hazard on miners, many countries and organizations have given the limit of DPM levels for mining industries, as shown in Table 2. In Germany, the DPM limit for underground non-coal mines and other surface workplaces are 0.3 mg/m^3 and 0.1 mg/m^3, respectively (AIOH, 2013). In Canada, 1.5 mg/m^3 (DPM measured as Respirable Combustible Dust) has been used by many provinces as the limit for the mining industry. The Canada Centre for Mineral and Energy Technology (CANMET) then lowered the limit to half (0.75 mg/m^3) (Cantrell & Watts Jr, 1997). The US Mine Safety and Health Administration (MSHA) recommended 0.16 mg/m^3 (DPM measured as TC) as the limit for the underground metal/nonmetal mines, which was effective on 20th May 2008 (MSHA, 2006). In Australia, the Australian Institute of Occupational Hygienists (AIOH) has recommended an 8-hour-time-weighted average (TWA) exposure limit of 0.1 mg/m^3 (measured as elemental carbon, EC) (DMP, 2013).

Table 2 DPM standard in different countries

Country (Agency)	Working Areas	Surrogate	Limit (mg/m^3)
Australia (AIOH)	Underground Mine	EC	0.1
USA (MSHA)	Underground Mine	TC	0.16
Canada	Underground Mine	RCD	0.4-1.5
Germany	Underground Mine	TDPM	0.3
	Surface Workplaces		0.1

2.3.4 DPM Controls

Currently, two main approaches have been used to control DPM emissions for the mining industries. One is called source controls, which control the DPM before it is emitted from the diesel engine. The other one is called exposure controls, which control the DPM after it is emitted to the working area. The comparison of different controls are summarized in Table 3.

Table 3 Comparison of different controls

Category	Methods	Features	Disadvantages
Source controls	Engine maintenance	1. First step to reduce DPM emissions 2. Low cost and easy implementation	N/A
	Engine design improvement	Reduce 90% of the DPM emissions	1. Need to change the current engine's structure even the whole powertrain system. 2. Costly and cannot achieve in a short time
	Alternative fuel	Reduce 15% to 66% of DPM	Increase of NO_x emission
	Aftertreatment devices (filters)	Reduce 20% to 50% diesel particles.	1. Performance depends on engine types 2. Require a certain range of temperature for the chemical reactions 3. Consumable
Exposure controls	Ventilation	1. Main and widely used method in underground mines 2. Effective way to dilute DPM in confined area	1. Impractical air quantity may be required when many diesel equipment works at the same time. 2. Difficult to separate the fresh air from the contaminated air.
Other controls	PPE	Protect miners from diesel exhaust	Cannot reduce the DPM concentration in working areas.
	Enclosed Cabin	Capture more than 90% of DPM	

2.3.4.1 Source Controls

The source controls mainly include engine maintenance, engine design improvement and the using biodiesel.

2.3.4.1.1 Engine maintenance and design improvement

Reducing the source of DPM should be the first consideration when controlling the DPM level. Diesel exhaust emission is the main source of DPM and diesel engine design is a vital factor affecting the diesel emission rate. Improving the diesel design contributes to the reduction of DPM emissions, which includes improving the combustion chamber design, improving the pump injection systems, increasing the number of intake valves and higher fuel injection pressures (Robert A. Haney, 1997; Turner, 2007). It was reported that the improvements to engine design can reduce as much as 90% of the DPM emissions (Robert A. Haney, 1997). However, this method may need to change the

current engine's structure, even the whole powertrain system, which is costly and time-consuming and it is impossible to make a technological breakthrough in a short time.

Regular engine maintenance is another method to keep the DPM emission at a low level. A poor condition diesel engine can generate much more DPM than a good one. McGinn (S McGinn, 2000) has studied the links between regular diesel engine maintenance and DPM emissions. The results showed that good maintenance of the diesel engine could significantly minimize the DPM emission from the diesel engine. Moreover, he developed a procedure and guidelines for engine maintenance. Another report by NIOSH (A. D. Bugarski et al., 2011) also indicated the importance of diesel engine maintenance for the DPM emission controls. Several diesel engine servicing procedures have been recommended for the mining industries, which include preventing dust from entering the engine, maintaining the efficiency of charge compression systems, cooling systems, external exhaust gas recirculation systems, fuel delivery and injection systems, and filtration systems. Due to its low cost and easy implementation, regular diesel engine maintenance can be the first step for DPM emissions control.

2.3.4.1.2 Fuel

Fuel is another main influencing factor in DPM generation. An appropriate fuel plays a vital factor in the performance of the diesel engine. The sulphur content of the fuel has a significant impact on the DPM emissions. Low sulphur diesel fuel usually generates fewer DPM emissions. It was reported that the use of low-sulphur fuel and lubricant reduced the engine particulate emissions by 30% (Robert A. Haney, 1997). The use of alcohol-diesel also contributes to the reduction of DPM emissions (Neeft et al., 1996).

Biodiesel is another proper choice to replace petroleum diesel. Generally, the use of biodiesel results in an apparent reduction in the DPM emission (Behçet, Oktay, Çakmak, & Aydin, 2015; A. D. Bugarski, Cauda, Janisko, Hummer, & Patts, 2010; A. D. Bugarski et al., 2011; A. D. Bugarski et al., 2007; Howell & Weber, 1997; Steven E Mischler & Colinet, 2009). Compared with petroleum diesel, biodiesel contains fewer aromatics and sulphur but has higher oxygen content. Howell et al. (Howell & Weber, 1997) conducted a study to compare the performance between biodiesel and normal diesel. The results showed that the use of biodiesel results in a 50% DPM reduction in the lab test and 55% time-weighted DPM reduction in the field test. NIOSH has conducted a series test to evaluate the effects of several different kinds of biodiesel on the DPM emission by underground diesel mining equipment (A. D. Bugarski et al., 2007). The results showed a 30 to 66% reduction in the total particulate matter when

using biodiesel. Bugarski et al. conducted a study to evaluate the effects of biodiesel on DPM size and mass concentration in an underground mine. The results suggested that the total and peak concentration of DPM decreases with an increase in the fraction of biodiesel blend. In Bugarski's other study (A. D. Bugarski et al., 2011), he reported a 47% DPM reduction by using FAME biodiesel compared with normal diesel. Behcet et al. (Behçet et al., 2015) studied the performance of two biodiesel-diesel fuel blends which were produced from animal fats. The results showed a 15.95% and 10.02% particulate matter reduction for the FOB20 and CFB20 biodiesel, respectively. Lutz et al. (Lutz, Reed, Lee, & Burgess, 2015) compared three different fuels: low-sulphur diesel, biodiesel/diesel blend (B75) and natural gas/diesel blend (GD) in a simulated pilot study. The result showed that both B75 and GD resulted in a DPM reduction. The use of GD fuel resulted in reduction of exposure for each set of analyzed data in this study. A.M. Ashraful et al. (Ashraful, Masjuki, & Kalam, 2015) investigated the impact of different percentages of biodiesel on the DPM emissions under different engine loads. The results showed a significant reduction in EC, OC and TC emission when using PB10 and PB20 biodiesel compared with diesel fuel. The EC reduction for PB10 and PB20 varied from 0.75% to 18% and 11.36% to 23.46% for different engine speeds, respectively. Lutz (Lutz, Reed, Lee, & Burgess, 2017) compared personal DPM exposure by using diesel fuel and 75% biodiesel blend (B75); a 22% reduction in respirable DPM was observed by using B75. However, some researchers demonstrated an increase of NO_x emission when using biodiesel (A. D. Bugarski et al., 2010; A. D. Bugarski et al., 2011; A. D. Bugarski et al., 2007; Y.-Y. Liu, Lin, Wang, & Ho, 2009).

2.3.5 Exposure Controls

The exposure controls mainly include ventilation and the use of aftertreatment devices. Other approaches, such as environmental cabs and personal protective equipment (PPE), are also used to protect the miners from the DPM exposure.

2.3.5.1.1 Aftertreatment Devices

Aftertreatment devices have the capability to remove pollutant from the exhaust gases before they are emitted to the environment. Aftertreatment devices mainly include diesel oxidation catalytic converters (DOCC), diesel oxidation catalysts (DOC), reusable ceramic filters (RCF), diesel particulate filters (DPF), disposable diesel exhaust filters (DDEF), and ceramic particulate filters (CPF) (Steven E Mischler & Colinet, 2009; Robert A. Haney, 1997; ZHENG, 2011).

A number of researchers illustrated that the filters can reduce diesel particulate emissions effectively. Haney et al. (Robert A. Haney, 1997) reported that DOCC can

reduce DPM emissions by 50%; particulate control systems have a range of 60% to 90% removal efficiencies by using DPF. Bugarski (A. Bugarski, Schnakenberg, et al., 2004) conducted a compared test between DPF and DOC. The results showed that both DPF and DOC result in a reduction of EC in the diesel exhaust. NIOSH studied the effectiveness of DPF, DFE and DOC on the DPM reduction (Steven E Mischler & Colinet, 2009). The results showed that the efficiencies of different DPF ranged from 81% to 87% in the DPM mass reduction; the DFE's efficiency is more than 80%. However, these filters could only reduce about 40% of the mass concentration when the engine was operated under the highest workload. The United States Environmental Protection Agency (U.S. EPA) and the California Air Resources Board (CARB) have tested several DOC products. The results showed that the reduction in CO and HC were 40% and 50%, respectively; the reduction in total DPM emissions varied from 20% to 35% (A. D. Bugarski et al., 2011).

Although aftertreatment devices are increasingly used for controlling the DPM levels for underground mines, they still have many disadvantages. The performance of a number of devices is critically dependent on the engine type because chemical reactions in filters rely on a certain range of temperature (A. D. Bugarski et al., 2011). Some DPFs, such as disposable paper filters, should be changed frequently. The disposable paper filters should be discarded after being used for 2 or 3 shifts (Robert A. Haney, 1997). In addition, one field test which was conducted by Bugarski et al. (A. Bugarski, Mischler, et al., 2004) showed that the DPM concentration was still over the limit even after using filters in the confined zone.

2.3.5.1.2 Ventilation

The main and widely used method for DPM control in underground mines is ventilation. Ventilation is important in a confined area (underground mine) because it carries fresh air to the working area and dilutes the DPM concentration. It was reported that the DPM concentration decreases with increasing air flow quantities (Robert A. Haney, 1997). A good mine ventilation system should be designed to meet the minimum legislative requirement in the areas where the diesel-powered devices are being used.

To control the DPM effectively, it is important to know the required quantity of airflow to dilute the DPM concentration. In the US, MASH has developed a "particulate index (PI)" to calculate the required quantity of air to reduce the DPM emission of a diesel engine to 1 mg/m^3 (MSHA, 2014). It is calculated that the amount of ventilation air quantity is 10 (1/0.1) times the PI number to dilute the DPM level to the standard of 0.1 mg/m^3. In Australia, the minimum ventilation requirements for the underground

mine is based on the power of a diesel engine, which is 0.06 m^3/s per kW; the ventilation requirements in China, Chile and South Africa are similar to that of Australia, with 0.067 per kW, 0.063 per kW and 0.063 per kW, respectively; in Canada, the ventilation requirement varies from 0.045 – 0.092 m^3/s per kW by province (Gangal, 2012). It is easy to maintain the DPM level under the standard when a single diesel device is working underground. However, it becomes difficult when many diesel devices are working together, because the minimum air flow quantity is the sum of the required air quantity for each diesel device (Robert A. Haney, 1997). This may require impractical amounts of air to maintain the DPM level below the limit. In addition, sufficient quantities of fresh air must be used to dilute the DPM exhaust. In fact, the air gets contaminated as it flows in the tunnel, and cannot dilute the DPM effectively at the workface. Because of the opening sizes in underground tunnels, it is difficult to separate the fresh air from the exhaust air (Turner, 2007). For these reasons, how to use the ventilation efficiently to reduce the DPM concentration needs to be studied further.

2.3.5.1.3 Other Exposure Controls

Environmental cabs and PPE (respirator filter media or mask) are effective methods to prevent miners from DPM exposure. Environmental cabs, also called enclosed cabins, are usually used by miners to avoid harmful noise. When installed with filtration systems in the cabin, it could also prevent the miners from DPM exposure (A. D. Bugarski et al., 2011; Turner, 2007). Noll et al. (James Noll, Cecala, & Organiscak, 2011) reported that the efficiency of a properly functioning enclosed cabin can be more than 90% at capturing DPM. For some high DPM exposure occupation, like diesel engine operators, wearing a proper respirator filter mask can largely reduce the DPM inhaled. Burton et al. (Burton, Whitelaw, Jones, & Davies, 2016) reported that a proper mask was over 94% efficient in DPM filtering. Those two methods can only prevent miners from DPM exposure and cannot reduce the DPM level in the working area.

2.3.6 Summary

In reviewing the literature, it was found that DPM emission has been a threat to underground miners. Numerous epidemiological and animal studies associated the long-term DPM exposure with a high risk of lung cancer. As mining industries increase the utilization of diesel equipment, many countries and agencies have set standard limits of DPM for underground mining industries. Based on the available information, an 8-hour TWA DPM exposure standard of 0.1 mg/m^3 (measured as submicron EC) is recommended for underground mining industries.

Both the source controls and exposure controls have been discussed in this paper. At present, ventilation is still the primary way to control DPM emission, but how to use the ventilation efficiently to reduce the DPM concentration needs to be studied further. Other approaches are also used for the DPM control. The current paper found that only a single control strategy is not enough to control the DPM effectively. For most cases, the combination of controls seems to be the best way to control the DPM level. Is it possible to find a way (other than ventilation) to reduce the DPM after emission. For example, by using water mist with an added surfactant to suppress the DPM. This will be studied in future research.

2.4 CFD Application for Mining

CFD is short for the computational fluid dynamics, which is a technique to analyse the physical phenomenon that involves fluid flows and thermal conduction by using numerical computation or analysis. The standard procedure of a CFD simulation study includes three steps: pre-processing, model solving and post-processing (Xu, Luxbacher, Ragab, Xu, & Ding, 2016). The pre-processing mainly includes simulation parameter set and domain construct (geometry, meshing, etc.). After that, a mesh independence study must be conducted before solving the model. The accuracy of a simulation result significantly depends on the quality and size of a mesh. Generally, a dense mesh gives a more accurate result than a coarse mesh. However, the computation cost increases with the size of mesh increasing. Thus, mesh independence should be achieved first. Once the mesh independence study finish, it comes to the second step, which is also the most important step, model solving. In this step, the model is usually governed and calculated by a solver, which is available in the CFD simulation software. An open source software OpenFOAM was mainly used in this study. After the model solving, the simulation results should be exported or visualized by a CFD post-processing software. This step calls post-processing. The standard CFD simulation procedure is illustrated in Figure 2.

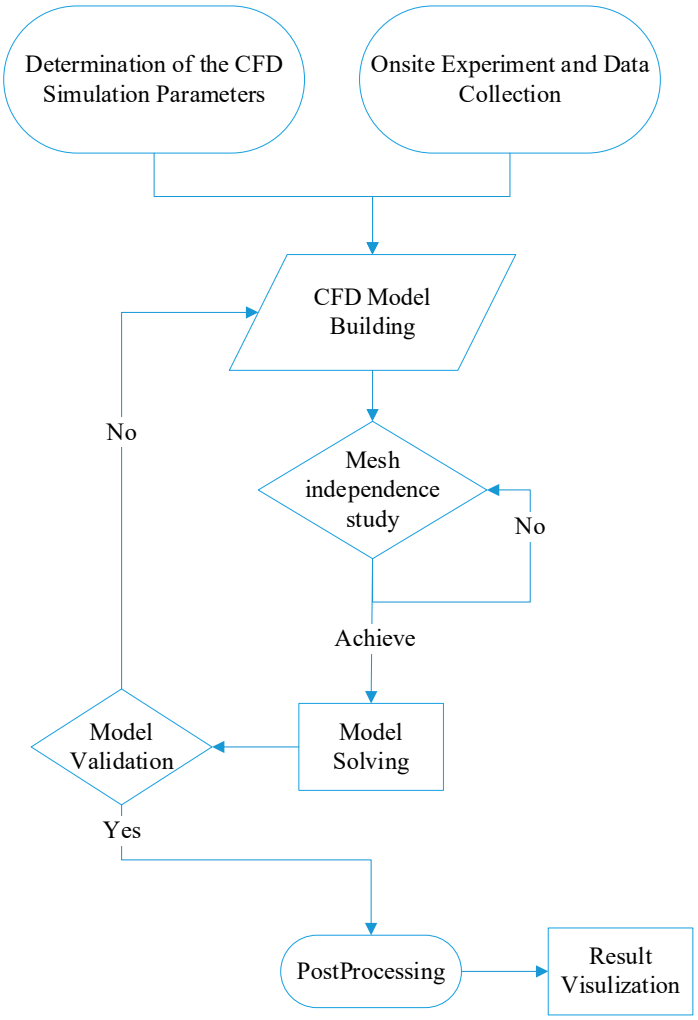

Figure 2 Standard procedure of CFD simulation

With the development of computing technology and large improvement of the computer hardware performance since the 21st century. The CFD modelling has been applied in a wide range of both research and industries to solve the fluid related problems due to its high efficiency, low labour consuming and high accuracy. In the mining industry, the CFD method has also been largely applied to study the health and safety related issues in the following fields:

2.4.1 Mine ventilation and airflow analysis

As an effective mean to analysis the airflow characteristics, CFD is commonly used to evaluate the ventilation performance, investigate airflow behaviours and optimize ventilation design in the mining industry.

Parra et al. (Parra, Villafruela, Castro, & Mendez, 2006) compared three ventilation systems, exhaust, blowing, and mixed, in a coal mine, by using the CFD modelling, the data was validated with the onsite experiment. The results showed a good agreement between the simulation results and experimental data.

Hargreaves et al (Hargreaves & Lowndes, 2007) applied the CFD method to analysis the ventilation airflow behaviours in a deep coal mines in UK under different mining stages and the data was further validated with the ventilation experiments. The results demonstrated that CFD modelling could be a reliable mean to identify the ventilation characteristics.

Aminossadati et al (Aminossadati & Hooman, 2008) examined the airflow patterns in underground mine cross-cut regions with the impact of brattice sails. The effects of the brattice sails' size and length on the airflow pattern were presented in the results.

Diego and co-authors (Diego, Torno, Toraño, Menéndez, & Gent, 2011) evaluated an underground ventilation system by both CFD method and a traditional method. The CFD results were compared with the data obtained by the traditional method. The results provided guidance on the practical use of CFD modelling for the underground ventilation analysis.

Ranjan et al. (Ranjan & Karan Kumar, 2013) applied the CFD modelling on the design of mine ventilation system for the underground bord and pillar mining system. The airflow patterns in this system were presented. The results helped to improve the designing and operation of the underground ventilation system.

Sasmito et al. (Sasmito, Birgersson, Ly, & Mujumdar, 2013) evaluated the ventilation performance on the methane removal in a "room-and pillar" structured underground coal mine. Four turbulence models were compared and validated with the experimental data. And the Spallart-Almaras model was selected to study the airflow characteristics under different ventilation. Then, the paper further compared the advantages and disadvantages of the different ventilation designs.

Kurnia (Jundika C Kurnia, Agus P Sasmito, & Arun S Mujumdar, 2014b) investigated a novel intermittent ventilation system in underground mines. By numerical simulation, both the energy cost and methane control efficiency of this ventilation system were evaluated. Results showed a significant energy saving when using this system.

Cheng et al. (D. F. Cheng, Urata, Yagihashi, & Hozumi, 2012) studied the effect of ventilation parameters on the gas and fire control by using the CFD simulation based on an underground coal mine in China. A list of various ventilation parameters was presented in the study. The optimum ventilation parameter was recommended for both methane maintenance and fire prevention purposes.

Guang et al. (Xu, Jong, Luxbacher, Ragab, & Karmis, 2015; Xu, Luxbacher, Ragab, & Schafrik, 2013) conducted a series simulation studies to remote analysis the

ventilation systems after incidents in the underground mines. He combined the gas tracer method and CFD models together to analysis the ventilation systems under different scenarios. The results can help the mining industry to quick identify the status of the ventilation system remotely when incidents happened in the underground mines.

A simulation study conducted by Wang et al. investigated the effect of air volume on the air curtain's coal dust efficiency in an underground working face. The optimum air volume parameters for the air curtain was suggested based on the simulation results (H. Wang, Nie, Cheng, Liu, & Jin, 2018).

Liu et al (X. Liu, Chang, Wang, Zhang, & Yang, 2018) investigated the dust removal performance of a vortex ventilation system in an underground development face. Both the traditional long blowing and short suction ventilation system and the new ventilation system were compared by CFD simulation. The results showed that the vortex ventilation system resulted in a significant reduction on the respirable coal dust.

2.4.2 Mine fire and spontaneous combustion

CFD has also been used to predict the fire and spontaneous combustion, and combustion control in the mines.

Edwards and Hwang (Edwards & Hwang, 2006) simulated the fire spread in an underground mine entry. The flame spread rate was studied in different places and a good agreement was observed between the simulation results and onsite measurements.

Yuan and co-authors conducted a series numerical studies to evaluate the effects of various parameters on the spontaneous combustion in underground coal mines (L Yuan & Smith, 2007, 2010; Liming Yuan & Smith, 2008).

The effects of gas emission from longwall gob areas, coals' activation energy and reaction surface areas on the spontaneous heating were investigated in one of his study (L Yuan & Smith, 2007). Based on the previous study, another study was presented to investigate the effect of coal properties on spontaneous combustion by Yuan and Smith (Liming Yuan & Smith, 2008). The results of this study were compared with the available test data, however more onsite data was still needed to improve the CFD model. Another study conducted by Yuan and Smith presented CFD models to simulate the coal spontaneous heating in longwall panels. In this study, the effect of pressure change on spontaneous combustion was evaluated. The results showed that the change of pressure led to a change in the oxygen concentration and finally affected the coal spontaneous heating (L Yuan & Smith, 2010).

A similar numerical study was presented by Zhu and Liu to examine the effect of methane drainage pattern on coal spontaneous combustion (Hongqing & Xingkui, 2012).

In this study, the CFD simulation was built to help understand the association between the tail roadway methane drainage and spontaneous combustion region in a gob area. The results indicated the adverse impact of methane drainage on the spontaneous combustion and the suggestion on combustion prevention was provided.

Li (Li, 2008) evaluated the coal spontaneous combustion phenomenon in a gob area with leaking air influence. He found that the coal spontaneous combustion was significantly determined by the air leakage position and the simulation results provided useful information for the combustion analyse and prevention.

Taraba (Taraba & Michalec, 2011) used the laboratory experimental data to construct CFD models to study the relationship between longwall face advance rate and spontaneous combustion in a goaf. A “favourable” zone was identified in this study which contributed to the development of spontaneous.

Zhang et al (J. Zhang, Zhang, Ren, Wei, & Liang, 2019) developed a CFD model to study the spontaneous heating in a longwall goaf. In this study, a proactive inertisation plan was made to prevent spontaneous combustion based on the simulation results. Nitrogen was used in this study to suppress the process of the coal spontaneous combustion and the best location for the release of nitrogen was identified.

2.4.3 Methane control

Methane is one of the main issues for the coal mine. In order to solve the methane issues and give the coal miners a safe working environment, many researchers applied CFD simulation to study the methane behaviours and methane control strategy for underground coal mines.

Toraño et al. (Javier Toraño, Torno, Menendez, Gent, & Velasco, 2009) studied the methane flow patterns in a heading face of an underground coal mine. In this study, two auxiliary ventilation systems, forcing system and exhausting system, were evaluated and the forcing system was used according to effective methane control. The methane behaviour under this ventilation system was then investigated by CFD mean. The potential hazardous zones were identified based on the simulation results.

Guo et al. (Guo, Yuan, Shen, Qu, & Xue, 2012) conducted a study on the strata behaviours and methane flow characteristics by using numerical modelling. This study provided comprehensive information about the effect of coal seam and geological parameters on the coal mine methane desorption and migration, which could be used for the coal methane extraction design.

Kurnia et al. (Jundika C Kurnia, Agus P Sasmito, & Arun S Mujumdar, 2014a) addressed the methane distributions in a mine tunnel by CFD modelling and validated

the results with the experimental data from another published paper. The effect of ventilation on the methane dispersion was studied in this research and a methane management strategy was suggested based on the results. A similar study was conducted by Tanguturi and Balusu to investigate the methane dispersion and control strategies in an underground coal mine (Tanguturi & Balusu, 2014). Both the methane and oxygen concentrations at a tailgate were analysed and the efficiency of gas control strategies such as gas drainage, back returning system and wind curtains application were also evaluated.

Zhou et al (L. Zhou, Pritchard, & Zheng, 2015) analysed the methane dispersion in a mining face under different curtain setback distances with both the onsite experiments and numerical modelling. A good agreement was found between the simulation and experimental data. The results suggested that the size of the high methane concentration zones extended with the increase of setback distance.

Fang et al (Fang, Fan, Kenneally, & Mooney, 2016) predicted the airflow and methane behaviours under a recirculation ventilation system in a long twin tunnel by CFD simulation. The methane accumulation zone was first identified under this ventilation system. Then jet fans combined with the recirculation ventilation system were applied to successful eliminate this zone.

Mishra et al (Mishra, Kumar, & Panigrahi, 2016) studied the methane distribution in a tailgate of a longwall mine under various air velocities. The study indicated that ventilation played an important role on the methane distributions and a minimum air velocity of 3 m/s was confirmed to maintain the methane under a safe level. Another simulation study presented by Mishra and his colleagues evaluated the effects of mining parameters on the methane distributions (Mishra, Panigrahi, & Kumar, 2018). A similar results was obtained as the pervious, 3 m/s of air velocity was adequate to control the methane under a safe level. The results also revealed that the increasing of surface roughness and inclination of mine seam leaded to lower DPM concentration distributions in the tailgate.

Hasheminasab (Hasheminasab, Bagherpour, & Aminossadati, 2019) evaluated the methane distributions with the impact of various ventilation system. The impact of intake air velocities, brattice size, brattice positions, ventilation duct size and duct positions on the methane distributions was investigated and the optimum auxiliary design on the methane control was suggested.

2.4.4 Coal dust

Another main safety issues for the coal mine is the coal dust during the mining activities. Especially for the excavation face, where is the main source of the coal dust. Understanding the coal dust dispersion behaviours contributes to the making of dust control strategy and optimization of ventilation design. A number of numerical studies have been conducted to achieve this goal.

Toraño et al. (J Toraño, Torno, Menéndez, & Gent, 2011) examined the coal dust behaviours under two auxiliary ventilation systems in an underground roadway by numerical modelling. Onsite measurement data was provided for validation purpose. The study indicated that the CFD modelling was an effective and economical method to modify the ventilation system and thus to improve the working environment and it was capable of predicting the coal dust distributions accurately.

Ren and co-authors conducted a series numerical studies to investigate the coal dust behaviours in different scenarios (Ren, Wang, & Cooper, 2014; Ren, Wang, & Zhang, 2018; Z. Wang & Ren, 2013). They studied both the airflow and coal dust behaviours above an underground bin (Ren et al., 2014; Z. Wang & Ren, 2013). A Lagrangian method was used in these studies to trach the coal dust particles. Based on the simulation results, an innovative dust suppression system was developed and a good coal dust removal efficiency was achieved (Ren et al., 2014). Another numerical study was conducted to study the dust movement patterns in an underground coal caving face (Ren et al., 2018). The effect of different ventilation systems on the dust behaviours was evaluated. The optimum ventilation design was recommended based on the simulation results.

Hu and his colleagues investigated the coal dust distributions in a roadway after blasting. The Eulerian-Lagrangian method was used to simulate the gas-solid two-phase fluids (Hu et al., 2016b; Hu, Wang, & Feng, 2015). The results presented in these studies could be used to better understand the dust movement patterns and help to make the dust control strategy. In another study conducted by Hu et al. (Hu et al., 2019), he analysed the coal dust behaviours in an excavation face by using CFD-discrete phase model. A good agreement was obtained between the simulation results and field measurements. The high coal dust concentration areas were identified in the study.

Similar studies were also presented in other literatures (Yu, Cheng, Wu, Wang, & Xie, 2017; G. Zhou, Zhang, Bai, Fan, & Wang, 2017). These studies provided valuable information for the dust distribution characterises in the excavation face and the results could be used to improve the miners working environment in this area.

Kurnia et al (Jundika Candra Kurnia, Agus Pulung Sasmito, & Arun Sadashiv Mujumdar, 2014) investigated the dust dispersion characteristics in a development face under different scenarios. Six different auxiliary ventilation system was introduced and the coal dust concentrations under different systems were presented. By comparison of the coal dust reduction performance of each ventilation system, the application of brattice in the development face provided the best dust control result.

Geng and co-authors (Geng et al., 2017; Y. Wang, Luo, Geng, Li, & Li, 2015) also studied the coal dust dispersion patterns under a hybrid ventilation system in an underground coal mine. The coal dust accumulation areas were identified and the coal dust reduction performance of the current ventilation system was provided.

Zhang et al. (Q. Zhang et al., 2018) analysed the coal dust dispersion in a longwall face by the discrete phase model. Overcame the current study limit, the behaviours of coal dust from multiple sources in the longwall were analysed by both the macroscopic and mesoscopic scales.

2.4.5 CFD application on DPM control

The CFD application on the DPM research is quite recent for the mining industry, the summary of current DPM studies by using CFD method is given in Table 4.

Zheng and co-authors conducted a series of CFD studies to investigate the DPM behaviours in underground mines (Y. Zheng, H. Lan, M. Thiruvengadam, & J. Tien, 2011a; Zheng, Thiruvengadam, Lan, & Tien C, 2015; Y. Zheng, M. Thiruvengadam, H. Lan, & C. J. Tien, 2015a; Y. Zheng, M. Thiruvengadam, H. Lan, & J. C. Tien, 2015b; Zheng & Tien, 2008, 2009). He studied the DPM distribution in a single heading in an underground mine and compared the DPM behaviours under two different auxiliary ventilation systems in this heading (Zheng & Tien, 2008). In another study, he built a CFD model based on an onsite experiment and studied the DPM distributions in an isolated zone (Zheng & Tien, 2009). In one of his study, both the onsite experiments and CFD modelling were conducted to evaluate the DPM dispersion (Zheng et al., 2011a). This study demonstrated that CFD simulation was able to predict the DPM concentration distribution. He also studied the DPM distributions with the effect of buoyancy force in a long roadway (Zheng, Thiruvengadam, Lan, & Tien C, 2015) and the effects of different auxiliary ventilation systems on the DPM dispersion in a dead-end entry (Zheng, Thiruvengadam, et al., 2015a; Zheng, Thiruvengadam, et al., 2015b).

It worth noting that he used a numerical method called species transport method in all his research to study the DPM behaviours. In his studies, the DPM was considered as a gas species and n-octane vapour was used to represent DPM. However, in one of his

study (Zheng & Tien, 2009), the difference between the simulation data and experiment measurement was up to 58.02%, which was not acceptable for the CFD simulations. There are two main reasons may cause this discrepancy. It is known that DPM is a kind of particles and treat it as a gas phase may result in an inaccurate result. Thus, the species transport model which consider the DPM as a gas species might be not suitable in this case. Second, the reprehensive gas (C8H18) of DPM he selected was not proper.

Kurnia et al. (Kurnia, Sasmito, Wong, & Mujumdar, 2014) also conducted a numerical study to predict the DPM dispersion in underground mines. He used the same simulation model (species transport model) as Zheng's studies. Four different ventilation systems were evaluated and the effect of the location of tailpipe on diesel exhaust distributions were also analysed. The results showed that side tailpipe and turned duct design gave the lowest hazardous gas concentrations.

Table 4 Summary of current DPM studies by using CFD

Reference	Modelling Method	Validation
Zheng and Tien (2008)	Species Transport Model	No validation presented
Zheng and Tien (2009)	Species Transport Model	Difference between the simulation data and experiment data is 58.02%
Zheng et al. (2011a)	Species Transport Model	Difference ranges from 0.1% to 56.5%
Zheng, Thiruvengadam, Lan, and Tien C (2015)		
Zheng, Thiruvengadam, et al. (2015a) Zheng, Thiruvengadam, et al. (2015b)	Species Transport Model	No validation presented
Jundika C Kurnia, Agus P Sasmito, Wai Yap Wong, et al. (2014)	Species Transport Model	The turbulence model was validated with onsite data, but no validation was presented for DPM simulation
Thiruvengadam, Zheng, and Tien (2016)	Species Transport Model Eulerian-Lagrangian Model	No validation presented, however, two simulations methods illustrated similar results

As known from above reviewed studies, species transport model is mostly used numerical model for DPM simulation. However, DPM is solid particles, Eulerian-Lagrangian model has potential to simulate gas-solid two phase fluids. In 2016, Zheng and his colleagues compared both the species transport method and Eulerian-Lagrangian method in a study(Thiruvengadam, Zheng, & Tien, 2016). The results showed that both the simulation methods presented similar DPM distributions.

In addition, in other field, many studies have used CFD modelling to study the evolution of DPM size distribution in a vehicle tailpipe(P. Jiang et al., 2005), investigate the effects of dilution, nucleation, condensation and coagulation on the DPM formation under different DPM dilution systems (Uhrner et al., 2007), evaluate the indoor DPM size and concentration distributions from the diesel lamps (Apple et al., 2010), and predict the DPM formation, evolution processes, and concentration distribution in a vehicle's wake area near the ground (Chan, Liu, & Chan, 2010; Y. Liu, He, & Chan, 2011).

2.4.6 Other applications

The CFD has also applied in another mining field. Edwards and Hwang (Edwards & Hwang, 1900) studied the mine fire smoke dispersion under reversal conditions in an underground mine. Humphreys and his colleagues (Humphreys, Collecutt, & Proud, 2010; Proud, Collecutt, & Humphreys, 2015) used the CFD method to study the coal dust explosion in underground coal mines and evaluate the design of suppression systems. Trevits et al. (Trevits, Yuan, Thibou, & Hatch, 2010) built a CFD model based on the onsite experiment conducted by NIOSH to evaluate the nitrogen (N_2) injection and its effect on oxygen (O_2) content in a sealed mine area. Torno et al. (Torno, Toraño, Ulecia, & Allende, 2013) analysed the blasting gas behaviours in an underground coal mine heading. The gas dilution models were also developed to help identify the safe condition in the heading. Panigrahi (Panigrahi & Mishra, 2014) simulated the effect of blade profiles on the energy consumption of mine ventilation fans by CFD method. A most energy efficiency blade profile was suggested by the simulation results.

2.5 Summary

In summary, long-term DPM exposure contributes to the high rate of lung cancer. And currently, the main DPM control method in the underground mine is ventilation. Thus, understanding the DPM dispersion and concentration distribution characteristics in underground mines will help to solve the DPM relate issues and optimize the ventilation design. The previous studies have demonstrated that CFD is a proper method to achieve these goals. However, the selection of numerical models is very important. Even for the same physical model, the simulations by different numerical models may vary. Thus, it is important to an optimum model for the DPM simulation. Currently, the Eulerian-Lagrangian method has been widely used to solve coal dust related problems. It is able to accurate analysis of the gas-solid two-phase fluid. Thus, this method has the potential to analysis the DPM behaviours better compared to the currently used method – species

transport method. The following chapter would try to compared different numerical models and recommend the applicability for each model.

3 Numerical study of diesel particulate matter distribution in an underground mine isolated zone

This chapter has been published on Power Technology. It was entirely written by Ping Chang with the editorial suggestions provided by Dr Guang Xu and Dr Benjamin Mullins. Please cited it as:

Xu, G., Chang, P., Mullins, B., Zhou, F., & Hu, S. (2018). Numerical study of diesel particulate matter distribution in an underground mine isolated zone. Powder Technology, 339, 947-957.

The literature reviews demonstrated that CFD is capable of simulation DPM dispersion behaviours in underground mines. However, the selection of the simulation model is important. In this chapter, a numerical simulation was built based on a published report. The DPM particles were treated as discrete phase and the Eulerian-Lagrangian method was used to simulate the air-DPM two-phase fluid. The results were further compared with the onsite experimental data and a published study which used another method to simulate the DPM.

3.1 Abstract

The increased use of diesel engines in underground mines, together with increased mine depth, cause challenges in maintaining diesel particulate matter (DPM) at acceptable levels in underground environments. In 2012, the International Agency for Research on Cancer (IARC) classified DPM as carcinogenic to humans. To control the DPM exposure, it is important to understand DPM distribution and dispersion characteristics. In this study, an isolated zone in an underground mine in the US was taken as the physical model and the computational fluid dynamics (CFD) method was used to study the DPM distribution for two operational scenarios. The simulation results were compared with existing validation data. Compared to studies that treat DPM as a continuous phase, a better agreement with the experimental data is achieved in this study which uses the discrete phase to represent DPM. High DPM concentrations were identified in the two scenarios. This information can be potentially used to optimise auxiliary ventilation designs.

3.2 Introduction

The use of diesel engines in underground mines has continuously increased since the 1960s due to the high thermal efficiency of the diesel combustion process and non-flammability of diesel fuel. However, diesel engines emit a high concentration of ultrafine particulate matter, mainly in the form of carbonaceous particles (soot), in addition to NO_x, CO, CO_2 and H_2O. This is a problem in confined spaces, such as underground mines, where it has the potential to overexpose underground miners to diesel particulate matter (DPM). In 2012, the International Agency for Research on Cancer (IARC) classified DPM as carcinogenic to humans (Group 1) (Lyon, 2012). While long-term exposure to DPM increases lung cancer risk, short-term or acute DPM exposure also may result in impaired respiratory function (Chang & Xu, 2017a; HEI, 2003; Turner, 2007), altered DNA Methylation (R. Jiang, Jones, Sava, Kobor, &

Carlsten, 2014; X. Zhang et al., 2016) and impaired blood-brain-barrier integrity (Heidari Nejad et al., 2015). Therefore, it is necessary to ensure effective ventilation to reduce DPM concentrations in underground mines to an acceptable level.

In order to minimize DPM health hazards, the DPM concentrations should be maintained below an acceptable limit. In Australia, the Australian Institute of Occupational Hygienists (AIOH) has recommended an 8-hour time weighted average (TWA) exposure guideline of 0.1 mg/m^3 and an action level of 0.05 mg/m^3 (measured as Elemental Carbon (EC)) (AIOH, 2017). Currently, two main strategies have been used to control DPM concentrations (DMP, 2013). One option is to control DPM through a combination of improved engine management, high pressure (common rail) electronic fuel injection, low sulphur fuels and exhaust aftertreatment. Off-highway vehicles in the US and Australia are classified via a Tier 1-4 rating system, which specifies increasingly lower emission limits for new vehicles, thereby requiring the implementation of the above strategies. The current specification in Australia is Tier 4i (i= interim), which specifies NOx reduction through Selective Catalytic Reduction (SCR), however does not require Diesel Particulate Filters (DPFs) (Dittler, 2017). While not a regulatory requirement, many Tier 1-3 mine vehicles are, however retrofitted with DPFs to control particulate emissions, such systems are typically inferior to original equipment manufacturer (OEM) systems fitted to on-road vehicles. The second strategy is of course to control DPM post-emission through dilution. This includes mine ventilation. Other strategies such as remote operation or electric mine vehicles also exist, however will not be addressed in detail here.

To effectively control DPM exposure, it is important to understand the distribution of DPM and dispersion characteristics in the flow field inside underground mines post emission. After emission, DPM disperses through mine roadways/tunnels and is transported with airflow. Therefore, understanding the two-phase (gas-solid) fluid characteristics in mine tunnels are the key issues to understand the DPM distribution and dispersion.

Computational fluid dynamics (CFD) has been widely used in many areas in the mining industry to investigate the properties of coal dust particles in roadways after blasting (Hu et al., 2016a; Hu et al., 2015), study dust behaviour and control strategies under different ventilation systems in underground mines (Geng et al., 2017; Kurnia, Sasmito, Hassani, & Mujumdar, 2015; Jundika Candra Kurnia et al., 2014; Ren et al., 2014; J Toraño et al., 2011; Yu et al., 2017), simulate tracer gases and investigate the level of damage to the ventilation system after incidents (Xu et al., 2015; Xu et al.,

2013), evaluate the performance of ventilation system in underground coal mines (Sasmito et al., 2013), and study hazardous gases dispersion and management in underground mines (Jundika C Kurnia, Agus P Sasmito, et al., 2014a; Jundika C Kurnia, Agus P Sasmito, Wai Yap Wong, et al., 2014; L. Zhou et al., 2015). These works demonstrated that CFD is an effective approach in the study of air and particle flow problems in the mining industry.

However, the application of CFD in studying DPM in underground mines is relatively recent, with only a small number of studies. Zheng et al. (Zheng et al., 2011a; Y. Zheng, H. Lan, M. Thiruvengadam, & J. C. Tien, 2011b; Zheng, Thiruvengadam, Lan, & Tien C, 2015; Zheng, Thiruvengadam, et al., 2015a; Zheng, Thiruvengadam, et al., 2015b; Zheng & Tien, 2008, 2009) conducted a series of studies of DPM in underground mines by using this computational method. These works typically considered DPM as continuous phase instead of the discrete phase. One CFD study (Zheng & Tien, 2009) developed a virtual recreation of an isolated zone experiment (A. Bugarski, Schnakenberg, et al., 2004) using CFD. The DPM concentrations between the simulated results and experimental measurements were compared, however the error between simulation and experiment was up to 58.02%. This error may be due to the use of continuous phase (Eulerian) methods, or may be due to the mismatch between the experimental cases and model boundary conditions. In real world (mine) experiments it is of course very difficult to characterise flow and concentration parameters on the fine spatial scales needed when constructing CFD simulations. Conversely, mine tunnel dimensions and roughness are typically simplified in CFD studies, compared to the real situation.

The aim of this paper is to simulate the DPM concentrations distribution in an isolated zone by using the discrete element (Lagrangian) method, in order to allow comparison with previous Eulerian simulations (Zheng & Tien, 2009) and field (experimental) data. This work also draws on previous experimental work (A. Bugarski, Schnakenberg, et al., 2004) as a model validation case. In the current work, the gas phase is solved by using a Eulerian method and the particle phase is solved via a Lagrangian approach. Both 2D and 3D models are constructed. A 2D simulation is used to first find the characteristics of the airflow and DPM concentrations distribution in an operating cycle. A 3D model is then constructed to provide more accurate and detailed information about the simulation. Areas of high DPM concentrations are identified and suggestions provided to help control DPM in such areas through improved ventilation. Finally, the results are compared with previous simulation (Zheng & Tien, 2009) and experimental

(A. Bugarski, Schnakenberg, et al., 2004) studies of the same case, with sources of discrepancy between the results analysed and discussed.

3.3 Problem statement and Mathematical models

3.3.1 Problem Statement

The physical model simulated in this paper is based on a published report by NIOSH (A. Bugarski, Schnakenberg, et al., 2004). The testing was conducted in an isolated zone in an underground mine, as shown in Figure 3. The length of the isolated zone is 462 m from inlet to outlet, and the cross-sectional dimensions are 3.6 m (height) × 2.7 m (width). There are two dead-ends in this isolated zone, which are the load/dump points marked in Figure 3. In the field tests, two sampling stations were setup: the downstream sampling station and the vehicle sampling station (shown in Figure 4). The experimental study only reports DPM concentrations at the downstream sampling station. A diesel-powered load-haul-dump truck (Caterpillar R1500 LHD) travels between the two load/dump points. The LHD executes three load/dump tasks at the upstream point then moves to the downstream point and repeats the same operation. The average cycle time was measured at approximately 13 minutes. Due to computational effort requirements, only two scenarios are investigated in this study: when the LHD works at the upstream load/dump point (scenario 1), and when it works at the downstream load/dump point (scenario 2). It is assumed that the LHD works at the torque converter stall (TCS) condition under which it produces the highest exhaust emissions.

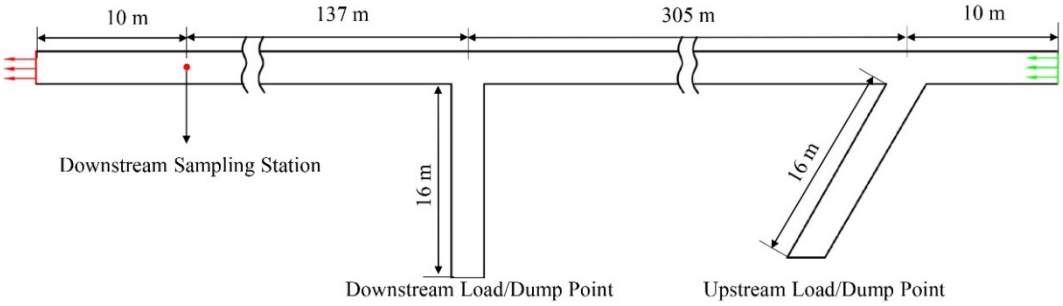

Figure 3 Schematic diagram for the area under study

3.3.2 Mathematical Models

Two main approaches that have been used to represent the gas-particle two-phase fluid (Van Wachem & Almstedt, 2003). The first is a Eulerian-Eulerian approach (or two-fluid approach) (Enwald, Peirano, & Almstedt, 1996; Gidaspow, Jung, & Singh, 2004). This approach considers both the gas and particle phase as a continuous phase governed by the Navier-Stokes equation. A more computationally intensive, however

potentially more accurate approach, is the Eulerian-Lagrangian approach, has been developed for applications such as gas-particle simulation (Deen, Annaland, Van der Hoef, & Kuipers, 2007; Zhu, Zhou, Yang, & Yu, 2007, 2008). In this approach, the gas phase is solved using the Eulerian approach and the particle phase tracked within the flow field via the Lagrangian approach. The Eulerian-Lagrangian approach is used in this paper. Particle-particle interactions are not considered as the particulate volume fraction is less than 0.1% (Afkhami, Hassanpour, Fairweather, & Njobuenwu, 2015; Van der Hoef et al., 2006). For the nano-size particles, Brownian diffusion plays a vital role in the motion of the particle. However, the turbulence dispersion has significantly greater effects on the particle motions than that of the Brownian diffusion (Ounis & Ahmadi, 1990). For this reason, the diffusion of particles caused by turbulence dispersion is accounted for. In order to reduce the computational cost, the particle phase is calculated using the computational parcels method (Andrews & O'rourke, 1996; O'Rourke & Snider, 2010). One parcel contains a group of particles that have the same dynamic properties. This approach is reasonable for gas-particle two-phase fluid systems where collisions can be neglected (Benyahia & Galvin, 2010; Patankar & Joseph, 2001).

3.3.3 Governing Equations

The gas phase is treated as an incompressible continuous fluid, and its continuity and momentum equations are described by the Navier-Stokes equation (J.Anderson, 2008), which are given by:

$$\begin{cases} \dfrac{\partial \epsilon_g}{\partial \mathrm{t}} + \nabla \cdot (\epsilon_g \boldsymbol{u_g}) = 0 \\ \dfrac{\partial \boldsymbol{u_g}}{\partial t} + \nabla(\boldsymbol{u_g u_g}) = \dfrac{1}{\epsilon_g \rho_g}\left(-\nabla p - \boldsymbol{F} + \nabla \cdot \left(\epsilon_g \bar{\bar{\tau}}_g\right) + \rho_g \epsilon_g \boldsymbol{g}\right) \end{cases} \tag{1}$$

where p, ρ_g, ϵ_g, $\boldsymbol{u_g}$and $\boldsymbol{g}$ are static pressure, gas density, gas volume fraction, gas velocity and gravity acceleration, respectively. $\bar{\bar{\tau}}_g$ is the viscous stress tensor, which is given by:

$$\bar{\bar{\tau}}_g = (\mu + \mu_t)\left(\nabla \boldsymbol{u_g} + \left(\nabla \boldsymbol{u_g}\right)^T\right) - \frac{2}{3}\left[(\mu + \mu_t)(\nabla \cdot \boldsymbol{u_g}) - \rho_g k\right]\boldsymbol{I} \tag{2}$$

where μ, μ_t, k and **I** are the molecular viscosity, turbulent viscosity, turbulent kinetic energy and unit tensor, respectively. **F** is the volumetric momentum transfer rate between particles and gas phases, which is given by

$$\boldsymbol{F} = \frac{\sum \boldsymbol{F_d}}{V_{cell}} \tag{3}$$

where V_{cell} is the computational cell volume, F_d is the fluid force on particles and is equivalent to the particle drag force.

The standard $k-\varepsilon$ model is the most widely used turbulence model in engineering, and thus, it is used in this paper. The equations of this model are given by:

$$\frac{\partial(\rho_g k)}{\partial t}+\nabla\cdot\left(\rho_g k\boldsymbol{u_g}\right)=\nabla\cdot\left[\left(\mu+\frac{\mu_t}{\sigma_k}\right)\nabla k\right]+G_k-\rho_g\varepsilon \tag{4}$$

$$\frac{\partial\left(\rho_g\varepsilon\right)}{\partial t}+\nabla\cdot\left(\rho_g\varepsilon\boldsymbol{u_g}\right)=\nabla\cdot\left[\left(\mu+\frac{\mu_t}{\sigma_\varepsilon}\right)\nabla\varepsilon\right]+C_{1\varepsilon}\frac{\varepsilon}{k}G_k-C_{2\varepsilon}\rho_g\frac{\varepsilon^2}{k} \tag{5}$$

where ε and G_k are turbulent dissipation rate and turbulent production, respectively. μ_t and G_k are given by:

$$\mu_t=C_\mu\rho_g\frac{k^2}{\varepsilon} \tag{6}$$

$$G_k=\mu_t\left(\nabla\boldsymbol{u_g}+\left(\nabla\boldsymbol{u_g}\right)^T\right)\nabla\boldsymbol{u_g} \tag{7}$$

The value of model coefficients C_μ, $C_{1\varepsilon}$, $C_{2\varepsilon}$, σ_k, σ_ε are 0.09, 1.44, 1.92,1, and 1.3, respectively. The particle dispersion due to the turbulence of the airflow is controlled by the Stochastic tracking model. The continuity and momentum equations are solved using the PIMPLE algorithm.

In the discrete phase, DPM is tracked by using the Lagrangian method. In the gas field, many forces act on solid particles, including drag force, lift force, buoyancy, gravity and pressure gradient force etc. However, only drag force and gravity are considered in the model and other non-significant forces are neglected. The governing equation for the motion of particles is calculated by Newton's second law, which is given by:

$$m_p\frac{d\boldsymbol{u_p}}{dt}=m_P\boldsymbol{g}+\boldsymbol{F_d} \tag{8}$$

where m_p and $\boldsymbol{u_p}$ are the particle mass and velocity, respectively. The drag force $\boldsymbol{F_d}$ is given by (Gidaspow, 1994):

$$\boldsymbol{F_d}=\frac{V_g\beta}{\left(1-\epsilon_g\right)}\left(\boldsymbol{u_g}-\boldsymbol{u_p}\right) \tag{9}$$

where β is the interphase momentum exchange coefficient and given by:

$$\beta=\begin{cases}0.75C_D\dfrac{\rho_g\epsilon_g\left(1-\epsilon_g\right)\left|\boldsymbol{u_g}-\boldsymbol{u_p}\right|}{d_p}\epsilon_g^{-2.65} & \epsilon_g\geq 0.8\\ \dfrac{150\left(1-\epsilon_g\right)^2\mu}{\epsilon_g d_p^2}+\dfrac{1.75\rho_g\left(1-\epsilon_g\right)\left|\boldsymbol{u_g}-\boldsymbol{u_p}\right|}{d_p} & \epsilon_g<0.8\end{cases} \tag{10}$$

$$C_D=\begin{cases}\dfrac{24}{Re_p}\left(1+0.15Re_p^{0.687}\right) & Re_p<1000\\ 0.44 & Re_p\geq 1000\end{cases} \tag{11}$$

$$Re_p = \frac{\rho_g \epsilon_g |\boldsymbol{u_g} - \boldsymbol{u_p}| d_p}{\mu} \quad (12)$$

where $C_D$is the drag force coefficient, d_p is the particle diameter, and Re_p is the particle Reynolds number.

3.3.4 Solver Selection

OpenFOAM is a Linux based C++ library which has been extensively applied to solve CFD-based problems. It provides a range of existing solvers and libraries, however also allows users to customize or write new solvers. Several existing solvers were evaluated, including simpleReactingParcelFoam, however, DPMFoam was been selected as the most appropriate solver for this work, as it included all relevant physics and did not have artificial constraints on particle concentrations or injection rates.

3.4 CFD Model Setup and Simulations

3.4.1 CFD Model Setup

The following boundary conditions and assumptions were implemented: air is incompressible; airflow is fully developed and turbulent; heat-transfer are not considered; gravity is 9.81 m/s^2; and no slip wall function is used. The boundary conditions and initial conditions used in this paper are identical to that used by Zheng (Zheng & Tien, 2009) except for the particle simulation approach. The particle density is set based on published data (Park, Kittelson, Zachariah, & McMurry, 2004) and the DPM emission rate is calculated according to Mine Safety and Health Administration (MSHA) data. Simulation parameters are given in Table 5. The pressure-velocity equation of the gas phase is solved by the SIMPLE algorithm. The numerical schemes used in this study are second-order discretization. The numerical schemes for the divergence and Laplacian derivatives are Gauss linearUpwind and Gauss linear corrected, respectively. The schematic diagram for the 2D and 3D models for the two scenarios are shown in Figure 4. Note that the position of the vehicle sampling station is slightly different for the simulation and the field test. In the field test, the vehicle sampling station is 0.61 m from the LHD operator cabin. In the simulation, the vehicle sampling is 0.61 m from the back of the LHD due to the spatial constraints in the 2D model. For direct comparison purpose, the vehicle sampling station for the 3D model is set at the same position as the 2D model.

Table 5 Boundary and initial conditions

Boundary	Value
Inlet	Air velocity: 2.43 m/s (23.6 m^3/s)
Outlet	Pressure: fixed-value 0 Pa
Wall	No slip wall
LHD tailpipe	Particle density:1.75×10^3 kg/m^3 Particle size: 78.7×10^{-9} m DPM mass rate: 2.49×10^{-6} kg/s Exhaust flow rate: 0.89 m^3/s (tailpipe size: 0.3 m ×0.16 m)

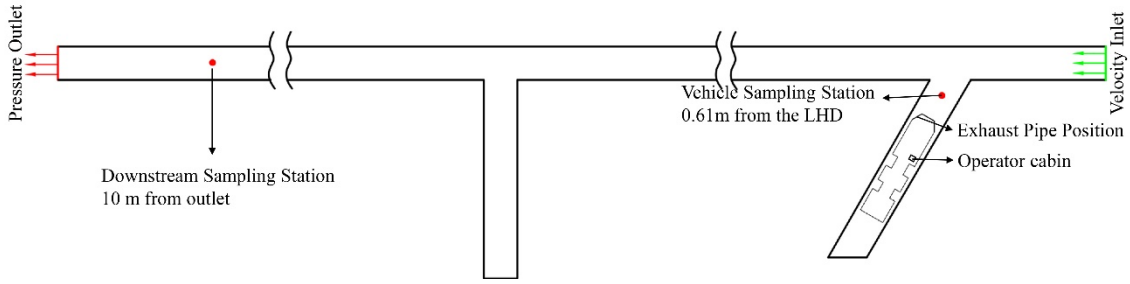

(a) Scenario 1

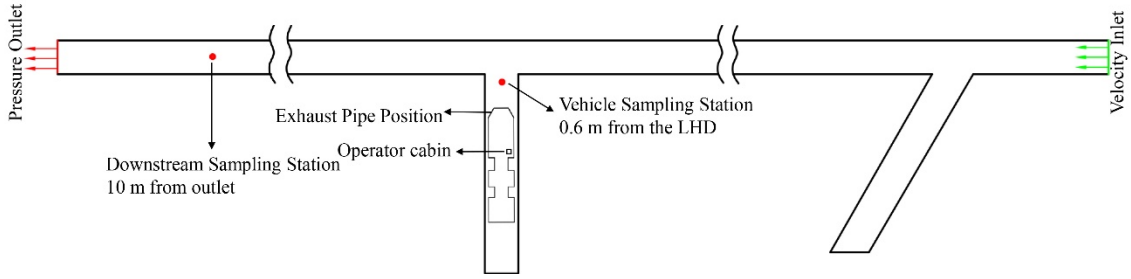

(b) Scenario 2

Figure 4 Schematic diagram for the CFD models

3.4.2 The 2D CFD Model

Both 2D and 3D CFD models were constructed. A 3D model can provide more accurate and detailed output data. However, 3D simulations greatly increase computational effort, especially for particle tracking simulations. The 2D model was built first to provide both initial results and parameter optimization/refinement for the model bounds, which then reduced the number of 3D model runs which needed to be executed.

The LHD in question has the vehicle sampling station located. In the 2D model, the LHD is simplified to its top view projection solid area, thus the actual vehicle sampling station cannot be represented in the model. Alternatively, in the 2D study, it is assumed that the vehicle sampling station is 0.61 m from the LHD, as shown in Figure 4. After

the flow field is established, 13 minutes of real time is simulated, representing is a full operating cycle.

3.4.3 The 3D CFD Model

As we are simulating what is expected to be a transition or turbulent flow fields, 3D models are built to provide a more accurate representation of the flow structures and hence particle dispersion. The 2D and 3D models are essentially the same Compared to the 2D model, the 3D model computation time is much more extensive, especially for the calculation of the Lagrangian particle motion. For this reason, the 3D simulation for the two scenarios is reduced to 240 seconds, which is believed long enough to analysis the DPM dispersion characteristics.

A mesh independence study was initially for both the 2D and 3D models, as per correct CFD protocol. In order to reduce space, only the mesh independence study for scenario 1 of the 3D model is presented here. In order to make sure the simulation results are independent of the mesh size, a medium and a fine mesh were tested in this study. The total number of cells for the medium and fine mesh are approximately 2.4 and 4.8 million, respectively. An unstructured mesh is used in the heading where the LHD is located, and the structured mesh is used in other parts of the model. In order to ensure the accuracy of the simulation, the mesh near the LHD was generated with higher density.

Velocity profiles across four lines at four different locations in the main roadway were used to check the mesh independence. Line 1 and line 2 are at the horizontal centreline 190 m and 430 m from the inlet, respectively. Line 3 and line 4 are 1 m from the upstream and downstream deadend entrance, respectively. As can be seen from Figure 5, it is observed that the velocity profiles of the medium mesh are highly matching that of the fine mesh for both monitor lines. The velocity difference for the two sections between medium mesh and fine mesh is calculated by using the root mean square deviation (Xu et al., 2016). For scenario 1, the difference is 2.38%, 1.65%, 2.85% and 1.34% for line 1, line 2, line 3 and line 4, respectively. As no significant difference was found between the medium and fine mesh, it is believed that a mesh independent solution had been achieved and the medium mesh was used in order to minimise computational time.

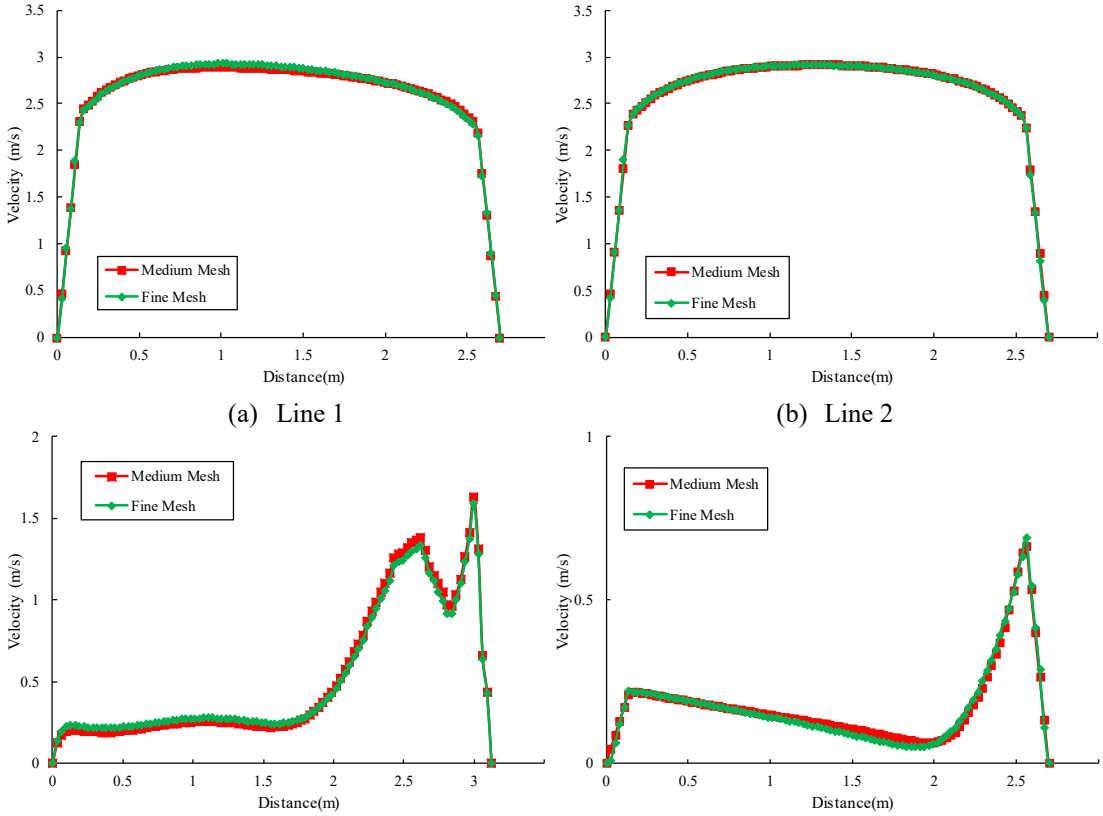

(a) Line 1 (b) Line 2

(c) Line 3 (d) Line 4

Figure 5 Velocity profiles at the monitor lines

3.5 Results and Discussion

3.5.1 2D CFD Model

To compare the simulated results to field measurements and other studies, the concentration values shown in Figure 6 have been averaged over the cross sectional area. The simulated change in DPM concentrations for 2D models are shown in Figure 6 (a). As can be seen, once the DPM reaches the monitor point, its concentrations increases rapidly and levels out at a stable value. This reveals a steady state has been achieved. The final concentration values are all below the limit of 0.1 mg/m^3. The DPM concentrations at the vehicle sampling station is higher than that at the downstream sampling station. These can be explained by the airflow features in the deadend entry for the two scenarios. As can be seen in Figure 7, the velocity and flow rate in the deadends for both scenarios are lower than that of the main roadway and therefore insufficient to dilute DPM. At the downstream sampling station, the DPM concentrations for scenario 2 is higher than scenario 1. Due to the deadend geometry difference, the distinct flow features around the LHD exhaust for the two scenarios result in different DPM flow behaviour, and the DPM is carried out to the main road quicker for scenario 2.

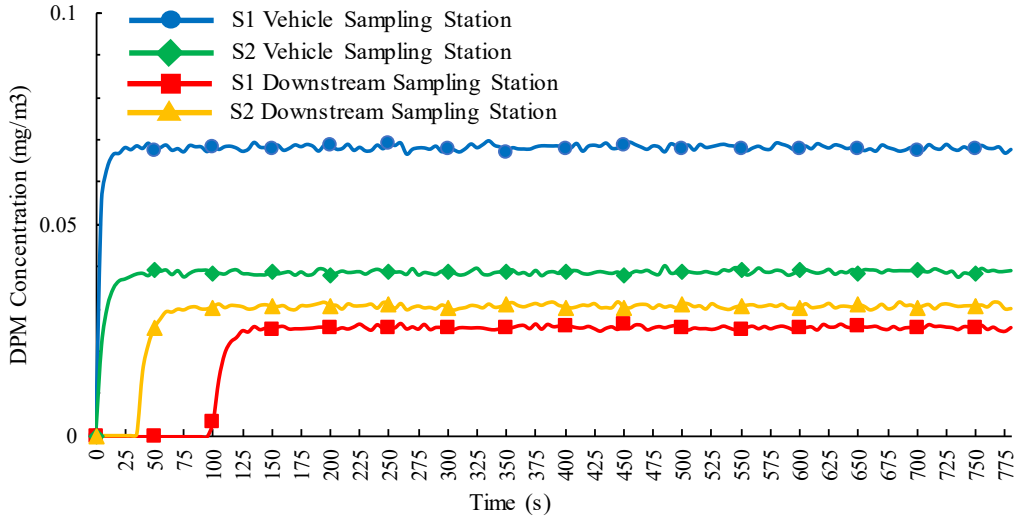

(a) 2D models

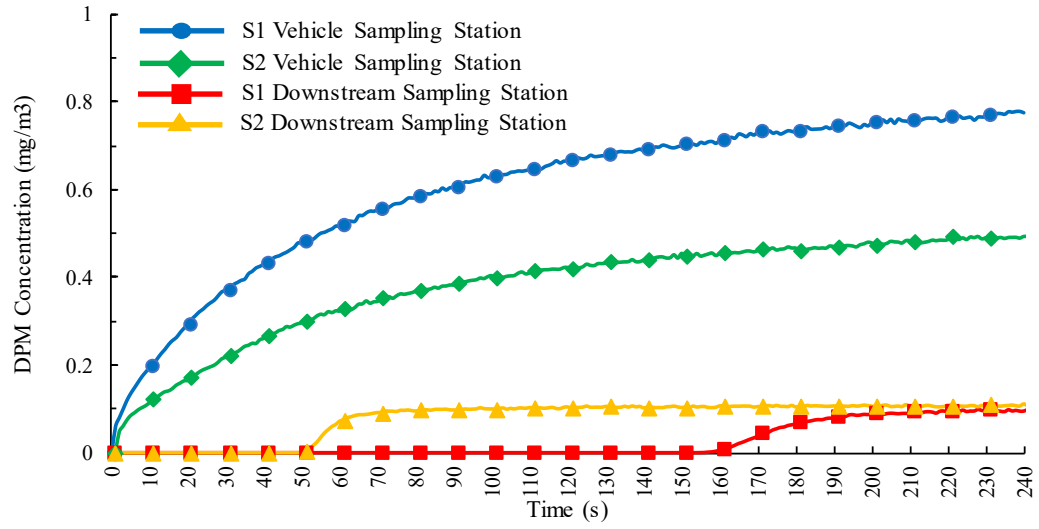

(b) 3D models

Figure 6 DPM concentration change at sampling stations

The circulation of the flows also causes the accumulation of DPM in the vortex, rather than carrying it out to the main flow for better dilution. For the upstream, due to the direction of airflow, there is no DPM accumulation. For the rest of areas in the main roadway, the DPM concentrations are similar and the DPM concentrations for two scenarios are quite close, they are about 0.027 mg/m^3 and 0.031 mg/m^3 for scenario 1 and scenario 2, respectively. These are much lower than the recommended limit of 0.1 mg/m^3. According to the DPM concentration changes in Figure 6, it is believed that the 2D simulations already achieved the stable state during a working cycle (13 mins).

Figure 8 displays the DPM concentrations distribution close to the vehicle sampling station for the two scenarios at the end of the simulation. The red shaded region indicates DPM concentrations equal to or greater than the recommendation limit (0.1 mg/m^3). For scenario 1, the high DPM concentration area is located at the back of the LHD on the

exhaust pipe side. However, for scenario 2, this area expands to one side of the deeper part of the deadend entry and some DPM accumulated at the front of the LHD although the concentrations were under the recommendation limit. This is caused by the different geometry of the two working areas. It means that, for different situations, if auxiliary ventilation duct is to be used for effective removal of DPM, the duct length should be different. Also, to which side of the entry the duct is installed can also influence the dilution efficiency. Due to the low diffusion coefficient and airflow velocity, initially most DPMs are concentrated to the deadend side of the main roadway where the vortex location is, as shown in Figure 7. The circulation of the flow in the vortex also contributes to DPM accumulation in these areas. The concentrations in this area are 0.04 mg/m^3 and 0.05 mg/m^3 for scenario 1 and scenario 2, respectively. As they flow to the downstream, DPM relatively quickly diffuses in the roadway (as can be seen in Figure 9) and its cross section area weighted average concentrations maintain at a stable value at around 0.03 mg/m^3 for both scenarios. Further inspection of Figure 9 demonstrates that after the DPM concentrations reach a stable state, it concentrates at the centre of the roadway. This will be investigated and explained in detail in section 3.5.2.

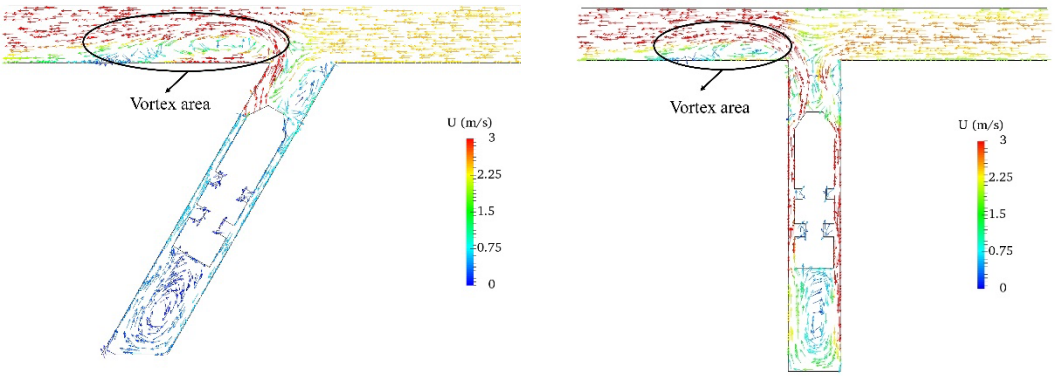

(a) Scenario 1 (b) Scenario 2

Figure 7 Airflow features in the deadend entries

3.5.2 3D CFD Model

Figure 6 (b) gives the DPM concentrations change for 3D models. Not the same with the 2D models, the DPM concentrations at the vehicle sampling station slowly increase and have not reached a stable value at the end of 240s. This is reasonable as the 2D model stabilizes faster without considering vertical diffusions. If the simulation time is further extended, it is believed stable concentrations can also be achieved. In addition, the DPM concentrations at this location exceed 0.1 mg/m^3 at 4 s and 7 s for scenario1 and 2, respectively. For the DPM concentrations at the downstream sampling station, the 3D results show the same trend as the 2D results but the final concentrations reached to about 0.1 mg/m^3 for both scenarios. Overall, the DPM concentrations for the 3D models

are higher than that of the 2D models, and the DPM arrival time to the downstream sampling station is longer for the 3D models. This is because the 2D model is not a physical representation of the actual flow. As a velocity inlet, the LHD exhaust causes a much higher flow quantity in the 2D model than that of the 3D. This causes the final velocity in the 2D model main roadway is considerably higher, which is not accurate and causes lower DPM concentrations and shorter arrival time.

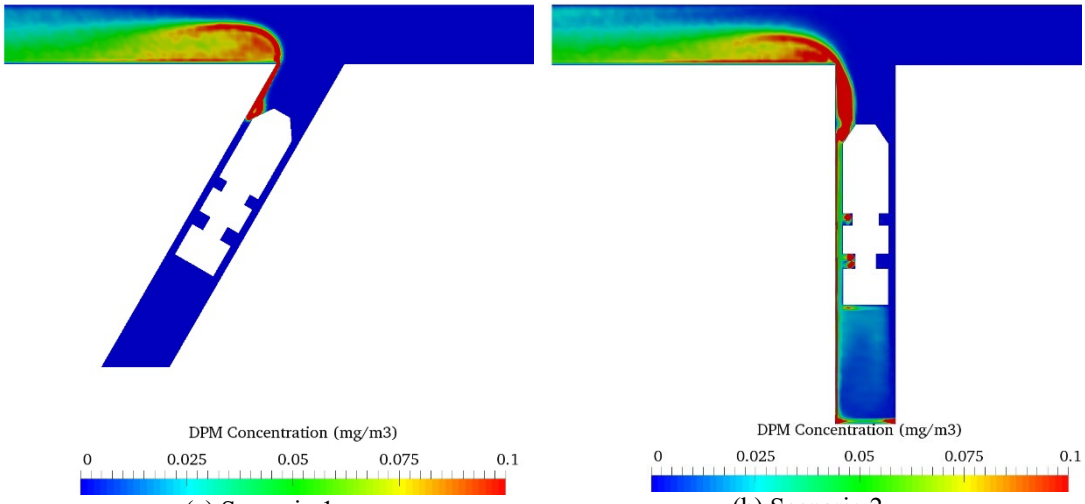

(a) Scenario 1 (b) Scenario 2

Figure 8 DPM concentration distributions in deadend entry at 780s

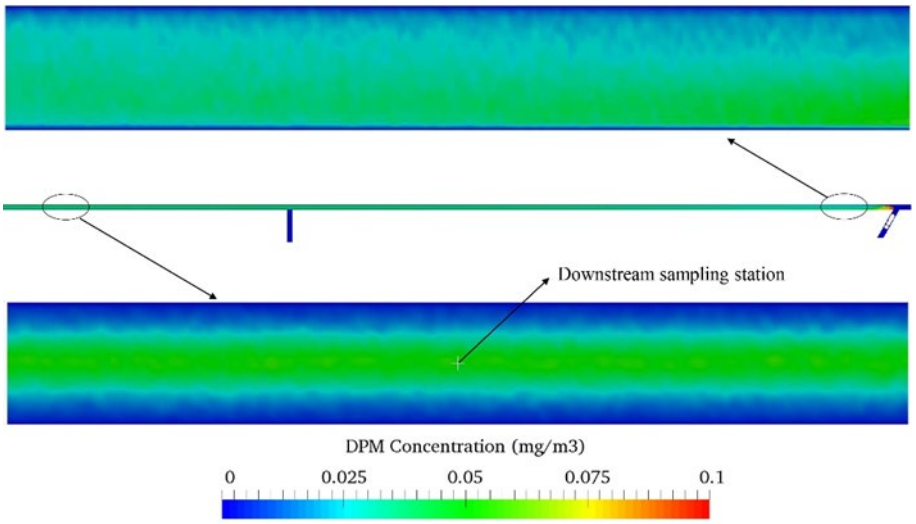

Figure 9 DPM concentration distribution in the main roadway for scenario1 at 780s

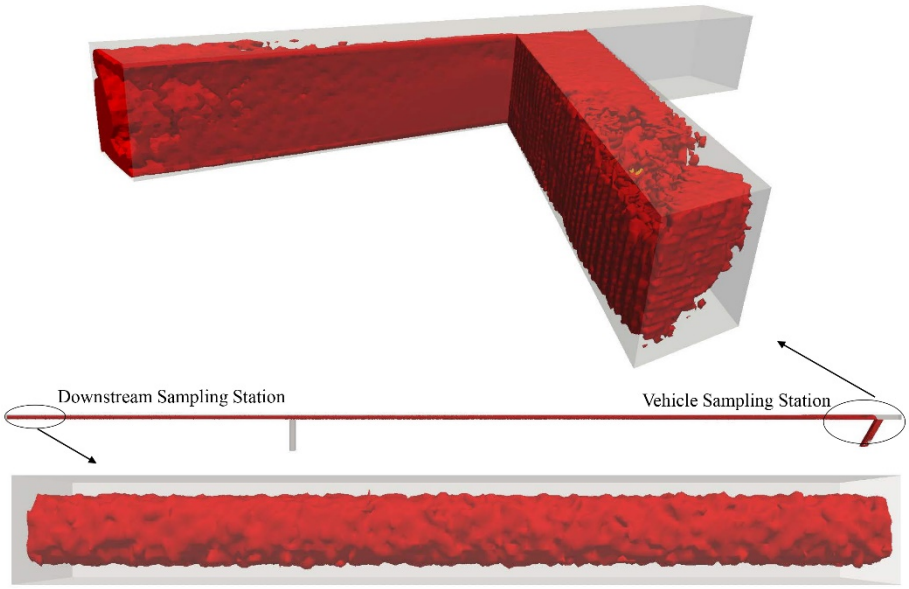

(a) Scenario 1

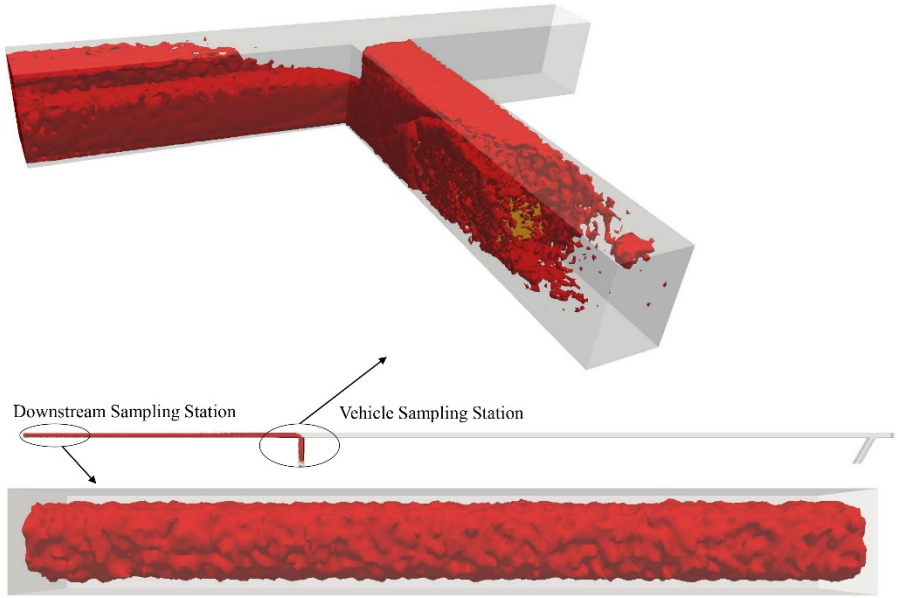

(b) Scenario 2

Figure 10 DPM distribution with the concentration ⩾ 0.1 mg/m3 at 240s

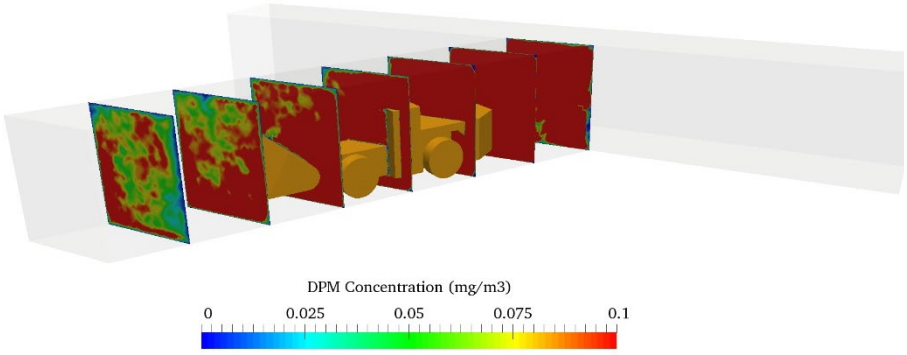

(a) DPM concentration distribution in deadend entry

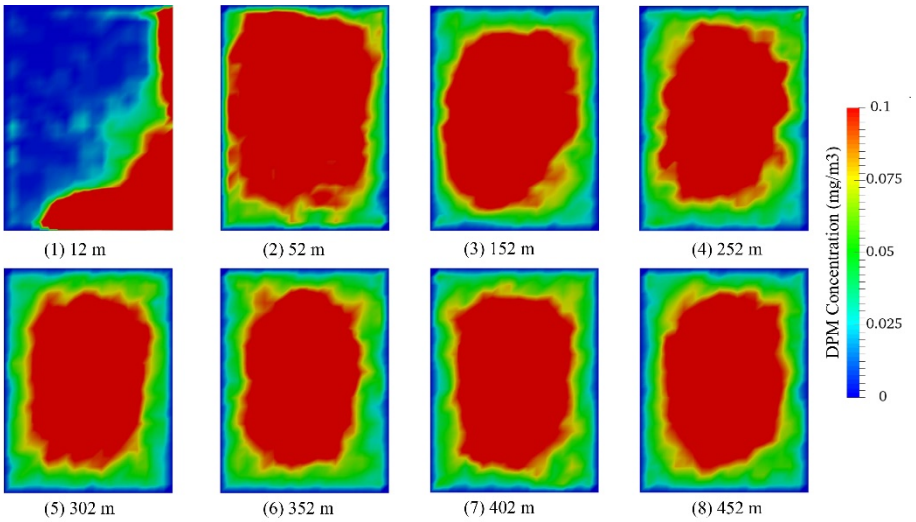

(b) Cross-sectional planes in the main roadway (distance from the inlet)

Figure 11 DPM distribution at cross-sectional planes for scenario 1 at 240s

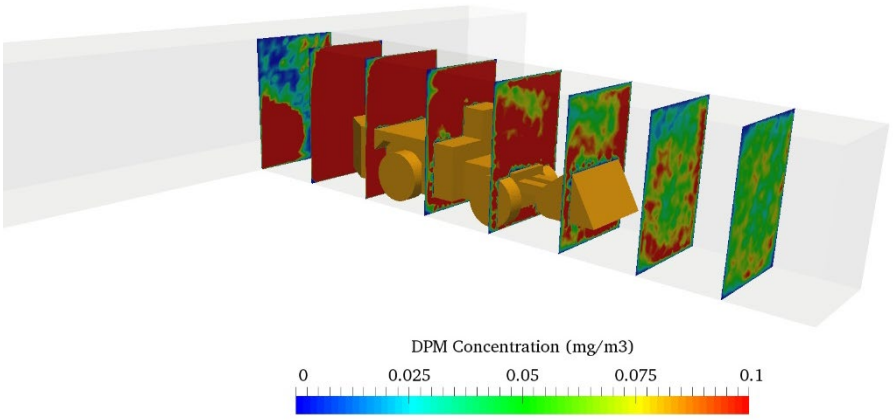

(a) DPM concentration distribution in deadend entry

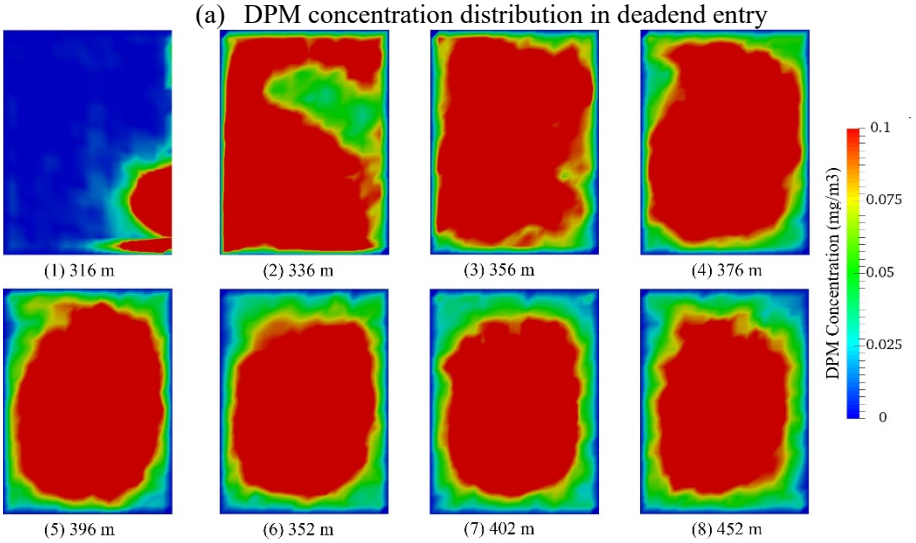

(b) Cross-sectional planes in the main roadway (distance from the inlet)

Figure 12 DPM distribution at cross-sectional planes for scenario 2 at 240s

The DPM distributions for the two scenarios at 240 s are shown in Figure 10. The red contours represented the DPM with the concentrations equal or above the exposure limit of 0.1mg/m^3. For both two scenarios, the DPM accumulates around the LHD, but the high DPM concentration area expands to the deeper part of the deadend entry in

scenario 1. Comparing the 2D results, more DPM are accumulated in the deadend entry. This is because the space on top of the LHD is not represented in the 2D models, but DPM accumulates in this area in the 3D models. The general locations of high DPM concentration area in the main roadway are highly consistent with that of the 2D simulations, with the high DPM concentration zone located in the central area of the roadway. This phenomenon is also observed in Figure 11 (b) and Figure 12 (b). This result may not be realistic and could be caused by two main reasons. First one is the stochastic dispersion model. In the anisotropic turbulence area near the wall, it was reported to give a poor prediction of the motion and the wall impaction rate of particles when the particle's diameter is at the nanoscale size (Longest & Xi, 2007; Zhao, Chen, & Lai, 2011). The other reason is the wall effects on the particles. In this paper, the collision between particles and wall is perfectly elastic without any kinetic energy loss. In fact, it may cause the kinetic energy loss when the particle rebound on the wall and some particles may stick on the wall due to this loss.

The DPM distributions at cross-sectional planes are shown in Figure 11 (a) and Figure 12 (a). It can be seen that a higher concentration of DPM occurred in most working areas in the deadend entry. For this reason, additional controls (e.g. auxiliary ventilation) should be applied to these areas, or additional protective equipment should be given to workers, to avoid over exposure to DPM. Figure 11 (b) and Figure 12 (b) show the DPM distribution at different cross sections in the downstream main roadway. It is observed that the plume initially accumulates at the one side of the main roadway. Later, due to a combination of dilution and dispersion, the plume dissipates and extends toward the other side of the roadway. With it flows to the downstream further, the DPM distributions become stable.

3.5.3 Results comparison

Only DPM concentrations at the downstream sampling station are reported in the onsite experiment (A. Bugarski, Schnakenberg, et al., 2004), thus the result of the current study is compared to it and a previous CFD study (Zheng & Tien, 2009) based on this location. In Zheng's study, six scenarios (LHD operating at six different locations) were simulated until the DPM concentrations reached steady state. The final DPM concentrations at the downstream sampling station were reported as 0.553 mg/m^3, which were the average of the results for the 6 scenarios. In the experimental work, during the measurement, five DPM samplers were used at the downstream sampling station, and their locations are illustrated in Figure 13. The data for the samples were averaged, and the DPM concentrations were reported as 0.35 mg/m^3 for an averaged

operating time. This actually represents the DPM concentrations in the centre area of the roadway. To better compare it with the CFD results, it is plotted in Figure 14 together with the result reported from Zheng's study and the DPM profile across the horizontal centre line in our study. It can be seen that Zheng's data overestimates experimental DPM levels by 58%. The average DPM concentrations of our simulation for this area are 0.217 mg/m^3. Although this underestimates by 38%, it represents a closer agreement with the experiment data.

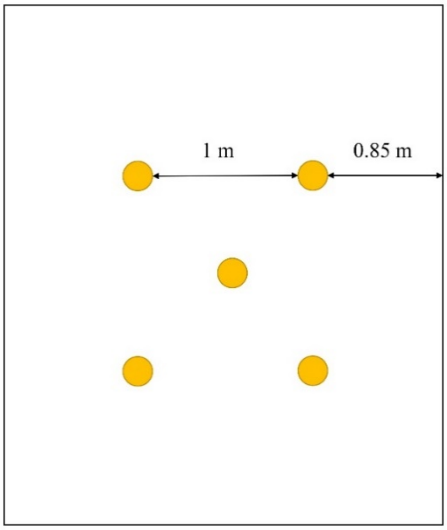

Figure 13 DPM sampler distribution at downstream sampling station

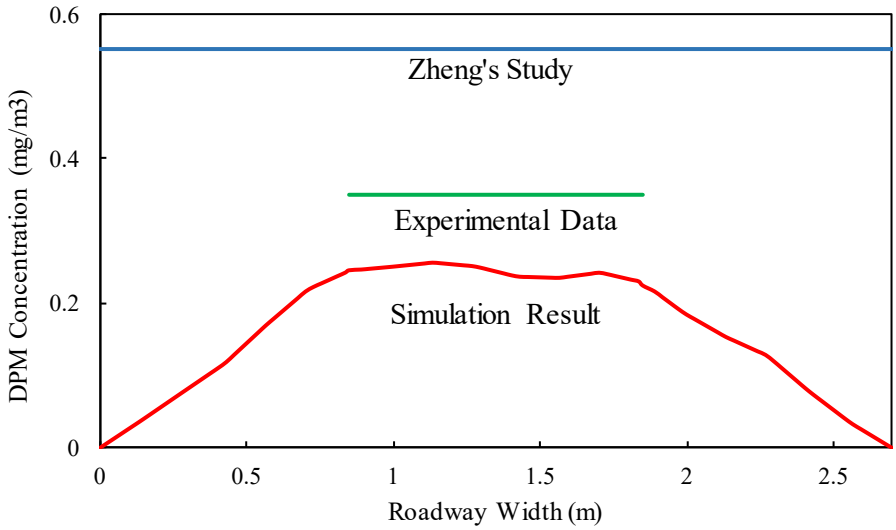

Figure 14 Results comparison at the cross sectional plane of downstream sampling station

The discrepancies in the results may be due to various factors. In Zheng's study, DPM is treated as the continuous phase, whereas in the current work DPM is treated as a discrete phase, which may account for some but not all of the variation between the studies. The DPM emission rate for the LHD is not identified in the NIOSH report. Zhang et al. have chosen a different emission rate (different data source) to the MSHA

data we have used here. This may be another source of error. In addition, during the DPM measurement in the mine, the LHD was driven from the upstream load/dump point to downstream load/dump point and then back to the upstream load/dump point to complete the cycle. This results in much higher DPM concentrations at the downstream sampling station when the LHD travels in the main roadway. Thus the method used here by taking the average values for the two scenarios is probably not very appropriate to predict DPM concentrations when vehicles are moving. To achieve a more accurate result, further research should be conducted to simulate the fluid disturbance of a moving LHD with the DPM input as either a moving line source (as opposed to a fixed point) in the underground mines.

3.6 Conclusion

In this paper, a CFD modelling study was conducted based on an isolated zone experiment (A. Bugarski, Schnakenberg, et al., 2004). Both 2D and 3D CFD models were built to simulate two operational scenarios: when the LHD works at the upstream load/dump point (scenario 1), and when it works at the downstream load/dump point (scenario 2). A gas-solid two-phase fluid study was conducted to analyze the DPM movement pattern and distribution characteristics between the discrete phase and the continuous phase. The results were compared with the isolated zone experimental data and plume dispersion simulation study by Zheng et al. (Zheng & Tien, 2009). The following conclusions have been drawn based on the results.

(1) For the isolated zones studied in this paper, DPM concentrations accumulated relatively quickly due to lower airflow velocity and the formation of airflow vortexes. DPM concentrations built-up quickly to exceed the recommended level limit, which then is difficult to clear with existing ventilation.

(2) High DPM concentration areas were identified for the two simulated scenarios. For both scenarios, the high DPM concentrations areas were found to be located around the LHD. However, the high concentration area for scenario 1 spread into the deeper part of the deadend entry. This indicates that different geometry will cause different flow features and thus DPM distribution will also be different. According to the simulation results, improved auxiliary ventilation designs can be proposed to alleviate the higher DPM concentration issues, which could be an avenue for further simulation studies.

(3) The change of DPM concentrations at the vehicle sampling station and downsampling station for the two scenarios shows a similar trend for the 2D

models. The DPM concentrations increased first and achieved a stable state after a short time of vehicle operation. For the 3D models, the DPM concentrations illustrate a growing trend in the vehicle sampling station during the simulation time (240 s) for both scenarios. It is believed that the concentrations may achieve a stable state with longer simulation time. The DPM in the main roadway shows the same distribution characteristic for both the 2D and 3D models. In the 3D models, the DPM accumulated near the deadend entrance, and the concentrations in this area for the two scenarios are 0.12 mg/m^3 and 0.13 mg/m^3, respectively. As it flows to the downstream, the DPM slowly diffuses in the roadway and the concentrations reduce to a stable value at around 0.1 mg/m^3 for both scenarios. In addition, the results also indicate that the DPM accumulated in the central area of the main roadway, which may attribute to the inaccuracy of the stochastic dispersion model.

(4) Compared to the experimental data, although the simulation underestimates the DPM value, a better agreement is achieved than studies that treat DPM as a continuous phase. The lower simulated values might be caused by two reasons. First, the DPM emission rate for the LHD is not identified in the NIOSH report. The emission rate used in the current paper is calculated according to the MSHA data, which may be different from the actual operational emission rate. Second, the scenarios that the LHD works in the main roadway are not simulated. For the scenarios which the LHD works in the deadend entry, most of the DPM is accumulated in the deadend entry instead of flowing into the main roadway, which could cause the lower DPM concentrations at the downstream sampling station.

This study intends to simulate the DPM concentration distributions for the loading activity in an underground isolated zone. However, the current method is not good enough to represent the moving vehicle during the mining activity. The dynamic meshing method will be used in future study to solve this issue.

3.7 Acknowledgement

This research project is supported by the Independent Research Projects of State Key Laboratory of Coal Resources and Safe Mining, CUMT (SKLCRSM15KF01); the Minerals Research Institute of Western Australia (M495); the Mining Education Australia Collaborative Research Grant Scheme (2018); and the computation resources

provided by the Pawsey Supercomputing Centre with funding from the Australian Government and the Government of Western Australia.

4 Minimizing DPM pollution in an underground mine by optimizing auxiliary ventilation systems using CFD

This chapter has been published on Tunnelling and Underground Space Technology. It was entirely written by Ping Chang with the editorial suggestions provided by Dr Guang Xu, Dr Benjamin Mullins and Dr S. Abishek. Please cited it as:
Chang, P., Xu, G., Zhou, F., Mullins, B., Abishek, S., & Chalmers, D. (2019). Minimizing DPM pollution in an underground mine by optimizing auxiliary ventilation systems using CFD. Tunnelling and Underground Space Technology, 87, 112-121.

For the DPM simulation, the previous chapter proofed that the Eulerian-Lagrangian method presented better results than that of species transport method. Thus, this method was applied in this chapter to optimize the auxiliary ventilation system in an underground development face. In this chapter, the onsite experiment was first conducted to obtain the data for the modelling construct. Then the CFD simulation was built to investigate the DPM removal performance of three auxiliary ventilation designs. The optimum auxiliary ventilation system was recommended based on the results.

4.1 Abstract

Diesel particulate matter (DPM) is a carcinogen to humans. Underground miners have the potential to expose to higher DPM concentrations since the working environment is confined. To address the DPM pollution issues and optimize the auxiliary ventilation system, a development face in an underground mine in Western Australia was taken as the physical model and the computational fluid dynamics was used to analyse the airflow characteristics and DPM concentration distributions in the development face. Then, the obtained simulation results were validated with the onsite measurement data. The DPM concentration distributions under 3 scenarios, with different duct lengths, were further compared with the AIOH standard for DPM (0.1 mg/m3). The results found that the current auxiliary ventilation system was not able to reduce the DPM concentration effectively, and the ventilation system with a duct length 5 m longer than the actual duct length provided a better DPM dilution performance. The finding of this paper is helpful for effective DPM control and auxiliary ventilation design for further mining activities.

4.2 Introduction

Diesel-powered equipment is extensively used in the underground mining industry. As a result, tens of thousands of underground miners are exposed to aerosols and gases emitted by diesel engines. Diesel particulate matter is generated due to the incomplete combustion in the diesel engine. It mainly consists of elemental carbon (EC), organic carbon (OC), sulphates and other components (water, ash etc.). Carbon is the main part of the DPM, which accounts for more than 40 % of the total mass and EC occupies about 40 % of the total carbon (HEI, 2002). Due to EC's large proportion of the DPM and few interferences for EC in the underground mines, it has been widely used as a surrogate to measure DPM level (Birch & Noll, 2004; DMP, 2013; JD Noll et al., 2006). Diesel particulate matter (DPM) can pose a very serious health problem. More than 90 % of the

DPM particles' diameter is less than 100 nm (D. B. Kittelson, 1998). Due to these ultrafine characteristics, they can be easily breathed by humans and absorbed in the deepest part of the lungs. Studies showed that both long-term and short-term exposure to high concentration DPM have adverse health effects on humans (Chang & Xu, 2017b; US.EPA, 2002). In 2012, the International Agency for Research on Cancer classified DPM as a carcinogen for humans (Group 1) (Lyon, 2012). This problem is particularly severe for underground miners, who work in confined spaces. Exposure of underground miners to DPM is recognized to be the highest among workers in all occupations, and it is reported that the DPM concentrations in underground mines could be a hundred times higher than the normal environmental concentrations (US.EPA, 2002). Thus, miners' over exposure to DPM has been an increasing concern for the government and mining industries.

The Australian Institute of Occupational Hygienists (AIOH) recommends an 8-hour time-weighted average (TWA) exposure limit of 0.1 mg/m^3 (measured as elemental carbon) for normal underground environments and an action TWA level of 0.05 mg/m^3 for investigation of suitable control strategies (AIOH, 2017). However, it is very challenging for most mines to meet this standard. Currently, many approaches have been used in underground mines to control DPM hazards, which include the usage of bio-diesel, the installation of aftertreatment devices (diesel filter), and the application of environmental cabs and ventilation (DMP, 2013).

Ventilation is still the most popular method for diluting the DPM. In an underground mine development face, a ventilation duct is commonly used for the auxiliary ventilation duty. The distance from the duct face to the heading face may have great impacts on the ventilation performance and DPM dilution efficiency. Generally, the distance should be less than 4 $\sqrt{S}$ to 5 $\sqrt{S}$ (S is the average section area of the development face) (G. Zhang, Tan, Chen, Liu, & Yang, 2007) . If the distance is too far, the airflow may not be strong enough to clear the DPM out of the heading. If the distance is too short, it requires extending the duct frequently which interrupts mining production. For this reason, an economic and effective auxiliary duct design (with optimum duct length) is necessary. Computational fluid dynamics (CFD) can be used for this purpose by visualizing how a different duct length impacts the DPM distribution in the development face.

CFD has been successfully applied in mining engineering research to solve various air and particle flow related problems. Numerous researchers (Geng et al., 2017; Ren et al., 2014; Y. Wang et al., 2015; Z. Wang & Ren, 2013; Yu et al., 2017) used the gas-

solid coupled method to simulate the coal dust dispersion and size distribution characteristics in underground mines, and used the results to optimize ventilation systems for effective coal dust control. Some researchers (Aminossadati & Hooman, 2008; Parra et al., 2006; Sasmito et al., 2013) conducted a number of numerical modelling studies to study the airflow behaviour and optimal ventilation design in underground mines, which helps to evaluate the ventilation performance and harmful gas remove efficiency. Kurnia et al. (Jundika C Kurnia, Agus P Sasmito, et al., 2014a, 2014b; Jundika C Kurnia, Agus P Sasmito, Wai Yap Wong, et al., 2014) studied the hazardous gases' dispersion behaviours and control methods under different ventilation conditions, and based on the simulation results, better ventilation designs were recommended to reduce the hazard effectively. Guang et al. (Xu et al., 2015; Xu et al., 2013) developed a methodology that uses CFD modelling and the tracer gas technique to evaluate and predict the extent of damage in the event of a mine emergency, which helps to manage the incident effectively, and to increase the safety for rescuers. However, the application of the CFD method on DPM studies in underground mines is relatively recent. Zheng et al (Thiruvengadam, Zheng, Lan, & Tien, 2016; Zheng, Thiruvengadam, Lan, & Tien C, 2015; Zheng, Thiruvengadam, et al., 2015a; Zheng, Thiruvengadam, et al., 2015b) conducted a series of CFD studies to depict the DPM dispersion pattern and concentration distribution under various ventilation scenarios. By visualizing the DPM distribution, it assisted in the understanding of DPM movement in underground mines. The results could be used for the selection of ventilation for optimal DPM dilution. In addition, for other industries, CFD approaches have been widely used to study the DPM formation, evolution and dispersion patterns near the vehicle wake region (Chan et al., 2010; Y. Liu et al., 2011), describe the evolution of DPM size distribution around the vehicle tailpipe (P. Jiang et al., 2005) and analyse the indoor DPM concentration and size distribution characteristics from diesel light (Apple et al., 2010). Nevertheless, in most of the DPM studies on mine site, the DPM was treated as a gas flow, which may perform differently with the solid particles. For the other research mentioned above, which considered the DPM as particles, the studies mainly focused on the formation or evolution progress of the DPM near the pipe area. However, few studies concerned the DPM concentration distribution characteristics, especially for the underground mines, thus the DPM dispersion behaviours in underground mines still need to be studied when treat DPM as particles. In addition, a pervious study (Xu, Chang, Mullins, Zhou, & Hu, 2018) on the DPM distributions in an underground mine isolated zone indicated that the simulation results by using the Eulerian- Lagrangian method had a better agreement with

the experimental data than the results which used the species transport model. For this reason, a study on the DPM distribution, especially the diesel particles' movement pattern under different ventilation conditions in the development face, is needed.

The aim of this article is to compare the DPM dispersion and concentration distribution with different ventilation duct positions in an underground development face. The CFD model is built based on a development face that undergoes shotcreting. The actual onsite scenario was modelled first, and the results were validated by comparing the airflow and DPM distribution measurement data. The validated models were used to further investigate the effectiveness of DPM dilution with different auxiliary duct lengths. The Eulerian-Lagrangian approach was used to simulate the gas-solid two-phase fluid. The airflow field characteristics for each scenario were first analysed and the critical areas which may affect the distribution of DPM were determined. Then the effect of 3 different ventilation designs on the DPM concentration distributions were analysed. The DPM concentrations at different locations in the development face for each scenario were compared with the DPM standard (0.1 mg/m^3). High DPM concentration zones were identified for each scenario. Finally, the DPM dilution effects were further discussed and the optimized auxiliary duct length was suggested. The results showed that ventilation through the current duct length was not enough to sufficiently reduce the DPM concentration. The findings in this paper provide a guidance for the selection of auxiliary duct length for further mining activities.

4.3 Model Description

4.3.1 Physical Model and Boundary Conditions

A computational model was built based on the physical conditions of a development face of a mine in Western Australia. The dimensions of the modelled section are labelled in Figure 15. The cross-section areas of the development roadway are uneven due to the rough blasted surface, and the average sectional dimensions are 5.5 m (height) × 6 m (width). Most of the cross-section dimensions are based on simplified data from the mine survey results; the section very close to the face was represented by the average dimension, due to inaccessibility for measurement. A 20.6 m depth cuddy is connected to the development roadway, and the average dimension for this area is 6.5 m (height) × 6 m (width). A 1.2 m diameter duct is used for forced auxiliary ventilation. The centre of the duct is 1.3 m from the side wall and 4.6 m from the floor. To better control the airflow direction from the duct, a part of the duct outlet is closed, as shown in Figure 16. The diameter of the open part of the duct is around 0.6 m. For the actual

scenario, the duct outlet is 15.2 m from the heading (scenario 1), as shown in Figure 15. To study the effects of duct length on DPM distributions, two more scenarios are built with different duct lengths. As mentioned in section 4.2, the distance between the duct outlet and heading should be less than $4\sqrt{S}$ to$5\sqrt{S}$. Thus, the distance should be less than 23.92 ~ 29.9 m. For scenarios 2 and 3, the distance between the duct outlet and heading face are 5 m shorter and longer than scenario 1, which is 10.2 m and 20.2 m, respectively. The model of diesel vehicle used for the shotcreting activity is Normet Spraymec 904. The Spraymec is 8.5 m away from the heading face. The exhaust tailpipe location is marked in Figure 15.

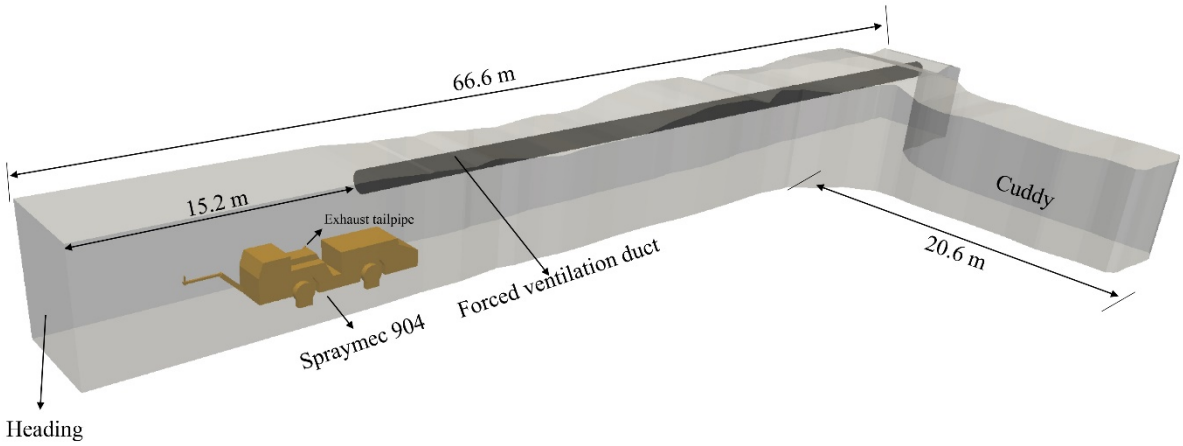

Figure 15 3D view of the CFD model geometry

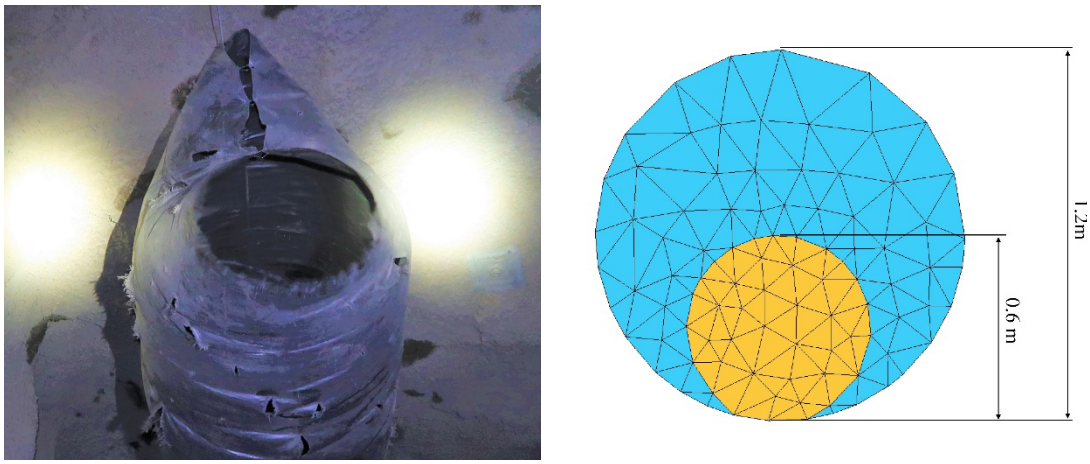

(a) Ventilation duct outlet (b) CFD duct outlet meshing

Figure 16 Actual duct outlet and its meshing in the model

OpenFOAM is a Linux based free and open source software, which has been widely used to solve CFD related issues. There are many solvers available in OpenFOAM to meet different problems in CFD application. OpenFOAM is used for all the simulations

in this study. In the simulations, the air is assumed to be incompressible; no heat-transfer is considered during the study, and gravity is 9.81 m/s^2. The standard $k-\varepsilon$ model (Hu et al., 2016b; Ren et al., 2014; J Toraño et al., 2011; Javier Toraño et al., 2009) is applied to simulate the continuous phase. The airflow was firstly simulated to achieve a steady-state by simpleFoam, after which the flow field was frozen before simulating DPM emissions. According to the actual Spraymec operating time, while conducting the shotcrete activity, the DPM was emitted for 440 s. The movement of particles was solved by DPMFoam. The time step Δt was set to 5×10^{-4} for the particle simulation. Other parameters are given as follows:

(1) No slip wall function is used.

(2) At the duct outlet, airflow rate is set as 21.2 m^3/s (74.93 m/s) based on the onsite measurement, the turbulent kinetic energy and dissipation rate is set as 5.1895 m^2/s^2 and 46.2504 m^2/s^3, respectively, based on the calculation.

(3) At the Spraymec tailpipe, the particle density is set to 1.77×10^3 kg/m^3 (Park et al., 2004); the particle's diameter is set to 78.7×10^{-9} m. According to the DPM emission rate information available from the MSHA's website (MSHA), the DPM emission mass rate is calculated and set to be 1.219×10^{-6} kg/s in the simulation; the tailpipe exhaust flow rate is calculated as 0.358 m^3/s according to "Exhaust Product Guide" (Donaldson).

(4) The density for air is calculated based on the following ideal gas equation:

$$\rho = \frac{PM}{RT} \tag{13}$$

where ρ, P, M, R and T is gas density, pressure, molar mass (0.029 kg/mol), ideal gas constant (8.314 J·mol^{-1}·K^{-1}) and gas temperature, respectively. In this study, the temperatures and pressures at 3 locations in the development face were measured, and the average temperature and pressure are 298.15 K and 103, 908 Pa, respectively. Based on these two values, the average air density was calculated as 1.206 kg/m^3 and used in the simulation.

(5) The average atmospheric pressure is prescribed at the development face outlet with static pressure set to 103,905 Pa.

4.3.2 Governing Equations

The Eulerian-Lagrangian approach (Patankar & Joseph, 2001) is applied to simulate the gas-solid two-phase fluid. The motion of air is governed by the Navier-Stokes equation. The mass conservation and momentum conservation equations of the gas phase are given as follows (Moukalled, Mangani, & Darwish, 2016):

$$\begin{cases} \nabla \cdot \boldsymbol{v_g} = 0 \\ \dfrac{\partial \rho_g \boldsymbol{v_g}}{\partial t} + \nabla \cdot \left(\rho_g \boldsymbol{v_g} \boldsymbol{v_g}\right) = -\nabla p + \nabla \cdot \boldsymbol{\tau} + \rho_g \boldsymbol{g} \end{cases} \tag{14}$$

where ρ_g, $\boldsymbol{v_g}$ and $\boldsymbol{g}$ is the gas density (air), gas velocity and gravitational acceleration, respectively. $\boldsymbol{\tau}$ is the viscous stress tensor and is given by:

$$\boldsymbol{\tau} = \mu\left(\nabla \boldsymbol{v_g} + \left(\nabla \boldsymbol{v_g}\right)^T\right) - \frac{2}{3}\mu\left(\nabla \cdot \boldsymbol{v_g}\right)\boldsymbol{I} \tag{15}$$

where μ and **I** are the molecular viscosity and unit tensor, respectively. In this study, the governing equations for the gas phase are solved by the SIMPLE algorithm. The numerical scheme for the convective derivatives is Gauss LinearUpwind (second order).

The Lagrangian particle tracking approach is used to track the trajectories of DPM. In this method, the motion of particles is governed by Newton's second law. Only drag force, gravity, pressure gradient force, lift force and the turbulence dispersion effects on particles are considered because other forces are considered not significant enough to affect the particle's motion (Hu et al., 2016b; Ren et al., 2014). The governing equation is given by:

$$m_p \frac{d\boldsymbol{v_p}}{dt} = m_P \boldsymbol{g} + \boldsymbol{F_d} + \boldsymbol{F} \tag{16}$$

where m_p, $\boldsymbol{v_p}$ is the particle mass and particle velocity, respectively. $\boldsymbol{F}$ is the sum of pressure gradient force, lift force and the turbulence dispersion effects on particles. $\boldsymbol{F_d}$ is the drag force, which is expressed as:

$$\boldsymbol{F_d} = \frac{3}{4}\frac{C_d Re}{d_p}|\boldsymbol{V_r}|\boldsymbol{V_r} \tag{17}$$

where Re and d_p is the Reynolds number and particle diameter, respectively. V_r is the relative velocity between particles and the gas phase, which is defined as $\boldsymbol{V_r} = \boldsymbol{v_p} - \boldsymbol{v_g}$. C_d is the drag coefficient, which is expressed by:

$$C_d = \begin{cases} \dfrac{24}{Re \cdot C_c} & Re \leq 1 \\ \dfrac{24(1 + 0.15Re^{0.687})}{Re} & 1 < Re \leq 1000 \\ 0.44 & Re > 1000 \end{cases} \tag{18}$$

where C_c is the Cunningham slip correction factor, which is expressed by

$$C_c = 1 + \frac{\lambda}{d_p}\left(2.514 + 0.8e^{\frac{-0.55d_p}{\lambda}}\right) \tag{19}$$

where λ is the mean free path of gas molecules, 68 nm is used based on the operation condition in this study.

4.3.3 Mesh Independence Study

A mesh independence study is conducted to ensure that both the accuracy and computation cost are within acceptable ranges. For scenario 1, three types of mesh, coarse, medium and fine mesh, are used for the mesh independence study. The total number of cells for different meshes are about 0.75 million, 1.57 million and 2.2 million. A hybrid mesh is used for the model. For the complicated geometry region near the heading face where the Spraymec is located, tetrahedral meshes are generated, while hexahedral meshes are used for the rest of the model. The overall quality of the meshes is above 0.3, the maximum non-orthogonality angle is below 70 degrees, and the maximum skewness is less than 3.5. The size of the mesh was increased two times by increasing the nodes number $\sqrt[3]{2}$ times on all three dimensions for the hexahedral mesh. For the tetrahedral mesh, the total number of mesh increased by decrease the maximum size of the cell. Such mesh qualities are acceptable for the solvers in OpenFOAM. The thickness of the first layer of the mesh is set as 0.017 m based on the calculation of $y+ \approx 30$. The height growth ratio of the layer is 1.2. A representative mesh is shown in Figure 17(medium mesh).

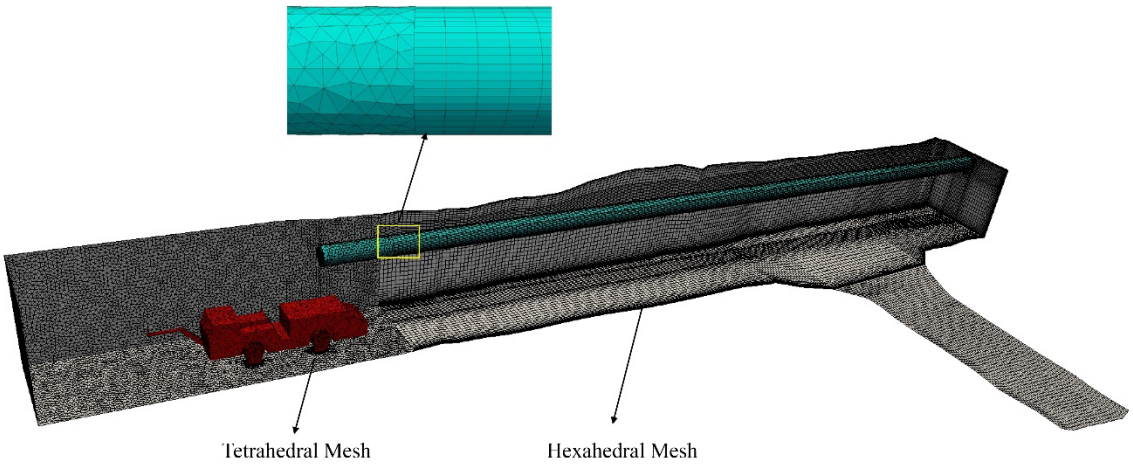

(a) Overview of the hybrid meshes

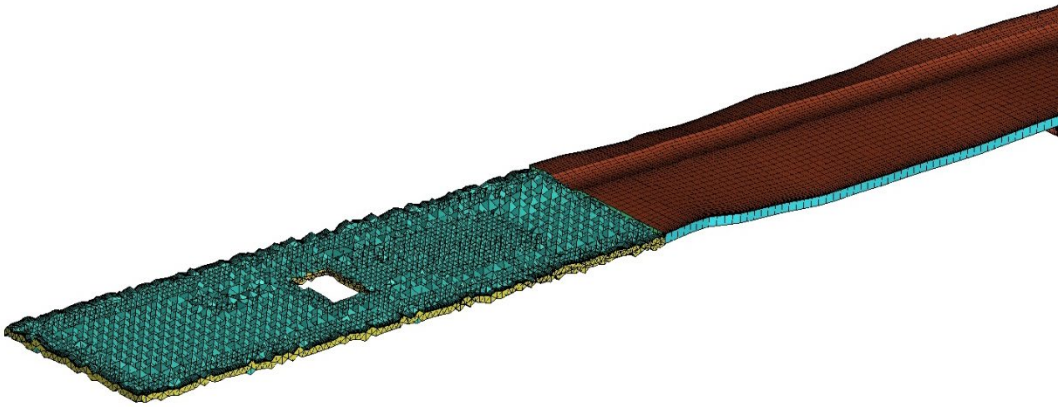

(b) Volume mesh distribution near the Spraymec
Figure 17 Overview of medium mesh

Air velocity profiles for three line monitors at different locations are compared. Line 1 and 2 are at the horizontal centreline 5 m and 30 m from the heading face, respectively, and line 3 is at the horizontal centreline 13 m from the cuddy heading face, as illustrated in Figure 18. Figure 19 depicts the air velocity profiles for different meshes. It is observed that the velocities of the medium mesh are highly matching that of the fine mesh. The root mean square deviation (Xu et al., 2016) is used to calculate the velocity difference at three line monitors among three sizes of mesh. The velocity differences between coarse mesh and medium mesh, medium mesh and fine are listed in Table 6. As can be seen, the velocity difference between medium mesh and fine mesh is less than 2%, which demonstrates that mesh independence has been achieved by using the medium mesh. Thus, the medium mesh is used in further simulations. Similar parameter setups for the mesh used in scenario 1 were used to generate the meshes for simulation scenario 2 and 3.

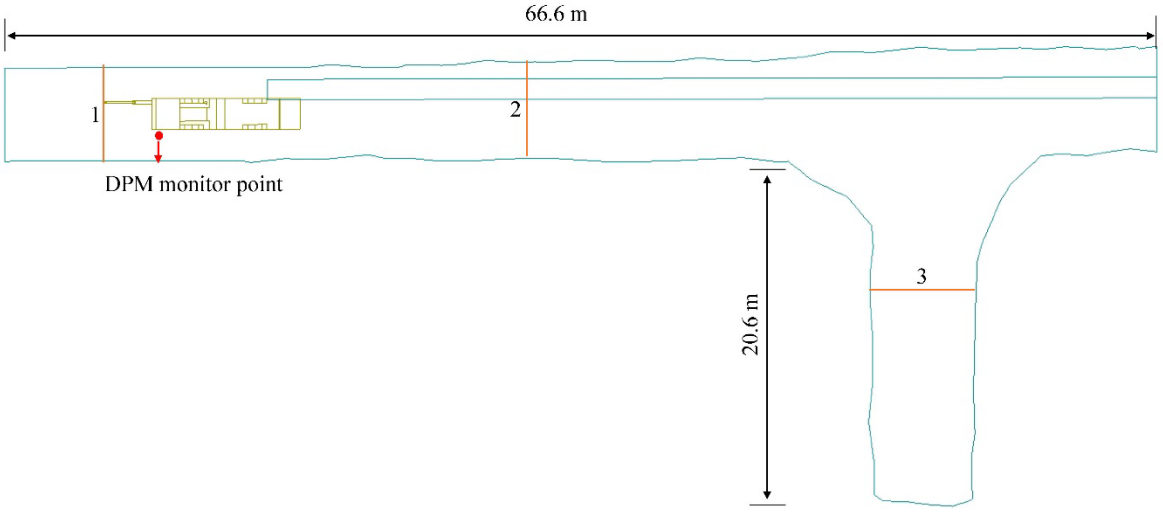

Figure 18 Position of monitor lines

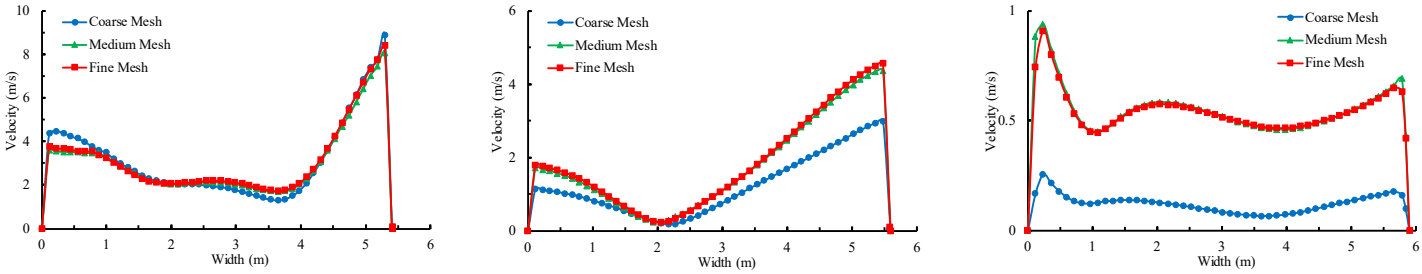

(a) Line 1 (b) Line 2 (c) Line 3

Figure 19 Velocity profile comparison for different meshes

Table 6 Velocity difference between medium mesh and other mesh at three line monitors

	Line 1	Line 2	Line 3
Coarse mesh	12.82%	48.62%	18.60%
Medium mesh	-	-	-
Fine mesh	1.73%	0.59%	0.05%

4.3.4 Model Validation

To ensure model accuracy, the simulated airflow field and DPM simulation were validated with onsite measured results. In this study, the velocity at 9 points on a cross-section 44.5 m away from the heading face was measured using an electronic velometer. The location of the points is shown in Figure 20. For each point, 10 velocity values were measured in 1 minute and the averaged value was used to compare with the CFD result. Table 7 shows the velocity at each point and the error compared to the measured data. As can be seen, the maximum discrepancy is at P7, with an error of 37.84%. However, the average error between the measured data and CFD results is less than 15%. When measuring the air velocity, the position of the velometer was estimated, which may not

be the exact same designed positions. Thus, may results in difference when compared to the simulation data. For this reason, the simulation results are taken as acceptable.

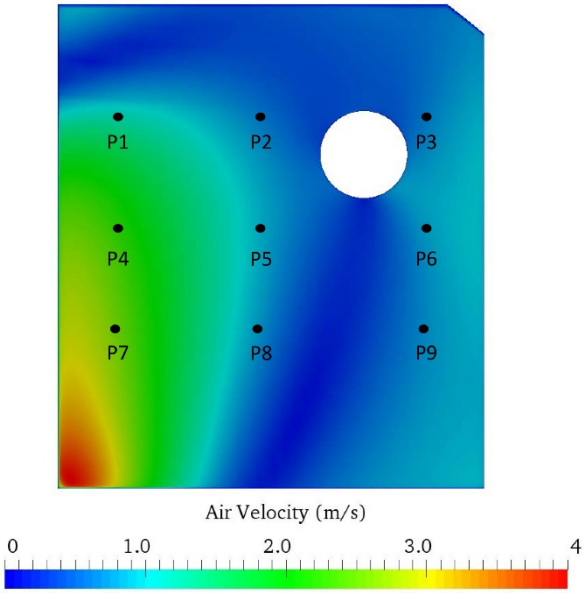

Figure 20 Velocity contour at cross section 44.5 m from the heading face

Table 7 Comparison between CFD results and measured data

Point number	P1	P2	P3	P4	P5	P6	P7	P8	P9
Measured data (m/s)	0.92	0.79	0.44	2.05	1.82	0.91	1.61	0.35	0.56
CFD results (m/s)	0.91	0.64	0.44	2.35	0.89	0.87	2.59	0.38	0.67
Error	1.10%	23.44%	0%	12.77%	7.87%	4.60%	37.84%	7.89%	16.42%

To validate the accuracy of the gas-solid coupled model, the real-time DPM concentrations on site were monitored and compared with the simulation result for scenario 1. The actual DPM concentrations were measured by an Airtec Diesel Particulate Monitor from FLIR® as shown in Figure 21. A default airflow rate of 1.7 L/min was used for the pump of the Airtec DPM monitor. This monitor is highly correlated with the NIOSH 5040 method and is able to provide real-time and TWA DPM concentration data. The sensitivity of the monitor is less than 15 µg/m^3 EC and the average bias between the Airtec monitor and NIOSH 5040 was less than 8.5% based on a previous study (JD Noll & Janisko, 2013). Due to the limitation of actual experimental field conditions and the limited available monitor, only the DPM concentrations of one point at the right front outside the Spraymec operator cabin were measured, as shown in Figure 18.

To compare the simulation data with the field measured data, the DPM concentration at 1 point in the same position as the monitor was selected. For the onsite experiment data, 5 sample point average data was used and the data collecting time

interval was 1 min. The comparison between the simulation results and field measured data is shown in Figure 22. As can be seen in Figure 22 (a), except for the data at 3 min, the field measured data and the simulated result shows a consistent trend. The mean difference between them is 23.37%. There may be a couple of reasons for the discrepancy. First, the experiment circumstance at the underground mine is complicated, which may generate unstable airflow near the monitor, thus affect the accuracy of the measurement. Second, during the measurement, the monitor was worn on the operator's uniform and the operator is not stationary, which causes the measurement of locations other than what had been compared in the model. Figure 22 (b) gives the correlation of DPM concentration between CFD data and measured data (exclusive of the data at 3 min). As can been seen the CFD data has a great agreement with the measured data, and the R^2 coefficient is 0.8222. Thus, the discrepancy between the actual and simulated results are considered acceptable taking all of the above factors into account.

Figure 21 Airtec Diesel Particulate Monitor

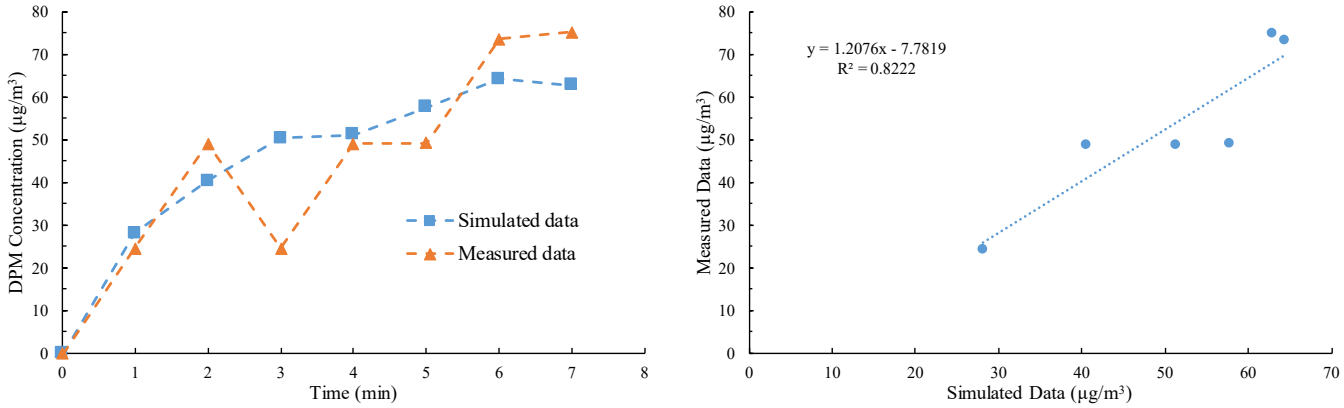

(a) DPM data comparison (b) DPM concentration correlation

Figure 22 Comparison between measured data and simulated data

4.4 Result and Discussion

4.4.1 Airflow Field

The DPM dispersion and concentration distributions are highly influenced by the airflow behaviour. With the different distances between the duct outlet and heading face, the airflow behaviour in the development face varies. And the position and size of the vortex play major roles in affecting the DPM accumulation. Thus, it is important to understand the airflow characteristics under different scenarios. Figure 23 shows the airflow streamlines around the Spraymec for the three simulated scenarios. The vortex areas in the airflow field, where the DPM may accumulate, were determined based on the simulation results. As can be seen, the airflow at the heading face is highly affected by the high-velocity air from the duct. The high-velocity air was emitted from the duct outlet and migrated towards the heading face, and the airflow direction reversed after hitting the heading face. Then a vortex area between the heading face and the duct head is generated for all scenarios due to the combined effect of the opposite direction airflow and the airflow from the duct. For scenario 1, the vortex was located between the Spraymec and the heading face. With the extension of the duct position, the vortex area decreased, as shown in scenario 2 (Figure 23 (b)). On the contrary, the vortex area expanded to the Spraymec with the increase of the distance between heading face and duct head, which is illustrated in Figure 23 (c). It seems that a greater distance between the duct outlet and the heading face results in a larger vortex zone. Due to the circulation of the airflow in vortex areas, these areas may be dangerous since the DPM accumulates in them.

To further analyse the airflow characteristics in the development face along the horizontal direction, the airflow velocity vectors at 3 m height from the floor are presented in Figure 24. The position of the vortex and low air velocity zones were observed. It is clearly seen that the extent of the vortex region for scenario 1, 2 and 3 is 0-6 m, 0-3 m and 0-12 m away from the heading face, respectively. The vortex area expands with an increase in the distance between the duct outlet and the heading face. For scenario 1 and 2, another vortex was generated just behind the Spraymec. Behind the Spraymec, the high-velocity zone was located at the non-duct side of the development face for scenario 1. Several small vortices formed under the duct and the airflow velocity at these areas was quite low. Therefore, the DPM had a high potential to accumulate in them. The airflow distribution in scenario 2 is more complex than that of scenario 1. As shown in Figure 24 (b), there were 3 big vortices in the roadway. Due to the complex airflow distribution, the DPM was hardly removed by the airflow for scenario 2. For scenario 3, two vortices were located 2-17 m away from the Spraymec. The airflow distribution in other areas behind the Spraymec was similar to scenario 1. In the cubby,

the airflow distribution for the 3 scenarios was similar. Several large vortices were generated in this area.

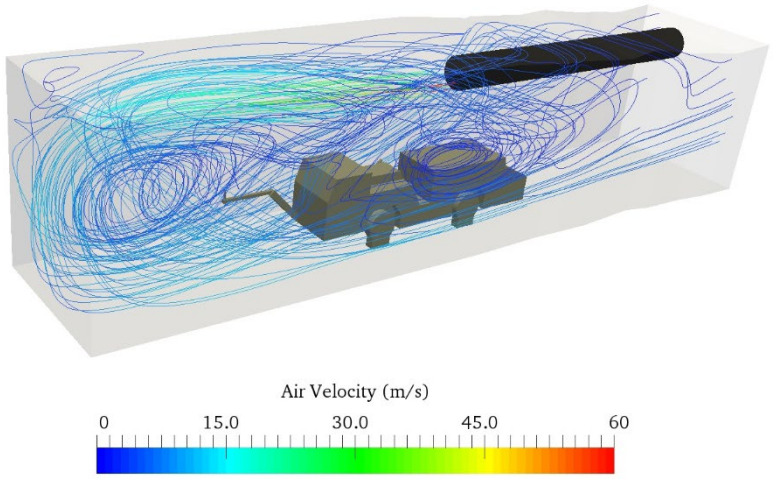

(a) Scenario 1 (15 m)

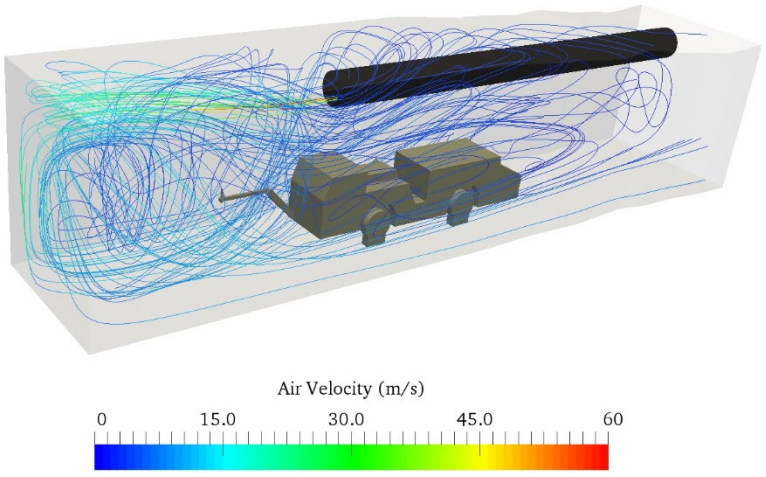

(b) Scenario 2 (10 m)

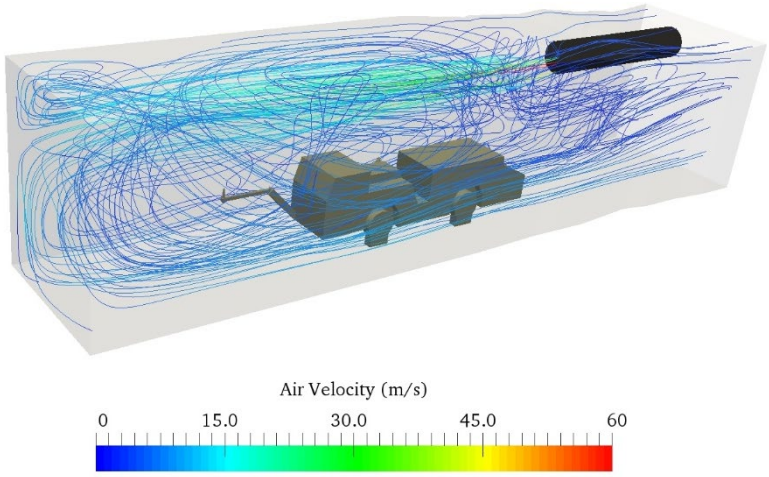

(c) Scenario 3 (20 m)

Figure 23 Airflow velocity distribution for different duct to face distances

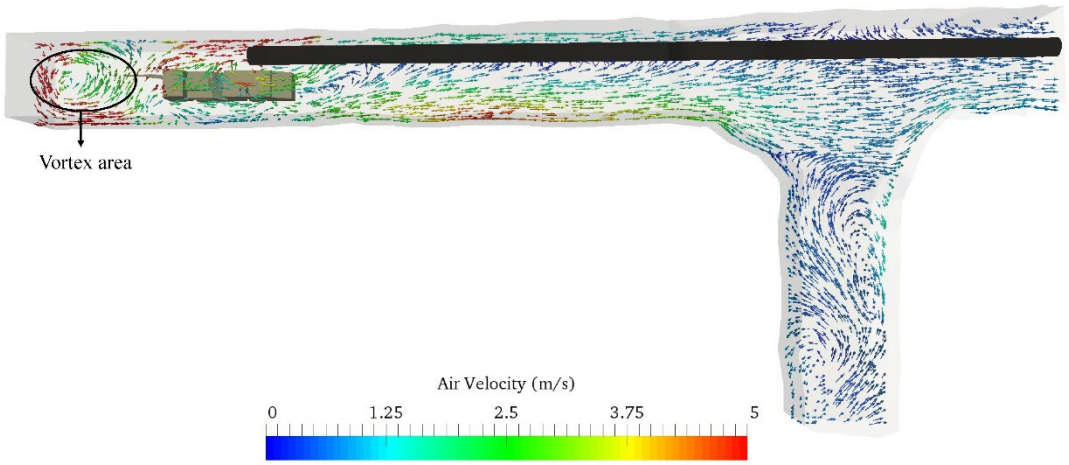

(a) Scenario 1 (15 m)

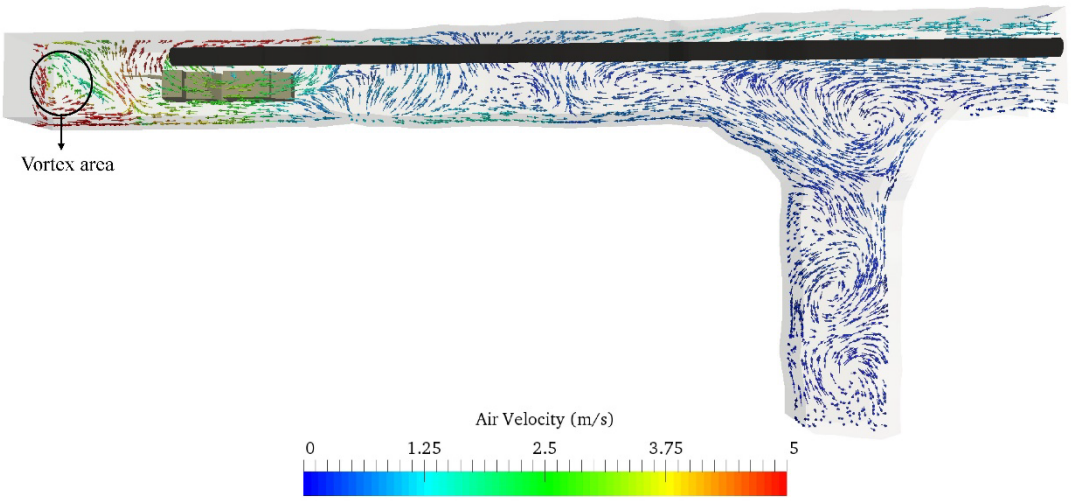

(b) Scenario 2 (10 m)

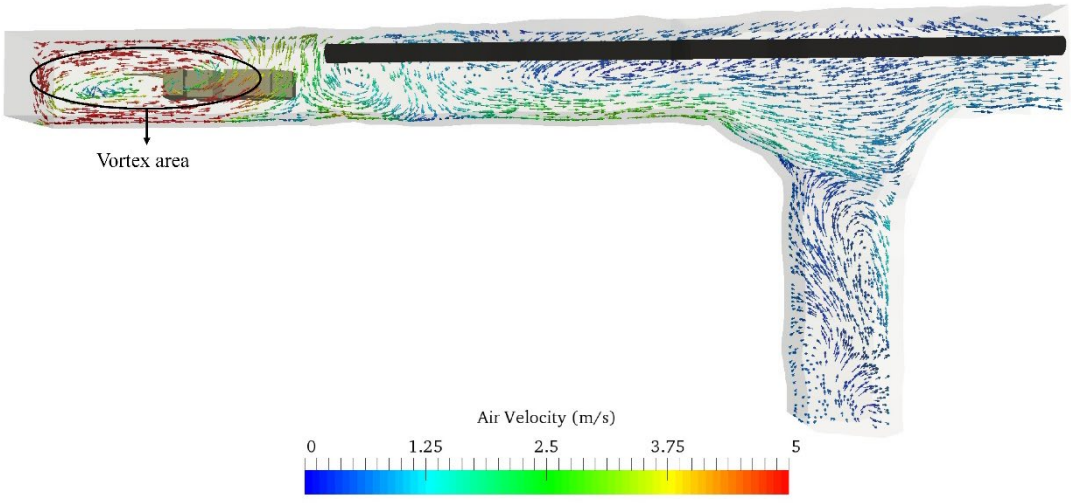

(c) Scenario 3 (20 m)

Figure 24 Airflow velocity vectors at plane 3 m height above the floor

4.4.2 DPM Distribution

The DPM distributions at the final state (440 s) of the simulations for the 3 scenarios are presented in Figure 25. The red colour in the planes indicates DPM concentrations greater than 100μg/m^3. In the left column of Figure 25, the vertical cross-sectional plane is 3.5 m from the duct-side wall; the horizontal cross-sectional plane is 3 m high from the floor. For the figures in the right column of Figure 25, the cross-sectional planes are selected every 4 m.

As expected, the DPM accumulation occurs in the vortex areas and low airflow velocity zones. Due to the recirculated airflow in the vortex areas, the DPM is hardly able to escape from the vortices. The DPM diffuses much slower in the low air velocity zones than in the high velocity zones, thus high DPM concentration zones are generated in these low velocity areas. For all the scenarios, less DPM is carried into the cuddy according to the main airflow direction in the roadway.

For scenario 1, it is observed that a high DPM concentration area formed at the front of the Spraymec about 3 m from the heading face due to the existence of a vortex in this area. It is also noticed that DPM accumulates around the Spraymec. According to the airflow distribution, there is a small vortex area around the tailpipe and a low airflow velocity zone just behind the Spraymec, as shown in Figure 24 (a). The existence of these areas results in the DPM accumulation. With the DPM migration with the airflow in the roadway, the DPM flows toward the outlet of the roadway in the airflow direction but accumulates at the ventilation duct side in the tunnel due to the low airflow velocity in this area. This area reduces gradually with the DPM diffusion with the airflow.

For scenario 2, the DPM mainly concentrated in 3 areas. One is at the front of the Spraymec, about 0-5 m away from the heading face, where the vortex is located. The second high DPM concentration zone occurs around the tailpipe, as shown in Figure 25 (b). Compared to scenario 1, both of the two areas are smaller due to the different size of the vortex area. The third high DPM concentration area is located at 30 m to 38 m away from the heading face. This is different from scenario 1, less DPM accumulates just behind of the Spraymec. Due to the formation of the vortex, it is relatively difficult for the DPM to escape from this area.

For scenario 3, although there is a large vortex at 0-12 m from the heading face, no DPM concentrated in this area. The DPM concentrated around the tailpipe of the Spraymec and then was diluted by the airflow before it reconcentrated at around 25-32 m away from the heading face at the duct side of the roadway, due to a low velocity vortex area. Then the DPM migrated to the outlet of the roadway and resulted in a reduction in the DPM concentrations.

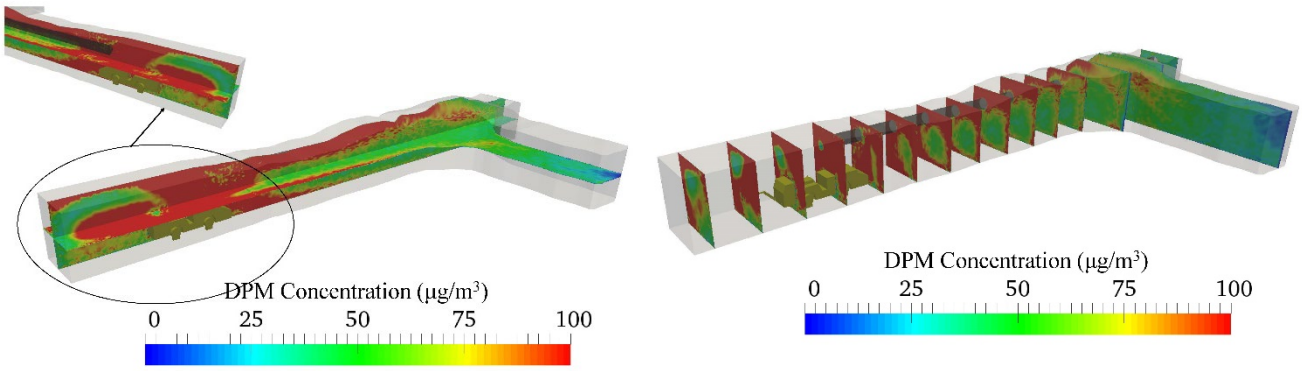

(a) Scenario 1 (15 m)

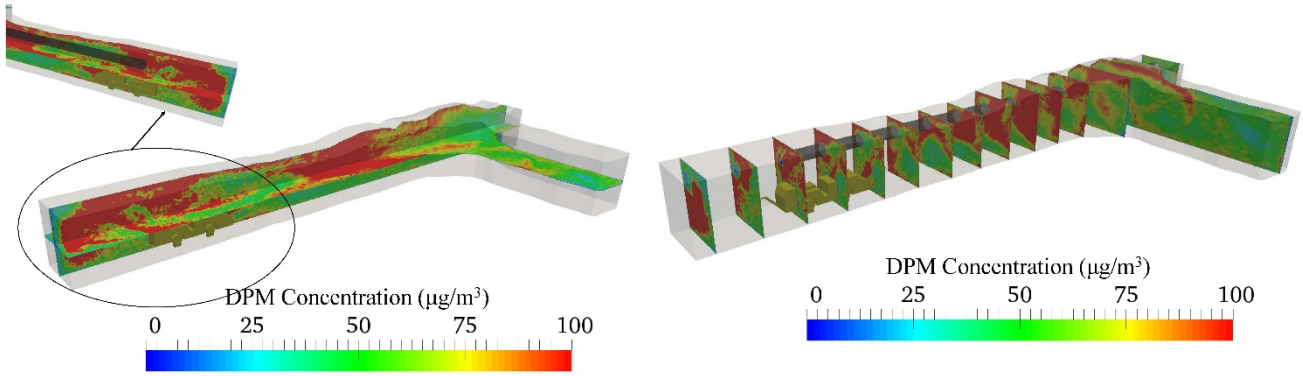

(b) Scenario 2 (10 m)

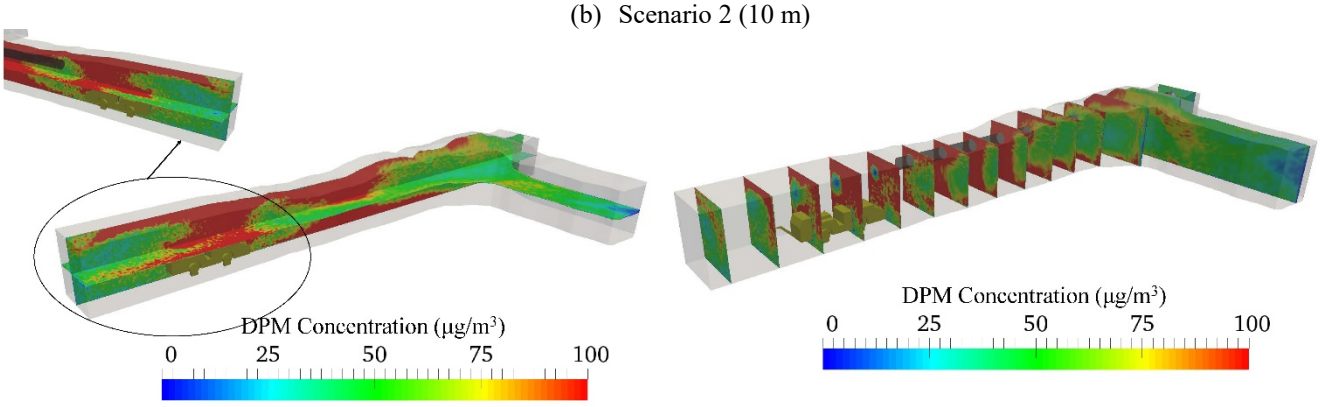

(c) Scenario 3 (20m)

Figure 25 DPM concentration distribution at horizontal and vertical cross-sectional planes

To further analyse the performance of each ventilation system for the 3 scenarios, the area-weighted average DPM concentration at different cross-sectional planes are presented against the distance from the heading face in Figure 26. It is clearly seen that scenario 1 gives the maximum average DPM values among the 3 scenarios, and scenario 2 provides the best DPM dilution performance.

For scenario 1, the DPM concentrations between 3 m and about 40 m away from the heading face exceed the standard limit. The maximum DPM concentration occurs 12 m away from the heading face, which is about 160 µg/m^3. For the area from 8.5 m to 17 m, where the Spraymec is located, the average DPM value is about 135 µg/m^3. The miners who work in this area should be given extra protective equipment to avoid the potential hazard from the high concentration DPM. The DPM concentrations for

scenario 2 are much lower than the other two scenarios. Similar to scenario 1, the DPM values peak at 12 m, where the Spraymec tailpipe is positioned. Except for this, another two high DPM values should be noted, which are both located around 35 m away from the heading face with concentrations slightly above the standard limit at around 103 $\mu g/m^3$. In addition, from around 2 m to 6 m away from the heading face, the DPM concentrations are relatively high due to the vortex, but the maximum value in this area is still below the limit. In general, for scenario 2, the DPM concentrations at most of the areas remain at a safe level. The DPM value for scenario 3 shows a "double hump" distribution. Except for the tailpipe region, the other high DPM concentration area is located at 32 m from the heading face, with a DPM value of around 136 $\mu g/m^3$. One possible reason for the high concentration is the existence of a vortex at this area. Although the dangerous zone for scenario 3 is smaller than that for scenario 1, the miners still have a high risk of exposure to a high concentration DPM in the main activity area (around the Spraymec), thus extra protective equipment should be given. With the DPM diffusion in the airflow, the DPM concentrations decrease gradually after 38 m and reach a stable level at around 50 $\mu g/m^3$ at the outlet of the roadway. Overall, the average DPM values are greatest for scenario 1 and least for scenario 2. Although the highest values for scenario 2 still exceed the limit of 100 $\mu g/m^3$, it is worth noting that the values are all around 103 $\mu g/m^3$, which are quite close to the limit and the DPM concentrations are in a safe range for most of the areas. From the DPM concentration comparison of the 3 scenarios, it seems that scenario 2, with the duct outlet 10.2 m from the heading face, gives a better DPM dilution.

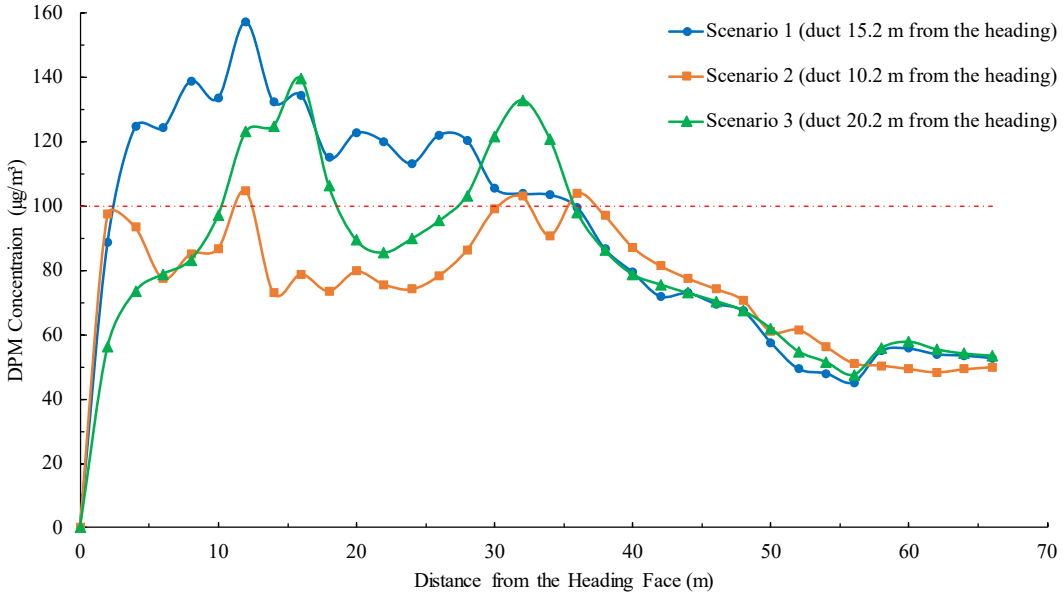

Figure 26 Area weighted average DPM concentrations at different cross-sectional planes

4.5 Conclusion

A computational study has been conducted to evaluate the DPM distribution behaviour in an underground development face under different ventilation designs for the shotcreting activity. Three different ventilation scenarios were created with the duct outlet 15.2 m, 10.2 m and 20.2 m away from the heading face, respectively. The performance of different ventilation designs on the DPM dilution was evaluated. The motion of airflow and DPM were solved by the Eulerian-Lagrangian method.

The results showed that a vortex region formed between the Spraymec and the heading face and this region became larger for shorter duct length. DPM accumulated in this zone. Scenario 1 (duct 15.2 m from the heading face) gave the highest average DPM concentrations of the 3 scenarios. The highest concentration zone occurred around the Spraymec and expanded to the middle area of the tunnel. Based on the DPM distribution, the section within 40 m away from the heading face should be given extra attention under current ventilation design (scenario 1). Scenario 2 (duct 10.2 m from the heading face) presented the lowest average DPM concentrations among the 3 scenarios. For most of the areas, the average DPM concentrations are lower than the limit of 100 $\mu g/m^3$. Although the concentrations for some areas were still high, these concentrations were quite close to the limit. For scenario 3 (duct 20.2 m from the heading face), the DPM concentration in two regions exceeded the limit. One is 10 to 19 m away from the heading face, which is also the location of the Spraymec. The other one is 28 to 36 m away from the heading face. It is advisable to provide personal protective equipment, masks for example, to the miners who work in this area.

In total, current ventilation design (duct 15.2 m from the heading face) cannot dilute the DPM effectively in the development anywhere. However, the ventilation design in scenario 2 (duct 10.2 m from the heading face) provides the best performance on DPM dilution. Although only 3 scenarios were investigated, it is apparent that a short distance between the duct outlet and heading face results in a better DPM control based on current research. More scenarios with different duct positions should be studied to draw a solid conclusion. However, the results in this study could still be used as a reference for optimal ventilation design. For the further research, more ventilation designs (distance between 10.2 m 15.2 m) will be studied to find out a proper auxiliary ventilation design (with the longest distance between the duct outlet and heading face) which could keep the DPM concentration below the limit.

4.6 Acknowledgement

This research project is supported by the Independent Research Projects of State Key Laboratory of Coal Resources and Safe Mining, CUMT (SKLCRSM15KF01), the Minerals Research Institute of Western Australia (M495), the Mining Education Australia Collaborative Research Grant Scheme (2018), and the computation resources provided by the Pawsey Supercomputing Centre with funding from the Australian Government and the Government of Western Australia.

5 Comparison of underground mine DPM simulation using discrete phase and continuous phase models

This chapter has been published on Process Safety and Environmental Protection. It was entirely written by Ping Chang with the editorial suggestions provided by Dr. Guang Xu, Dr. Benjamin Mullins and Dr. S. Abishek. Please cite it as:
Chang, P., Xu, G., Zhou, F., Mullins, B., & Abishek, S. (2019). Comparison of underground mine DPM simulation using discrete phase and continuous phase models. Process Safety and Environmental Protection, 127, 45-55.

Chapter 3 and 4 illustrated that the Eulerian-Lagrangian model was an accurate method to present the DPM behaviours in underground mines. However, this method is more computational expensive than species transport. To find out the best simulation method for DPM simulation, this chapter compared three commonly used numerical models for contaminant simulations. The advantages and disadvantages for each model were compared and the applicability was recommended according to different situations.

5.1 Abstract

Diesel particulate matter (DPM) is carcinogenic to humans. DPM concentrations in underground mines are much higher than other working environments, thus pose substantial health threats to miners due to overexposure. Computational fluid dynamics is commonly used to study the DPM dispersion and assess the concentration distribution in various working environments. However, most such studies for underground mines treated DPM as a continuous phase (gas phase) in the model. DPM is a solid discrete phase, and its behaviours could be quite different from that of gaseous contaminants. This study compared DPM concentration distributions by using three modelling methods: the Eulerian-Lagrangian method and the Eulerian-Eulerian method that treats DPM as discrete phase particles, and the species transport method that treats DPM as a continuous phase gas. The model was based on a typical underground mine development face with a forcing auxiliary ventilation setup. It was found that the general DPM concentration distribution for the three numerical methods was similar for simple geometry with more uniform flow regions. However, large discrepancies existed in the development heading with complex geometry and flow features. The findings suggest that when simulating DPM, although the species transport method can provide relatively accurate results with much less computational time, the parameters of the modelled gas need to be carefully calibrated to get a better simulation result. For key areas where the diesel machinery and miners are usually located, the Eulerian-Lagrangian method should be used for more accurate analysis.

5.2 Introduction

Diesel particulate matter (DPM) is generated by diesel equipment due to incomplete combustion. The increased use of diesel equipment in underground mines has put the miners under the threat of overexposure to DPM. It was found that the exposure to DPM in underground mines is hundreds of times more than other environments where the use of diesel equipment is common (US.EPA, 2002). More than 90% of the DPM particles'

diameter is less than 0.1 μm, which can easily enter the deepest part of human lungs and result in adverse health effects (D. B. Kittelson, 1998; NIOHS, 1988). Many research projects have indicated that both short-term and long-term DPM exposure has adverse health effects on human beings, such as irritation, cough, light headiness, and even lung cancer (Attfield et al., 2012; Chang & Xu, 2017a; Silverman et al., 2012; US.EPA, 2002; Vermeulen et al., 2014). In 2012, the International Agency for Research on Cancer (IARC) classified DPM as carcinogenic to humans (Group 1) (Lyon, 2012).

A general time-weighted average (TWA) exposure limit of 0.1 mg/m^3 (measured in elemental carbon) is used in most countries, and the Australian Institute of Occupational Hygienists (AIOH) even proposed an action level of 0.05 mg/m^3 in the latest position paper (AIOH, 2017). However, these limits are challenging to meet in most mines. Currently, ventilation dilution is the main approach to control DPM (DMP, 2013; Robert A. Haney, 1997). However, solely relying on the main ventilation system to reduce DPM concentration may require an unpractical air flow quantity to dilute DPM below the acceptable limit. A report (DMP, 2013) showed that the required air quantity could be 6 to 8 times greater than the current ventilation in most mines to adequately maintain DPM below the recommended limit. This cannot be practically achieved due to the facility and economic restrictions. The development and production headings are generally where most mining activities occur, and thus these locations have higher DPM levels. Optimised auxiliary ventilation is an effective control measure, which can be achieved by studying DPM distribution and dispersion characteristics, and identifying high DPM concentration zones in such areas. Usually, DPM concentration at a specific position can be easily measured by the DPM monitor. The concentration limit of 0.1 mg/m^3 is required in the underground mines. However, when a diesel vehicle is working in the development heading, it is not safe to measure the DPM concentration around the vehicle. Besides, the concentrations at multiple locations are needed to study the DPM distribution characteristics. In this situation, the DPM measurement would be time-consuming and non-cost-effectively. With the development of computer technology, computational fluid dynamics (CFD) could be an economic and high-efficiency method to simulate the DPM distribution and address the high DPM concentration areas. Based on the simulation results, protective measures could be applied to reduce DPM concentration and protect the miners' health.

Computation Fluid Dynamics (CFD) is widely used in the mining-related researches due to its effective, economic and high accuracy. J. Cheng et al. (2016) used the CFD modelling to optimise the underground ventilation for gas control and fire

preventing purpose and the optimizing ventilation parameters were suggested to ensure the mining safety; H. Wang et al. (2018) evaluate the air curtain dust suppression effectiveness by adjusting the air flow parameters in an underground rock tunnel, the air parameters for the best dust dispersion performance were recommended based on the simulation results; X. Liu et al. (2018) compared two auxiliary ventilation systems in an excavation face by the CFD simulation and the results showed that a vortex ventilation system gave a better dust collection performance; G. Zhou et al. (2017) analysed the respirable dust diffusion behaviours by CFD and the effective dust control measures were provided based on the results. Currently, three methods are commonly used for DPM simulation: the species transport method (STM), the Eulerian-Lagrangian method (ELM), and the Eulerian-Eulerian method (EEM). The STM treats DPM as a gas phase, and a substitute gas is generally used to represent the diesel exhaust particles. Jundika C Kurnia, Agus P Sasmito, Wai Yap Wong, et al. (2014) conducted a study by the usage of the STM to evaluate the performance of different ventilation systems to control DPM and other hazardous gases. Zheng and co-authors (Thiruvengadam, Zheng, Lan, et al., 2016; Zheng et al., 2011a; Zheng, Lan, Thiruvengadam, Tien, & Li, 2017; Zheng, Thiruvengadam, Lan, & Tien C, 2015; Zheng, Thiruvengadam, et al., 2015a; Zheng, Thiruvengadam, et al., 2015b) also used this method to analyse the DPM dispersion characteristics and concentration distribution in underground mines under different scenarios. However, the ultrafine DPM is a solid phase, and its behaviours could be quite different from that of gaseous contaminants (DMP, 2013). Both ELM and EEM treat particles as a solid phase and are used for the gas-solid two-phase flow in CFD simulation. The ELM considers the particles as a discrete phase; while the EEM treats the particles as a continuous phase. Uhrner et al. (2007) used a coupled Eulerian-Eulerian simulation method to study the DPM formation and growth in the exhaust pipe at two different vehicle operating conditions. Xu et al. (2018) investigated the DPM concentration distribution in an underground mine isolated zone by using ELM. They compared the simulation results with a study that used the STM method and found that the ELM simulation results have better agreements with the experimental measured data.

Previous studies have also compared the EEM and ELM methods. Vegendla et al. (Vegendla, Heynderickx, & Marin, 2011) applied these two methods to simulate dilute gas-solid riser flow and compared with the experimental data. They found a better agreement with the experimental results by applying the ELM. Chiesa et al. (Chiesa, Mathiesen, Melheim, & Halvorsen, 2005) studied the particles behaviour of a lab-scale fluidized bed by using these two methods. The results from both approaches showed a

similar pattern with the experiment, but the ELM gave a better agreement with the experiments. A similar study was conducted by De Jong et al. (De Jong, Dang, van Sint Annaland, & Kuipers, 2012). Both approaches gave well results compared with the experimental data. The above studies showed that the two methods illustrated a similar result, but ELM performed slightly better with a closer agreement to the experimental data.

The literature review illustrates that there are mainly three numerical methods, STM, ELM, and EEM, are used to study the particle contaminant behaviours. However, no study is conducted to compare the difference between the three methods in mimicking the DPM. As the simulation results are significantly dependent on the selected numerical methods, it is important to understand their impact to the results and the advantages and disadvantages of each method in order to select the proper method for DPM simulation. The aim of this paper is to compare the difference of simulation results by applying different numerical methods when simulating DPM in an underground mine development heading. When it is treated as a gas, the STM is applied and n-octane (C_8H_{18}) and SF_6 are used to represent DPM. C_8H_{18} has been used in other studies (Thiruvengadam, Zheng, Lan, et al., 2016; Zheng et al., 2011a; Zheng, Thiruvengadam, Lan, & Tien C, 2015; Zheng, Thiruvengadam, et al., 2015a; Zheng, Thiruvengadam, et al., 2015b) to represent DPM in CFD modelling. SF_6 is an ideal tracer gas because it is non-toxic, odorless, inert and it can be detected even in low concentration. It has been widely used to represent the hazard gases in industries (Boadi & Wittenberg, 2002; Kilgallon et al., 2017; Wilhelm, Seibt, Bich, Vogel, & Hassel, 2005). Thus, it can possibly be used to study DPM flow behaviour in underground mines. When the DPM is treated as discrete particles, the EEM and ELM approaches are used. The CFD model is constructed based on a typical conceptual mine development heading. The difference in the simulation results by using different numerical methods are further compared and analysed. The proper numerical method for the DPM simulation is suggested based on the results.

5.3 Model Description

5.3.1 The Development Heading

A main roadway with a development heading conjunction is the most common used tunnel shape on the mine site and it has been widely used in many related CFD studies as the physical model for different objectives (Aminossadati & Hooman, 2008; Sasmito et al., 2013; Zheng, Thiruvengadam, et al., 2015b). Thus, for the purpose of this study, a

conceptual mine development heading is used as the prototype (Figure 27). A load haul dump truck (LHD) works in a 3.6 m (height) × 2.7 m (width) development heading. The model of the LHD used is Caterpillar R1500 LHD, which is assumed to work at the highest exhaust emission rate. A 0.8 m diameter ventilation duct is used for forcing auxiliary ventilation. The outlet end of the duct is 4.7 m from the development face, and the centre of the duct is 0.675 m from the side wall and the roof.

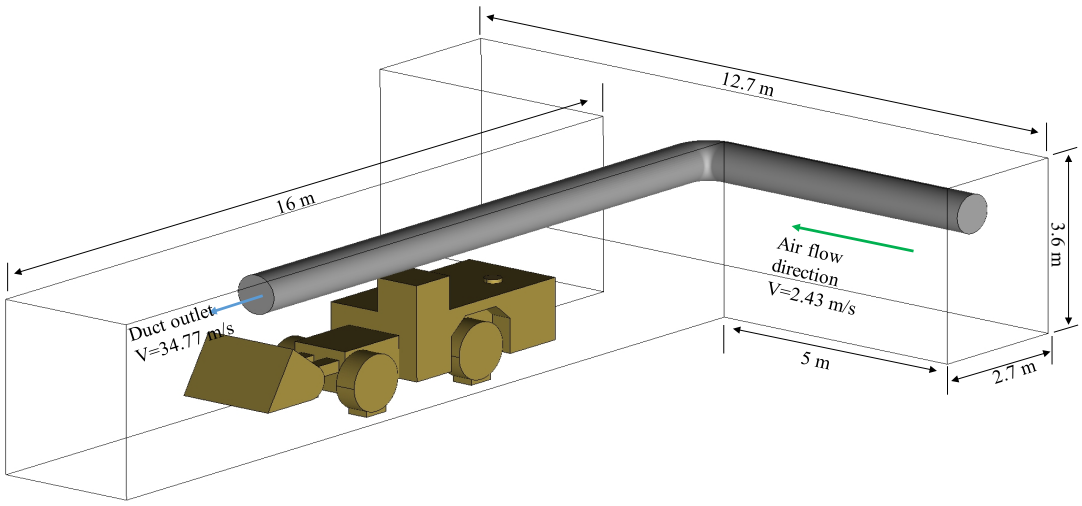

Figure 27 Model prototype geometry

5.3.2 CFD Model Setup

In this study, the airflow is incompressible (Jundika C Kurnia, Agus P Sasmito, et al., 2014b; Ren et al., 2018; H. Wang et al., 2018); no heat-transfer is considered, the temperature is assumed as 288 K; and the gravity is 9.81 m/s^2. The standard $k-\varepsilon$ model is one of the most widely used turbulent models in the simulation of air flow in underground mines due to its accuracy and efficiency (Hu et al., 2016b; J Toraño et al., 2011; Javier Toraño et al., 2009; Z. Wang & Ren, 2013; Xu et al., 2015). Thus, this turbulent model is applied in this study. The airflow was simulated to initially achieve a steady-state by using simpleFoam solver, after which DPM was emitted for 120 s. The simulation of the airflow is solved by the SIMPLE algorithm. The numerical scheme for the convective derivatives is Gauss LinearUpwind (second order). All the simulation were carried out by using of OpenFOAM 5.0 with 16 cores on the supercomputing facility Magnus, provided by Pawsey Supercomputing Centre, Perth, Australia. Other parameters are given as follows:

(1) No slip wall function is used
(2) At the inlet, air velocity is 2.43 m/s (flow rate 23.6 m^3/s)
(3) Standard atmospheric pressure is prescribed at the outlet with static pressure set to 101 kPa

(4) At the duct outlet, air velocity is 34.77 m/s (9.84 m^3/s). This is based on the 0.06 m^3/s per kW of diesel equipment, which is the Australian minimum air flow requirement in underground working areas. The engine power of the LHD is 164 kW, which requires a minimum air flow of 9.84 m^3/s.

(5) At the LHD tailpipe, the particle density is set to 1.77×10^3 kg/m^3 (Park et al., 2004); the particle's diameter is set to 78.7×10^{-9} m. According to the DPM emission rate information available from the MSHA's website (MSHA), the DPM emission mass rate is calculated and set to be 2.49×10^{-6} kg/s in the models; the exhaust flow rate is set as 0.89 m^3/s referred to a previous study (Zheng & Tien, 2009). For the ELM and EEM, the same particle parameters are used. The volume fraction for particle_2 at the tailpipe is calculated and set as 4.584×10^{-7}.

(6) The air density, dynamic viscosity and kinematic viscosity are set as 1.213 kg/m^3, 1.81×10^{-5} Pa/s and 1.49×10^{-5} m^2/s, respectively, based on the assumed temperature and pressure. The gas species emission rate is calculated by the division of the particle mass rate and exhaust flow rate, which is 4.287×10^{-6} kg/m^3. The diffusion coefficient in the air (D) for C_8H_{18} and SF_6 is 5.0×10^{-6} (Zheng, Li, Thiruvengadam, Lan, & Tien, 2017) and 5.9×10^{-6} (Xu et al., 2013), respectively.

The solver used in this study and the initial conditions for different species at tailpipe are summarised in Table 8.

Table 8 Solvers used and initial conditions at the tailpipe for the numerical modelling

Method	Species	Solver	Initial condition at tailpipe
Steady simulation	Air flow	SimpleFoam	0.581 m3/s
Eulerian-Eulerian method	Particle_1	twoPhaseEulerFoam	2.49×10^{-6} kg/s
Eulerian-Lagrangian method	Particle_2	DPMFoam	2.49×10^{-6} kg/s
Species transport method	C8H18 SF6	Customized scalarTransportFoam (with the effect of turbulent dispersion)	4.287×10^{-6} kg/m3

5.4 Governing Equations

5.4.1 The Eulerian-Eulerian Model

There are two main approaches to numerically model the gas-solid two-phase flow: multiphase Eulerian model (EEM) and Lagrangian particle tracking (ELM). For the EEM, both the air flow and dispersed phase (DPM) are described as interpenetrating continua and therefore share the same governing equations. The continuity and momentum equations are given as (Abishek, King, & Narayanaswamy, 2017):

$$\begin{cases} \dfrac{\partial \varphi_n}{\partial \mathrm{t}} + \nabla \cdot (\varphi_n \boldsymbol{u_n}) = 0 \\ \dfrac{\partial \boldsymbol{u_n}}{\partial t} + \nabla(\boldsymbol{u_n}\boldsymbol{u_n}) = \dfrac{1}{\alpha_n \rho_n}(-\nabla p - \boldsymbol{F} + \nabla \cdot (\alpha_n \bar{\bar{\tau}}_n) + \rho_n \alpha_n \boldsymbol{g}) \end{cases} \tag{20}$$

where ρ_n, α_n, $\boldsymbol{u_n}$, $\boldsymbol{g}$ and $\bar{\bar{\tau}}_n$are the fluid density, volume fraction, fluid velocity, gravity, and viscous stress tensor, respectively. The symbol *n* is the index for different phases, e.g. ρ_g and ρ_{DPM} denote the air density and DPM density, respectively. The sum of volume fraction for each phase is unity: $\sum \alpha_n = 1$. $\bar{\bar{\tau}}_n$ is the viscous stress tensor, which is given by (Moukalled et al., 2016):

$$\bar{\bar{\tau}}_g = (\mu + \mu_t)(\nabla \boldsymbol{u_n} + (\nabla \boldsymbol{u_n})^T) - \frac{2}{3}\left[(\mu + \mu_t)(\nabla \cdot \boldsymbol{u_g}) - \rho_n k\right]\boldsymbol{I} \tag{21}$$

where μ, μ_t, k and **I** are the dynamic viscosity, turbulent viscosity, turbulent kinetic energy and unit tensor, respectively. **F** is the volumetric momentum transfer rate between different phases, which is given by:

$$\boldsymbol{F} = \frac{\sum \boldsymbol{F_i}}{V_{cell}} \tag{22}$$

where V_{cell} is the computational cell volume, F_i is the interaction forces between different phases, which includes the particle drag force and turbulent dispersion. GidaspowErgunWenYu drag model (Gidaspow, 1994) is applied for both the EEM and ELM.

5.4.2 The Eulerian-Lagrangian Model

Lagrangian particle tracking approach is employed when DPM is treated as a discrete phase. In this method, the air flow is still governed by equation (14). The motion of particles is governed by Newton's second law. There are many forces would influence the motion of particles, such as drag force, gravity, Brownian force, virtual mass force, thermophoretic force, buoyancy, Saffman's lift force and Magnus force. In this paper, no heat transfer is considered, thus thermophoretic force are neglected. Brownian force less influences the particles behaviours compared with the turbulence diffusion, thus is ignored as well. The Magnus force is generated due to the spin of the solid particles in the fluid, in this paper, particle collision and spin are not considered, thus Magnus force is ignored. The virtual mass force is significant when the particles density much less than the air density. Hence, this force is neglected due to the large particle density. Saffman's lift force becomes significant when the particles near the wall, which is not interested in this study, thus the lift is also ignored. According to the above reasons, only drag force and gravity are considered in this study. (Hu et al., 2019; Ren et al., 2018; Xia et al., 2016; Zheng and Silber-Li, 2009). The governing equation is given by:

$$m_p \frac{d\boldsymbol{u_p}}{dt} = m_P \boldsymbol{g} + \boldsymbol{F_d} \tag{23}$$

where m_p and $\boldsymbol{u_p}$ are the particle mass and particle velocity, respectively. $\boldsymbol{F_d}$ is the drag force, which is expressed as:

$$\boldsymbol{F_d} = \frac{1}{2} C_d \rho_g A_p |V_r| V_r \tag{24}$$

where A_p is the projected area of the particle, and V_r is the relative velocity between particles and air flow. C_d is the drag coefficient, which is expressed by (Gidaspow, 1994):

$$\begin{cases} \dfrac{24}{Re_p \cdot C_c} & Re_p \leq 1 \\ C_d = \dfrac{24\left(1 + 0.15{Re_p}^{0.687}\right)}{Re_p} & 1 < Re_p \leq 1000 \\ 0.44 & Re_p > 1000 \end{cases} \tag{25}$$

where Re_p and C_c are the particle Reynolds number and Cunningham slip correction factor, respectively. C_c is expressed by

$$C_c = 1 + \frac{\lambda}{d_p}\left(2.514 + 0.8e^{\frac{-0.55 d_p}{\lambda}}\right) \tag{26}$$

where λ and d_p are gas mean free path and particle diameter, respectively.

5.4.3 The Species Transport Model

When DPM is treated as a gas species (C_8H_{18} and SF_6), the species transport method is used. The transport equation for the gas species is given by:

$$\frac{\partial C_i}{\partial t} + \frac{\partial u_i C_i}{\partial x_i} - \frac{\partial}{\partial x_i}\left[\frac{\partial C_i}{\partial x_i}\left(D + \frac{\mu_t}{S_{Ct}}\right)\right] = S \tag{27}$$

where S is the source term, D is the diffusion coefficient in air (m^2/s), and S_{Ct} is the turbulent Schmidt number, with a value of 0.85 (Launder & Spalding, 1983). C is the passive scalar, which is SF_6 or DPM concentration (kg/m^3) for in this study.

5.5 Mesh Independence Study

5.5.1 Mesh Quality and Size

The flow field is modelled using a coarse, medium and fine mesh for conducting the mesh independence study. The overall mesh quality is above 0.2, the max aspect ratio is less than 1.2, the max non-orthogonality angle is below 70 degrees, and the maximum high skewness is less than 4. Such mesh qualities are acceptable for the solvers used in this study, as shown in Table 8. The number of control volumes for the coarse, medium and fine mesh is about 1.35 million, 2.83 million and 5.21 million, respectively. High

density meshes are used near the duct, wall and LHD to ensure computational accuracy. The first layer of the mesh is set to be 0.004 m based on the calculation of y+ ≈ 30. The height growth ratio of the layer is 1.2. The medium mesh is shown in Figure 28 as a representative.

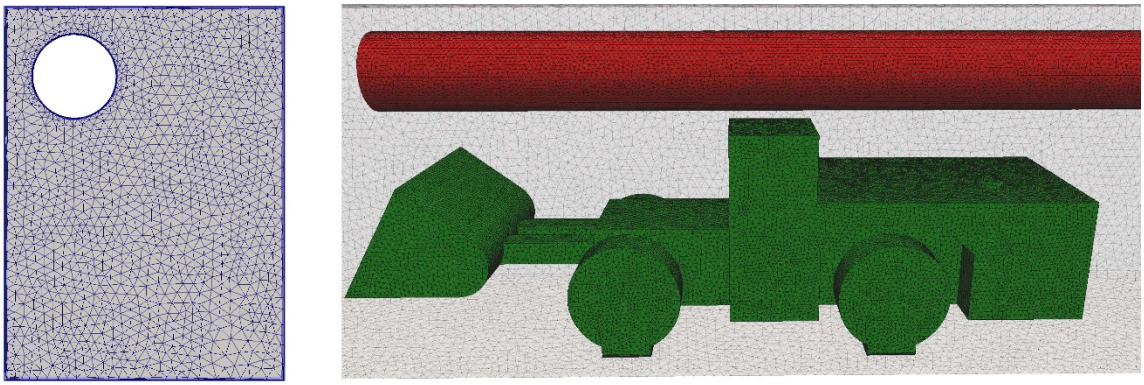

Figure 28 Overview of the medium mesh

5.5.2 Solution Convergence

The air flow field is simulated to a steady state for the convergence study. To guarantee the solution is converged, the residual values for each governing equation reached 1×10^{-4}. In addition to this, three monitor points are set and the velocity at these points is monitored until it no longer changes with the iterations. These monitoring points are in the centre of the roadway. Point 1 and point 2 are 6 m and 9 m away from the inlet of the main roadway, and point 3 is 4 m away from the development face, as shown in Figure 29. The velocity change at the three monitor points for the medium mesh is shown in Figure 30. The mesh independence study will be discussed in the next section.

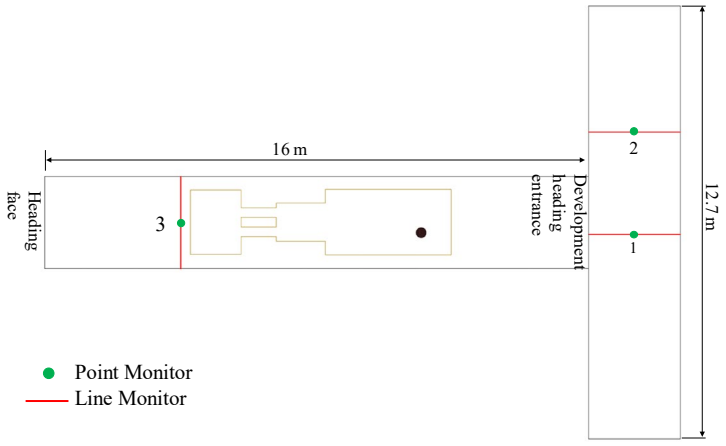

Figure 29 Position of monitor points and lines

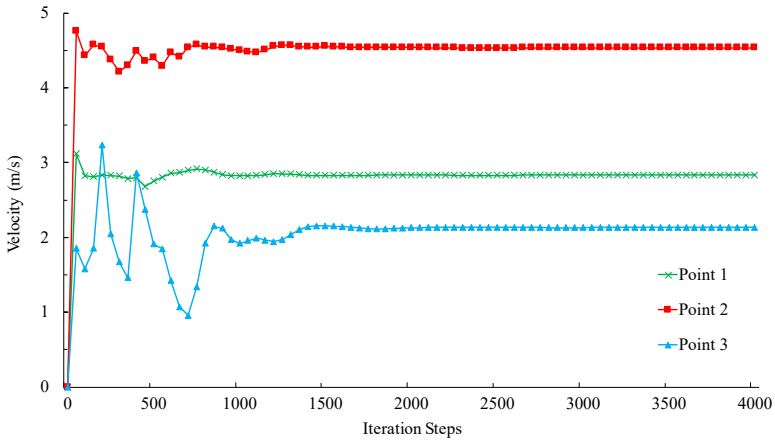

Figure 30 The velocity change at monitor points

5.5.3 Mesh Independence Study

The simulation results are highly dependent on the mesh quality. Normally, a denser mesh leads to a more accurate simulation result with a higher computational cost. In this study, the computational time for 5000 iteration steps for coarse mesh, medium mesh and fine mesh are about 36 mins, 108 mins and 146 mins, respectively. A mesh independence study is conducted to balance solution accuracy and computational cost. In this study, air velocity profiles are shown in Figure 31 for three line monitors. Lines 1, 2 and 3 are at the horizontal central line 6 m, 9 m from the roadway inlet and 4 m away from the development heading, respectively, as shown in Figure 29. As can be seen, the velocity profiles of the medium mesh are closely matching that of the fine mesh. This indicated that mesh independence has been achieved. The medium mesh is used in the study to save computational cost.

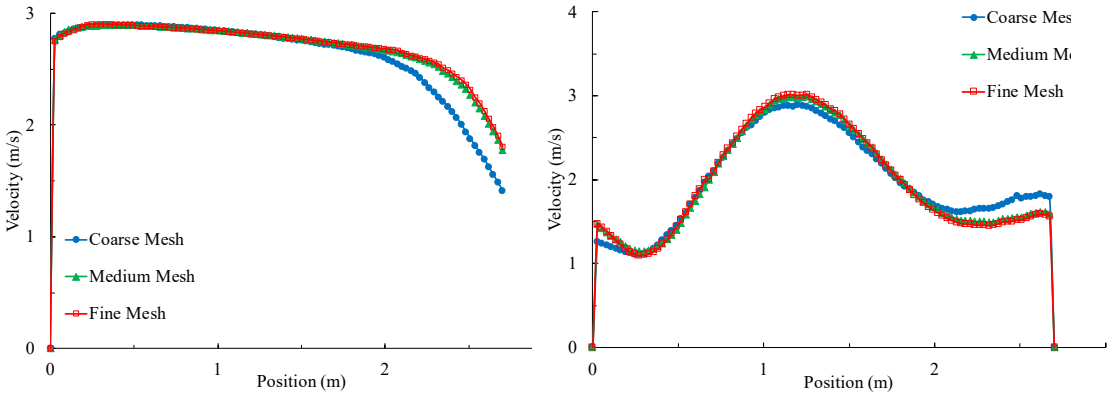

(a) Line monitor 1 (b) Line monitor 2

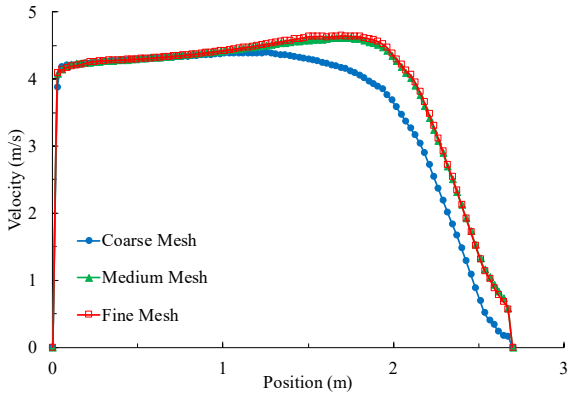

(c) Line monitor 3

Figure 31 Velocity profiles at the line monitors (left to right: line monitor 1 to 3 as shown in Figure 29)

5.6 Result

5.6.1 Analysis of Airflow Field

The dispersion pattern and distribution characteristics of DPM are significantly impacted by the airflow characteristics. For this reason, it is important to understand the airflow characteristics in the roadway, which include the airflow velocity, direction, and the airflow recirculate area location. Figure 32 shows the airflow pathlines coloured by velocity magnitude. After air blew out from the duct, the airflow collided and rebounded at the development face. There is an airflow recirculate area in front of the LHD. The circulation of the airflows in this area may cause the accumulation of DPM. In order to analyse the airflow characteristics in the domain in more detail, the air velocity contours at different cross-sectional planes are presented in Figure 33 and Figure 34. At the entrance of the development heading (d=0 m), the airflow velocity was uniformly distributed. The velocity near the left-side wall is higher than in other regions. At d=3 m, a large low-speed airflow zone was formed near the right bottom region, which is located at the back of the LHD. With the low-air velocity, the DPM is hard to escape when the DPM diffuses to this area and results in an accumulation. However, the DPM is also dominated by the exhaust flow direction. The accumulation of DPM will be further analyzed in the following section. At d=6 m, the high-speed airflow zones are located at the bottom of the LHD. The airflow velocity under the duct was lower due to the blockage of the LHD operating cabin. Figure 33 (d) shows the position that is at the front of the LHD operating cabin. The high-speed airflow zones are located at the bottom, left and right side of the LHD. The airflow velocity near the duct ranged from 0.5 m/s to 1.5 m/s, which is lower than in other regions. Figure 34 illustrates that the velocity distribution trend is similar for the three locations in the main roadway with a lower velocity close to the wall on the development heading side.

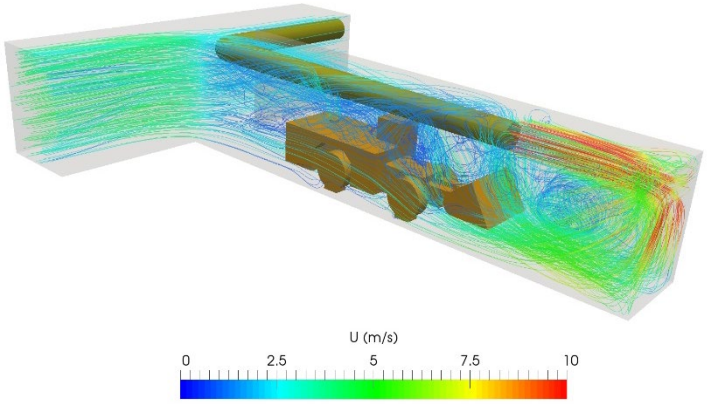

Velocity magnitude range 0 - 10 m/s

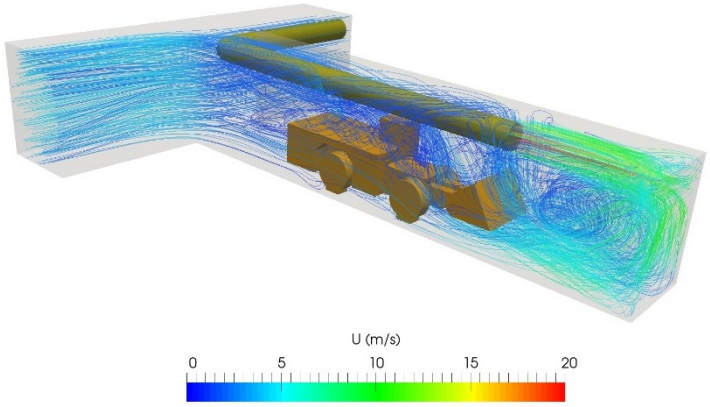

Velocity magnitude range 0 - 20 m/s

Figure 32 Airflow field path lines

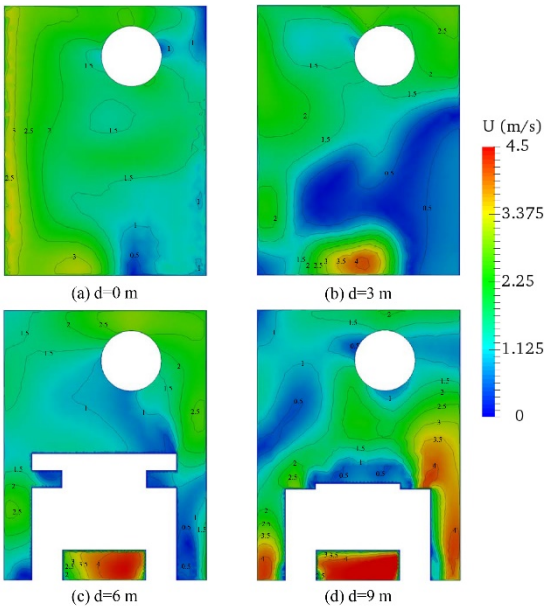

Figure 33 Airflow velocity at cross sectional planes in the development heading (distance from the heading entrance)

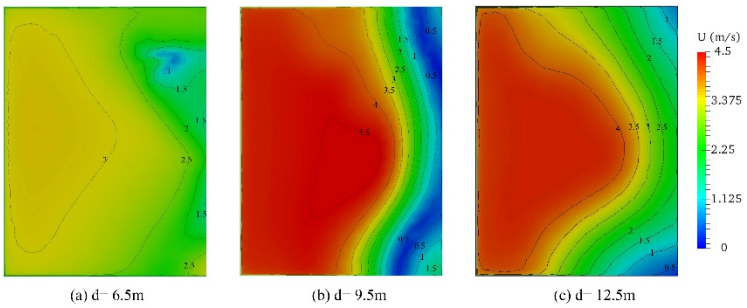

Figure 34 Airflow velocity at different cross sectional planes (distance from the inlet)

5.6.2 Analysis of DPM Distribution

For the four species used to represent the DPM in the simulation, namely Particle_1, Particle_2, SF_6 and C_8H_{18}, the DPM distributions at the steady state were first achieved. The area weighted average DPM concentrations at 2 m from the development heading entrance for four species were monitored until they no longer changed with the simulation time, as shown in Figure 35.

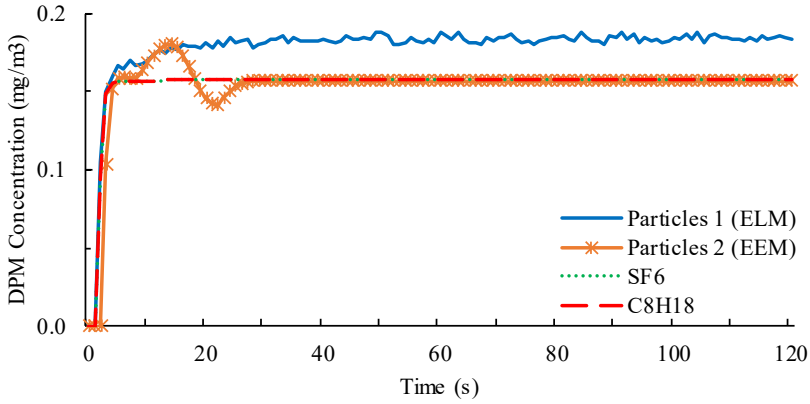

Figure 35 Area weighted average DPM concentration change with time (2 m from the development heading entrance)

Figure 36 gives DPM distributions for four species. The red contour represents the DPM concentration equal or exceeds 0.1 mg/m^3. Particle_1, Particles_2 and two gas species (SF_6 and C_8H_{18}) were simulated by ELM, EEM, and STM respectively. It is noticed that the general profile of the high DPM concentration areas for the four species is similar. After being emitted from the exhaust, DPM flows toward the main roadway with the air flow direction but concentrates in the top part of the development heading entry due to the initial exhaust velocity. Because of the ventilation duct extends to the front of the LHD, no DPM flows to the deep part of the development heading. The DPM gradually spreads out as it flows downstream. In the main roadway, although DPM spreads out more quickly due to higher fresh air dilution, it is still concentrated on one

side of the roadway which corresponds to the low velocity regions demonstrated in Figure 34.

Some apparent differences among the four modelling results also exist. For the Particle_2 (EEM), SF_6 and C_8H_{18}, there is no DPM accumulation behind the LHD. All DPM diffused quickly from the development heading to the roadway. For Particle_1 (ELM), however, a high DPM concentration zone is found behind the LHD. This difference is mainly caused by the different species' diffusion rate. Gravity impacts more significantly on the particles due to the large density compared with the other species. For Particle_2 (EEM), it performs more like a gas phase rather than particles. Not like the Particle_1, no DPM accumulates at the back of the LHD. It is noted that Particle_2 illustrates a similar distribution as that of two gas species in the development heading. And in the main roadway, Particle_2 diffuses more easily in air than the other 3 species and results in the smallest high DPM concentration zone among all the modelling For the two gas species SF_6 and C_8H_{18}, the distribution patterns are almost the same due to the similar gas diffusion coefficient in air, 5.9×10^{-6} and 5.0×10^{-6} respectively for SF_6 and C_8H_{18}. Another observation is that the EEM and STM model results show a smooth DPM profile compared with that of the ELM model due to the continuous character of the simulated phase.

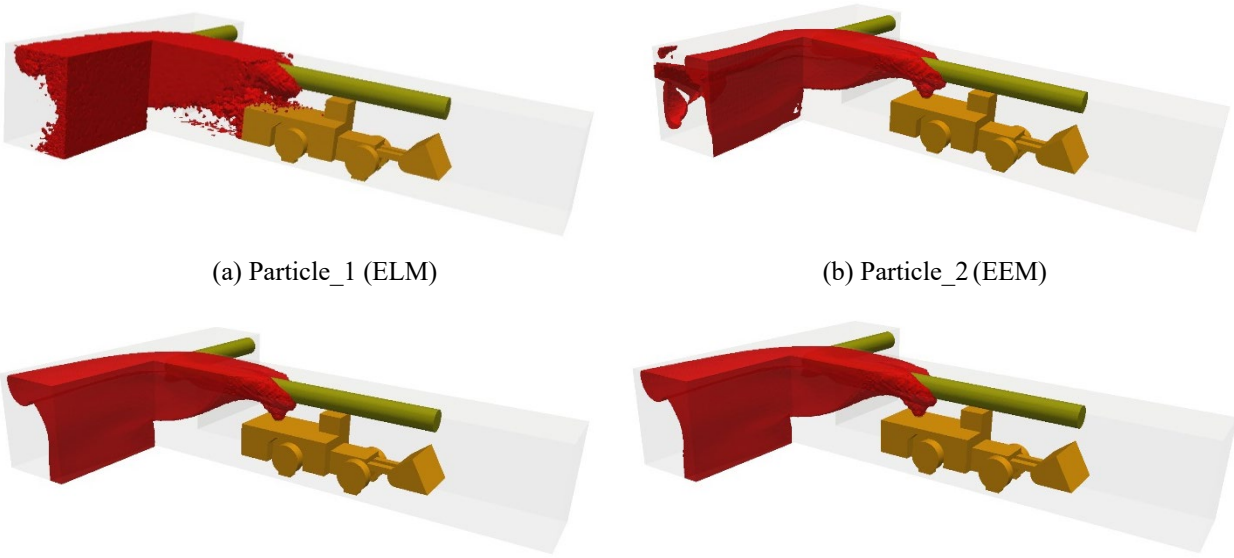

(a) Particle_1 (ELM) (b) Particle_2 (EEM)

(c) SF_6 (STM) (d) C_8H_{18} (STM)

Figure 36 DPM distribution with concentrations ≥ 0.1 mg/m^3

DPM distribution at cross-sectional planes for the four species are shown in Figure 37. The red colour in the planes shows DPM concentration ≥ 0.1 mg/m^3. It can be seen that the results of EEM and STM models give a similar DPM concentration distribution

in the development heading. However, it is apparently different for the results of the ELM model. For the Particle_1, Particle_2, SF_6 and C_8H_{18}, most of the DPM migrate to the roadway with the airflow. However, Particle_1 migrate slower than the other three species, and some particles diffuse to the low-speed airflow zone that is located behind the LHD and accumulated in this area. It is noticed that the high-DPM-concentration zone for Particle_1 in the roadway is larger than that of the other species. This is because the discrete particles diffused slower than the gas species. However, the area of the high-DPM-concentration zone for Particle_2 in the roadway is the smallest in the four models. For Particle_2 (EEM), with low particle fraction rate, the particles behave like a gas and diffuse faster than other species. As expected, the two gas species, SF_6 and C_8H_{18}, give the same DPM distributions in the entire simulated area.

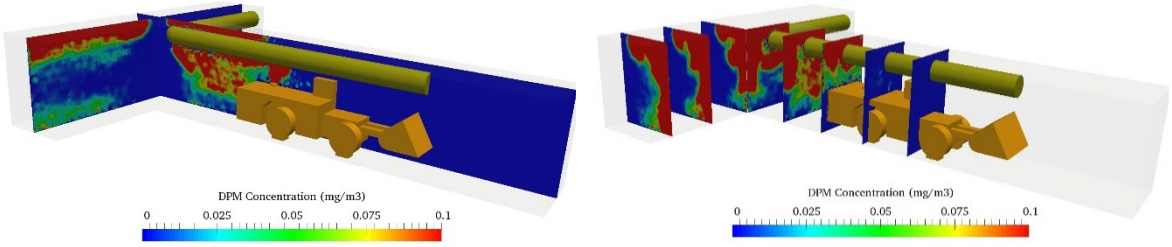

(a) Particle_1 (ELM)

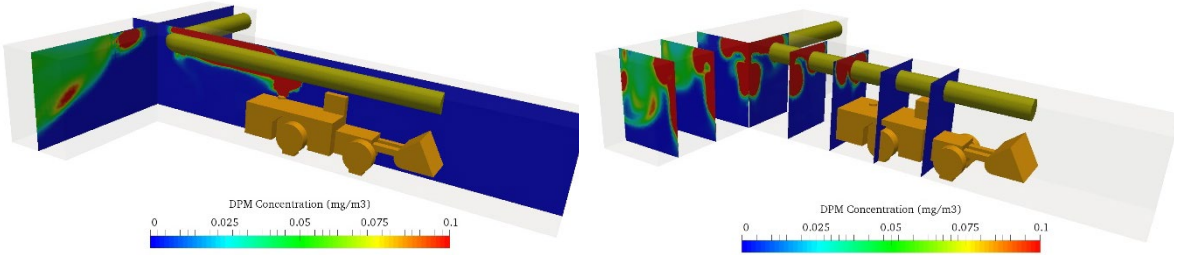

(b) Particle_2 (EEM)

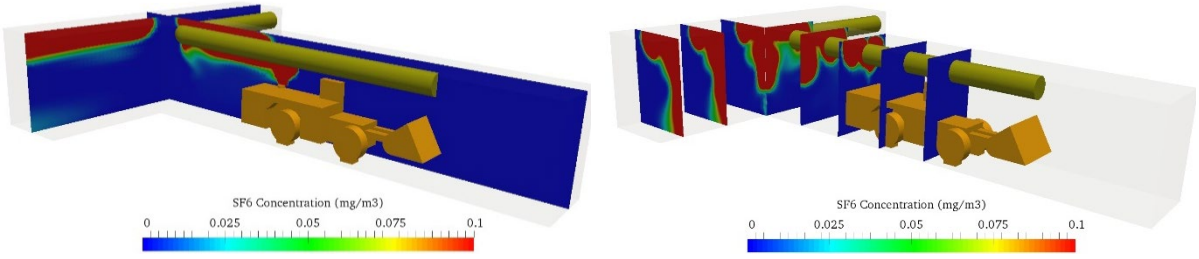

(c) SF6 (STM)

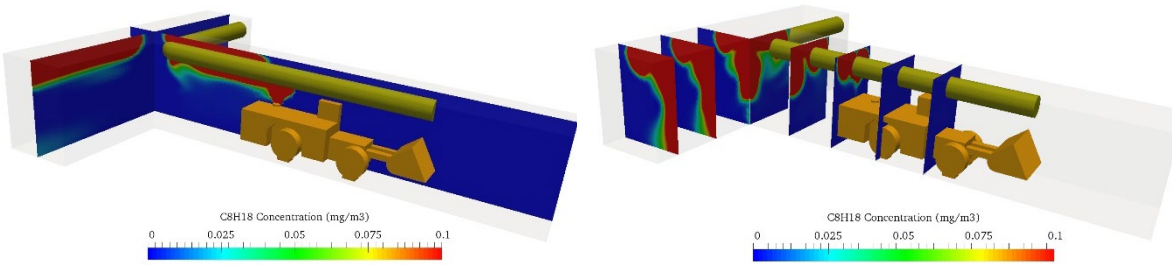

(d) C8H18 (STM)

Figure 37 DPM concentration distribution at cross-sectional planes

Figure 38 presents the area weighted average DPM concentration at different cross sections in the development heading and the roadway. As demonstrated earlier, the DPM concentration for Particle_1 (ELM) is higher than that of the other species in the development heading entry and the concentration for Particle_2 (EEM) is the lowest in the main roadway. In Figure 38 (a), it can be seen that the general spatial distribution trend is similar for the four different species. The DPM concentration peaks at 9 m from the heading face where is near the LHD tailpipe location and then decreases as it flows to the main roadway. As displayed in Figure 38 (b), the general DPM concentration trend for Particle_1 and the two gas species are similar. With the Particle_1 flowing to in the main roadway, Partilce_1 concentration becomes the same as the other two gas species based on the same inlet mass flow rate. The DPM concentration for the four species rises sharply to the limit of 0.1 mg/m^3 at around 8 m. After that, the increasing trend for Particle_1 and the two gas species becomes slow and then the concentration drops slowly due to ventilation dilution. It is worth noting that the concentration for Particle_2 decreases gradually after 8 m in the main roadway. It is believed that the DPM concentration would become stable as it flows further downstream and the final concentration difference between the four species should be minimal.

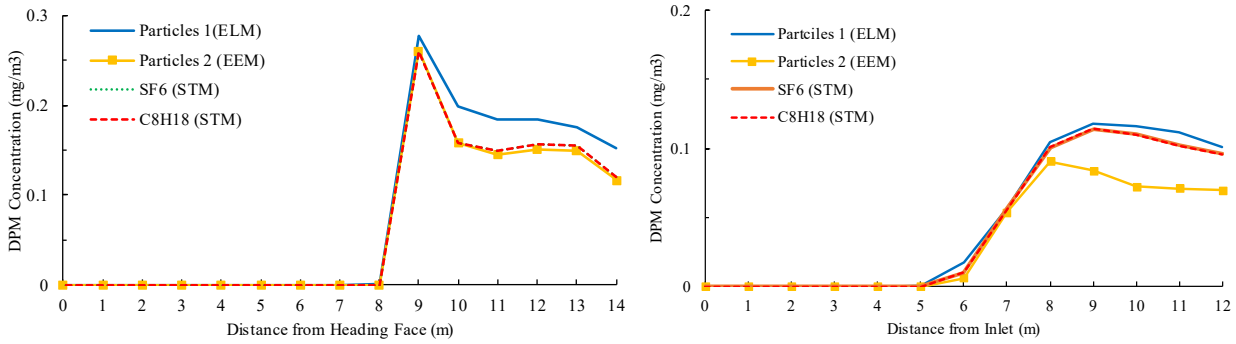

Development heading entry Main roadway

Figure 38 Area weighted average DPM concentration at different cross sections

5.6.3 Model Validation

Model validation is an important part of any CFD study to guarantee the accuracy of simulation results. However, in this study, the numerical models were built based on a conceptual development heading. Thus, no measurement data is available for validation purposes. However, a similar study was conducted by the authors to analyse DPM distributions in an underground development face by using the E-L method (Chang, Xu, Zhou, Mullins, Abishek, et al., 2019). The simulation results have been validated for both the airflow and DPM concentration. The average error between the onsite data and simulation data for the airflow and DPM concentration were 12.44% and 23.37%, respectively. Due to complicated ventilation and tunnel conditions and the measurement environment, such errors were deemed to be acceptable. According to the previous study, it is believed that the ELM method is able to provide acceptable results. Thus, it is believed that the ELM provides a more accurate result among the 3 simulation methods and it is reasonable to use this method to estimate the DPM distributions.

5.7 Discussion

Based on the results above, the general profile of high DPM concentrations zones for the four species significantly depends on the airflow behaviours. In the development heading, most of the DPM firstly flow to the roof due to the initial exhaust airflow direction, then it is carried to the main roadway. No DPM diffuses to the front of the LHD. In the main roadway, the DPM accumulates at the low-velocity areas as shown in Figure 36 and Figure 37.

It is noted that DPM accumulation at the back of the LHD occurs only in the simulation of Particle_1. Compared to the other three species, the distribution of Particle_1 (ELM) is influenced more by gravity, and it diffuses the slowest. Only the ELM method showed DPM accumulation closely on the back of the LHD, based on the previous study (Chang, Xu, Zhou, Mullins, Abishek, et al., 2019; Xu et al., 2018), it is believed that the ELM give a more accurate simulation results compared to other methods.

In the main roadway, Particle_2 presents the smallest high DPM concentration zone among the four models. This can be caused by two reasons. The first reason is that Particle_2 in the EEM models performs more like a gas phase rather than a particle phase, and it diffuses the fastest of all the other methods. The particle is treated as a continuous phase in this method and it is governed by the same equation as the airflow. Thus, the Particles_2 presents the gas characteristics as the SF6 and C8H18, such as smooth DPM profile. The second reason is that the EEM is not suitable to simulate a

dilute particle phase whose particulate volume fraction is less than 10^{-3} (Van der Hoef et al., 2006). In this study, the particulate volume fraction at the LHD tailpipe is much smaller than this value. It is reported that the equations for EEM are not applicable when the particles flow becomes dilute (Crowe, 2005). For this reason, it is believed that the EEM method gives an inaccurate result on the DPM simulation.

It is worth noting that the DPM distributions of SF_6 and C_8H_{18} are almost the same because of their close diffusion coefficients. In this study, the emission rate (kg/m^3) is applied as the passive scalar for the STM. According to equation (27), the calculation of this passive scalar is dominated by the diffusion coefficient and airflow filed velocity. With the same airflow field and close diffusion coefficients, the concentrations are almost the same for two gaseous species. Although the DPM concentration of SF_6 and C_8H_{18} are lower than that of the Particles_1 in the development heading, the concentration change trends at different locations are the same for three species. With the DPM flowing to the main roadway, the DPM concentrations become similar for all the three species. Thus, it is reasonable to use STM to present DPM distribution characteristics. However, the selection of species is important. Based on the study, a gaseous species with a lower diffusion coefficient is recommended to better represent the DPM. For the emission rate of SF_6 should be carefully calibrated to get good results.

5.8 Conclusion

Prior research has used CFD methods to address DPM distribution and dispersion characteristics in different areas. However, most such studies treated DPM as a gas species in the model and applied the species transport method. DPM is a solid discrete phase and its behaviours could be quite different from those of gaseous contaminants. To compare the differences by applying different numerical methods, simulations were performed based on a typical underground mine development heading with a forcing auxiliary ventilation setup. Four species (Particle_1, Particles_2, SF_6 and C_8H_{18}) with three simulation methods were used to model DPM dispersion in a typical underground mine development heading. The Eulerian–Lagrangian method (ELM) and Eulerian–Eulerian method (EEM) were used when DPM is treated as discrete phase particles, and the species transport model (STM) was used when it is regarded as gases.

This study demonstrated that the ELM simulation produces the highest DPM concentration in the development heading due to the low diffusion rate and the more apparent gravity effect on particles. Compared with other methods, the biggest DPM distribution discrepancy is at the behind of the LHD, where airflow velocity is low. From

the results, the ELM method gives a better prediction on the DPM distribution around the vehicles, and a high DPM concentration area was observed behind the LHD. However, no DPM accumulation occurs in this area for the other two methods. Results showed that DPM distributions are very similar when using the STM regardless of what gas properties (SF_6 or C_8H_{18}) are set to represent DPM. The EEM simulation results in a similar DPM distribution with that using the STM, but the DPM diffuses slightly faster and results in a lower DPM concentration distribution in the main roadway.

Since the general distribution trend for the three methods is quite similar, STM simulation is recommended for any preliminary studies due to its low computational cost and memory requirement. However, the current study indicated that the modelled species (SF_6 or C_8H_{18}) diffuse faster than particles. For improved simulation accuracy, the parameters (such as diffusion coefficient and inlet mass flow rate) for the modelled species need to be carefully calibrated to achieve a closer agreement with reality. For the important regions around the diesel vehicle areas, the result from ELM seems more realistic based on previous studies (Chang, Xu, Zhou, Mullins, Abishek, et al., 2019; Xu et al., 2018), especially in the low velocity and complex flow area. Due to longer computational time, complications, and inaccurate results for the dilute particle flow in the EEM, this method is not recommended for the DPM modelling.

The simulation results are highly dependent on the selection of numerical methods. Therefore, it is important to select the appropriate numerical method to study the DPM dispersion behaviours. This numerical study is conducted based on a typical scenario of an underground mine development face. In this study, three commonly used numerical methods are compared, and the advantages and disadvantages of each method are analysed. To our knowledge, such comparisons have not been previously done for DPM simulation studies in underground mines. DPM is treated as one of the possible biggest occupational health threats for underground miners and has drawn much attention in its research. The findings in this paper could be used to better understand the difference in DPM behaviours by using different modelling methods. Also, this study can help the researchers to select a proper modelling approach in related simulation studies to accurately understand, predict, and alleviate DPM exposure in underground mines.

5.9 Acknowledgement

This research project is supported by the Independent Research Projects of State Key Laboratory of Coal Resources and Safe Mining, CUMT (SKLCRSM15KF01), the Minerals Research Institute of Western Australia (M495), the Mining Education

Australia Collaborative Research Grant Scheme (2018), and the computation resources provided by the Pawsey Supercomputing Centre with funding from the Australian Government and the Government of Western Australia.

6 Numerical investigation of diesel particulate matter dispersion in an underground development face during key mining activities

This chapter is planning to be submitted to a mining-related academic journal. It was entirely written by Ping Chang with the editorial suggestions provided by Dr Guang Xu.

Chapter 5 illustrated that the species transport method could provide convincing results with proper simulation parameters. This method is more computational-economic compared with the Eulerian-Lagrangian method. The species transport is an ideal method when simulating the DPM dispersion during numbers of mining activities with a large computational domain. This chapter presented the DPM dispersion during key mining activates, such as shotcreting, loading, and charging, in an underground development face by using the species transport method with a lower DPM diffusivity rate in air. The auxiliary ventilation performance of DPM removal for each activity was also evaluated.

6.1 Abstract

Diesel particulate matter (DPM) is carcinogenic to humans. Underground miners have high risk to over-exposure to high concentrations of DPM. To control DPM effectively, it is essential to understand the DPM dispersion characteristics. In this study, the DPM distributions of three key and representative mining activities, shotcreting, loading and charging activity, in an underground development face were studied. A computational model for the mining activities was developed using 3D imagery, onsite data and OpenFOAM. Tracer gas experiments were first conducted in the underground mines for the validation purpose for the CFD simulation. The simulations were carried out at a steady state using the standard k-ε turbulence model, while the transport and dispersion of DPM was modelled using a segregated species transport model. Then the DPM distribution characteristics for each mining activity were analysed and the high concentration zones were identified. At last, the efficiency of current auxiliary ventilation system on DPM dilution was evaluated based on the simulation results. The results show that the current ventilation design cannot maintain the DPM concentration under an acceptable level for loading activity. And this issue could be solved by simply increasing the ventilation rate. The findings in this paper could be used for optimizing the auxiliary ventilation design for future mining activities in this development face.

6.2 Introduction

With the rapid development of mechanization in the mining industry, diesel equipment has been widely used for mining actives. Nevertheless, this also generates a severe health issue on the miners - overexposure to diesel particulate matter (DPM). Previous study (D. B. Kittelson, 1998) showed that more than 90 % of the diesel particles' diameters by mass are less than 100 nm. Such size of particles are capable to

penetrate to the human respiratory system and deposit at the deepest part of the human lung (Chang & Xu, 2017b). In 2012, the International Agency for Research on Cancer (IARC) classified DPM as a carcinogen to humans (Group 1) (IARC, 2013). A number of studies (IARC, 2013; Ris, 2007; US.EPA, 2002) indicated that both acute- and long-term exposure to high concentration could result in adverse health effects, such as asthma, headedness, lung cancer, etc. Due to the confined working environment, the underground miners have a high risk of over-exposure to high DPM concentration than that of the worker who works in a normal environment. For this reason, it is vital to remain the DPM concentration under an acceptable level. In 2017, the Australian Institute of Occupational Hygienists recommends an 8-hour time-weighted average (TWA) exposure limit of 0.1 mg/m^3 and an "action limit" of 0.05 mg/m^3 on the basis of elemental carbon (EC) for underground mines (AIOH, 2017). However, it is very challenging for most of mining industries to meet this standard.

Currently, ventilation is still the main stragety to dilute DPM. In an underground development face, usually, the auxiliary ventilation set up does not change in a complete mining cycle, including shotcreting, loading, charging actives, etc. Diesel particulate emissions vary in the mining cycle due to the different type of diesel equipment used. Thus, it is important to understand the DPM dispersion characteristices in the development face for different mining activities, especially for the key mining activities which highly rely on diesel machines. With the rapid development of computer technology, computational fluid dynamic (CFD) is an effective way to simulate the DPM distribution based on the on-site experiments.

Numerous studies have used CFD simulation to investigate the contaminant behaviours in underground mines. Kurnia et a. (Jundika C Kurnia, Agus P Sasmito, et al., 2014a) used species transport method to simulate the methane behaviours in an underground mine tunnel. Various methane release conditions were evaluated and the effects of the ventilation on the methane distributions were also investigated. The results showed that the methane behaviours were highly influenced by the gas release conditions, such as release location, release rate and source numbers. Based on the methane distributions under different scenarios, the effective methane management was provided. A numerical study was conducted by Fang et al (Fang et al., 2016) to investigate gas dispersion in a twin tunnels by using the species transport method. The effects of the ventilation systems parameters, such as duct air flow quantity, auxiliary fan locations on the gas dilution efficiency were also evaluated. An auxiliary ventilation system with a jet fan placed at 50 m before the cross-aisle was recommended to effective

control the gas concentration. A similar study was conducted to analyse the methane distribution in an underground development face (Hasheminasab et al., 2019). The species transport model was applied to study the gas dispersion characteristics. The performance of different auxiliary ventilation systems on the gas control was studied and the best auxiliary ventilation system design was suggested based on the simulation results. Torno and his colleagues (Torno et al., 2013) analysed the blasting gas behaviours after blasting in underground headings by using the CFD methods. The results were validated with the onsite gas concentrations during 40 minutes and a good agreement was obtained. In addition, the species transport method was also used to predict diesel exhaust behaviours in underground. Kurnia et al (Jundika C Kurnia, Agus P Sasmito, Wai Yap Wong, et al., 2014) used this method to investigate the hazardous gases from the diesel emission in an underground development face under various auxiliary ventilation systems. The auxiliary ventilation systems performance on hazard gases dilution were further evaluated and the hazardous gases control strategies were provided based on the numerical results. Zheng and his colleagues conducted a series numerical studies to investigate diesel particles' dispersion and distribution characteristics using the species transport method. They predicted the DPM distributions in an underground isolated zone with a loader at 6 locations to present the dynamic activity (Zheng & Tien, 2009); they evaluated the buoyancy effect on the DPM dispersion in an underground development face (Zheng, Thiruvengadam, Lan, & Tien C, 2015);they investigated the efficiency of four auxiliary ventilation systems on DPM dilution (Zheng, Thiruvengadam, et al., 2015b); and they also analysed the DPM patterns with the impact of motion vehicle in a heading face (Zheng, Li, et al., 2017). Diesel particulate matter is a solid phase. However, in Zheng's studies, DPM was treated as a gaseous phase by using species transport model. Two studies have compared two simulation numerical models when treated DPM as solid particles or a gas species (Chang, Xu, Zhou, Mullins, & Abishek, 2019; Thiruvengadam, Zheng, & Tien, 2016). Both of the studies showed that species transport model could provide similar results as the model which considers DPM as solid particles. Since its computational economic and relatively high accuracy, the species transport method was applied in this study to predict the DPM dispersion characteristics in underground mines.

The aim of this study is to use CFD method to study the DPM dispersion characteristics under various key mining activities and evaluate the efficiency of the current auxiliary ventilation system on DPM dilution in an underground development face. This study is based on an on-site experiment in a development face in a gold mine

in Western Australia. A steady sate CFD simulation was carried out to study the particulate matters' dispersion characteristics by using a standard k-ε turbulence and the transport and dispersion of DPM was modelled by using a segregated species transport model. The high DPM concentration areas were identified where the ventilation could be improved. In addition, SF_6 was used in the on-site experiment as a tracer gas for the CFD validation purpose. The results provided in this study may be used for improving the design of ventilation system to better control the DPM concentration in the development face.

6.3 Model Description

6.3.1 Physical Model Geometry

The studied area is an underground development face in a Western Australian gold mine. The 3D geometry of the region was obtained for the simulation from the onsite survey. As shown in Figure 39, the length of the development face considered for the study is 66.5 m, which has an average cross-sectional dimensions of about 6.5 m (height) × 5.5 m (width). A 20.6 m depth cuddy is connected to the development face, with an average cross-section of 6.5 m (height) × 6 m (width). A forcing auxiliary ventilation system with a duct diameter of 1.2 m and an outlet diameter of 0.6 m (partially blocked – as shown in Figure 39 (a)) was used for providing ventilation. The duct outlet was 15.2 m away from the heading face for shotcreting and loading activities. For the charging activity, the region was extended for 4 m, but the length of duct kept the same. The vehicle model used for shotcreting, loading and charging activities are Normet Spraymec 904 (90 kW), Caterpillar Loader R3000H (305 kW) and Normet Charmec 1614B (110 kW), respectively. For the shotcreting activity, the Spraymec was positioned 8.5 m from the heading face, as shown in Figure 39 (a). For the charging activity, the Charmec was located at a distance of 5 m from the heading face, as shown in Figure 39 (c). Unlike the shotcreting or charging activities that involve the vehicle to be at a particular location, loading involves the vehicle to be in motion for most of the duration of work. Hence, three representative locations of the Loader in the development face were chosen for the simulation. As shown in Figure 39 (b), the three chosen locations correspond to the loader being 5 m and 30 m away from the heading face for cases 1 and 2 and 5 m from the cuddy heading for case 3.

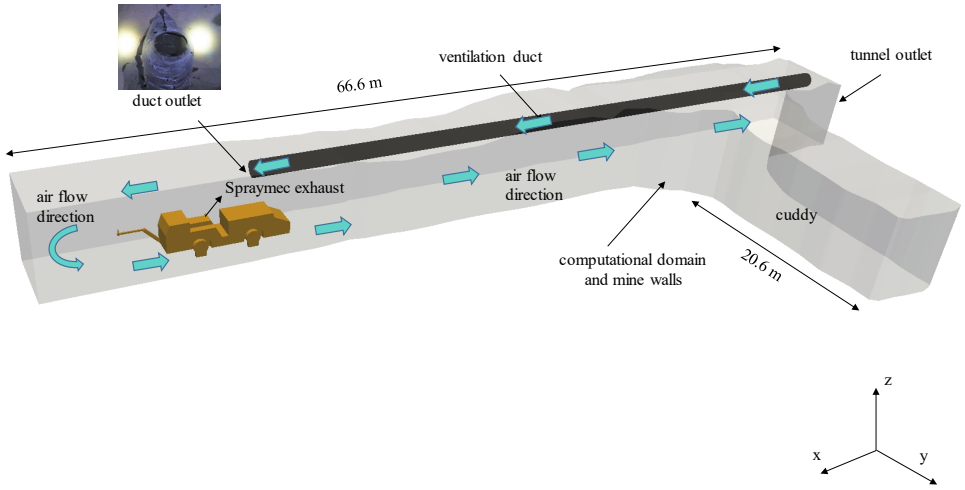

(a) shotcreting activity

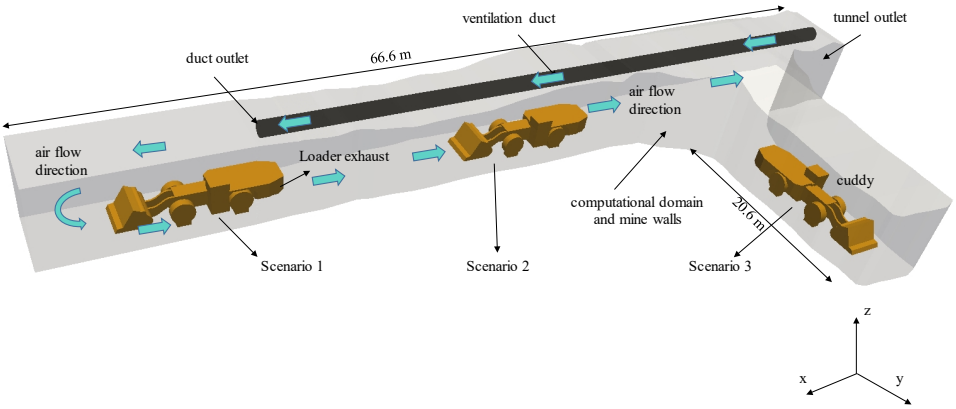

(b) loading activity for 3 scenarios

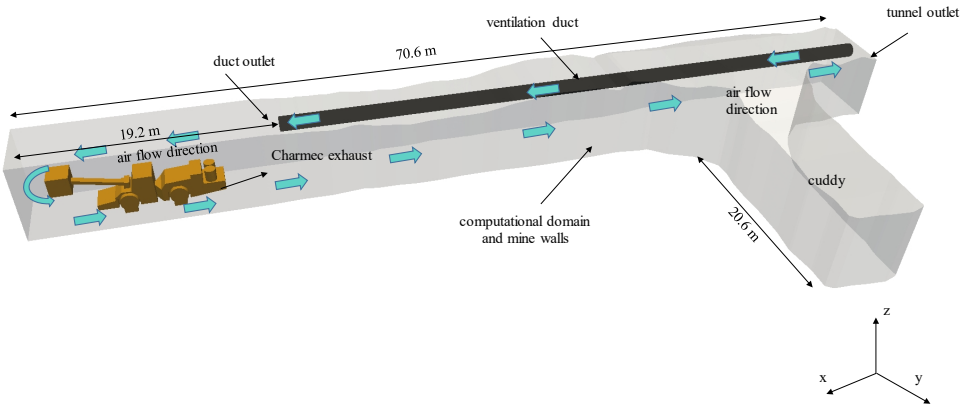

(c) charging activity

Figure 39 Model prototype geometry for different activities

6.3.2 Boundary Conditions and Numerical Schemes

An open source CFD tool – OpenFOAM was used for conducting the simulations. Airflow in the region was first simulated to achieve a stable state by using a steady-state solver – simpleFoam with the standard $k-\varepsilon$ turbulent model. The SIMPLE algorithm

was used to solve the pressure-velocity coupled equation. The numerical schemes used in this study were second-order discretization, as shown in Table 9. The DPM was simulated by using a customized (including dispersion due to turbulence) scalarTransportFoam solver. All the species transport simulations were achieved a steady state. The air dynamic viscosity and kinematic viscosity were 1.82×10^{-5} Pa/s and 1.51×10^{-5} m^2/s, respectively. The DPM diffusion coefficient in air was set as 9.494×10^{-6} m^2/s. The boundary conditions for each mining activity are listed in Table 10. All the simulations reported here were carried out by using 64 to 128 cores on a Cray XC40 supercomputer -Magnus, which is located at the Pawsey Supercomputing Centre, Perth, Australia.

Table 9 Numerical schemes

Gradient	Divergence	Laplacian	Interpolation	SnGrads
Gauss linear	Gauss linearUpwind	Gauss linear corrected	linear	corrected

Table 10 Operating conditions for each activity

Activity	Boundary	Material	Flow rate
-	Duct outlet	Air (m^3/s)	21.2
		Air (m^3/s)	0.358
Shotcreting	Spraymec exhaust	DPM (kg/s)	1.219×10^{-6}
		SF_6 (m^3/s)	3.58×10^{-5}
Loading	Loader exhaust	Air (m^3/s)	1.215
		DPM (kg/s)	6.056×10^{-6}
		SF_6 (m^3/s)	-
Charging	Charmec	Air (m^3/s)	0.437
		DPM (kg/s)	3.083×10^{-6}
		SF_6 (m^3/s)	3.58×10^{-5}

The accuracy of the simulation results highly depends on the quality of the meshes. Thus, a mesh independence must be achieved before further simulation. Such a study has been done in a previous study for the shotcreting activity (Chang, Xu, Zhou, Mullins, Abishek, et al., 2019). Three sizes of mesh, coarse mesh (0.75 million), medium mesh (1.57 million) and fine mesh (2.2 million), were tested. The velocities at 3 monitor points of each mesh were compared and it was found that the mesh independence had been achieved by the medium mesh. The same mesh size was applied in this study. A hybrid mesh, generated by ANSYS ICEM, was used for the simulation. For the complicated geometry region near around the diesel vehicle, tetrahedral meshes are generated, while hexahedral meshes are used for the rest of the model. The generated mesh for the loading activity (scenario 1) is shown in Figure 40 as a representative.

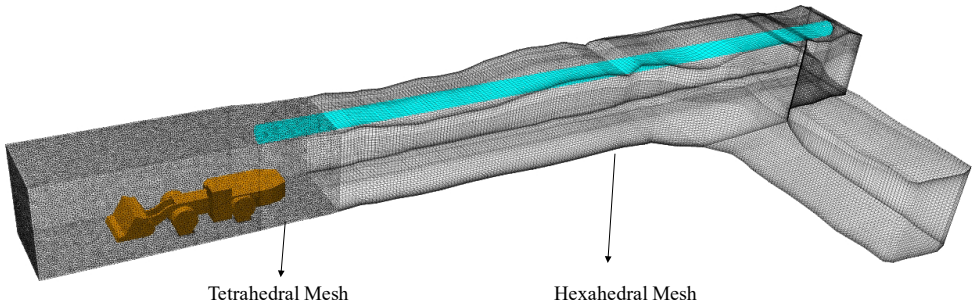

Figure 40 Overview of the mesh generation for loading activity

6.3.3 Governing Equations

The region air flow is assumed incompressible and no head transfer is considered in the simulation. Navier-Stokes equations are used to describe the motion of air. The incompressible continuity and momentum equations are given by (Xu et al., 2016):

$$\begin{cases} \dfrac{\partial u_i}{\partial x_i} = 0 \\ \dfrac{\partial (u_i u_j)}{\partial x_j} = -\dfrac{1}{\rho}\dfrac{\partial p}{\partial x_i} + \dfrac{1}{\rho}\dfrac{\partial}{\partial x_j}\left[(\mu + \mu_t)\left(\dfrac{\partial u_i}{\partial x_j} + \dfrac{\partial u_j}{\partial x_i}\right)\right] + \boldsymbol{g} \end{cases} \tag{28}$$

where u_i is the air flow velocity vector (m/s), ρ is the air density (kg/m^3), p is the pressure (Pa), μ is dynamic viscosity of air (Pa/s), μ_t is turbulent viscosity (Pa/s), $\boldsymbol{g}$ is the gravity acceleration (m/s^2) and i, j is the coordinate direction.

The passive scalar transport equation is given by:

$$\frac{\partial u_i}{\partial x_i} C = \frac{\partial}{\partial x_i}\left[\frac{\partial C_i}{\partial x_i}\left(D + \frac{\mu_t}{S_{Ct}}\right)\right] \tag{29}$$

where D is the diffusion coefficient (m^2/s), and S_{Ct} is the turbulent Schmidt number, with value of 0.85 (Launder & Spalding, 1983). C_i is the passive scalar, which is the SF_6 or DPM concentration in this study.

6.3.4 Model Validation

To ensure the accuracy of simulation results for further analysis, the results were compared with onsite measured results for the validation purpose. The air velocities in the region for shotcreting activity have been validated in previous research (Chang, Xu, Zhou, Mullins, Abishek, et al., 2019). The DPM concentration validation was not available due to the limit of DPM monitors. However, a tracer gas (SF_6) experiment was conducted to meet the validation requirement. For the shotcreting and charging activities, SF_6 was released at the vehicle tailpipe at a constant flow rate specified in Table 10. The loader kept motion during the loading activity, and thus, no SF_6 experiment was

conducted due to safety consideration. The SF_6 concentrationwas measured by a MIRAN SapphIRE Portable Ambient Analyzers which is designed by Thermo Scientific^{TM}. The SF6 concentrations were continuously monitored untilstable state. Same simulation method was used for both the SF6 and DPM simulation. For the validation of SF_6 concentrations, two monitor points were measured for each activity. Point 1 was near the release source, besides the vehicle and Point 2 was located at about 1.7 m above the floor and 30 m away from the heading, as shown in Figure 41 (shotcreting activity as a representative). The comparison between CFD results and measured data is given in Table 11. It worthing noting that the average measurement error is 13.45%. The average error between the measured data and CFD results is less than 20%. Since the complicated measurement environment, this error is acceptable for the simulation.

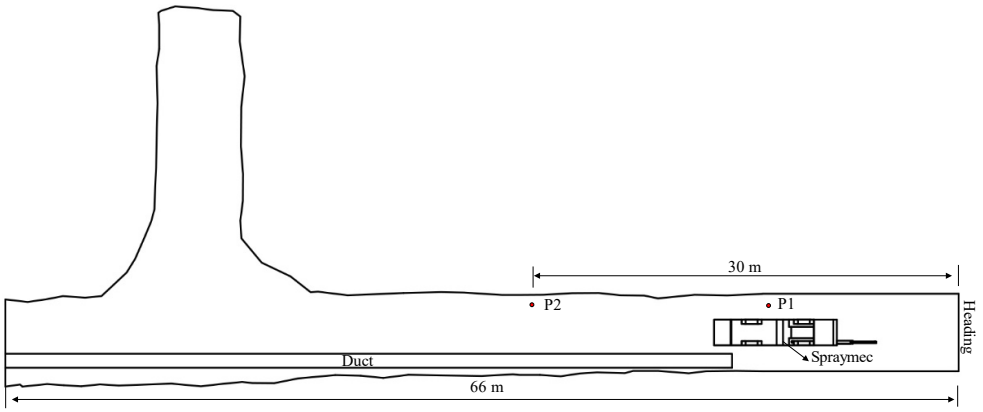

Figure 41 Position of monitor points (Shotcreting activity)

Table 11 Comparison between CFD results and measured data

Activities	Shotcreting		Charging	
Point number	P1	P2	P1	P2
Measured data (ppb)	4000±7.5%	2400±8.3%	4500±20%	2200±18%
CFD results (ppb)	4211	1778	3533	1713
Error	5.28%	25.92%	21.49%	22.14%

6.4 Result and Discussion

6.4.1 Shotcreting Activity

The DPM dispersion is predominantly controlled by the mean flow and turbulence levels in the air stream. Thus, it is important to understand airflow behaviours in the development face. The airflow velocity vectors at 3m height above the floor are given in Figure 42. As can be seen, a recirculation area is generated at the front of the Spraymec due to the combined effects of the airflow from the duct and reversed airflow after hitting the heading face. Another small recirculation area existed at the behind of the Spraymec. In the tunnel, the air velocity near the duct side wall was lower than that near

the other side. The pollutant may accumulate in the low-velocity zone and recirculation area areas.

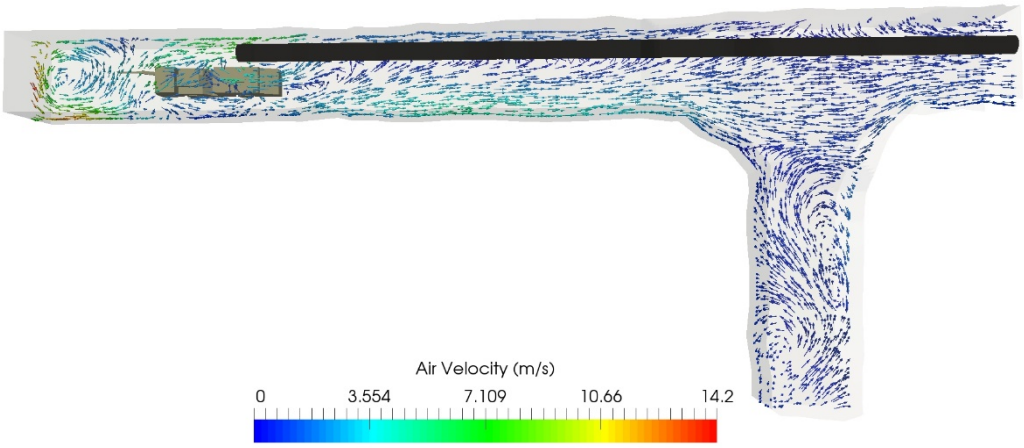

Figure 42 Airflow velocity vectors at 3 m height above the floor

The DPM distributions at vertical and horizontal cross sections are given in Figure 43. Concentrations greater than 0.1 mg/m^3 are represented in red. As can be seen, a uniform DPM distributions is illustrated in the tunnel except for the vicinity of the exhaust pipe. As the tailpipe is located at the top of the Spraymec (front of the duct outlet), the DPM is seen to be carried by airflow to the front of the Spraymec first and then disperses to the outside part of the tunnel. The confinement, and hence the limited airflow into the cuddy due to its geometry, resulted in relatively lower concentrations of DPM in the cuddy.

Figure 44 shows the DPM plume with the concentrations large than 0.1 mg/m^3. In this situation, most of the tunnel is under the same limit, thus, the operator does not have the hazard to over-expose high levels of DPM under the current ventilation conditions during the shotcreting activity.

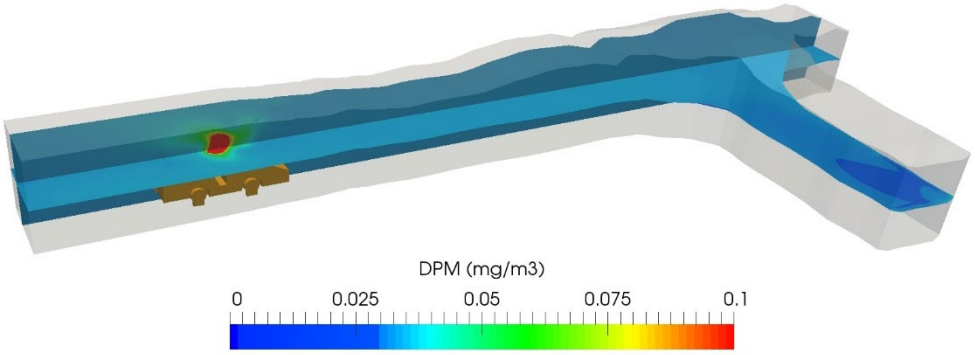

Figure 43 DPM concentration distributions at cross sections for shotcreting activity

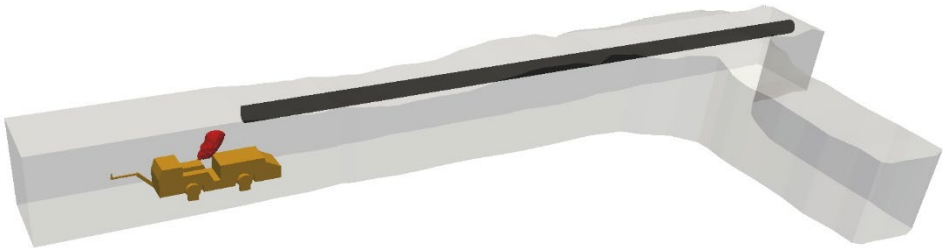

Figure 44 DPM distributions with the concentration large than the limit (0.1 mg/m^3)

6.4.2 Loading Activity

The airflow velocity vectors at 3m height above the floor for the loading activity are given in Figure 45. As can be seen, a recirculation area is generated near the face heading for the 3 scenarios. For scenario1 and 2, the exhaust tailpipe is located behind of the duct outlet, which results in a relatively lower concentration of DPM ahead of the loader. However, for scenario 3, appreciable concentrations of DPM are possible as seen in the figure due to the lower air velocities in the cuddy. The velocity vectors in the cuddy are also indicated of the greater residence time for DPM when the loader is working in this area.

The DPM concentration distributions for the 3 scenarios are presented in Figure 46. The red color contour indicates the DPM concentrations greater than 0.1 mg/m^3. It is evident from the figure that for scenario 1, the DPM concentrations behind the vehicle are in great excess to the allowable limit. This is indicative miners who work in the vicinity of the loader in such a configuration, downstream of the tunnel are potentially at a high risk to over-exposure to hazardous levels of DPM. Hence, protective measures such as protective equipment must be worn to eliminate continued over-exposure. For the areas in the front of the loader, the DPM concentrations are at safe levels due to the fresh air from the duct. It is seen from the figure that the relative location of the loader from the cuddy also has a significant influence on the DPM concentrations. Figure 46 shows that DPM concentrations in the cuddy are relatively lower for scenarios 2 and 3 as compared to that of scenario 1. The loader for scenario2 is located near the cuddy. Most of the DPM is carried to the downstream by fresh air before it diffused to the cuddy. For scenario 3, the DPM accumulation can be seen near the duct-side wall due to the loader exhaust orientation. The downstream presents a relatively higher DPM concentration for scenarios 2 and 3 compared the concentration in cuddy with the DPM flowing to the outlet.

Figure 47 presents the DPM distribution with the concentrations large than the limit (0.1 mg/m^3). As expected, most of the regions downstream of the loader show DPM levels exceeding 0.1 mg/ m^3 when the loader works near the heading face (scenario 1). When the loader moves to the mid-way of the tunnel, this area occurs between the cuddy and outlet of the tunnel (scenario 2). However, for scenario 3, DPM is first injected to the duct-side wall, thus generated a high DPM concentration zone. Then this zone expanded to the downstream due to the main airflow direction in the tunnel. It is noticed that a small region of high DPM concentration zone also exists at the upstream, due to the location of a re-circulation recirculation area, as shown in Figure 45 (c).

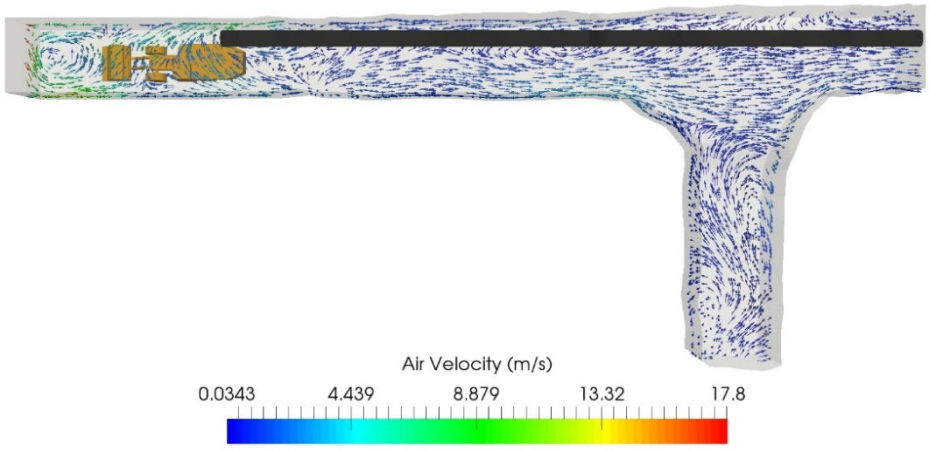

(a) Scenario 1

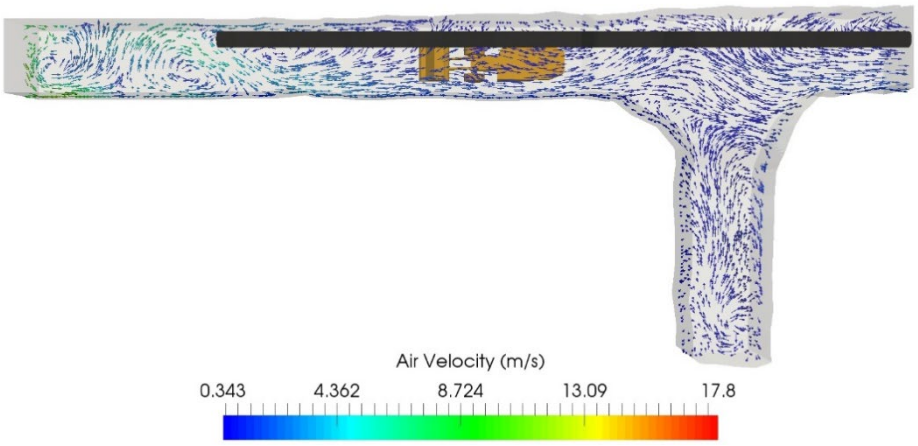

(b) Scenario 2

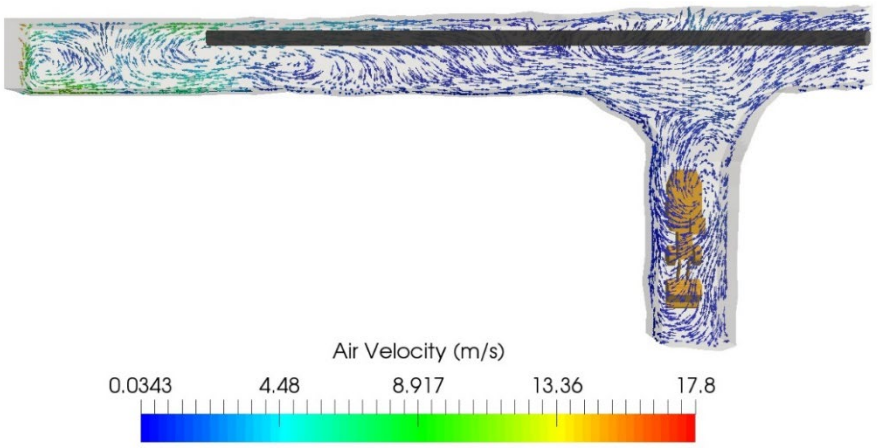

(c) Scenario 3

Figure 45 Airflow velocity vectors at 3 m height above the floor

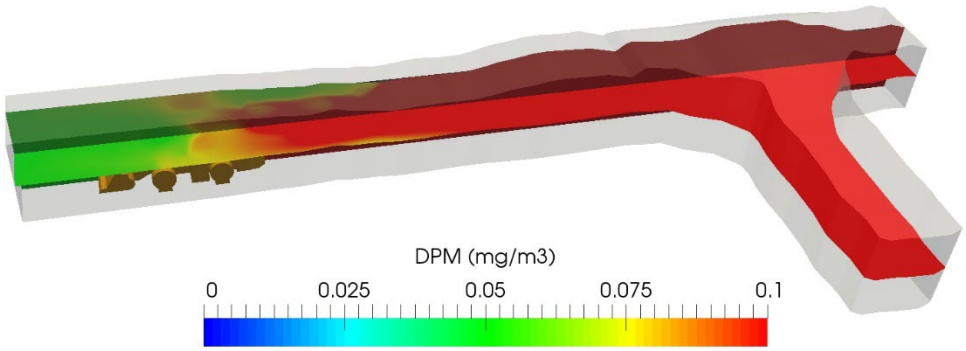

(a) scenario 1

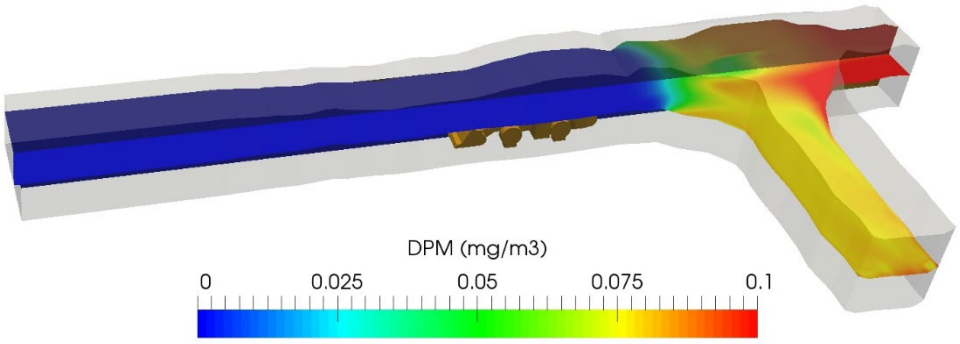

(b) scenario 2

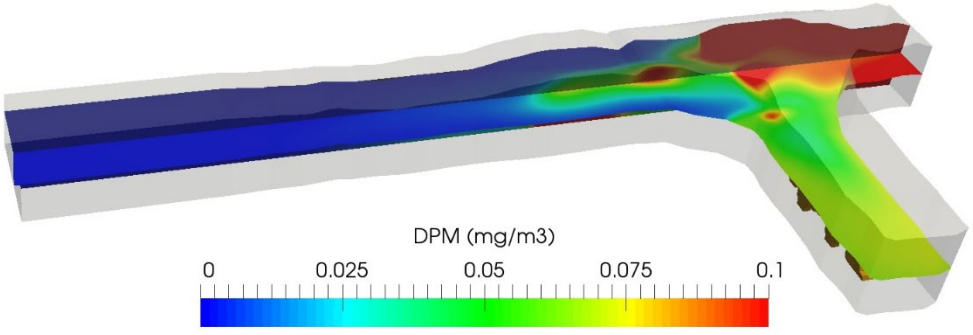

(c) Scenario 3

Figure 46 DPM concentration distributions at cross sections for loading activity

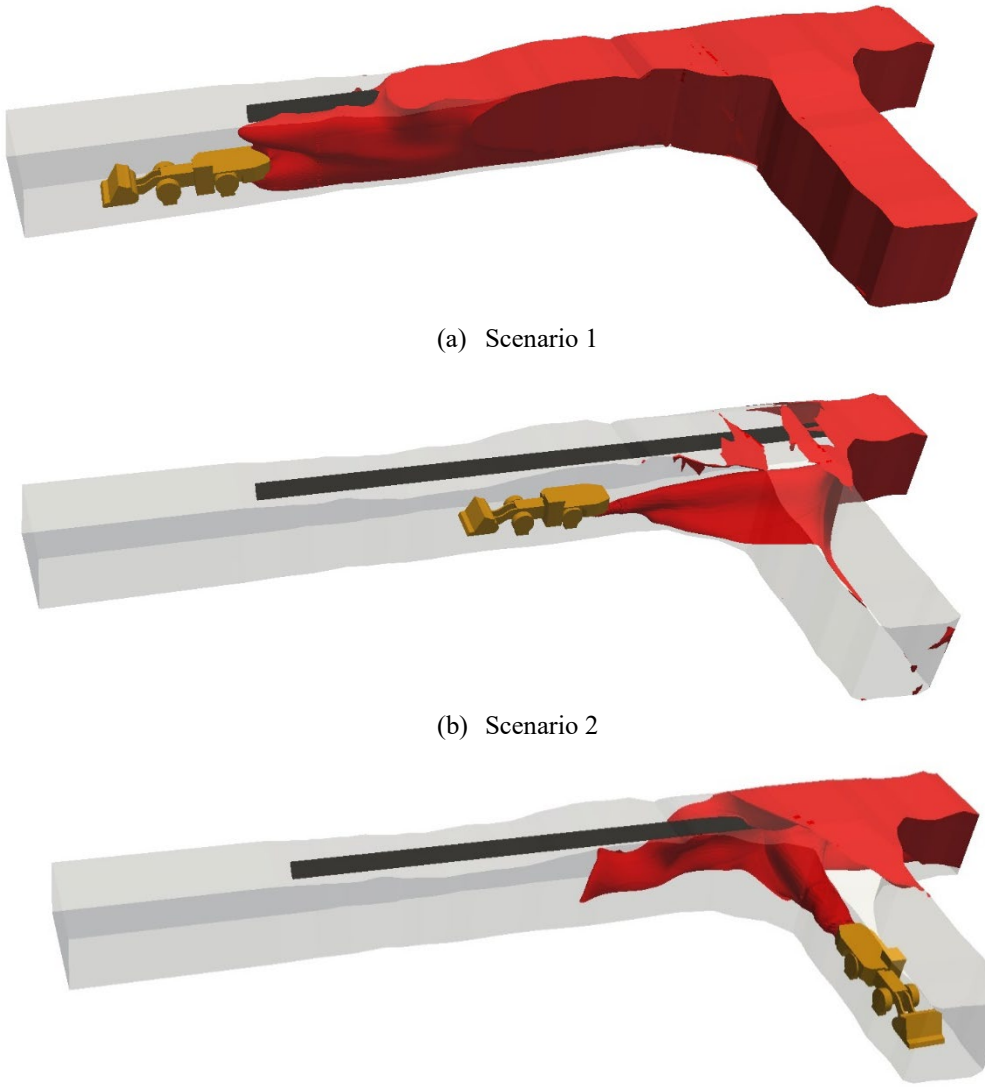

(a) Scenario 1

(b) Scenario 2

(c) Scenario 3

Figure 47 DPM distributions with the concentration large than the limit (0.1 mg/m^3) for loading activity

6.4.3 Charging Activity

The airflow velocity vectors at 3 m height above the floor for charging activity are given in Figure 48. As shown in Figure 48, a local recirculation region exists around the Charmec bucket. However, as the exhaust pipe is located at the bottom of the Charmec, the airflow in the region was not sufficient to carry any significant fraction of the DPM upstream from the vehicle. This, along with Figure 49 indicates that DPM concentrations during charging are mostly lower than the allowable limits. As shown in Figure 48, a low-velocity zone exists downstream of the Charmec, which can be expected to retain greater DPM concentrations. The airflow velocity in the non-duct side wall is large enough for the DPM to diffuse sufficiently with the air at this side first and then disperses to other areas slowly in the tunnel.

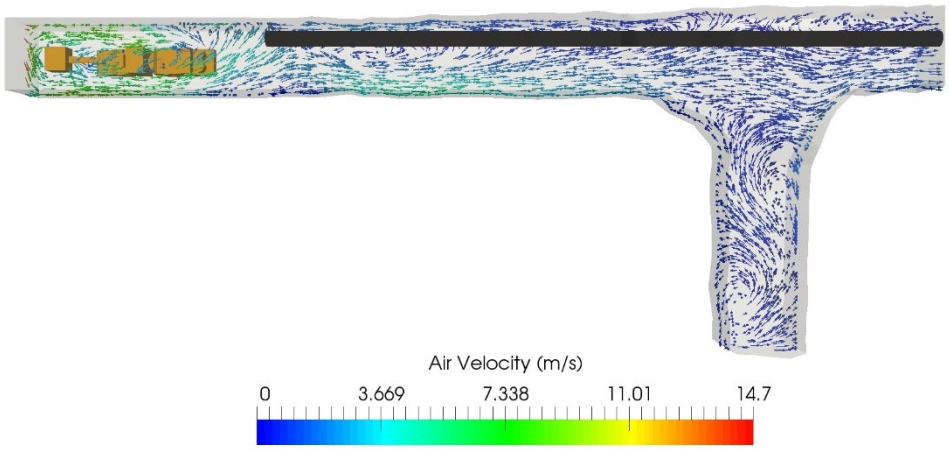

Figure 48 Airflow velocity vectors at 3 m height above the floor for charging activity

The DPM distributions at vertical and horizontal cross section are given in Figure 49. As expected, the DPM concentration around the Charmec was quite low. Some DPM accumulated at the right behind of the Charmec due to the low-velocity recirculation region, as shown in Figure 49. Beyond about 3 m downstream from the Charmec, a uniform distribution of DPM can be seen in the figure at the steady state. Figure 50 illustrates the DPM distribution with the concentrations large than the limit. It is noticed that no DPM concentration in the tunnel exceeded the limit except the area close to the exhaust pipe. Compared to the DPM concentration distribution of shotcreting activity, the concentrations are relatively lower for charging activity. Thus, the position of exhaust pipe also plays an important role in the distribution of DPM. In summary, the DPM levels in the vicinity and downstream of the Charmec are relatively lower than the safe levels. For the miners who work in this situation do not have the potential to over-exposure to DPM.

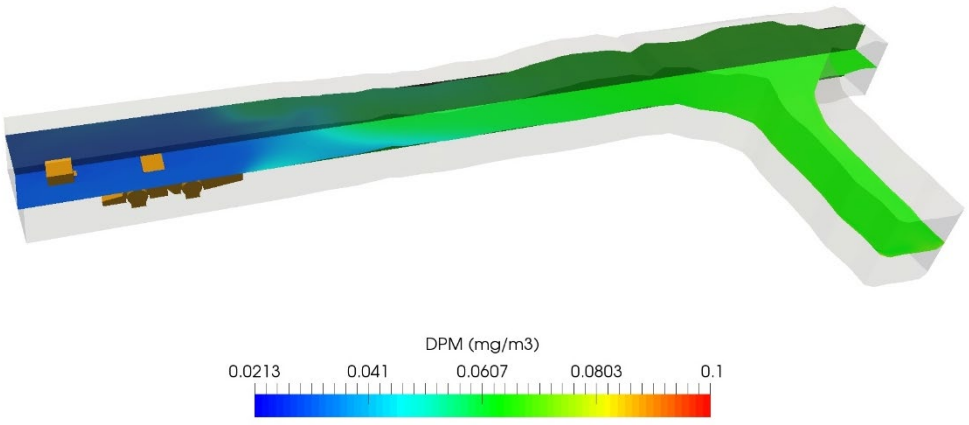

Figure 49 DPM concentration distributions at cross sections for charging activity

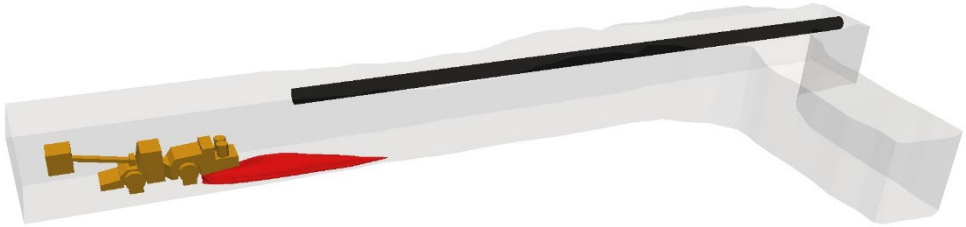

Figure 50 DPM distributions with the concentration large than the limit (0.1 mg/m^3) for charging activity

6.4.4 Ventilaton optimization for laoding activity

As analyzed in 6.4.1to 6.4.3, the DPM concentrations have exceed the limit (0.1 mg/m^3) in most of the areas only in the loading activity due to the higher engine power (305 kW) of the loader. Based on the diesel engine power (kW), the minimum requirement of ventilation rate in underground mines is regulated 0.06 m^3/s per kW in Australia (Chang & Xu, 2019). In this study, the minimum ventilation rate for the loader can be calculated as following:

$$Minimum\ ventilation\ rate = 0.06\,m^3/s \cdot kW \times 305\,kW = 18.3\ m^3/s$$

The actual ventilation rate in this development face is 21.2 m^3/s (as shown in Table 10), which has already met the minimum requirement. Generally, to dilute the diesel exhaust, the ventilation rate ranges from 0.06 to 0.1 m^3/s per kW in underground mines (Hedges, Djukic, & Irving, 2007). To dilute the DPM concentration of the loading activity below the requirement, another simulation (scenario 1 as the representative) was conducted with the ventilation rate set as 0.1 m^3/s per kW (air quantity as 30.5 m^3/s). The results are presented in Figure 51 and Figure 52. As can be seen, with the ventilation rate increase, the diesel particles concentration has been diluted below the limit expect the area near the exhaust pipe. The average DPM concentration is about 0.08 mg/m^3, which is close to but still under the limit (0.1 mg/m^3). Thus, the high DPM concentration issues can be solved by increase the ventilation rate to 30.5 m^3/s (0.1 m^3/s per kW).

In addition, a different ventilation rate requirement for the diesel machine is regulated by Mine Safety and Health Administration (MSHA) in the US. MSHA uses particulate index (PI) to calculate the required ventilation rate. The details of the minimum air quantity calculation has been presented in MSHA's report (MSHA, 2014). According to MSHA's regulation, the required minimum air quantity for Caterpillar Loader R3000H is 56.64 m^3/s, which is almost double the air quantity used in the simulation. It is obvious that such a ventilation rate would result a better DPM dilution performance, because the DPM concentration drops with the increase of ventilation rate. However, higher ventilation rate also cost more. Based on the simulation results, it

seems 30.5 m^3/s (0.1 m^3/s per kW) is optimum ventilation rate to maintain the pollutant under the limit.

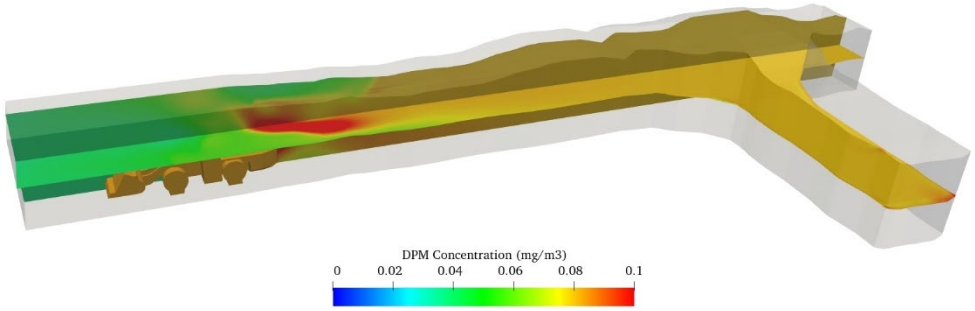

Figure 51 DPM concentration distributions at cross sections for loading activity (air quantity 30.5 m^3/s)

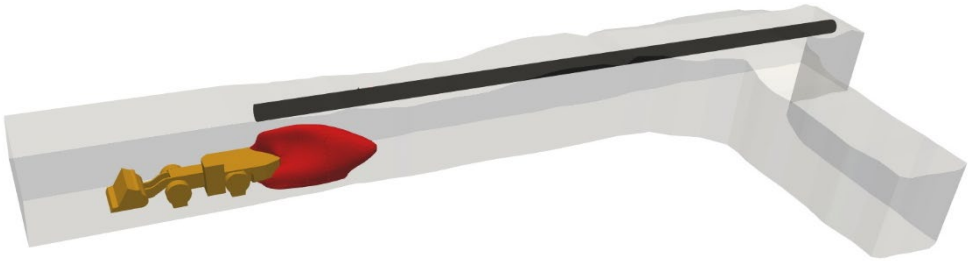

Figure 52 DPM distributions with the concentration large than the limit (0.1 mg/m3) for loading activity (air quantity 30.5 m^3/s)

6.5 Conclusion

Steady-state CFD simulations of DPM dispersion in a development face were conducted for three typical mining activities which include the shotcreting activity, loading activity, and charging activity. The tracer gas SF_6experiments were first conducted on the mine site and then the CFD modellings were built. The simulation results were validated with the onsite data. Then, the high DPM concentration ($\geq$ 0.1 mg/m^3) zone was determined for each activity. The results are summarized as follow:

1. The mean flow and turbulence are the key factors affecting the DPM dispersion in the development face under considered operating conditions.
2. For shotcreting activity and charging activity, the concentration of DPM in the tunnel is consistently lower than the acceptable limit except for the areas close to the exhaust tailpipe. For these two activities, the current ventilation system is sufficient to ensure the miners are not over-exposed hazardous levels of DPM. However, for loading activity, the DPM concentrations in most of the downstream areas of the loader exceed the limit. The miners who work in the downstream regions are likely to be exposed to the high concentrations of DPM.

For this activity, additional considerations are necessary to avoid over-exposure to DPM.

3. The exhaust pipe position of vehicles and relative location between the exhaust pipe and the duct outlet highly influence the DPM distributions in the development face. For shotcreting activity, the DPM concentrations in the whole region are similar. However, the DPM concentrations at the upstream of the Charmec and the loader are relatively lower than that at other regions in the development face.
4. The power of diesel vehicles is various for different activities. Loader, for example, has a more powerful diesel engine than the Spraymec and Charmec. Thus, it generates more DPM than the other two vehicles. Although for the shotcreting and charging activity, the current auxiliary ventilation system can dilute the DPM effectively, it cannot maintain the DPM concentration below the limit for loading activity. For this reason, different ventilation could be used for different activities to ensure the DPM levels are maintained below the allowable limits at all times. For loading activity, the DPM concentration could be decreased by increasing the fresh air through the ventilation duct. An optimum ventilation rate of 30.5 m3/s (0.1 m3/s per kW) has been obtained to keep the diesel plume under the limit (0.1 mg/m3).

In this study, it has shown that the CFD simulations by using the species transport method give a less computational cost and present a good agreement with the onsite data of SF_6 concentration. Compared to the traditional one-dimensional methods for the mine ventilation designs, CFD simulation could give more accurate results and presents more details for the ventilation system. The results presented in this study could be potentially used for the further auxiliary ventilation system optimization for the DPM dilution purpose in the development face, thus reduce the underground miners' occupational exposure.

6.6 Acknowledgement

This research project is supported by the Minerals Research Institute of Western Australia (M495), and the computation resources provided by the Pawsey Supercomputing Centre with funding from the Australian Government and the Government of Western Australia.

7 Numerical study on DPM dispersion and distribution in an underground development face based on dynamic mesh

This part has been presented on the 17th North American Mine Ventilation Symposium, Montreal, Canada. It was entirely written by Ping Chang with the editorial suggestion by Dr Guang Xu. Please cited it as:

Chang, P., & Xu, G. (2019). Numerical study on DPM dispersion and distribution in an underground development face based on dynamic mesh. Paper presented at the Proceedings of the 17th North American Mine Ventilation Symposium.

The vehicle equipment is a dynamic status for some of the mining activities, such as loading. The previous chapter presented the DPM distribution of a moving vehicle by simulating that of different positions. Although this method could provide accurate results by modelling the DPM distribution at enough positions. However, it is computational costly. Thus, this chapter provided a method named dynamic mesh method to simulate the DPM distribution of a moving vehicle.

7.1 Abstract

In 2012, the International Agency for Research on Cancer (IARC) classified diesel particulate matter (DPM) as a carcinogen to human. With the increased usage of diesel equipment in underground mines, miners have a high risk of over-exposure to DPM, which has drawn many concerns by the public. This study used computational fluid dynamics (CFD) to analyse the DPM dispersion and concentration distribution characteristics in an underground development face based on an on-site experiment. The DPM emitted from a moving loader under forcing auxiliary ventilation was simulated. The motion of the LHD in the tunnel was represented by a dynamic mesh method. The species transport approach was applied to study the DPM behaviours. High DPM concentration zones were then identified based on the simulation results. The results could provide guidelines for work practices and could be helpful to an optimum auxiliary ventilation design to reduce underground miner exposure.

7.2 Introduction

Since the 1960s, the diesel based machinery has been largely used in the mining industry due to its good performance in the mining activities compared to gasoline equipment. However, the extensive usage of diesel machines generates diesel particulate matter (DPM) issues on the mine site, especially for the underground mines, where space are confined. In such areas, the miners have the potential to expose to a high concentration of DPM. Previous researches (Chang & Xu, 2017b; HEI, 2003; Lyon, 2012) have associated both short- and long-term exposure to a high concentration of DPM to adverse health effects on humans. Also, the International Agency for Research on Cancer (IARC) classified DPM as a Group 1 carcinogenic to humans based on sufficient epidemiological and animal studies in 2012 (Lyon, 2012). To protect the underground miner's health, it is important to control the DPM concentration below an acceptable level. Currently, the Australia Institute of Occupational Hygienists (AIOH) recommended an 8-hour time weighted-average DPM exposure concentration of 0. 1

mg/m^3 (measured as elemental carbon) as a guidance value for the underground mines. In this paper, this value is also used as the DPM limit.

There are two main approaches to control the DPM on the mine sites (Chang & Xu, 2019). One is called source control, which controls the DPM before it is released from the diesel engine. This method mainly includes diesel engine regular maintenance and the usage of bio-diesel or low-sulphate diesel. The other method is exposure control, which controls the DPM after it is emitted in the work environment. This method mainly includes the usage of diesel filters, the usage of environmental cabs and the mine ventilation. Currently, mine ventilation is still the main approach to control the DPM concentrations. Therefore, understanding the DPM distribution characterises and dispersion behaviours will be beneficial to make an effective and economic ventilation strategy. This is particularly important for the underground development face, where the ventilation performance highly relies on the auxiliary ventilation design.

With the development of computer science, computational fluid dynamics is widely used to solve the mining-related issues. It has been used to evaluate the different ventilation system performance in underground mines (Aminossadati & Hooman, 2008; Parra et al., 2006; Sasmito et al., 2013); study the contaminant behaviours under different ventilation designs (Boadi & Wittenberg, 2002; Jundika C Kurnia, Agus P Sasmito, et al., 2014a; Javier Toraño et al., 2009; L. Zhou et al., 2015); investigate the coal dust distribution characteristics and management(Gong, Xia, Wu, Mo, & Zhang, 2017; Hu et al., 2016b; X. Liu et al., 2018; Proud et al., 2015) and simulate the tracer gas to evaluate the damage of the ventilation system after the incident in underground mines (Xu et al., 2015; Xu et al., 2013).

In addition, the CFD method has also been used to study the DPM behaviour in underground mines. Kurnia used species transport method predicted the diesel emissions under four types of auxiliary ventilation systems in an underground mining face. The control effectiveness of each ventilation design was evaluated and the most effective control strategy was suggested (Kurnia et al., 2014b). Zheng and his colleagues carried out a series of studies to address the DPM issues in underground mines (Zheng et al., 2017; Zheng et al., 2015a; Zheng et al., 2015b; Zheng et al., 2015c). Similar as Kurnia's study, the species transport model was used to simulate the DPM dispersion pattern. In Zheng's studies, C8H18 was used to represent the DPM. He investigated the DPM dispersion pattern under the effect of buoyancy in a long single entry (Zheng et al., 2015a). The results showed that DPM preferred to accumulate near the roof and top area in the tunnel due to the influence of buoyancy. With the same simulation method, he and

his colleagues also studied DPM distributions under four different auxiliary ventilation designs in a development face (Zheng et al., 2015b; Zheng et al., 2015c).By the comparison of four ventilation designs, the authors indicated that the short push and curved pull tubing ventilation system gave the best DPM control performance. Another numerical study conducted by Zheng et al. (Zheng et al., 2017) investigated the effect of the tunnel inclination on the DPM dispersion pattern. The results found that DPM accumulated easily in the upward dead end due to combination effects of the roadway inclination and buoyancy. In this situation, the DPM was hard to be removed by the current ventilation. The ventilation rate need to be increased by three times to lower the DPM under the limit. Guang et al (Xu et al., 2018) has built the CFD models to study the DPM distribution in an underground isolated zone. In this study, Eulerian-Lagrangian method was applied to simulate the gas-solid two phase fluid and a good agreement with the onsite experimental data has been achieved. Chang et al. (Chang et al., 2019b) used the same simulation method to evaluate the effectiveness of the different auxiliary ventilation systems on the DPM dilution. The study was conducted in an underground development face and three auxiliary ventilation designs with different duct length was evaluated. The results suggested that the duct length with 5 m longer than the current design gave the best DPM control results. However, in all the previous studies, only the diesel vehicle worked at a stationary state was simulated. In fact, the diesel vehicles, like loader and truck, move around during the working activities. It is believed that the DPM behaviours is highly affected by the motion of the vehicle. Thus, it is necessary to understand the DPM distribution and dispersion under the effect of the vehicle motion. Besides, how the ventilation affect the DPM distribution during the vehicle motion also need to be investigated.

The aim of this study is to simulate the DPM concentration distributions during a loading activity in an underground development face. Previous studies illustrated that both the Eulerian-Lagrangian method and species transport method can be used to simulate the DPM dispersion patterns (Chang, Xu, Zhou, Mullins, & Abishek, 2019; Thiruvengadam, Zheng, & Tien, 2016).However, species transport method needs less computational expense. Thus, this method is applied to simulate the DPM behaviours. According to Zheng's study (ZHENG, 2011; Zheng et al., 2011a; Zheng, Thiruvengadam, et al., 2015a; Zheng, Thiruvengadam, et al., 2015b), and C_8H_{18} is used to represent the DPM. The motion of the loader is presented by a dynamic mesh method in ANSYS Fluent. This study is still at its initial stage, only a 2D model is presented to

reveal airflow characteristics and the DPM behaviours due to the low computational cost. The 3D models will be built in further studies.

7.3 Model Description

7.3.1 Physical Model Geometry

The physical model is built based on an underground development face in a gold mine in Western Australia. The schematic diagram for the underground development face is shown in Figure 53. The length and average width of the development face is 84.5 m and 6 m, respectively. A cuddy is connected to the development face, which is 28.5 m from the development face entrance. The width and depth of the cuddy are 6 m and 20.6 m, respectively. The 1.2 m diameter forcing duct system is installed in the development face and the duct outlet is 15.2 m from the heading face. A loader is initially parked at 3.9 m from the development entrance. The whole loading activity is assumed to be 126 s, which includes three statuses. The first status is from 0 s to 33 s, the loader moves from the initial parking place to the front of the heading face. The second status is from 33 s to 93 s, the vehicle keeps stationary at the front of the heading face to represent the loading activity. The third status is from 93 s to 126 s, the loader reverses back to the initial parking place after the loading activity. During the motion, the loader is assumed to be moving at a constant speed of 2 m/s for both forward and reverse motion. The distance between the initial parking place and the loading place at the front of the heading face is 66 m, as shown in Figure 53. The loader used in this activity is Caterpillar Loader R3000H, Tier 3.

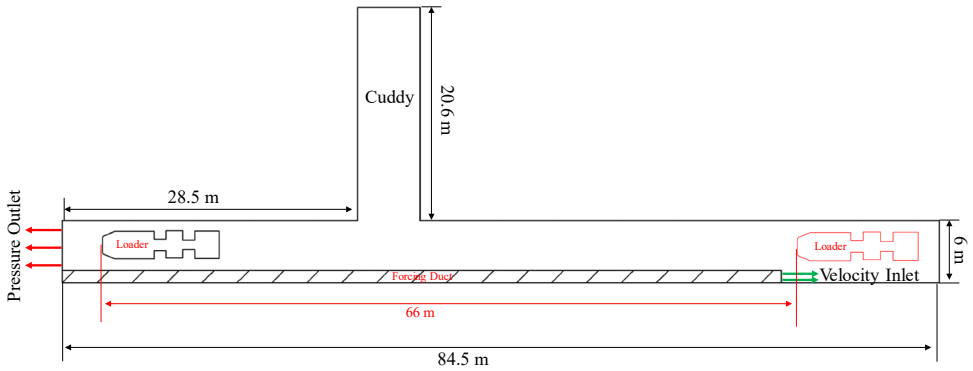

Figure 53. The schematic diagram for the CFD model

7.3.2 CFD Model Setup

ANSYS Fluent 19. 1 was used for the CFD simulation. The airflow was assumed to be incompressible. Standard $k-\varepsilon$ turbulent model is widely used in mining-related studies (Hu et al., 2016b; Ren et al., 2014; J Toraño et al., 2011; Javier Toraño et al.,

2009), and this turbulent model was also used in this study to simulate the airflow region. The Species Transport model is used to simulate the DPM. No heat-transfer was considered in the study. The model was first simulated to a steady-state with the loader parked at the initial parking area before the dynamic mesh simulation for 126 s. Pressure – Velocity coupling is solved by SIMPLEC. The solution spatial discretization used for the simulation is illustrated in Table 12. The convergence criteria for the parameters is set as 1×10^{-3}.

There are 3 dynamic mesh methods available in Fluent, smoothing, layering and remeshing. Smoothing and remeshing methods were selected in this paper. In the ANSYS Fluent user's Guide (ANSYS, 2018), the tetrahedral mesh is recommended for the smoothing and remeshing methods. Thus, this kind of mesh was generated in the paper. Mesh independence is an important part of a simulation study to guarantee the numerical solution independent on the size of the mesh. For this reason, two meshes, medium mesh and fine mesh, are generated. The total elements for medium mesh and fine mesh are 8082 and 15037, respectively. In order to obtain accurate results, high density meshes were generated for the critical areas (near the loader and duct) where the airflow may be complex, the medium mesh is given in Figure 54 as a representative. Air velocities at a vertical monitor line 20 m from the pressure outlet for different meshes are shown in Figure 55. As can be seen, the air velocities for medium mesh are highly close to that of fine mesh, thus the mesh independence is achieved and medium mesh is used for the simulation.

The properties of C_8H_{18} used in this paper referred to Zheng's study (Zheng, Thiruvengadam, et al., 2015a). Other initial conditions were determined based on the onsite measurement. All the boundary conditions needed for the CFD simulation are listed in Table 13. A time step $\Delta t = 0.005\ s$ was used for the 126 s transient simulation. CFD simulation was carried out on a workstation with 16 processors and it took about 40 hours to complete the simulation. More details about the governing equations could be found in the ANSYS Fluent user's Guide (ANSYS, 2018).

Table 12 Numerical schemes

Spatial Discretization	Description
Gradient	Green-Gauss cell based
Pressure	Second order
Momentum	Second order upwind
Turbulent kinetic energy	Second order upwind
Turbulent dissipation rate	Second order upwind
C_8H_{18}	Second order upwind

Table 13 Boundary and initial conditions

Boundary	Value
Air	Density: 1.225 kg/m^3
	Dynamic Viscosity: 1.789×10^{-5} (Pa/s)
	Turbulence Viscosity: 1.461×10^{-5} (m^2/s)
Duct inlet	Air velocity: 18.75 m/s
Outlet	Pressure: 0 Pa (static pressure)
	Velocity: 22. 757 m/s
Exhaust pipe	C8H18 mass fraction: 4.069×10^{-6}
	C8H18 diffusion coefficient in air: 5×10^{-6} (m2/s)
Loader and Walls	No slip wall function

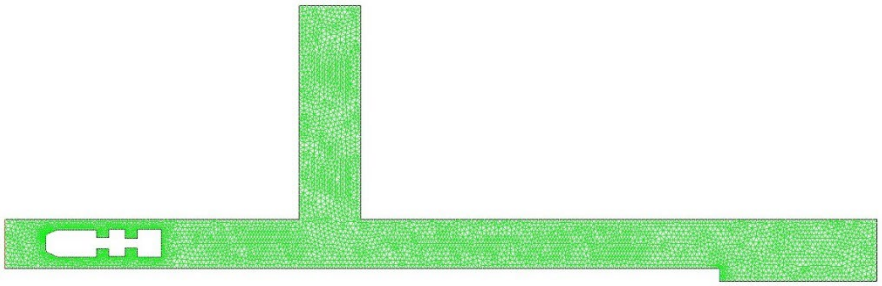

Figure 54. Mesh generation for the CFD modelling (Medium mesh)

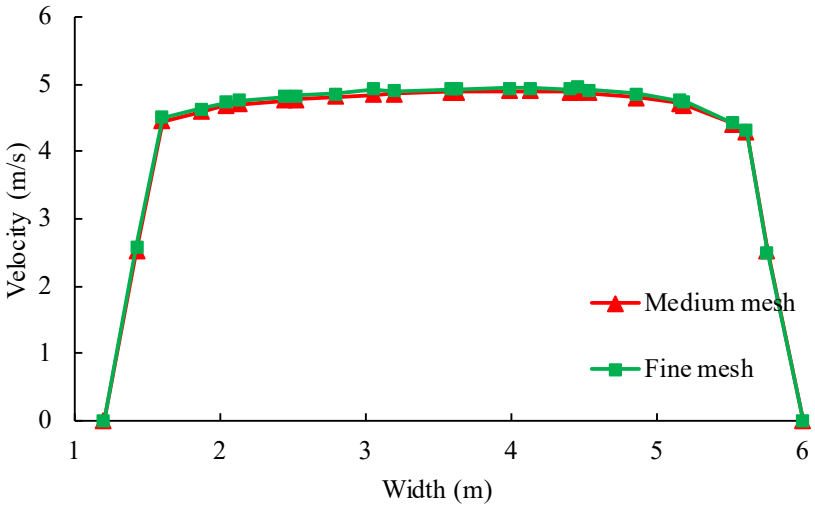

Figure 55. Air velocities for different meshes

7.4 Results and Discussion

7.4.1 Airflow Distribution

The airflow features in the development face highly affect the DPM behaviours. For the area where the vortex is located, the DPM may accumulate and result in a DPM overexposure. Therefore, it is necessary to make clear the airflow behaviours. The airflow velocity vectors at 5 different simulation times are presented in Figure 56. As can be seen, the vehicle at t = 0 s and t = 16s illustrate a similar airflow velocity distribution. At these times, the loader moves against the airflow and results in a high-

velocity areas besides the two sides of the loader. Due to the blockage of the loader, a low-velocity zone occurs at the behind of the loader, which may result in the DPM accumulation. It is worth to notice that a recirculation area was generated between the duct inlet and the heading face. However, no DPM would concentrate in this area because of the loader's location and airflow direction. At t = 63 s, as shown in Figure 56 (c), the loader keeps stationary at the front of the heading face. At this position, the high-air-velocity area was located at the cuddy side wall and a large low-air-velocity zone was generated at the behind of the loader near the non-cuddy side wall. This area might be hazardous because of the potential high DPM concentration exposure. During the loader reverse activity, a significant difference in the airflow features is discovered. The airflow velocity at the two sides of the loader was much closer to the airflow velocity at the other areas of the development face, as shown in Figure 56 (d). This is because the loader moved in the same direction as the airflow. A similar situation was observed at t =126 s when the vehicle arrived at the initial parking place, the velocity of the airflow at the sides of the loader at this time was much lower than that of t = 0s. In addition, it worth noting that the air velocity in the cuddy area was low during the whole loading activity. With the loader working in the development face, DPM diffused slow to the cuddy area and resulted in a high DPM concentration zone due to the poor ventilation condition in the cuddy.

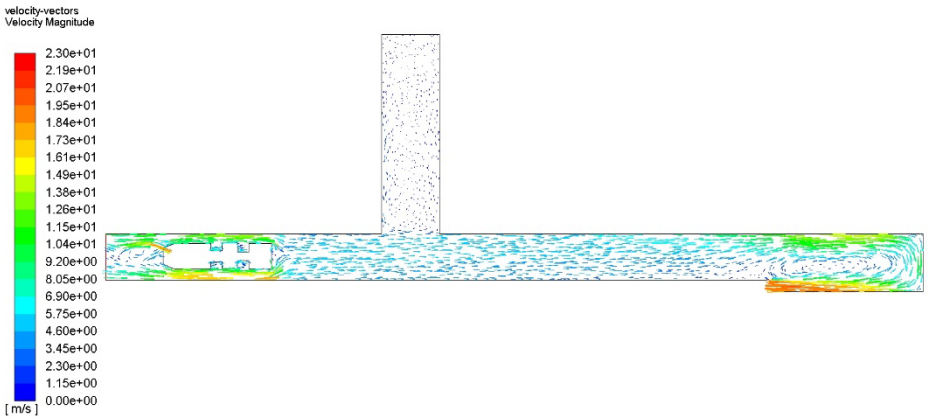

(a) t=0 s (initial parking place)

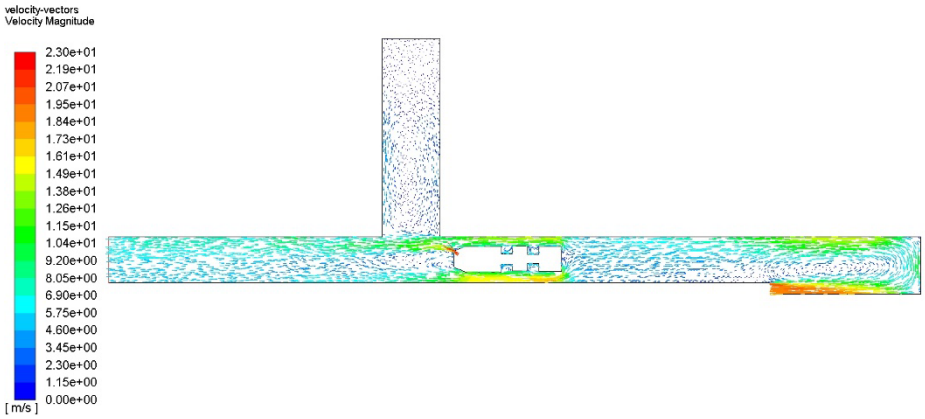

(b) t=16 s (32 m from the initial parking place)

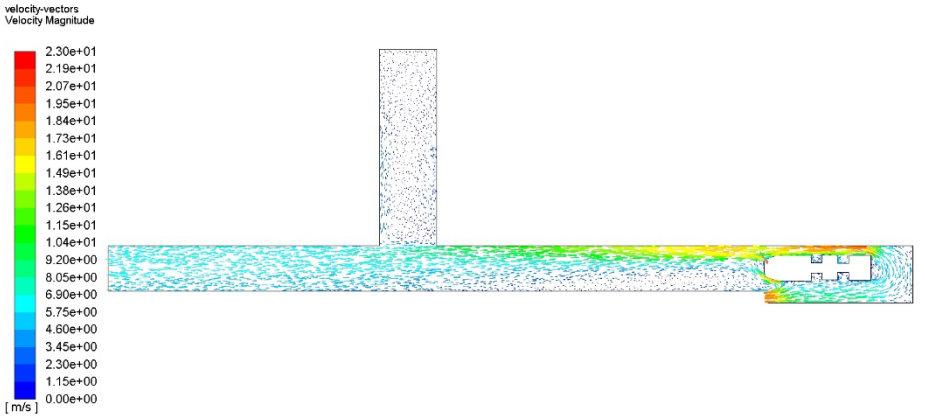

(c) t=63 s (66 m from the initial parking place)

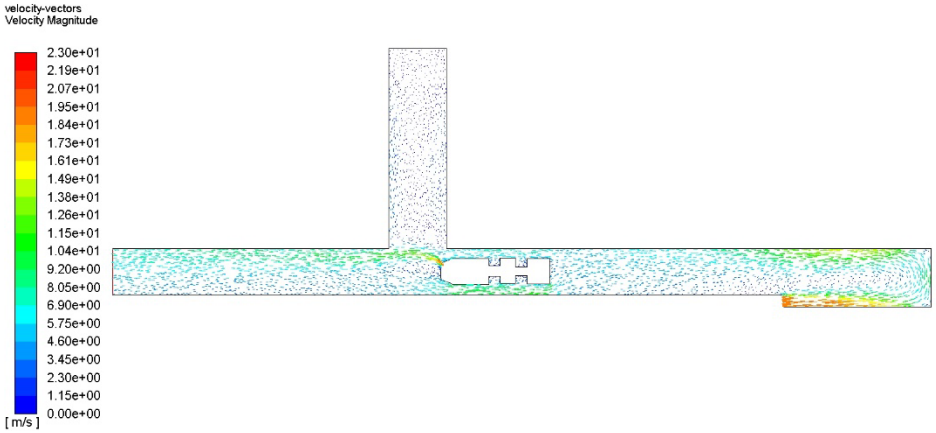

(d) t=110 s (32 m from the initial parking place)

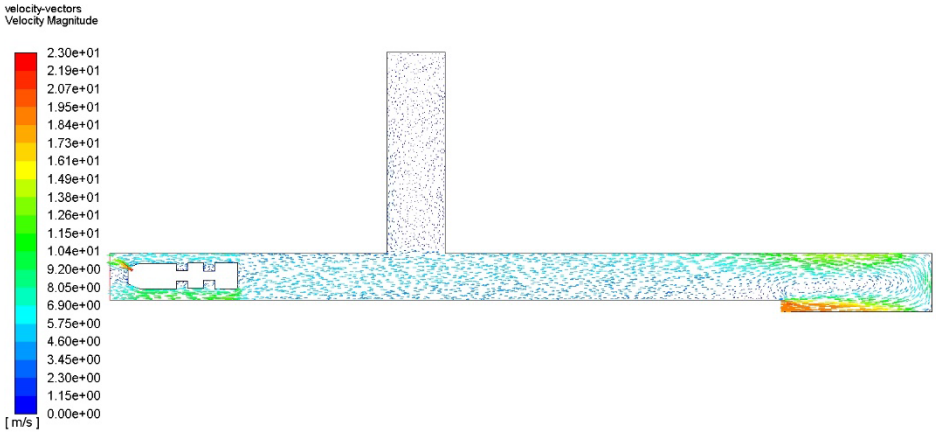

(e) t=126 s (initial parking place)
Figure 56. Airflow velocity vectors at different simulation time

7.4.2 DPM Distribution

The DPM distributions (≥ 0.1 mg/m^3) in the development heading at different times are shown in Figure 57. As expected, in the beginning, DPM accumulated at the back of the loader near the tailpipe due to the low-velocity airflow at this area. With the loader moving forward, the DPM diffused slowly to the other areas behind the loader. It can be observed that no DPM concentrated at the cuddy at 16 s, as shown in Figure 57 (b) due to to the main airflow direction in the development face. When the loader moving to the heading face, the DPM diffused slowly to the cuddy area (Figure 57 (c)). When the loader arrived at the front of the heading face, it can be seen that the downstream areas in the development face were filled with high concentration DPM. The DPM spread slowly with the loader working at the front of heading face and the cuddy was full of high levels of DPM at 63 s, as can be seen in Figure 57 (d). When the vehicle moving to the downstream, the high concentration areas at the front of the loader were quickly diluted by the fresh airflow from the auxiliary duct, as shown in Figure 57 (e) - (f). It worth noting that although the DPM concentrations at other areas at the upstream of the loader were reduced to an acceptable level, the cuddy was still filled with the high concentrations of DPM due to the poor ventilation condition. During the whole loading activity, no high concentration areas occurred at the upstream of the loader. However, the current ventilation system was not able to keep the DPM concentrations below the limit anywhere in the development face, espcecially for the downstream and cuddy areas. Thus, the additional protective approaches should be applied to protect the miner who work in these areas from the high DPM exposure.

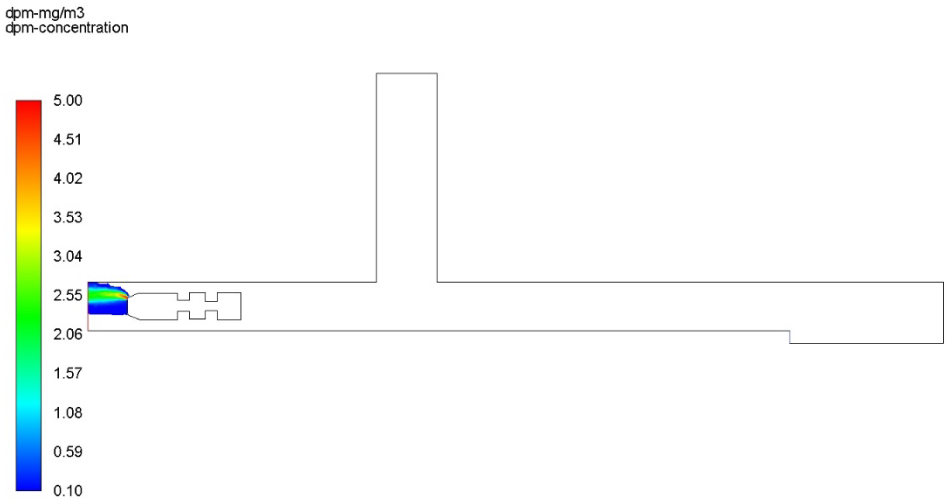

(a) t=0 s (the initial parking place)

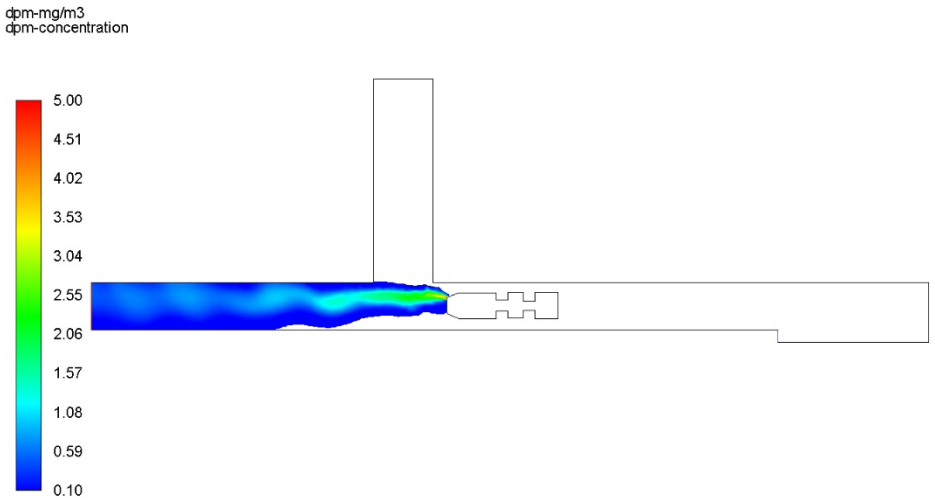

(b) t=16 s (32 m from the initial parking place)

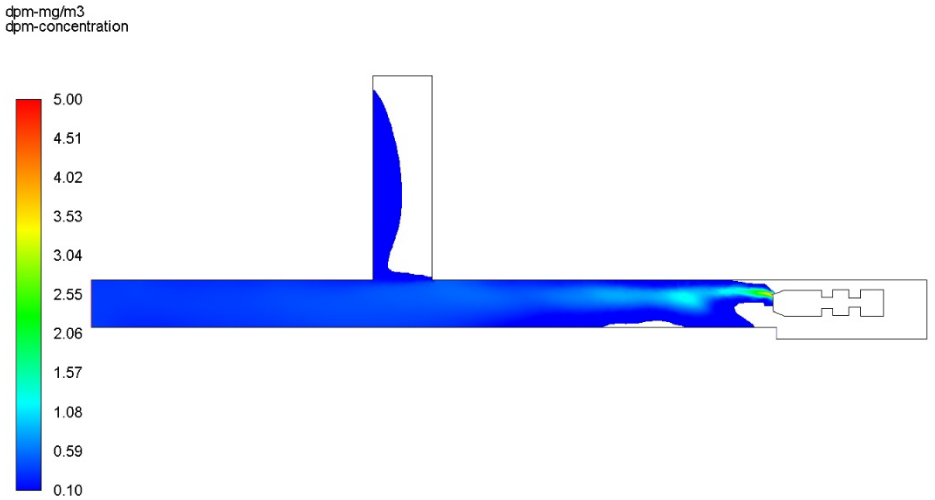

(c) t=33 s (66 m from the initial parking place)

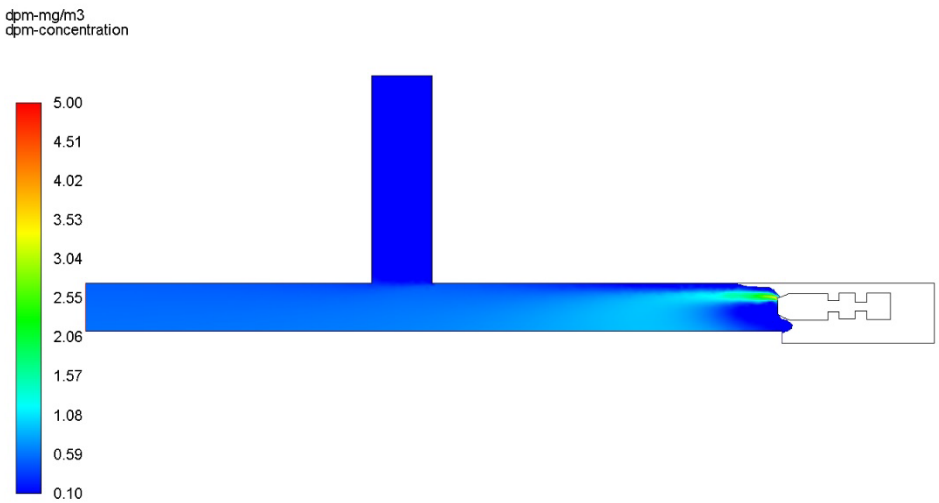

(d) t=63 s (66 m from the initial parking place)

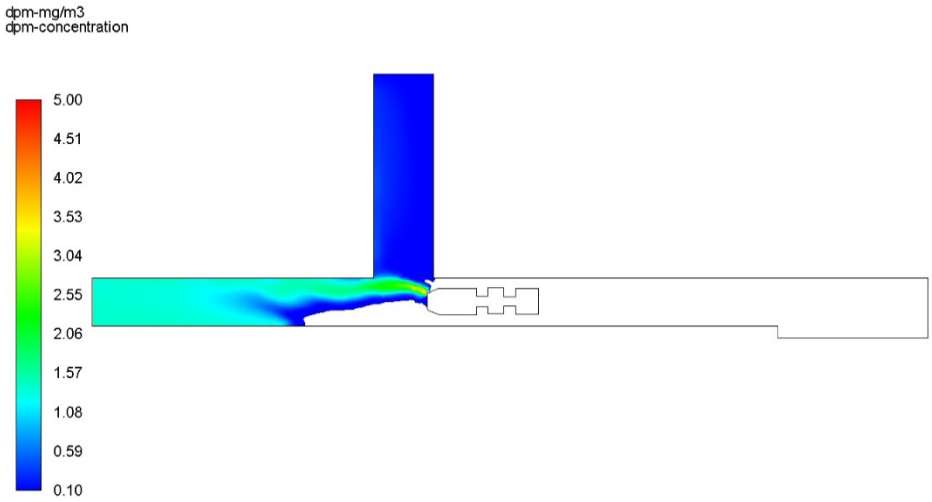

(e) t=110 s (32 m from the initial parking place)

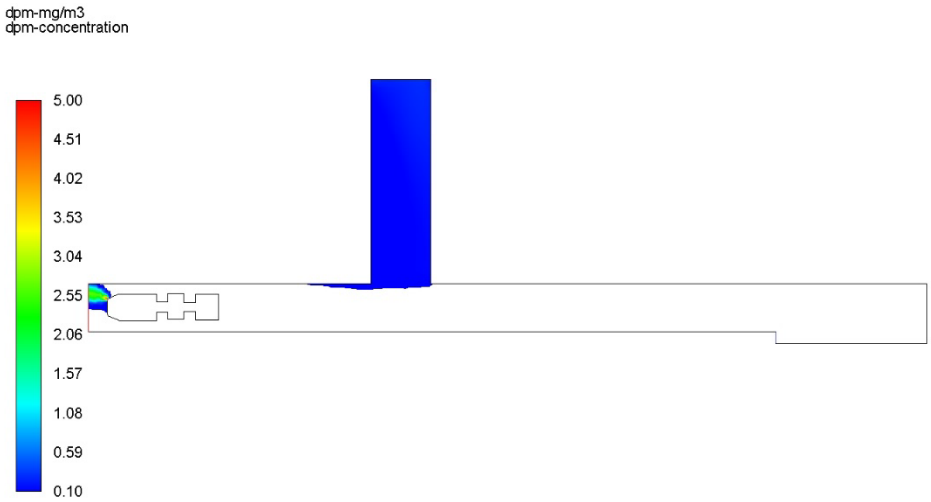

(f) t=126 s (initial parking place)

Figure 57. DPM distribution at different simulation time

7.5 Conclusion

In this paper, a 2D CFD study was conducted to simulate the DPM distribution for a loading activity in an underground development face. The dynamic mesh method was applied to study the motion of the loader. The airflow features and DPM concentration distributions under the combined effects of vehicle motion and auxiliary ventilation were presented. The simulation results indicated that the current ventilation system failed to maintain the DPM concentration below the limit. The high DPM concentration zones mainly occurred at the downstream of the loader due to exhaust flow and airflow direction. With the loader working in the development face, the DPM diffused slowly to the cuddy. When the loader moving to the downstream follow the airflow, the high DPM concentration areas at upstream were diluted quickly by the fresh airflow except the cuddy since the poor ventilation condition. Miners in the high concentration areas

mentioned above should be given additional protective equipment to avoid DPM over-exposure.

This study is still at its initial stage, thus only 2D simulation was presented. However, it can still reveal the DPM distribution characteristics for the moving vehicle. To understand the DPM behaviours under the combined effects of the vehicle motion and ventilation will contribute to a better auxiliary ventilation design in the development heading. For further research, a 3D simulation study will be conducted with the dynamic mesh approach to acquire a more accurate result.

8 Conclusions, Limitation and Future Works

8.1 Conclusions

This research illustrated that CFD modelling is an effective method to analysis the DPM dispersion and concentration distributions in underground mines. Both the Eulerian-Lagrangian method and species transport method were used to mimic the DPM in underground mines. The onsite experiments were also conducted and used for simulation validation purposes. Good agreements were found between the numerical results and measurements data. The results could be used for the mining industries to better understand the DPM behaviours and optimize the ventilation design.

Hundreds of literature were reviewed and illustrated a positive relationship between the long-term high DPM concentration exposure and lung cancer risk. Currently, no single DPM control strategy can maintain it under the acceptable level effectively. Combined approaches are usually applied to protect the miners from high DPM exposure. However, ventilation is still the mining method to control DPM in underground mines, especially for the space confined areas, such as development face. The current research demonstrated that CFD modelling is a cost and time economic mean to address the DPM issues on the mine site.

Based on a published report, numerical models were built to study the DPM distributions in an isolated underground zone. The DPM was treated as a solid phase and the Eulerian-Lagrangian method were used to simulate the gas-solid two-phase flow. The results were further compared with a study which treated DPM as the gas phase. A closer agreement between the simulation results and onsite data was achieved when DPM was treated as solid particles. Two scenarios with different LHD locations were simulated to present the motion mining activity. 2D simulations were first conducted to determine the initial parameters for the 3D simulations. Then the 3D models were constructed to provide more accurate results. The high DPM concentration areas were identified and the appropriate DPM control methods were suggested based on the simulation results. The results indicated that the Eulerian-Lagrangian method is capable of providing more accurate results than the current numerical method on the DPM simulation.

According to the information provided in chapter 3. The Eulerian-Lagrangian method was applied to evaluate the performance of different auxiliary ventilation systems on DPM maintenance in an underground development face. The onsite measurement was first conducted before built the CFD modelling. Then the CFD models were built based on the onsite data. The DPM distributions for the shotcreting activity in the development face was predicted. Three auxiliary ventilation systems with different

duct lengths were evaluated. The results showed that the current ventilation system could not meet the recommended DPM level. And the ventilation system with the shortest distance between the duct outlet and heading face gave the best DPM control performance.

Following the previous studies, the three most commonly used numerical methods for the solid contaminant simulation in mining industries were summarized and compared. The Eulerian–Lagrangian method and Eulerian–Eulerian method was used when DPM was treated as discrete particles, and the species transport model was used when it is regarded as gases. Due to computational cost and result's accuracy, Eulerian-Eulerian method was not recommended for the DPM simulation. And the Eulerian-Lagrangian method could provide better results compared to other methods, especially for the critical areas around the diesel vehicle. The species transport method was suggested to be used for any preliminary studies according to the computational cost efficiency. However, the gas parameters, such as the diffusion coefficient in air, should be selected carefully to obtain a more reliable result.

Accordingly, the species transport method was used to investigate the DPM concentration distributions during key mining activities. The modelling of three activities, shotcreting, loading, and charging were constructed. For the loading activity, three scenarios with LHD located at different positions were constructed to present the dynamic loading activity. The ventilation system was evaluated. It was found that the current ventilation design could maintain the DPM effectively for both shotcreting and charging activities but not for loading due to the different engine powers. The CFD also highlighted the DPM accumulation areas where the ventilation could be optimized for the loading activity.

At last, the dynamic mesh method was provided to study the DPM distribution with the impact of vehicle motion. For safe consideration, it is usually hard to measure the DPM concentrations during the mining activity with the diesel vehicle moving around. The dynamic mesh modelling provided a safe and effective mean to identify the DPM accumulated areas the ventilation need to be improved. Although only the 2D model was built, it still demonstrated that CFD has the potential to solve such dynamic issues.

This study demonstrated that CFD predictions were in good agreement with the onsite measurement data. Compared to the traditional one-dimensional methods currently used on the mine site for mine ventilation design. The method presented in this study could be a potential alternative for underground mine auxiliary ventilation optimization. Furthermore, CFD could also be employed to predict the high DPM

concentration zones and optimize the desired airflow rates in specific areas according to the intended mining activities. Based on the above advantages, CFD will benefit in the DPM control and hence result in a lower occupational exposure in underground mines.

8.2 Limitation and Future works

Although this research provided an effective and cost-economic method for the DPM distribution prediction and ventilation optimization in the underground mines, the following limits still exist and future work will be done to solve these limits.

For the isolated study, although the Eulerian-Lagrangian method presented better simulation results. However, the discrepancy between the onsite data and simulation results was still up to 38%. To minimize the error, more scenarios (LHD operates at different locations) should be considered in future work.

In this study, all the simulations were conducted based on a sole diesel equipment work with a full load. In fact, multiple diesel equipment may operate together for some mining activities. In this situation, the DPM concentration would be much higher and extra protective measures should be applied for the miners. Besides, for most cases, the diesel machine does work with a full load, this should also be taken into account.

The DPM particle's size was assumed as an average diameter with 78.7×10^{-9} m when it was considered as a discrete solid phase. Different size particles may present different behaviours during the simulation. In addition, no heat transfer was considered in the simulation because the DPM would reduce to the environment temperature quickly once it left the tailpipe. Nevertheless, the temperature near the vehicle tailpipe is higher than the environmental temperature and the buoyancy caused by the temperature difference would impact the particles' dispersion. The consideration of particles size and the heat transfer will help to improve the accuracy of the simulation.

In chapter 4, the auxiliary ventilation system with only three duct lengths was compared. More scenarios with different duct positions should be studied to get the most optimum ventilation design.

For the stationary diesel vehicle simulation, the stable state could be achieved easily. However, there is no stable state for dynamic simulation. And 3D dynamic mesh simulation is computational cost expensive. It is almost impossible to simulate long duration mining activity by using this method. Although 2D simulation could be used sometimes, it is obvious that 3D simulation gives more accurate results. Hence, future work will focus on finding a computational cost economic method to achieve this goal.

References

Abishek, S., King, A. J., & Narayanaswamy, R. (2017). Computational analysis of two-phase flow and heat transfer in parallel and counter flow double-pipe evaporators. *International Journal of Heat and Mass Transfer, 104*, 615-626.

Afkhami, M., Hassanpour, A., Fairweather, M., & Njobuenwu, D. (2015). Fully coupled LES-DEM of particle interaction and agglomeration in a turbulent channel flow. *Computers & Chemical Engineering, 78*, 24-38.

AIOH. (2013). *Diesel Particulate Matter and Occupational Health Issues*. Retrieved from AIOH Exposure Standards Committee: https://www.aioh.org.au/documents/item/15

AIOH. (2017). *Diesel Particulate Matter and Occupational Health Issues Position Paper*. Retrieved from

Aminossadati, S. M., & Hooman, K. (2008). *Numerical simulation of ventilation air flow in underground mine workings.* Paper presented at the 12th US/North American Mine Ventilation Symposium 2008.

Anderson, J. O., Thundiyil, J. G., & Stolbach, A. (2012). Clearing the air: a review of the effects of particulate matter air pollution on human health. *Journal of Medical Toxicology, 8*(2), 166-175.

Andrews, M., & O'rourke, P. (1996). The multiphase particle-in-cell (MP-PIC) method for dense particulate flows. *International Journal of Multiphase Flow, 22*(2), 379-402.

ANSYS. (2018). FLUENT user's guide. *ANSYS Inc, Canonsburg*.

Apple, J., Vicente, R., Yarberry, A., Lohse, N., Mills, E., Jacobson, A., & Poppendieck, D. (2010). Characterization of particulate matter size distributions and indoor concentrations from kerosene and diesel lamps. *Indoor air, 20*(5), 399-411.

Ashraful, A., Masjuki, H., & Kalam, M. (2015). Particulate matter, carbon emissions and elemental compositions from a diesel engine exhaust fuelled with diesel–biodiesel blends. *Atmospheric Environment, 120*, 463-474.

Attfield, M. D., Schleiff, P. L., Lubin, J. H., Blair, A., Stewart, P. A., Vermeulen, R., . . . Silverman, D. T. (2012). The diesel exhaust in miners study: a cohort mortality study with emphasis on lung cancer. *Journal of the National Cancer Institute, 104*(11), 869-883.

Behçet, R., Oktay, H., Çakmak, A., & Aydin, H. (2015). Comparison of exhaust emissions of biodiesel–diesel fuel blends produced from animal fats. *Renewable and Sustainable Energy Reviews, 46*, 157-165. doi:http://dx.doi.org/10.1016/j.rser.2015.02.015

Benyahia, S., & Galvin, J. E. (2010). Estimation of numerical errors related to some basic assumptions in discrete particle methods. *Industrial & Engineering Chemistry Research, 49*(21), 10588-10605.

Berlo, D. v., Albrecht, C., Knaapen, A. M., Cassee, F. R., Gerlofs-Nijland, M. E., Kooter, I. M., . . . Krutmann, J. (2010). Comparative evaluation of the effects of short-term inhalation exposure to diesel engine exhaust on rat lung and brain. *Archives of toxicology, 84*(7), 553-562.

Birch, M., & Cary, R. (1996). Elemental carbon-based method for monitoring occupational exposures to particulate diesel exhaust. *Aerosol Science and Technology, 25*(3), 221-241.

Birch, M. E. (2003). Monitoring of diesel particulate exhaust in the workplace. *NIOSH Manual of Analytical Methods (NMAM)*, 2003-2154.

Birch, M. E., & Cary, R. A. (1996). Elemental carbon-based method for occupational monitoring of particulate diesel exhaust: methodology and exposure issues. *Analyst, 121*(9), 1183-1190.

Birch, M. E., Dahmann, D., & Fricke, H.-H. (1999). Comparison of two carbon analysis methods for monitoring diesel particulate levels in mines. *Journal of Environmental Monitoring, 1*(6), 541-544.

Birch, M. E., & Noll, J. D. (2004). Submicrometer elemental carbon as a selective measure of diesel particulate matter in coal mines. *Journal of Environmental Monitoring, 6*(10), 799-806.
Boadi, D., & Wittenberg, K. (2002). Methane production from dairy and beef heifers fed forages differing in nutrient density using the sulphur hexafluoride (SF6) tracer gas technique. *Canadian Journal of Animal Science, 82*(2), 201-206.
Boffetta, P., Dosemeci, M., Gridley, G., Bath, H., Moradi, T., & Silverman, D. (2001). Occupational exposure to diesel engine emissions and risk of cancer in Swedish men and women. *Cancer Causes & Control, 12*(4), 365-374.
Borak, J., Sirianni, G., Cohen, H., Chemerynski, S., & Wheeler, R. (2003). Comparison of NIOSH 5040 method versus Aethalometer™ to monitor diesel particulate in school buses and at work sites. *Aiha Journal, 64*(2), 260-268.
Bugarski, A., Mischler, S., Noll, J., Schnakenberg, G., Crum, M., & Anderson, R. (2004). An Evaluation of the Effects of Diesel Particulate Filter Systems on Air Quality and Personal Exposure of Miners at Stillwater Mine Case Study: Production Zone. *Report to M/NM Diesel Partnership, April, 1*.
Bugarski, A., Schnakenberg, G., Noll, J., Mischler, S., Patts, L., Hummer, J., . . . Anderson, R. (2004). The Effectiveness of Selected Technologies in Controlling Diesel Emissions in an Underground Mine—Isolated Zone Study at Stillwater Mining Company's Nye Mine. *Draft Report,''NIOSH, Pittsburgh Research Laboratory*.
Bugarski, A. D., Cauda, E. G., Janisko, S. J., Hummer, J. A., & Patts, L. D. (2010). Aerosols emitted in underground mine air by diesel engine fueled with biodiesel. *Journal of the Air & Waste Management Association, 60*(2), 237-244.
Bugarski, A. D., Cauda, E. G., Janisko, S. J., Mischler, S. E., & Noll, J. D. (2011). *Diesel Aerosols and Gases in Underground Mines: Guide to Exposure Assessment and Control*: Department of Health and Human Services, Public Health Service, Center for Disease Control and Prevention, National Institute for Occupational Safety and Health, Office of Mine Safety and Health Research.
Bugarski, A. D., HUMMER, J., Mischler, S. E., Noll, J. D., Patts, L. D., & SCHNAKENBERG, G. (2007). Effectiveness of Selected Diesel Particulate Matter Control Technologies for Underground Mining Applications: Isolated Zone Study, 2004.
Burton, K. A., Whitelaw, J. L., Jones, A. L., & Davies, B. (2016). Efficiency of Respirator Filter Media against Diesel Particulate Matter: A Comparison Study Using Two Diesel Particulate Sources. *Annals of occupational hygiene*, mew026.
Campen, M. J., Babu, N. S., Helms, G. A., Pett, S., Wernly, J., Mehran, R., & McDonald, J. D. (2005). Nonparticulate components of diesel exhaust promote constriction in coronary arteries from ApoE−/− mice. *Toxicological Sciences, 88*(1), 95-102.
Campen, M. J., McDonald, J. D., Gigliotti, A. P., Seilkop, S. K., Reed, M. D., & Benson, J. M. (2003). Cardiovascular effects of inhaled diesel exhaust in spontaneously hypertensive rats. *Cardiovascular toxicology, 3*(4), 353-361.
Cantrell, B. K., & Watts Jr, W. F. (1997). Diesel exhaust aerosol: Review of occupational exposure. *Applied Occupational and Environmental Hygiene, 12*(12), 1019-1027.
Chan, T., Liu, Y., & Chan, C. (2010). Direct quadrature method of moments for the exhaust particle formation and evolution in the wake of the studied ground vehicle. *Journal of Aerosol Science, 41*(6), 553-568.
Chang, P., & Xu, G. (2017a). A review of the health effects and exposure-responsible relationship of diesel particulate matter for underground mines. *International Journal of Mining Science and Technology*.
Chang, P., & Xu, G. (2017b). A review of the health effects and exposure-responsible relationship of diesel particulate matter for underground mines. *International Journal of Mining Science and Technology, 27*(5), 831-838.
Chang, P., & Xu, G. (2019). *Review of Diesel Particulate Matter Control Methods in Underground Mines.* Paper presented at the Proceedings of the 11th International Mine Ventilation Congress.

Chang, P., Xu, G., Zhou, F., Mullins, B., & Abishek, S. (2019). Comparison of underground mine DPM simulation using discrete phase and continuous phase models. *Process Safety and Environmental Protection, 127*, 45-55.
Chang, P., Xu, G., Zhou, F., Mullins, B., Abishek, S., & Chalmers, D. (2019). Minimizing DPM pollution in an underground mine by optimizing auxiliary ventilation systems using CFD. *Tunnelling and Underground Space Technology, 87*, 112-121.
Cheng, D. F., Urata, C., Yagihashi, M., & Hozumi, A. (2012). A statically oleophilic but dynamically oleophobic smooth nonperfluorinated surface. *Angewandte Chemie, 124*(12), 3010-3013.
Cheng, J., Li, S., Zhang, F., Zhao, C., Yang, S., & Ghosh, A. (2016). CFD modelling of ventilation optimization for improving mine safety in longwall working faces. *Journal of Loss Prevention in the Process Industries, 40*, 285-297.
Chiesa, M., Mathiesen, V., Melheim, J. A., & Halvorsen, B. (2005). Numerical simulation of particulate flow by the Eulerian–Lagrangian and the Eulerian–Eulerian approach with application to a fluidized bed. *Computers & Chemical Engineering, 29*(2), 291-304.
Crowe, C. T. (2005). *Multiphase flow handbook*: CRC press.
Dahmann, D., & Bauer, H.-D. (1997). Diesel particulate matter (DPM) in workplaces in Germany. *Applied Occupational and Environmental Hygiene, 12*(12), 1028-1031.
De Jong, J., Dang, T., van Sint Annaland, M., & Kuipers, J. (2012). Comparison of a discrete particle model and a two-fluid model to experiments of a fluidized bed with flat membranes. *Powder technology, 230*, 93-105.
Deen, N., Annaland, M. V. S., Van der Hoef, M., & Kuipers, J. (2007). Review of discrete particle modeling of fluidized beds. *Chemical Engineering Science, 62*(1), 28-44.
Diego, I., Torno, S., Toraño, J., Menéndez, M., & Gent, M. (2011). A practical use of CFD for ventilation of underground works. *Tunnelling and Underground Space Technology, 26*(1), 189-200.
Dittler, A. (2017). The Application of Diesel Particle Filters—From Past to Present and Beyond. *Topics in Catalysis, 60*(3-5), 342-347.
DMP. (2013). *Management of diesel emissions in Western Australia mining operations*. 100 Plain Street EAST PERTH WA 6004: Resources Safety
Donaldson. Exhaust Product Guide
Edling, C., Anjou, C.-G., Axelson, O., & Kling, H. (1987). Mortality among personnel exposed to diesel exhaust. *International archives of occupational and environmental health, 59*(6), 559-565.
Edwards, J., & Hwang, C. (1900). CFD analysis of mine fire smoke spread and reverse flow conditions.
Edwards, J., & Hwang, C. (2006). *CFD modeling of fire spread along combustibles in a mine entry.* Paper presented at the Proceedings of the SME Annual Meeting.
Enwald, H., Peirano, E., & Almstedt, A.-E. (1996). Eulerian two-phase flow theory applied to fluidization. *International Journal of Multiphase Flow, 22*, 21-66.
Fang, Y., Fan, J., Kenneally, B., & Mooney, M. (2016). Air flow behavior and gas dispersion in the recirculation ventilation system of a twin-tunnel construction. *Tunnelling and Underground Space Technology, 58*, 30-39.
Gaillard, S., McCullough, E., & Sarver, E. (2016). Area monitoring and spot-checking for diesel particulate matter in an underground mine. *Mining Engineering, 68*(12).
Gangal, M. (2012). *Summary of worldwide underground mine diesel regulations.* Paper presented at the Proceedings of the 18th MDEC Conference, Toronto, Ontario.
Garshick, E., Laden, F., Hart, J. E., Davis, M. E., Eisen, E. A., & Smith, T. J. (2012). Lung cancer and elemental carbon exposure in trucking industry workers.
Garshick, E., Laden, F., Hart, J. E., Rosner, B., Smith, T. J., Dockery, D. W., & Speizer, F. E. (2004). Lung cancer in railroad workers exposed to diesel exhaust. *Environmental Health Perspectives*, 1539-1543.

Garshick, E., Laden, F., Hart, J. E., Smith, T. J., & Rosner, B. (2006). Smoking imputation and lung cancer in railroad workers exposed to diesel exhaust. *American Journal of Industrial Medicine, 49*(9), 709.

Garshick, E., Schenker, M. B., Muñoz, A., Segal, M., Smith, T. J., Woskie, S. R., . . . Speizer, F. E. (1987). A Case-Control Study of Lung Cancer and Diesel Exhaust Exposure in Railroad Workers. *American Review of Respiratory Disease, 135*(6), 1242-1248.

Garshick, E., Schenker, M. B., Muñoz, A., Segal, M., Smith, T. J., Woskie, S. R., . . . Speizer, F. E. (1988). A retrospective cohort study of lung cancer and diesel exhaust exposure in railroad workers. *American journal of respiratory and critical care medicine, 137*(4), 820-825.

Geng, F., Luo, G., Zhou, F., Zhao, P., Ma, L., Chai, H., & Zhang, T. (2017). Numerical investigation of dust dispersion in a coal roadway with hybrid ventilation system. *Powder technology, 313*, 260-271.

Gidaspow, D. (1994). *Multiphase flow and fluidization: continuum and kinetic theory descriptions*: Academic press.

Gidaspow, D., Jung, J., & Singh, R. K. (2004). Hydrodynamics of fluidization using kinetic theory: an emerging paradigm: 2002 Flour-Daniel lecture. *Powder technology, 148*(2), 123-141.

Gillies, S., & Wu, H. W. (2005). *Evaluation of a new real time personal dust meter for engineering studies on mine faces.* Paper presented at the Queensland Mining Industry Health and Safety Conference 2005.

Gong, X.-Y., Xia, Z.-X., Wu, Y., Mo, J.-M., & Zhang, X.-Y. (2017). *Research of Dust Field Optimization Distribution Based on Parameters Change of Air Duct Outlet in Fully Mechanized Excavation Face of Coal Mine.* Paper presented at the IOP Conference Series: Earth and Environmental Science.

Gordon, C. J., Schladweiler, M. C., Krantz, T., King, C., & Kodavanti, U. P. (2012). Cardiovascular and thermoregulatory responses of unrestrained rats exposed to filtered or unfiltered diesel exhaust. *Inhalation Toxicology, 24*(5), 296-309.

Guo, H., Yuan, L., Shen, B., Qu, Q., & Xue, J. (2012). Mining-induced strata stress changes, fractures and gas flow dynamics in multi-seam longwall mining. *International Journal of Rock Mechanics and Mining Sciences, 54*, 129-139.

Hansen, A., Rosen, H., & Novakov, T. (1984). The aethalometer—an instrument for the real-time measurement of optical absorption by aerosol particles. *Science of the Total Environment, 36*, 191-196.

Hargreaves, D., & Lowndes, I. (2007). The computational modeling of the ventilation flows within a rapid development drivage. *Tunnelling and Underground Space Technology, 22*(2), 150-160.

Hasheminasab, F., Bagherpour, R., & Aminossadati, S. M. (2019). Numerical simulation of methane distribution in development zones of underground coal mines equipped with auxiliary ventilation. *Tunnelling and Underground Space Technology, 89*, 68-77.

Hazari, M. S., Haykal-Coates, N., Winsett, D. W., Krantz, Q., King, C., Costa, D. L., & Farraj, A. K. (2011). TRPA1 and sympathetic activation contribute to increased risk of triggered cardiac arrhythmias in hypertensive rats exposed to diesel exhaust. *Environmental Health Perspectives, 119*(7), 951-957.

Hedges, K., Djukic, F., & Irving, G. (2007). *Diesel Particulate Matter in Underground Mines–Controlling the Risk (an update).* Paper presented at the tekijä: Queensland Mining Industry Health & Safety Conference.

HEI. (2002). *Research Directions to Improve Estimates of Human Exposure and Risk from Diesel Exhaust*. Retrieved from

HEI. (2003). *Research on Diesel Exhaust and Other Particules Health Effects Institute*. Retrieved from Charlestown Navy Yard, 120 Second Avenue, Boston MA 02129-4533 USA:

Heidari Nejad, S., Takechi, R., Mullins, B. J., Giles, C., Larcombe, A. N., Bertolatti, D., . . . Mamo, J. (2015). The effect of diesel exhaust exposure on blood–brain barrier integrity and function in a murine model. *Journal of applied toxicology, 35*(1), 41-47.

Heinrich, U., Fuhst, R., Rittinghausen, S., Creutzenberg, O., Bellmann, B., Koch, W., & Levsen, K. (1995). Chronic inhalation exposure of Wistar rats and two different strains of mice to diesel engine exhaust, carbon black, and titanium dioxide. *Inhalation Toxicology, 7*(4), 533-556.

Heinrich, U., Muhle, H., Takenaka, S., Ernst, H., Fuhst, R., Mohr, U., . . . Stöber, W. (1986). Chronic effects on the respiratory tract of hamsters, mice and rats after long-term inhalation of high concentrations of filtered and unfiltered diesel engine emissions. *Journal of applied toxicology, 6*(6), 383-395.

Henderson, R., Pickrell, J., Jones, R., Sun, J., Benson, J., Mauderly, J., & McClellan, R. (1988). Response of rodents to inhaled diluted diesel exhaust: biochemical and cytological changes in bronchoalveolar lavage fluid and in lung tissue. *Toxicological Sciences, 11*(1), 546-567.

Hongqing, Z., & Xingkui, L. (2012). Theoretical investigation on the relationship between tail roadway methane drainage and distribution of easily spontaneous combustible region in gob. *Safety science, 50*(4), 618-623.

Howell, S., & Weber, A. (1997). Biodiesel use in underground metal and non-metal mines. *Dieselnet site http://www. dieselnet. com*.

Hu, S., Feng, G., Ren, X., Xu, G., Chang, P., Wang, Z., . . . Gao, Q. (2016a). Numerical study of gas–solid two-phase flow in a coal roadway after blasting. *Advanced Powder Technology*.

Hu, S., Feng, G., Ren, X., Xu, G., Chang, P., Wang, Z., . . . Gao, Q. (2016b). Numerical study of gas–solid two-phase flow in a coal roadway after blasting. *Advanced Powder Technology, 27*(4), 1607-1617.

Hu, S., Liao, Q., Feng, G., Huang, Y., Shao, H., Fan, Y., & Ye, Y. (2019). Numerical study of gas-solid two-phase flow around road-header drivers in a fully mechanized excavation face. *Powder technology, 344*, 959-969.

Hu, S., Wang, Z., & Feng, G. (2015). Temporal and Spatial Distribution of Respirable Dust After Blasting of Coal Roadway Driving Faces: A Case Study. *Minerals, 5*(4), 679-692.

Humphreys, D., Collecutt, G., & Proud, D. (2010). *CFD simulation of underground coal dust explosions and active explosion barriers.* Paper presented at the Seventh International Conference on CFD in the Minerals and Process Industries CSIRO, Melbourne, Australia.

IARC. (1989). Diesel and gasoline engine exhausts and some nitroarenes. *46*. Retrieved from http://monographs.iarc.fr/ENG/Monographs/vol46/

IARC. (2013). Diesel and gasoline engine exhausts and some nitroarenes. *105*.

Iwai, K., Adachi, S., Takahashi, M., Möller, L., Udagawa, T., Mizuno, S., & Sugawara, I. (2000). Early oxidative DNA damages and late development of lung cancer in diesel exhaust-exposed rats. *Environmental Research, 84*(3), 255-264.

J. D. NOLL, A. D. B., L. D. PATTS, S. E. MISCHLER, AND L. MCWILLIAMS. (2007). Relationship between Elemental Carbon, Total Carbon, and Diesel Particulate Matter in Several Underground Metal/Non-metal Mines. *Environment Science Technology*(41).

J.Anderson, E. D., G.Degrez. (2008). *Computational fluid dynamics: an introduction*: Springer Science & Business Media.

Janisko, S., & Noll, J. (2008). *Near real time monitoring of diesel particulate matter in underground mines.* Paper presented at the Proceedings of the 12th US/North American Mine Ventilation Symposium.

Järvholm, B., & Silverman, D. (2003). Lung cancer in heavy equipment operators and truck drivers with diesel exhaust exposure in the construction industry. *Occupational and environmental medicine, 60*(7), 516-520.

Jiang, P., Lignell, D. O., Killy, K. E., Lighty, J. S., Sarofim, A. F., & Montgomery, C. J. (2005). Simulation of the evolution of particle size distributions in a vehicle exhaust plume with unconfined dilution by ambient air. *Journal of the Air & Waste Management Association, 55*(4), 437-445.

Jiang, R., Jones, M. J., Sava, F., Kobor, M. S., & Carlsten, C. (2014). Short-term diesel exhaust inhalation in a controlled human crossover study is associated with changes in DNA methylation of circulating mononuclear cells in asthmatics. *Particle and fibre toxicology, 11*(1), 71.

Kilgallon, R., Gilfillan, S., Edlmann, K., McDermott, C., Naylor, M., & Haszeldine, R. (2017). Experimental determination of noble gases and SF6, as tracers of CO2 flow through porous sandstone. *Chemical Geology*.

Kittelson, D., Watts, W., & Johnson, J. (2002). Diesel Aerosol Sampling Methodology–CRC E-43. *Final report, Coordinating Research Council*.

Kittelson, D. B. (1998). Engines and nanoparticles: a review. *Journal of Aerosol Science, 29*(5), 575-588.

Kurnia, J. C., Sasmito, A. P., Hassani, F. P., & Mujumdar, A. S. (2015). Introduction and evaluation of a novel hybrid brattice for improved dust control in underground mining faces: A computational study. *International Journal of Mining Science and Technology, 25*(4), 537-543.

Kurnia, J. C., Sasmito, A. P., & Mujumdar, A. S. (2014a). CFD simulation of methane dispersion and innovative methane management in underground mining faces. *Applied Mathematical Modelling, 38*(14), 3467-3484.

Kurnia, J. C., Sasmito, A. P., & Mujumdar, A. S. (2014). Dust dispersion and management in underground mining faces. *International Journal of Mining Science and Technology, 24*(1), 39-44.

Kurnia, J. C., Sasmito, A. P., & Mujumdar, A. S. (2014b). Simulation of a novel intermittent ventilation system for underground mines. *Tunnelling and Underground Space Technology, 42*, 206-215.

Kurnia, J. C., Sasmito, A. P., Wong, W. Y., & Mujumdar, A. S. (2014). Prediction and innovative control strategies for oxygen and hazardous gases from diesel emission in underground mines. *Science of the Total Environment, 481*, 317-334.

Laden, F., Hart, J. E., Eschenroeder, A., Smith, T. J., & Garshick, E. (2006). Historical estimation of diesel exhaust exposure in a cohort study of US railroad workers and lung cancer. *Cancer Causes & Control, 17*(7), 911-919.

Laden, F., Hart, J. E., Smith, T. J., Davis, M. E., & Garshick, E. (2007). Cause-specific mortality in the unionized US trucking industry. *Environmental Health Perspectives*, 1192-1196.

Launder, B. E., & Spalding, D. B. (1983). The numerical computation of turbulent flows. In *Numerical Prediction of Flow, Heat Transfer, Turbulence and Combustion* (pp. 96-116): Elsevier.

Lewis, T., Green, F., Moorman, W., Burg, J., & Lynch, D. (1989). A chronic inhalation toxicity study of diesel engine emissions and coal dust, alone and combined. *International Journal of Toxicology, 8*(2), 345-375.

Li, Z.-x. (2008). CFD simulation of spontaneous coal combustion in irregular patterns of goaf with multiple points of leaking air. *Journal of China University of Mining and Technology, 18*(4), 504-515.

Liu, X., Chang, P., Wang, E., Zhang, Z., & Yang, S. (2018). Numerical Study of the Respirable Coal Dust Removal Performance of a Vortex Ventilation System at an Excavation Face. *Energies, 11*(9), 2449.

Liu, Y.-Y., Lin, T.-C., Wang, Y.-J., & Ho, W.-L. (2009). Carbonyl compounds and toxicity assessments of emissions from a diesel engine running on biodiesels. *Journal of the Air & Waste Management Association, 59*(2), 163-171.

Liu, Y., He, Z., & Chan, T. (2011). Three-dimensional simulation of exhaust particle dispersion and concentration fields in the near-wake region of the studied ground vehicle. *Aerosol Science and Technology, 45*(8), 1019-1030.

Longest, P. W., & Xi, J. (2007). Effectiveness of direct Lagrangian tracking models for simulating nanoparticle deposition in the upper airways. *Aerosol Science and Technology, 41*(4), 380-397.
Lucking, A. J., Lundbäck, M., Barath, S. L., Mills, N. L., Sidhu, M. K., Langrish, J. P., . . . Gerlofs-Nijland, M. E. (2011). Particle traps prevent adverse vascular and prothrombotic effects of diesel engine exhaust inhalation in men. *Circulation, 123*(16), 1721-1728.
Lutz, E. A., Reed, R. J., Lee, V. S., & Burgess, J. L. (2015). Occupational exposures to emissions from combustion of diesel and alternative fuels in underground mining—a simulated pilot study. *Journal of occupational and environmental hygiene, 12*(3), 18-25.
Lutz, E. A., Reed, R. J., Lee, V. S. T., & Burgess, J. L. (2017). Comparison of Personal Diesel and Biodiesel Exhaust Exposures in an Underground Mine. *Journal of occupational and environmental hygiene*(just-accepted).
Lyon. (2012). *IARC: Diesel Engine Exhaust Carcinogenic*. Retrieved from France:
Mauderly, J. L., Jones, R. K., Griffith, W. C., Henderson, R. F., & McClellan, R. O. (1987). Diesel exhaust is a pulmonary carcinogen in rats exposed chronically by inhalation. *Toxicological Sciences, 9*(2), 208-221.
McGinn, S. (2000). The relationship between diesel engine maintenance and exhaust emissions—final report. In.
McGinn, S. (2009). Controlling Diesel Emissions in Underground Mining within an Evolving Regulatory Structure in Canada and the United States of America.
Mills, N. L., Törnqvist, H., Gonzalez, M. C., Vink, E., Robinson, S. D., Söderberg, S., . . . Blomberg, A. (2007). Ischemic and thrombotic effects of dilute diesel-exhaust inhalation in men with coronary heart disease. *New England Journal of Medicine, 357*(11), 1075-1082.
Mills, N. L., Törnqvist, H., Robinson, S. D., Gonzalez, M., Darnley, K., MacNee, W., . . . Sandstrom, T. (2005). Diesel exhaust inhalation causes vascular dysfunction and impaired endogenous fibrinolysis. *Circulation, 112*(25), 3930-3936.
Mischler, S. E., Bugarski, A. D., & Noll, J. D. (2006). Instrumentation for diesel particulate matter emissions research. *Proceedings of the 11th U.S./North American Mine Ventilation Symposium, University Park, Pennsylvania, June 5-7, 2006*.
Mischler, S. E., & Colinet, J. F. (2009). *Controlling and monitoring diesel emissions in underground mines in the United States.* Paper presented at the Mine Ventilation: Proceedings of the Ninth International Mine Ventilation Congress, New Delhi, India.
Mishra, D. P., Kumar, P., & Panigrahi, D. C. (2016). Dispersion of methane in tailgate of a retreating longwall mine: a computational fluid dynamics study. *Environmental Earth Sciences, 75*(6), 475.
Mishra, D. P., Panigrahi, D. C., & Kumar, P. (2018). Computational investigation on effects of geo-mining parameters on layering and dispersion of methane in underground coal mines-A case study of Moonidih Colliery. *Journal of Natural Gas Science and Engineering, 53*, 110-124.
Möhner, M., Kersten, N., & Gellissen, J. (2013). Diesel motor exhaust and lung cancer mortality: reanalysis of a cohort study in potash miners. *European journal of epidemiology, 28*(2), 159-168.
Moukalled, F., Mangani, L., & Darwish, M. (2016). The finite volume method in computational fluid dynamics.
MSHA. Engine approval numbers. Retrieved from https://lakegovprod2.msha.gov/ReportView.aspx?ReportCategory=EngineAppNumbers#. from https://lakegovprod2.msha.gov/ReportView.aspx?ReportCategory=EngineAppNumbers# https://lakegovprod2.msha.gov/ReportView.aspx?ReportCategory=EngineAppNumbers#

MSHA. (2001a). 30 CFR 72 Diesel Particulate Matter Exposure of Underground Metal & Non Metal Miners. *Federal Register*, 5706-5912.
MSHA. (2001b). Diesel Particulate Matter Exposure of Underground Metal & Non Metal Miners. *Federal Register*, 5706-5912.
MSHA. (2005a). 30 CFR Part 57 Diesel Particulate Matter Exposure of Underground Metal and Nonmetal Miners. *Federal Register, 70*(107), 32868.
MSHA. (2005b). Issues Final Rule Final Rule Strengthening Protections for Underground Metal/Nonmetal Miners Exposed to Diesel Particulate Matter. Retrieved from http://arlweb.msha.gov/MEDIA/PRESS/2005/NR050606.asp
MSHA. (2006). 30 CFR 57 Diesel Particulate Matter Exposure of Underground Metal & Non Metal Miners. *Federal Register*, 28924-29012.
MSHA. (2014). 30 CFR 7 Mineral Resources. *Federal Register*.
MSOD. (2008). Guideline for the management of diesel engine pollutants in underground environments. *Mine Safety Operations Division,New South Wales Department of Primary Industries*.
Neeft, J. P., Makkee, M., & Moulijn, J. A. (1996). Diesel particulate emission control. *Fuel processing technology, 47*(1), 1-69.
Nemmar, A., Al-Maskari, S., Ali, B. H., & Al-Amri, I. S. (2007). Cardiovascular and lung inflammatory effects induced by systemically administered diesel exhaust particles in rats. *American Journal of Physiology-Lung Cellular and Molecular Physiology, 292*(3), L664-L670.
Neumeyer-Gromen, A., Razum, O., Kersten, N., Seidler, A., & Zeeb, H. (2009). Diesel motor emissions and lung cancer mortality—Results of the second follow-up of a cohort study in potash miners. *International Journal of Cancer, 124*(8), 1900-1906.
Nikula, K., Snipes, M., Barr, E., Griffith, W., Henderson, R., & Mauderly, J. (1995). Comparative pulmonary toxicities and carcinogenicities of chronically inhaled diesel exhaust and carbon black in F344 rats. *Toxicological Sciences, 25*(1), 80-94.
NIOHS. (1988). Carcinogenic Effect of Exposure to Diesel Exhaust,Current Intelligence Bulletin 50,U.S. Retrieved from http://www.cdc.gov/niosh/nas/RDRP/appendices/chapter5/a5-29.pdf
NIOSH. (1986). *Evaluation of the potential health effects of occupational exposure to diesel exhaust in underground coal mines*. Retrieved from
Noll, J., Cecala, A., & Organiscak, J. (2011). The effectiveness of several enclosed cab filters and systems for reducing diesel particulate matter. *Transactions, 330*, 408.
Noll, J., Gilles, S., Wu, H. W., & Rubinstein, E. (2015). The relationship between elemental carbon and diesel particulate matter in underground metal/nonmetal mines in the United States and coal mines in Australia. *Journal of occupational and environmental hygiene, 12*(3), 205-211.
Noll, J., & Janisko, S. (2007). *Using laser absorption techniques to monitor diesel particulate matter exposure in underground stone mines.* Paper presented at the Optics East 2007.
Noll, J., & Janisko, S. (2013). Evaluation of a wearable monitor for measuring real-time diesel particulate matter concentrations in several underground mines. *Journal of occupational and environmental hygiene, 10*(12), 716-722.
Noll, J., Janisko, S., & Mischler, S. E. (2013). Real-time diesel particulate monitor for underground mines. *Analytical Methods, 5*(12), 2954-2963.
Noll, J., Mischler, S., Schnakenberg, G., Bugarski, A., Mutmansky, J., & Ramani, R. (2006). *Measuring Diesel Particulate Matter in Underground Mines Using Sub Micron Elemental Carbon as a Surrogate.* Paper presented at the Proceedings for the 11th US North American Mine Ventilation Symposium.
Noll, J., Volkwein, J., Janisko, S., & Patts, L. (2013). Portable instruments for measuring tailpipe diesel particulate in underground mines. *Mining Engineering, 65*(10).
Nordenhall, C., Pourazar, J., Blomberg, A., Levin, J.-O., Sandstrom, T., & Adelroth, E. (2000). Airway inflammation following exposure to diesel exhaust: a study of time kinetics using induced sputum. *European Respiratory Journal, 15*(6), 1046-1051.

Nordenhäll, C., Pourazar, J., Ledin, M., Levin, J.-O., Sandström, T., & Ädelroth, E. (2001). Diesel exhaust enhances airway responsiveness in asthmatic subjects. *European Respiratory Journal, 17*(5), 909-915.

O'Rourke, P. J., & Snider, D. M. (2010). An improved collision damping time for MP-PIC calculations of dense particle flows with applications to polydisperse sedimenting beds and colliding particle jets. *Chemical Engineering Science, 65*(22), 6014-6028.

Olsson, A. C., Gustavsson, P., Kromhout, H., Peters, S., Vermeulen, R., Brüske, I., . . . Brüning, T. (2011). Exposure to diesel motor exhaust and lung cancer risk in a pooled analysis from case-control studies in Europe and Canada. *American journal of respiratory and critical care medicine, 183*(7), 941-948.

Ounis, H., & Ahmadi, G. (1990). A comparison of Brownian and turbulent diffusion. *Aerosol Science and Technology, 13*(1), 47-53.

Panigrahi, D. C., & Mishra, D. P. (2014). CFD simulations for the selection of an appropriate blade profile for improving energy efficiency in axial flow mine ventilation fans. *Journal of Sustainable Mining, 13*(1), 15-21.

Parent, M.-E., Rousseau, M.-C., Boffetta, P., Cohen, A., & Siemiatycki, J. (2007). Exposure to diesel and gasoline engine emissions and the risk of lung cancer. *American journal of epidemiology, 165*(1), 53-62.

Park, K., Kittelson, D. B., Zachariah, M. R., & McMurry, P. H. (2004). Measurement of inherent material density of nanoparticle agglomerates. *Journal of Nanoparticle Research, 6*(2), 267-272.

Parra, M., Villafruela, J., Castro, F., & Mendez, C. (2006). Numerical and experimental analysis of different ventilation systems in deep mines. *Building and Environment, 41*(2), 87-93.

Patankar, N., & Joseph, D. (2001). Modeling and numerical simulation of particulate flows by the Eulerian–Lagrangian approach. *International Journal of Multiphase Flow, 27*(10), 1659-1684.

Proud, D., Collecutt, G., & Humphreys, D. (2015). *Computational Fluid Dynamics Modelling of Coal Dust Explosions and Suppression Systems*.

Ranjan, M., & Karan Kumar, S. K. (2013). Mine ventilation in a bord and pillar mines using CFD. *International Journal of Emerging Technology and Advanced Engineering, 3*(3).

Ren, T., Wang, Z., & Cooper, G. (2014). CFD modelling of ventilation and dust flow behaviour above an underground bin and the design of an innovative dust mitigation system. *Tunnelling and Underground Space Technology, 41*, 241-254.

Ren, T., Wang, Z., & Zhang, J. (2018). Improved dust management at a longwall top coal caving (LTCC) face–A CFD modelling approach. *Advanced Powder Technology, 29*(10), 2368-2379.

Ris, C. (2007). US EPA health assessment for diesel engine exhaust: a review. *Inhalation Toxicology, 19*(sup1), 229-239.

Robert A. Haney, G. P. S., Robert W. Waytulonis. (1997). An Overview of Diesel Particulate Exposures and Control Technology in the U.S. Mining Industry. *Applied Occupational and Environmental Hygiene, 12*(12), 6.

Rudell, B., ., Ledin, M. C., Hammarstr?M, U., ., Stjernberg, N., ., Lundb?Ck, B., ., & Sandstr?M, T., . (1996). Effects of symptoms and lung function in humans experimentally exposed to diesel exhaust. *Occupational & Environmental Medicine, 53*(10), : 658–662.

Rudell, B., Ledin, M. C., Hammarstr, M., U., Stjernberg, N., Lundb?Ck, B., & Sandstr?M, T. (1996). Effects of symptoms and lung function in humans experimentally exposed to diesel exhaust. *Occupational & Environmental Medicine, 53*(10), : 658–662.

Rudell, B., Sandström, T., Hammarström, U., Ledin, M. L., Hörstedt, P., & Stjernberg, N. (1994). Evaluation of an exposure setup for studying effects of diesel exhaust in humans. *International Archives of Occupational & Environmental Health, 66*(2), 77-83.

Rudell, B., Sandström, T., Stjernberg, N., & Kolmodin-Hedman, B. (1990). Controlled diesel exhaust exposure in an exposure chamber: pulmonary effects investigated with bronchoalveolar lavage. *Journal of Aerosol Science, 21*, S411-S414.

Salvi, S., Blomberg, A., Rudell, B., Kelly, F., Sandstrom, T., Holgate, S. T., & Frew, A. (1999). Acute inflammatory responses in the airways and peripheral blood after short-term exposure to diesel exhaust in healthy human volunteers. *American journal of respiratory and critical care medicine, 159*(3), 702-709.

Salvi, S., Nordenhall, C., Blomberg, A., Rudell, B., Pourazar, J., Kelly, F. J., . . . Frew, A. J. (2000). Acute exposure to diesel exhaust increases IL-8 and GRO-α production in healthy human airways. *American journal of respiratory and critical care medicine, 161*(2), 550-557.

Sasmito, A. P., Birgersson, E., Ly, H. C., & Mujumdar, A. S. (2013). Some approaches to improve ventilation system in underground coal mines environment–A computational fluid dynamic study. *Tunnelling and Underground Space Technology, 34*, 82-95.

Schwab, J. A., & Zenkel, M. (1998). Filtration of particulates in the human nose. *The Laryngoscope, 108*(1), 120-124.

Silverman, D. T., Samanic, C. M., Lubin, J. H., Blair, A. E., Stewart, P. A., Vermeulen, R., . . . Travis, W. D. (2012). The diesel exhaust in miners study: a nested case–control study of lung cancer and diesel exhaust. *Journal of the National Cancer Institute, 104*(11), 855-868.

Steenland, K., Deddens, J., & Stayner, L. (1998). Diesel exhaust and lung cancer in the trucking industry: exposure-response analyses and risk assessment. *American Journal of Industrial Medicine, 34*(3), 220-228.

Takiff, L., & Aiken, G. (2010). *A real-time, wearable elemental carbon monitor for use in underground mines.* Paper presented at the Proc. 13th United States/North American Mine Ventilation Symposium, Hardcastle & McKinnon (eds).

Tanguturi, K., & Balusu, R. (2014). CFD modeling of methane gas distribution and control strategies in a gassy coal mine. *The Journal of Computational Multiphase Flows, 6*(1), 65-77.

Taraba, B., & Michalec, Z. (2011). Effect of longwall face advance rate on spontaneous heating process in the gob area–CFD modelling. *Fuel, 90*(8), 2790-2797.

Thiruvengadam, M., Zheng, Y., Lan, H., & Tien, J. C. (2016). A diesel particulate matter dispersion study inside a single dead end entry using dynamic mesh model. *International Journal of Mining and Mineral Engineering, 7*(3), 210-223.

Thiruvengadam, M., Zheng, Y., & Tien, J. C. (2016). DPM simulation in an underground entry: Comparison between particle and species models. *International Journal of Mining Science and Technology, 26*(3), 487-494.

Toraño, J., Torno, S., Menéndez, M., & Gent, M. (2011). Auxiliary ventilation in mining roadways driven with roadheaders: Validated CFD modelling of dust behaviour. *Tunnelling and Underground Space Technology, 26*(1), 201-210.

Toraño, J., Torno, S., Menendez, M., Gent, M., & Velasco, J. (2009). Models of methane behaviour in auxiliary ventilation of underground coal mining. *International Journal of Coal Geology, 80*(1), 35-43. doi:http://dx.doi.org/10.1016/j.coal.2009.07.008

Torno, S., Toraño, J., Ulecia, M., & Allende, C. (2013). Conventional and numerical models of blasting gas behaviour in auxiliary ventilation of mining headings. *Tunnelling and Underground Space Technology, 34*, 73-81.

Trevits, M. A., Yuan, L., Thibou, M., & Hatch, G. (2010). Use of CFD modeling to study inert gas injection into a sealed mine area.

Turcotte, K. B., Edwardson, E., & Laflamme, G. (1998). Evaluation of Existing Diesel Particulate Matter Sampling and Analysis Methods at a High Sulphide Ore Mine.

Turner, S. (2007). Diesel particulate exposure and control in western australia underground mines. Retrieved from http://www.gastech.com.au/files/dpm/Diesel%20Particulate%20Report%202006.pdf

Uhrner, U., Von Löwis, S., Vehkamäki, H., Wehner, B., Bräsel, S., Hermann, M., . . . Wiedensohler, A. (2007). Dilution and aerosol dynamics within a diesel car exhaust plume—CFD simulations of on-road measurement conditions. *Atmospheric Environment, 41*(35), 7440-7461.

US.EPA. (2002). *Health assessment document for diesel engine exhaust*: National Center for Environmental Assessment.

Van der Hoef, M., Ye, M., van Sint Annaland, M., Andrews, A., Sundaresan, S., & Kuipers, J. (2006). Multiscale modeling of gas-fluidized beds. *Advances in chemical engineering, 31*, 65-149.

Van Wachem, B., & Almstedt, A.-E. (2003). Methods for multiphase computational fluid dynamics. *Chemical Engineering Journal, 96*(1), 81-98.

Vegendla, S. P., Heynderickx, G. J., & Marin, G. B. (2011). Comparison of Eulerian–Lagrangian and Eulerian–Eulerian method for dilute gas–solid flow with side inlet. *Computers & Chemical Engineering, 35*(7), 1192-1199.

Vermeulen, R., Silverman, D. T., Garshick, E., Vlaanderen, J., Portengen, L., & Steenland, K. (2014). Exposure-response estimates for diesel engine exhaust and lung cancer mortality based on data from three occupational cohorts. *Environmental Health Perspectives, 122*(2), 172.

Walter, S., Ashok, T., Erwin, A., Klaus, R., Georg, S., Peter, S., . . . Wolf, R. (2005). Chronic nose-only inhalation study in rats, comparing room-aged sidestream cigarette smoke and diesel engine exhaust. *Inhalation Toxicology, 17*(11), 549-576.

Wang, H., Nie, W., Cheng, W., Liu, Q., & Jin, H. (2018). Effects of air volume ratio parameters on air curtain dust suppression in a rock tunnel's fully-mechanized working face. *Advanced Powder Technology, 29*(2), 230-244.

Wang, Y., Luo, G., Geng, F., Li, Y., & Li, Y. (2015). Numerical study on dust movement and dust distribution for hybrid ventilation system in a laneway of coal mine. *Journal of Loss Prevention in the Process Industries, 36*, 146-157.

Wang, Z., & Ren, T. (2013). Investigation of airflow and respirable dust flow behaviour above an underground bin. *Powder technology, 250*, 103-114.

Watson, J. G., Chow, J. C., & Chen, L.-W. A. (2005). Summary of organic and elemental carbon/black carbon analysis methods and intercomparisons. *Aerosol Air Qual. Res, 5*(1), 65-102.

Wilhelm, J., Seibt, D., Bich, E., Vogel, E., & Hassel, E. (2005). Viscosity measurements on gaseous sulfur hexafluoride. *Journal of Chemical & Engineering Data, 50*(3), 896-906.

Wu, H., & Gillies, A. (2008). *Developments in real time personal diesel particulate monitoring in mines.* Paper presented at the Proceedings, 12 th US Mine Ventilation Symposium.

Xu, G., Chang, P., Mullins, B., Zhou, F., & Hu, S. (2018). Numerical study of diesel particulate matter distribution in an underground mine isolated zone. *Powder technology, 339*, 947-957. Retrieved from http://www.sciencedirect.com/science/article/pii/S0032591018307137

Xu, G., Jong, E. C., Luxbacher, K. D., Ragab, S. A., & Karmis, M. E. (2015). Remote characterization of ventilation systems using tracer gas and CFD in an underground mine. *Safety science, 74*, 140-149.

Xu, G., Luxbacher, K. D., Ragab, S., & Schafrik, S. (2013). Development of a remote analysis method for underground ventilation systems using tracer gas and CFD in a simplified laboratory apparatus. *Tunnelling and Underground Space Technology, 33*, 1-11.

Xu, G., Luxbacher, K. D., Ragab, S., Xu, J., & Ding, X. (2016). Computational fluid dynamics applied to mining engineering: a review. *International Journal of Mining, Reclamation and Environment*, 1-25.

Yokota, S., Furuya, M., Seki, T., Marumo, H., Ohara, N., & Kato, A. (2004). Delayed exacerbation of acute myocardial ischemia/reperfusion-induced arrhythmia by

tracheal instillation of diesel exhaust particles. *Inhalation Toxicology, 16*(5), 319-331.
Yokota, S., Ohara, N., & Kobayashi, T. (2008). The effects of organic extract of diesel exhaust particles on ischemia/reperfusion-related arrhythmia and on pulmonary inflammation. *The Journal of toxicological sciences, 33*(1), 1-10.
Yokota, S., Seki, T., Furuya, M., & Ohara, N. (2005). Acute functional enhancement of circulatory neutrophils after intratracheal instillation with diesel exhaust particles in rats. *Inhalation Toxicology, 17*(12), 671-679.
Yu, H., Cheng, W., Wu, L., Wang, H., & Xie, Y. (2017). Mechanisms of dust diffuse pollution under forced-exhaust ventilation in fully-mechanized excavation faces by CFD-DEM. *Powder technology, 317*, 31-47.
Yuan, L., & Smith, A. (2007). Computational fluid dynamics modeling of spontaneous heating in longwall gob areas. *transactions-society for mining metallurgy and exploration incorporated, 322*, 37.
Yuan, L., & Smith, A. (2010). *Modeling the effect of barometric pressure changes on spontaneous heating in bleederless longwall panels.* Paper presented at the SME Annual Meeting and Exhibit.
Yuan, L., & Smith, A. C. (2008). Numerical study on effects of coal properties on spontaneous heating in longwall gob areas. *Fuel, 87*(15-16), 3409-3419.
Zhang, G., Tan, Y., Chen, K., Liu, Z., & Yang, Y. (2007). *Mine Ventilation and Safety*: China University of Mining and Technology Press.
Zhang, J., Zhang, H., Ren, T., Wei, J., & Liang, Y. (2019). Proactive inertisation in longwall goaf for coal spontaneous combustion control-A CFD approach. *Safety science, 113*, 445-460.
Zhang, Q., Qian, X., Yuan, M., Zhao, L., Zhao, Y., Fan, T., . . . Fu, L. (2018). CFD investigation on diffusing dynamics of respirable dust coupled with multiple sources on a longwall face: A case study from meso-scale. *Powder technology*.
Zhang, X., Li, J., He, Z., Duan, H., Gao, W., Wang, H., . . . Zheng, Y. (2016). Associations between DNA methylation in DNA damage response-related genes and cytokinesis-block micronucleus cytome index in diesel engine exhaust-exposed workers. *Archives of toxicology, 90*(8), 1997-2008.
Zhao, B., Chen, C., & Lai, A. C. (2011). Lagrangian Stochastic Particle Tracking: Further Discussion. *Aerosol Science and Technology, 45*(8), 901-902.
ZHENG, Y. (2011). *Diesel Particulate Matter Dispersion Analysis in Underground Metl/Nometal Mines Using Computational Fluid Dynamics.* (Doctor of Philosophy). MISSOURI UNIVERSITY OF SCIENCE AND TECHNOLOGY,
Zheng, Y., Lan, H., Thiruvengadam, M., & Tien, J. (2011a). DPM dissipation experiment at MST's experimental mine and comparison with CFD simulation. *Journal of Coal Science and Engineering (China), 17*(3), 285-289. doi:10.1007/s12404-011-0311-1
Zheng, Y., Lan, H., Thiruvengadam, M., & Tien, J. C. (2011b). DPM dissipation experiment at MST's experimental mine and comparison with CFD simulation. *Journal of Coal Science and Engineering (China), 17*(3), 285-289.
Zheng, Y., Lan, H., Thiruvengadam, M., Tien, J. C., & Li, Y. (2017). Effect of single dead end entry inclination on DPM plume dispersion. *International Journal of Mining Science and Technology, 27*(3), 401-406.
Zheng, Y., Li, Y., Thiruvengadam, M., Lan, H., & Tien, J. C. (2017). DPM dispersion inside a single straight entry using dynamic mesh model. *International Journal of Coal Science & Technology, 4*(3), 234-244.
Zheng, Y., Thiruvengadam, M., Lan, H., & Tien C, J. (2015). Simulation of DPM distribution in a long single entry with buoyancy effect. *International Journal of Mining Science and Technology, 25*(1), 47-52. doi:http://dx.doi.org/10.1016/j.ijmst.2014.11.004
Zheng, Y., Thiruvengadam, M., Lan, H., & Tien, C. J. (2015a). Effect of auxiliary ventilations on diesel particulate matter dispersion inside a dead-end entry. *International Journal of Mining Science and Technology, 25*(6), 927-932.

Zheng, Y., Thiruvengadam, M., Lan, H., & Tien, J. C. (2015b). Design of push–pull system to control diesel particular matter inside a dead-end entry. *International Journal of Coal Science & Technology, 2*(3), 237-244.

Zheng, Y., & Tien, J. C. (2008). *DPM dispersion study using CFD for underground metal/nonmetal mines.* Paper presented at the Proceedings of the 12th US/North America Mine ventilation Symposium, Reno.

Zheng, Y., & Tien, J. C. (2009). *Reconstruction of diesel emissions distribution based on an isolated zone experiment by using CFD method.* Paper presented at the Proceedings of the 9th International Mine Ventilation Congress. New Delhi.

Zhou, G., Zhang, Q., Bai, R., Fan, T., & Wang, G. (2017). The diffusion behavior law of respirable dust at fully mechanized caving face in coal mine: CFD numerical simulation and engineering application. *Process Safety and Environmental Protection, 106*, 117-128.

Zhou, L., Pritchard, C., & Zheng, Y. (2015). CFD modeling of methane distribution at a continuous miner face with various curtain setback distances. *International Journal of Mining Science and Technology, 25*(4), 635-640.

Zhu, H., Zhou, Z., Yang, R., & Yu, A. (2007). Discrete particle simulation of particulate systems: theoretical developments. *Chemical Engineering Science, 62*(13), 3378-3396.

Zhu, H., Zhou, Z., Yang, R., & Yu, A. (2008). Discrete particle simulation of particulate systems: a review of major applications and findings. *Chemical Engineering Science, 63*(23), 5728-5770.

Appendix

Declaration of Authorship

To Whom It May Concern

I, Ping Chang, contributed:

- 90% of design and analysis to the publication entitled "A review of the health effects and exposure-responsible relationship of diesel particulate matter for underground mines". Dr. Guang Xu supervised the study and provided the editorial suggestion and reviewed the paper.
- 85% of design and analysis to the publication entitled "Numerical study of diesel particulate matter distribution in an underground mine isolated zone". Dr. Guang Xu supervised the study and provided the editorial suggestion and reviewed the paper. Prof. Benjamin Mullins and Prof. Fubao Zhou assisted with the design and analysis of the study and reviewed the paper. Prof. Shengyong Hu assisted with the CFD model set-up and reviewed the paper.
- 85% of design and analysis to the publication entitled "Minimizing DPM pollution in an underground mine by optimizing auxiliary ventilation systems using CFD". Dr. Guang Xu supervised the study and provided the editorial suggestion and reviewed the paper. Prof. Benjamin Mullins and Prof. Fubao Zhou assisted with the design and analysis of the study and reviewed the paper. Dr. S. Abishek assisted with the CFD model set-up and reviewed the paper. Mr. Duncan Chalmers provided the ventilation design suggestion.
- 80% of design and analysis to the publication entitled "Comparison of underground mine DPM simulation using discrete phase and continuous phase models". Dr. Guang Xu supervised the study and provided the editorial suggestion and reviewed the paper. Prof. Benjamin Mullins and Prof. Fubao Zhou assisted with the design and analysis of the study and reviewed the paper. Dr. S. Abishek assisted with the CFD model set-up and reviewed the paper.

Ping Chang Date: 24/09/2019

I, as a Co-Author, endorse that this level of contribution by the candidate indicated above is appropriate.

Dr. Guang Xu
Supervisor and co-au Date: 9/20/2019

Prof. Benjamin Mullins
Co-author Date: 24/09/2019

Prof. Fubao Zhou
Co-author Date: 2019/9/23

Prof. Shengyong Hu
Co-author Date: 20/09/2019

Dr. S. Abishek
Co-author Date: 20/09/2019

Mr. Duncan Chalmers
Co-author Date: 2019/9/19